AD-A129 016 A HIGH PRESSURE MERCURY TURBINE CYCLE FOR USE IN SPACECRAFT AND TERRESTRI..(U) MASSACHUSETTS INST OF TECH LEXINGTON LINCOLN LAB R M LERNER 22 MAR 83 TR-577 1/ 3

UNCLASSIFIED ESD-TR-82-176 F19628-80-C-0002 F/G 13/2• NL

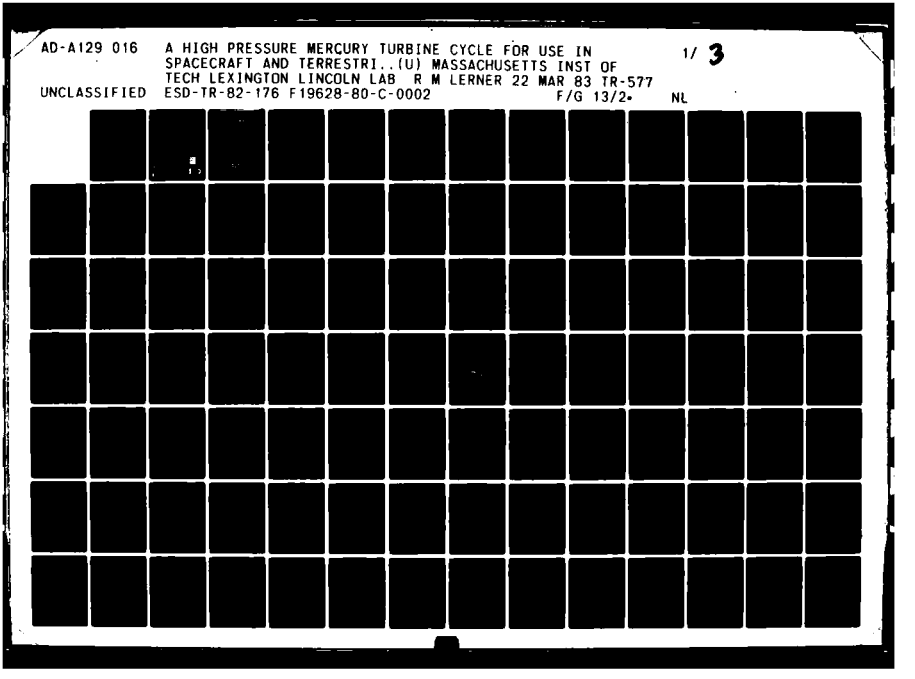

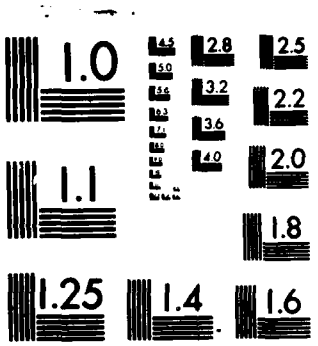

MICROCOPY RESOLUTION TEST CHART
NATIONAL BUREAU OF STANDARDS-1963-A

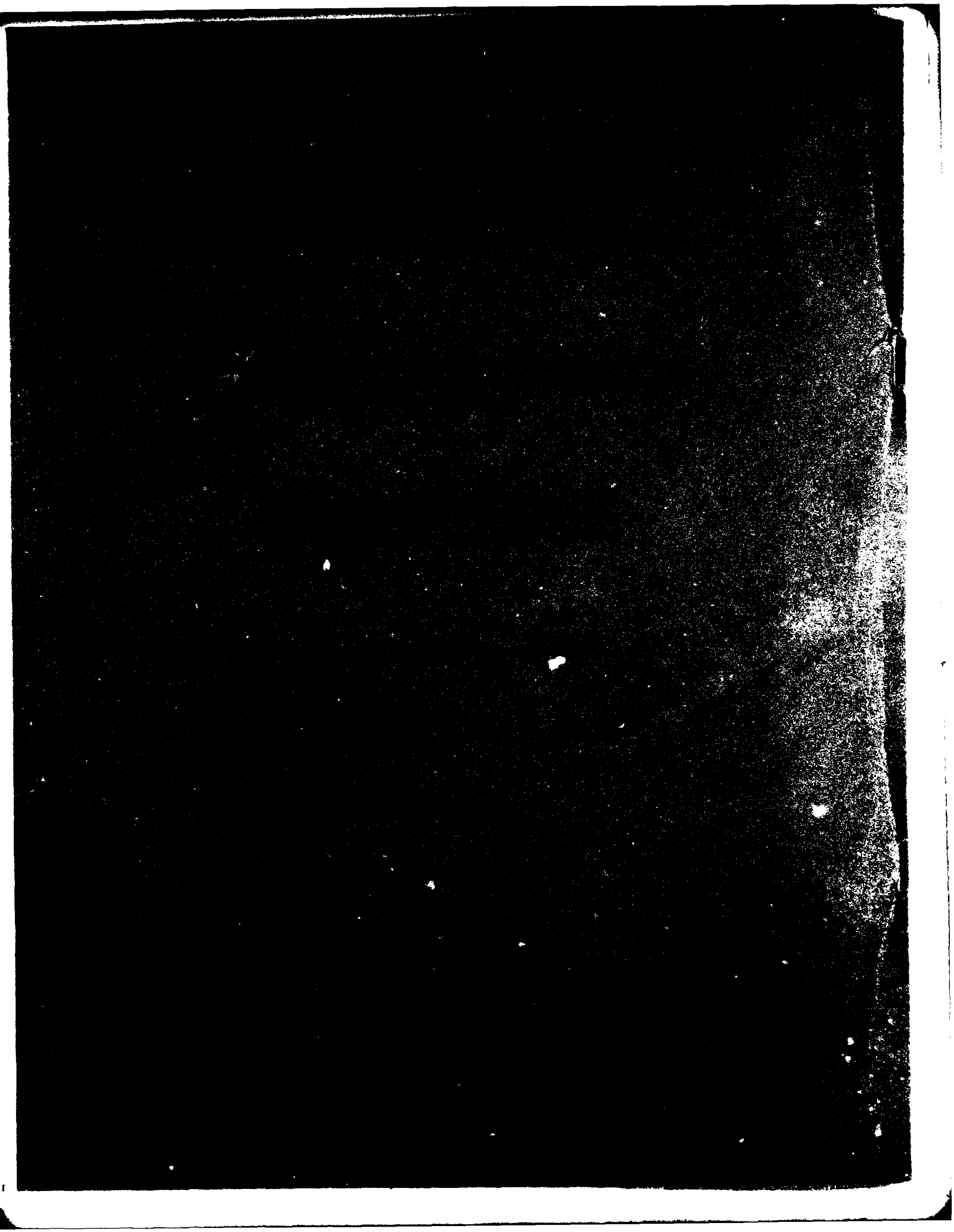

MASSACHUSETTS INSTITUTE OF TECHNOLOGY
LINCOLN LABORATORY

A HIGH PRESSURE MERCURY TURBINE CYCLE FOR USE IN SPACECRAFT AND TERRESTRIAL POWER PLANTS

R.M. LERNER
Group 68

TECHNICAL REPORT 577

22 MARCH 1983

LEXINGTON MASSACHUSETTS

ABSTRACT

A high pressure thermomechanical cycle using mercury as the working fluid can be made practical at close to theoretical thermodynamic efficiency between a hot shoe temperature of about 1200°K (3000 psia "boiler" pressure) and 600°K condenser. Means are proposed for utilizing a simple "Rankine" cycle without superheat, in which liquid droplets are vaporized by radiative heat transfer after being sprayed into the boiler chamber as a mist; and in which vapor wetness is controlled (by the addition of further hot mist if need be) prior to expansion in a nozzle; and in which, after expansion, the kinetic energy of both droplet and vapor phases is utilized in a turbine. Potential non-equilibrium flow phenomena and potential turbine blade erosion by wet fluid are controlled by utilizing a condensate droplet radius of the order of 1 μm during expansion and power extraction.

Rough calculations are made of boiler and radiator size and weight for use in orbit, at the 100/300 kW output power level for use as a replacement for a thermopile in a spaceborne reactor system, at the 30 kW output power level for use with a radioisotope thermal source or with a concentrating solar collector. Specific power for the 100/300 kW case ranges up to 100 W/lb. In all cases, the overall space plant thermodynamic efficiency is in the range 25% to 35%; in a terrestrial power plant a 40% practical efficiency is possible, ranging up to 55% if a conventional medium pressure steam plant is added as a bottoming cycle.

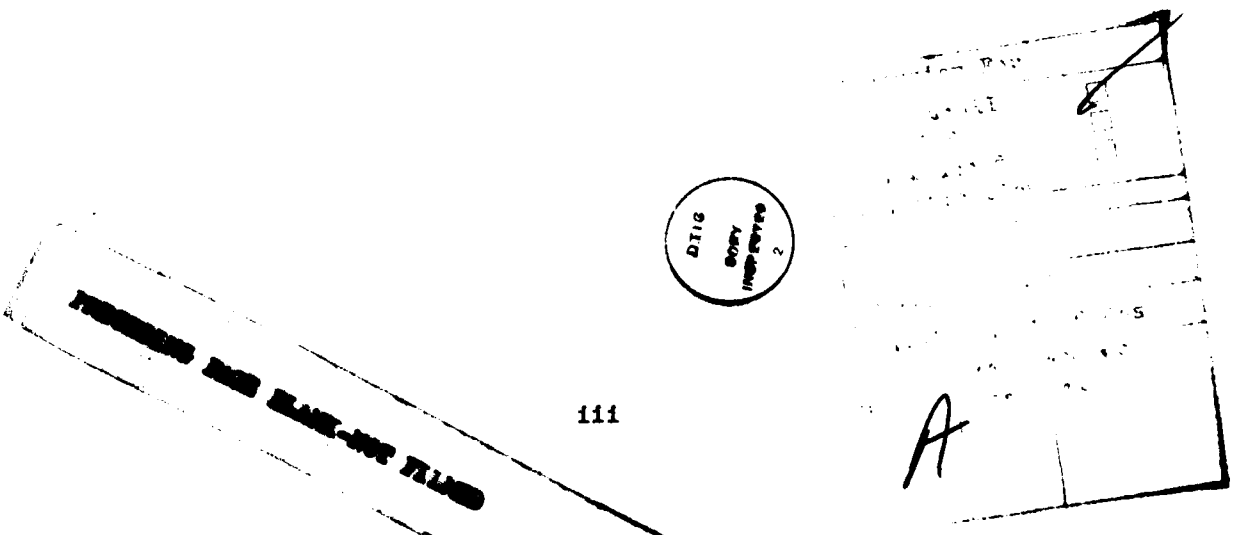

CONTENTS

PREFACE

There are dangers in writing a report as long as this one is. The first is that no one will read it; it is too long. The second danger is that someone will read it and still find it too long; sketchy where it should have given more detail, intuitive where it should have been precise, and tedious where it should have been succinct. The author therefore wishes to share with his potential readers his objectives in treating the subject matter as he has done.

First and foremost, the writer has sought an affirmative answer to a question that arose during the construction of Lincoln Experimental Satellites LES-8 and LES-9, which utilized radio-isotope power sources having a hot shoe temperature of about 1000°C (1300°K) and a radiator temperature at about 300°C (600°K). Is it possible to put a power plant into a synchronous-altitude satellite that will extract power from such nuclear sources with an efficiency which is comparable to theoretical thermodynamic efficiency? In particular, given the 5 kW of radioisotope thermal power available on LES-8 or on LES-9, could it be practical to obtain 1.5 kW of electrical power rather than the 300 W available from a thermopile?

This report does not give a clean answer to the question at the level of 5 kW input, 1.5 kW output, in part because this power level is not a good one for the particular types of rotating machinery considered. Some of the length of the report therefore comes from the detail of investigation necessary to establish how far down useful power levels can be pushed. The investigation does give a clear "yea" for outputs upwards of 30 kW (inputs upwards of 100 kW); and an enthusiastic affirmative answer for the use of high pressure mercury as a high temperature topping cycle in a central (earthbound) power plant. At the 100 kW thermal power input level, the source can be a solar concentrator; but at central station power levels the source is almost certain to be a nuclear reactor.

The suitability of the high pressure mercury turbine cycle to terrestrial power plants raises design issues with which the author cannot conveniently cope.

All engineering is done on the basis of experience and aesthetic rules-of-thumb which differ with the application; the practical aesthetics of satellite design are different in both objectives and scale from those of earthbound enterprises. The terrestrial power plant is physically and economically an end-in-itself, not tied to the design of the loads which are connected to it; the satellite power plant is a mere subsystem whose design and stability are intricately interrelated to the design of the loads to be served. Designs are weight-limited in orbit; dollar-limited on earth. Simple thruster nozzles and flywheels are familiar to the satellite engineer (who must keep track of every micropound-inch of unbalanced torque); multiply re-entrant boilers and expansion turbines are the bread and butter of the power plant engineer. What the author has done has been to mention the central-station level of technology in passing, but to concentrate on the simple nozzle and flywheel-turbine systems more likely to be familiar and acceptable to the satellite engineer.

A major technical innovation of this report is to directly expand wet mercury vapor in a nozzle and to use the resulting kinetic energy of the condensed phase, as well as the gas phase, to drive the turbine. In proposing to do this one must face much conventional wisdom that it cannot be done. The objections include difficulty in maintaining condensation equilibrium during expansion, problems arising out of potential supersonic velocities in the flow at nozzle exits and turbine blade inlets, sandblasting of turbine blades by condensate, and boiler wall corrosion by boiling liquid metal.

In each instance, the answer appears to lie in the use of droplets in the 1 μm size range, together with controlled blade and nozzle geometry. In the boiler, the large area-to-mass ratio of such droplets facilitates boiling by radiative heat transfer in a very dry "boiler" in which liquid does not have to touch the walls. In expansion, the same large area permits rapid exchange of heat between droplets and expanding gas. In striking surfaces at glancing angles, such droplets can be small enough so that thermal diffusion (in the wall struck) can dissipate the effects of such hot spots as may tend to form (by several mechanisms) at the points of contact.

In arguing for the plausibility of the scheme in the face of conventional wisdom, the writer has been propelled into a more detailed exploration of a wide variety of technical issues than he had intended to undertake. Simply because an author had to plow through much detail in order to convince himself about a technical issue is no excuse for inflicting the same level of detail upon his readers. Some of the tutorial material on thermodynamics, liberally scattered throughout the report, may be subject to this criticism. There have been some technical matters, however, in which the author has deliberately erred on the side of too much (he hopes) rather than too little exposition: where the literature is confusing (the thermodynamic properties of mercury); where the device is novel (the radiative heat transfer boiler); and where an otherwise old-hat technology is being used in an unexpected regime (supersonic flow through turbine blades when the blades can easily move with the speed of sound in the gas; and also flow in an expansion nozzle with change of state that is quasi-isentropic rather than quasi-isothermal). On other matters the author assumes the reader to be broadly familiar with the relevant technology and has sought to err on the side of terseness.

Most of the apparatus described in this report has not been built; most of the experiments suggested have not yet been done. To the extent that the author succeeds in motivating himself, his colleagues, or others to carry out appropriate experiments and to build equipment to put his suggestions to acid tests, he will deem his present work successful. To the extent that he merely stakes an intellectual claim for having had a useful idea that "was not obvious" and for pursuing it far enough in design to have "reduced it to practice," he will deem his present work a failure. Time will be the judge.

I. INTRODUCTION

In terms of weight per unit of power for the entire power plant, the internal combustion engine stands unrivalled at the top of the ladder. If for some reason the source of energy must be outside the engine, then unrivalled second place belongs to the Rankine cycle turbine expansion engine; the price is a boiler and a condenser for the working fluid, both of which can be cumbersome, but need not be so given the proper choice of working temperatures and working fluids.

The space environment is compatible with high temperature engines, both in terms of the ease of providing insulation in a vaccum environment and in terms of the difficulty in dumping excess heat by radiation at low temperature. Conveniently high temperatures can be reached in space and on the ground without combustion and without gas heat transfer by the use of solar concentrators and by the use of nuclear fuels. Indeed, one of the initial motivations for this study was to improve the conversion efficiency of radio-isotope powered spacecraft power supplies from the 7% class (typical of thermopiles) to the 45% class where it thermodynamically belongs, given hot shoe temperatures at 1300°K and radiator temperature of 600°K*.

To utilize high temperature up to 1000°C, whether on the scale of a satellite or the scale of a modern nuclear power plant, requires a better working fluid than water. The critical temperature of water is slightly under 375°C (slightly over 705°F). Thus a heat engine with water as working fluid cannot follow an ideal Rankine cycle to the temperatures used in modern power plants, around 600°C (1000°F), even if the engineering problems of a Rankine cycle without superheat are solved. It was recognized early in the 20th century, about 1910, by engineers at the General Electric Company that mercury was a nearly ideal working fluid at high temperature;

---

* Parameters typical of the power supplies used in experimental satellites LES-8 and LES-9, and others.

that with the mercury condenser acting as the heat source for a medium pressure conventional steam plant a high practical conversion efficiency of heat to power was available.[1]

Between the conception and the reduction to practice lay formidable problems in construction and metallurgy, but by the late 1930's at least one plant with 20 MW mercury-driven turbine capacity was in commercial use, by no means a tiny plant for its day. Indeed, it did have the highest operating efficiency of the plants then in service.

Though the metallurgical and operational problems of the mercury topping cycle were in time solved brilliantly, they were solved too late. It is pointless to speculate what might have happened if the answers had come in 1920 instead of 1940. By the 1940's steam technology had made tremendous strides. The commercial mercury turbine retired along with the generation of engineers and scientists who conceived it and made it work.

The scheme underwent a brief reincarnation in the early 1960's in the form of NASA's SNAP-8 35 kW_e (later revised to 90 kW_e) space reactor program [25]. There were the same problems of premature full scale design, boiler corrosion, and seals, followed by solutions after the program had ended, with history now telescoped into a few years instead of a few decades.

Just as surely as the brilliant idea of 1910 was past its time by 1940, so too the power plant technology of the 1940's and 1950's has begun to show inadequacies for the 1980's and beyond. The working efficiencies of steam plants has had to be cut back because the boiler tubes couldn't take the stress of the pressure and temperature required to reach towards 40% plant efficiency. The graft of a light-water conventional steam plant to a nuclear pile, once the hope of the future, has (literally) begun to spring embarrassing leaks. The resulting cutbacks of power plant efficiency and availability looms ever more serious as the cost of exploiting fossil fuels escalates, despite the fact that one of those fossil fuels, uranium oxide, is naturally a high temperature source around which an efficient plant might be built.

The mercury-working-fluid turbine system proposed here has little in common with the old General Electric system or with the SNAP-8 design. It is high pressure, and uses only a tenth of the weight of mercury per kW of capacity as did the old systems. Its "boiler" does not rely on heat transfer at wetted walls; its boiler "tubes" are nearly empty of liquid. It utilizes a simple single-pass Rankine cycle with little or no superheat, with condensed liquid droplets allowed to impinge on the turbine blades. It is conceived as a system that can operate at a few kW in a spacecraft, powered by a hot shoe at 1000°C with up to 45% efficiency without a "bottoming" cycle. It is also a system adaptable to use in main-station utility power plants with a bottoming cycle for overall efficiency near 60%.

Below, we explore the principle features of the system.

- A "boiler" that vaporizes liquid droplets at flux densities of tens to hundreds of kW per sq m by radiative heat transfer, permitting the small physical size required to withstand the high pressure (3000 psia) and temperature (1000°C).
- Full expansion in nozzles to permit single-pass extraction of mechanical energy, thus easing the need for close tolerances and high temperature - high pressure packings.
- Use of turbine blades that can withstand the sandblasting of liquid droplets in the expanded fluid stream and can extract useful power from them.
- Use of close-to-atmospheric pressure in the condenser, resulting in modest condenser size.

Since this report is the theoretical reduction-to-practice of a concept rather than a description of experimental results, there are a variety of nuts-and-bolts issues that are unresolved. For example, it has been necessary to assume a model for the thermodynamic properties of mercury in the useful temperature range, in particular the variation of latent heat of vaporization with temperature. We are also forced to speculate about the actual degree of condensation in expansion nozzles.

Barring unanticipated problems, and admitting the need for experimental measurement of some performance parameters, it would nevertheless appear that a turbo-electric system of the sort proposed here could be designed to operate in space using either concentrated sunlight or nuclear materials as the source of heat to produce power with efficiency around 30%, perhaps ranging up to 40%, to condenser temperatures similar to those which have been used in RTG* -equipped spacecraft.

In what follows, we review the thermodynamics of the Rankine cycle, present the required thermodynamic properties of mercury and their effect on cycle efficiency (Sections II & III); describe the manner in which radiation can be used to "boil" droplets in the 1000°K to 1300°K temperature range (Sections IV and V), investigate the flow in nozzles and on turbine blades taking into account a variety of non-equilibrium effects Sections VI-IX; and estimate the order of magnitude of a variety of losses in a practical system configuration (Sections X and XI); and estimate the dimensions and weight for three possible satellite borne systems with input power levels ranging from 5 kW to 1 MW (Section XII). At the high power end of the scale, 100 W/lb may be practical for the entire power system.

The overall tenor of this report is engineering science, i.e., components rather than systems. The discussion of results in Section XIII, however, takes a system point of view. It is suggested there that components be designed for demonstration with a solar concentrator power source at the thermal level of 30 to 50 kW input to a high pressure mercury boiler (the midrange power level of the three discussed in Section XII). Such a demonstration would be of a scale and type of show the plausibility of the high pressure mercury cycle for uses both on satellites and in terrestrial power plants.

This introduction closes with a compilation of individual chapter summaries.

---

*Radio-isotope Thermoelectric Generator

CHAPTER SUMMARIES

Chapter II: THE RANKINE CYCLE USING MERCURY

Ideal Carnot and Rankine cycles are reviewed as they relate to temperature T, pressure P, molar volume V, molar entropy S, molar enthalpy H, heat exchanged Q, and external work W. The working ranges of mercury and water as thermodynamic working fluids are compared; mercury is superior for high temperature engines, having a ratio of critical temperature to 1 atm condensing temperature of almost 2.5 to 1.

Chapter III: THERMODYNAMIC PROPERTIES OF MERCURY

Experimental Data obtained in England, Germany, and Russia during the 1960's and 1970's is used with various thermodynamic equations to obtain "steam tables" for mercury over the temperature range between 300°K and 1600°K, with errors of at most a few percent in the range of interest between 500°K and 1300°K. Use is made of what may be an original discovery with respect to the principle of corresponding states, in the form of a "universal" for the heat of vaporization as a function of temperature.

Chapter IV: MERCURY BOILER (First Part)

The wetting and corrosion problems normally associated with the use of mercury boilers are avoided by spraying droplets into the "boiler" tube and by relying on radiative heat transfer between the tube wall and the resulting droplet mist. Published experimental data for the electrical conductivity of mercury is used with both approximate and exact equations for the electromagnetic reflectivity to establish the insensitivity of such heat transfer to droplet size, over a temperature range of 600°K to 1400°K and for droplet radii down to a few tenths of a micrometer. Radiative transfer theory is then used to establish conditions under which the mist exhibits diffuse absorption in the range 75% to 100% for source temperatures between 1000°K and 1400°K. Heat transfer is at the rate of 50 to 150 KW/m^2 with the boiler walls roughly 150° hotter than the boiling liquid.

CHAPTER V: MERCURY BOILER (Second Part)

A radiative heat transfer boiler has very low thermal mass. The working fluid cannot be relied on as a coolant, so that alternate means must be found for rerouting source heat not demanded by the eventual mechanical load. When the boiler is at the focus of a solar concentrator, the optical absorption of the mist can be used to switch the absorption of sunlight. In general, other cooling is required, which may take the form of a secondary low-pressure boiler and heat-pipe condenser system.

CHAPTER VI: ENERGY CONVERSION — STATIC EXTRACTION

The relationship between the enthalpy H of a working fluid and the work done in adiabatic processes is reviewed. The enthalpy-entropy (H-S) diagram for mercury is used to obtain the efficiency of ideal and modified Rankin cycles, permitting expanding vapor to become wet as in a piston expansion engine. The efficiency of a practical mercury Rankine cycle working between 1200°K and 600°K is found to be more than 90% of the ideal Carnot efficiency.

CHAPTER VII: KINETIC ENERGY EXTRACTION — DYNAMIC EQUILIBRIUM

An introductory analysis is made of the impulse turbine, in which expansion takes place in a stationary nozzle and in which the turbine reacts to the kinetic energy of the resulting flow. Ideal and non-ideal paths for the expansion are traced on the H-S diagram and on the P-V diagram. An equilibrium expansion from 1200° and 220 bar to 600° and 0.6 bar results in a 1 to 150 volume expansion.

CHAPTER VIII: KINETIC ENERGY EXTRACTION — SUPERSONIC FLOW

The speed of sound in Mercury vapor is calculated as a function of thermodynamic state variables. To avoid supersonic speed in the nozzle exits in a 1200°K to 600°K expansion, as many as a dozen successive stages of expansion might be needed. However, mercury is so dense that the speed of sound (150 to 250 m/s) is comparable with convenient peripheral speed for a turbine rotor. It is found that fully expanded flow at Mach 2.8 (M* 1.7) can be turned through

180° with only modest losses during startup. It is found that a single-pass extraction flow at Mach 1.4 (M* 1.26) can be shocked down to a subsonic flow through the blades and be re-expanded at the blade exits with only a few percent loss due to irreversibility. The equilibrium flow of mercury through the throat of a supersonic nozzle is considered both by analysis and by numerical integration of the thermodynamic properties of mercury vapor, with results presented as curves of flow vs nozzle area.

CHAPTER IX: NON-EQUILIBRIUM FLOW PHENOMENA

Droplets can exchange energy with the surrounding vapor only by friction or by thermal conduction, both of which are processes that introduce significant time lags. Droplets in wet mercury steam travel several thousand diameters beyond a velocity discontinuity or change of direction in the vapor flow. Droplets of sufficient size will not follow flow streamlines through the turbine blades, but will strike them, with impact conditions not unlike buck-shot striking armor plate. Analysis of impact forces and potential causes of temperature rise at contact (including so-called "cavitation") indicates advantages of micron to submicron droplet size and glancing angles of incidence on impact. Unless the total droplet area is large enough, there is not sufficient time for the mercury vapor to condense as it expands through the nozzle, returning the heat of condensation by thermal conduction to the vapor to permit it to do work. Even with the deliberate introduction of enough droplet nuclei to condense the vapor into droplets of only a micrometer radius, 100°K temperature differential between the droplets and the expanding vapor may be needed to drive the heat transfer. A substantial reducton of the heat transfer design constraint can be effected by deliberately introducing wet steam into the expansion nozzle. A variety of configurations for the entire cycle are considered in order to be able to satisfy separately droplet size requirements for proper operation of the boiler and of the expansion nozzles.

CHAPTER X: NOZZLE DESIGN AND NOZZLE LOSS

The three constraints on nozzle design are the power at the nozzle throat, the permitted friction, and the temperature disequilibrium permitted between

droplet mist and expanding vapor; each may be improved at the expense of the others. Graphical analysis is made of several nozzle designs having a constant temperature difference between mist and vapor. For 30 kW to 40 kW power flow through the throat, a nozzle operating on vapor 50% wet has 1/3 the length and 1/3 the friction losses of one whose inlet vapor is dry. A nozzle for the 100 to 300 kW power range has a 5 mm throat, a length of about a meter, and total losses of about 10%. A nozzle for 2 kW would have a 0.5 mm throat, a 5 cm length, and losses over 35%.

CHAPTER XI: OVERALL PERFORMANCE

A variety of losses in a practical mercury cycle are identified: pipe and turbine blade friction; windage and bearing friction; losses due to non-equilibrium heat transfer in boiler, nozzles, and condenser; feedpump and atomizer losses; and other miscellaneous losses. Sums of conservative estimates of such losses run from 30% at the 100 kW level up to 40% at the 10 kW output level. In a careful integrated design, overall losses may be lower, ranging from 10% at the central station scale up to 20% at the 30 kW satellite power plant scale. Overall efficiency from a hot shoe at 1100°C to a condenser at 300°C for a 30 kW satellite power supply is estimated to be 35% of the thermal input; using a bottoming cycle, central power plant efficiency is estimated to be 55% of thermal input.

CHAPTER XII: FEASIBILITY OF LIGHT WEIGHT POWER SUPPLY

Total weight and pounds-per-Watt for a variety of source and power conversion technologies are compared. Detailed estimates of weight and performance are made for boiler, waste heat radiator, turbine, and alternator. A possible application to RTG heat sources at the 10W/lb, 1 to 3 kW output level is suggested, using a reaction turbine. It is speculated that a LASL proposal for a 1 MW reactor in space can be scaled down in weight and power level with 100 kW of output at 100 W/lb. A developmental program to obtain 30 kW output for satellite use from a 10-meter diameter focussed solar collector is suggested, also sized for 100 W/lb (without storage for shadow).

CHAPTER XIII: DISCUSSION OF RESULTS

The devices and techniques orientation of this report is contrasted with the system engineering approach needed to assemble and integrate an actual system exploiting the technology. The techniques which have been introduced avoid the major system problems of the old low-pressure mercury system and the SNAP-8 program, at a cost of introducing new technology. It is urged that laboratory level testing of all system components exercise those components well beyond their intended stress levels to avoid limited-lifetime surprises at the pilot plant or full system level of application.

PART 1

THERMODYNAMIC BACKGROUND

Chapter Summaries

Chapter II
THE RANKINE CYCLE USING MERCURY

Ideal Carnot and Rankine cycles are reviewed as they relate to temperature T, pressure P, molar volume V, molar entropy S, molar enthalpy H, heat exchanged Q, and external work W. The working range of mercury and water as thermodynamic working fluids are compared; mercury is superior for high temperature engines, having a ratio of critical temperature to 1 atm condensing temperature of almost 2.5 to 1.

Chapter III
THERMODYNAMIC PROPERTIES OF MERCURY

Experimental Data obtained in England, Germany, and Russia during the 1960's and 1970's is used with various thermodynamic equations to obtain "steam tables" for mercury over the temperature range between 300°K and 1600°K, with errors of at most a few percent in the range of interest between 500°K and 1300°K. Use is made of what may be an original discovery with respect to the principle of corresponding states, in the form of a "universal" rule for the heat of vaporization as a function of temperature.

II. THE RANKINE CYCLE USING MERCURY

Absolute temperature, T, is defined on the basis of the equation of state of an ideal gas

$$PV = RT \qquad \text{(II-1)}$$

P being pressure, V the volume of one mole (6×10^{23} molecules) of gas, and R a universal gas constant which is directly proportional to Boltzmann's constant, K:

$$R = 6 \times 10^{23} K \quad . \qquad \text{(II-2)}$$

If pressure is measured in bars* and molar volume in cc, then R is 83.144 Joule/mol.

It is extremely difficult to build a high power density engine which reversibly (i.e., efficiently) exchanges heat with the surroundings during expansion or compression, while also executing an efficient exchange of real mechanical work with the external world. Consequently, modern heat-expansion engines are designed to exchange real mechanical work with the surroundings with little or no exchange of heat Q. For such processes, an important thermodynamic property of the working fluid is the entropy S, defined for reversible processes by

$$dS = \frac{dQ_{rev}}{T} \quad . \qquad \text{(II-3)}$$

An ideal expansion process that is both reversible and exchanges no heat with the surroundings is called isentropic (one which generally exchanges no heat but may not be reversible is called adiabatic). The equation of state for an ideal gas undergoing isentropic expansion or compression is

$$PV^{\gamma} = \text{const} \qquad \text{(II-4)}$$

γ being the ratio of specific heats at constant pressure and at constant volume.

If the specific heats are measured on a molar basis (as they almost always are in physics) then for an ideal gas

*One bar is 10^6 dyne/cm. One standard atmosphere is 1.01325 bar.

$$C_p = C_v + R \quad . \tag{II-5}$$

Moreover, C_v per molecule is $\frac{1}{2}DK$, where D is the number of classical degrees of freedom per molecule. On a molar bassis this fact becomes

$$C_v = DR/2 \quad . \tag{II-6}$$

For monatomic gases like mercury and argon, D is 3, for three translational degrees of freedom. One deduces from Eqs. (II-5) and (II-6) that for these gases γ is 5/3. For polyatomic gases, one must add two rotational degrees of freedom for the molecule as a whole, giving γ of 1.4. In general, for temperatures under 1000°C, quantum mechanical considerations prevent other degrees of freedom within the molecule from storing much random energy. But as temperature rises, or at sufficiently high density, there is a tendency to thermally excite these vibrational and rotational modes, with the consequence that γ of a polyatomic gas tends to decrease as temperature rises.

An "ideal" heat engine cycle using isentropic expansion was invented by Carnot in the mid-nineteenth century to bound the potential efficiency available from heat engines working between two given temperatures. The cycle is shown in Fig. 1(a) on a P-V diagram, and in Fig. 1(b) on a T-S diagram of the working fluid.

Work on a P-V diagram is given at constant pressure by $\Delta W = P\Delta V$, while reversible heat exchange at constant temperature on a T-S diagram is given by $\Delta Q = T\Delta S$. Because the First Law of Thermodynamics states that the work extracted cannot exceed the heat consumed by the engine, Carnot argued that the efficiency of his reversible cycle is η

$$\eta = (T_1 - T_2)/T_1 \quad . \tag{II-7}$$

He then showed by the Second Law that no engine could be more efficient.

The Carnot engine working with an ideal gas is not a practical device. In Fig. 1(a) (which has been drawn to log scales to make the curves segments of straight lines) no part of the cycle is at constant volume or at constant pressure. It follows that mechanical work must be exchanged with the

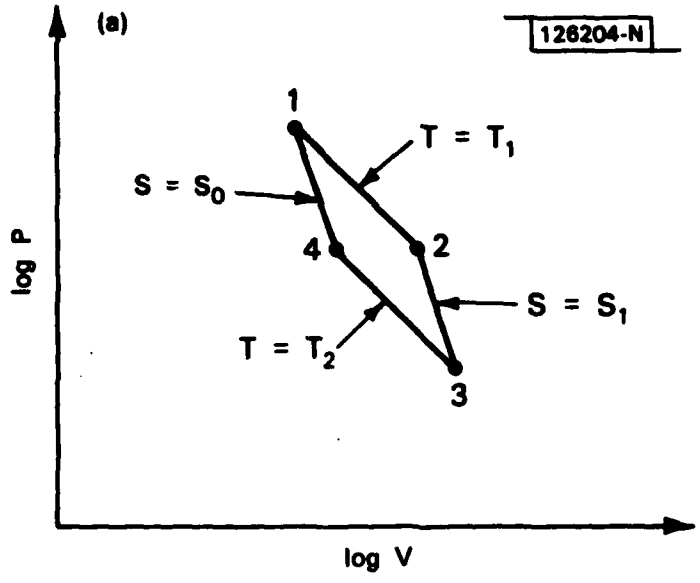

Fig. 1(a) Carnot cycle on P-V diagram.

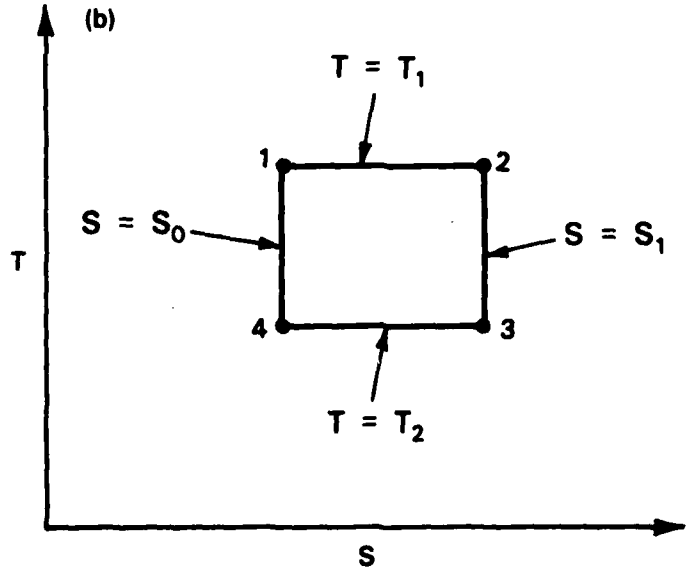

Fig. 1(b) Carnot cycle on T-S diagram.

surroundings on all four branches of the cycle, whether the fluid flows through the cycle or is carried through the cycle in a single container.

The simple Rankine cycle shown in Fig. 2 is close to being a Carnot cycle, but obviates many of the difficulties by utilizing change-of-state from liquid to gas to accomplish the constant-temperature addition or discard of heat. Change of phase from liquid (in some cases, solid) to gas provides an exception to the difficulty of doing work and exchanging heat simultaneously, because in such cases heat is exchanged by mass transfer rather than by conduction or convection. Thus vaporization and condensation takes place at constant pressure as well as taking place (ideally) at constant temperature. As a consequence, in a flowing-fluid heat engine cycle no net external mechanical work is required in the heat exchangers (other than that required to overcome incidental frictional losses in flow).

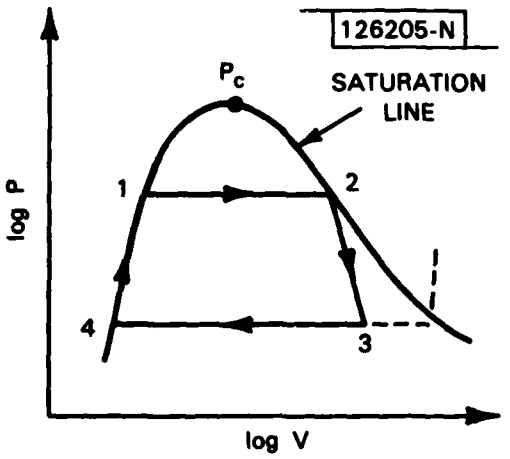

Fig. 2 Simple rankine cycle in P-V plane.

The Carnot and Rankine cycles also differ in that in the Rankine the compression (from 1 to 4 on the cycle diagrams), required before adding heat, is performed on a nearly incompressible liquid, so that comparatively little work is expended in that part of the cycle.

The natural diagram on which to plot the Rankine cycle is the enthalpy-entropy diagram. Enthalpy H has the dimensions of energy and is the natural thermodynamic potential for a flow process because it is independent of the extent to which the actual energy of the fluid is distributed between potential energy, kinetic energy, and internal (static) energy

$$H = U + PV \quad . \tag{II-8}$$

Here U is the sum of all of the energy that must be supplied to bring a mole of the gas from a standard initial state to its present condition. The PV term takes account of the fact that in a flowing-fluid system the work done on the fluid as it leaves a given volume is exactly counterbalanced by the work supplied to the fluid which enters that volume.

For a flow process at <u>*constant pressure*</u>, a change in enthalpy is equal to the heat exchanged

$$\Delta H_p = \int C_p \, dT = \Delta q \quad . \tag{II-9}$$

For an <u>adiabatic</u> flow process, the work done is also equal to the change in enthalpy. These relationships are true whether or not the process is reversible. Thus boiling can take place at a surface much hotter than the equilibrium temperature at the boiler pressure without changing the latent heat of boiling ΔH_{lg}. Thus also, flow through a porous plug or throttling valve, which is entirely irreversible, takes place with ΔH equal to zero because neither work nor heat is exchanged with the surroundings.

The advantage of the entropy-enthalpy diagram is that the heat supplied and the work done can be scaled directly from the diagram as enthalpy changes. Such diagrams, with added lines to show topology at constant pressure, temperature, and volume (and fraction in gas phase in the two-phase region) are called "Mollier Charts" in steam engineering practice.

The Rankine cycle is shown on the P-V diagrams in Fig. 2, and on the H-S diagram in Fig. 3. The branch of the cycle from 4 to 1 is not quite isentropic. In practice, one first brings the working fluid as a liquid up to the working pressure of the boiler. Then one heats it up, still as a liquid, to boiler temperature. To do so requires sensible heat and a change in entropy ΔS:

$$\Delta S = \int_{P_4}^{P_1} \frac{PdV}{T} + \int_{T_4}^{T_1} \frac{C_{pl}dT}{T} \quad . \qquad \text{(II-10)}$$

The process is not wholly reversible in that heat is supplied at T_1 and absorbed at $T < T_1$ as the liquid is heating up. As a result, this ΔS is slightly larger than the ΔS for reversible heating.

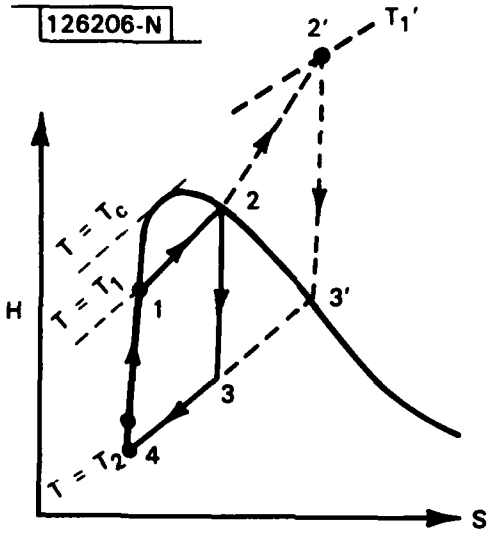

Fig. 3 Rankine cycle on H-S diagram.

The key fact is that this change ΔS is modest compared with the entropy of vaporization between 1 and 2. Thus, whatever part of it is due to irreversibility should not have a large effect on the overall efficiency of the cycle. The fact that the latent heat is large compared with the sensible heat is a substantial practical advantage of the Rankine cycle; it results in much more energy exchange and external work per cycle than would be available from the same working fluid used between the same two temperatures as an ideal gas.

The simple Rankine cycle would be efficient as well as practical in old piston-type stationary steam engines if the working parts were thermally insulating and thus consumed no heat as they alternately warm and cool during the cycle. Turbines are the practical alternatives, in which thermal energy is converted to kinetic energy in expansion nozzles and then extracted by change-of-vector-velocity as the fluid passes through the turbine blades. However, the isentropic expansion from 2 to 3 produces a two-phase fluid which is part vapor, part droplet mist*. In the moving gas stream of an expansion nozzle, a significant fraction of the kinetic energy will be carried by these droplets. But if they are allowed to strike the working parts of the turbine blades, they exert high local pressures and erode the blades by sandblasting. Some turbines are indeed designed to work with slightly "wet" (i.e., partially condensed to droplets) steam. But the droplets are simply separated from the dry steam by centrifugal action; they and the energy they carry are discarded.

Thus, most Rankine turbine cycles are modified to "superheat" the steam from 2 to 2', so when it does pass through the expansion engine, it comes out "dry" at 3' (see Fig. 3).

With water as the working fluid, this scheme has the advantage of permitting upper working temperatures T_1' which may be higher than the critical temperature T_c (see below). At the same time, however, there are

*If the droplet mist does not form, the heat of condensation cannot be extracted.

complications in the use of superheat. The heat transfer in superheat from 2 to 2' is not boiling transfer; it therefore requires greater heat exchanger area than would be the case if temperature T_1' were directly accessible from change-of-state. The average condition of the fluid moves toward ideal gas conditions, with the result that the greater volumes of gas must be handled by the condenser, and intermediate expansion and reheat devices, than would be the case with the simple Rankine cycle (Fig. 2) operating (with a different working fluid) between the same temperature limits. Finally the latent heat of evaporation is not directly recoverable as mechanical work in a superheat cycle (although some of it is recovered in practice by bleeding off partially expanded steam and using it to reheat more fully expanded steam in reheat-heat exchangers).

It is in avoiding the need to superheat in order to reach high theoretical efficiency in a simple Rankine cycle that mercury is superior to water. All fluids have a critical temperature above which the distinction between liquid and gas vanishes. As that temperature, T_c, is approached from below, there is a temperature, T_{max}, roughly 90% of T_c on an absolute scale, above which the heat of vaporization, and the volume difference between liquid and gas, drop precipitously. On the other hand, below the normal (1 atm pressure) boiling point the specific volume of the working fluid increases enormously, requiring corresponding large heat exchangers for condensing the vapor along the branch (3')-3-4 of the cycles in Figs. 2 and 3. Thus, this boiling point T_o tends to define a lower bound to the working temperature range.

Comparing water and mercury on the basis of 1 atmosphere pressure at the condenser leads to the following:

	Water	Mercury
Critical Temperature T_c	647°K	1760°K
Max useful boiling point T_{max}	580°K	1580°K
1 atm condenser Temp T_o	373°K	630°K
Freezing Point T_f	273°K	233°K
Carnot efficiency between T_{max} and T_o	36 %	62 %
Molar latent heat at T_o	40 kJ	50 kJ
Molar latent heat at T_{max}	20 kJ	25 kJ

Most fluids are like water, in that the temperature of boiling at one atmosphere is more than half of critical temperature. Thus mercury tends to occupy a unique position as a fluid that does not have to be expanded to very large specific volumes to achieve high efficiency in a Rankine cycle (provided the temperatures are available). Another limit on the use of a fluid in a Rankine cycle, even if we assume arbitrary specific volume as being possible, is the freezing point. Again, most fluids are like water in having a freezing point close (on the thermodynamic scale) to the boiling point, whereas the freezing point of mercury is roughly a seventh of T_{max}, roughly an eighth of T_c, and just over a third of T_o.

III. THERMODYNAMIC PROPERTIES OF MERCURY

In order to design a thermodynamic cycle using mercury as a working fluid, it is necessary to have a tabulation of the actual densities, pressures, and heats at various temperatures throughout the cycle, across the two-phase region. When two phases are present, the removal of heat increases the fraction x which is in the liquid phase. This fraction is called the "wetness".* If evaporation or condensation takes place under conditions of constant pressure, the equilibrium temperature also remains constant until the boundaries x = 0 or x = 1 of the region are reached.

In spite of a long history as a key liquid in Physics, and in spite of the early engineering interest in using (modest pressure) mercury vapor in power turbines, the thermodynamic properties of mercury at high pressure and temperature were not thoroughly investigated until the mid 1960's, for the purpose of establishing the nature of the metal-to-nonmetal transition which occurs for densities greater than about 9 gr/cm^3 (the "gas" above the critical point is a metallic conductor at sufficient density!)[2-5]. Even the temperature T_c and pressure P_c at the critical point are not precisely known ($\pm$10°K, $\pm$20 atm). We shall use T_c = 1760°K, P_c = 1500 atm (1520 bar)[3].

Because it is not easy to measure, the critical density ρ_c is still not well-established. Modern values range from 4.2 to 5.7 gr/cm^3 [3,4].

There appear to be only four primary sources of modern experimental data of the kind required to establish the thermodynamic properties on, and between, the liquid and vapor saturation lines.

(a) Constant pressure specific heat data, C_p, up to the normal boiling point[7].

(b) English pressure, volume, and temperature (PVT) data up to about 1000°C[2].

(c) Russian PVT data near the critical point[4].

---

*The symbol x is also used in the literature for "quality", which is 1-x as defined here.

(d) German data on the liquid density along the saturation line[3] and PVT near the critical point.

Because the working range of temperature and pressure for a mercury turbine cycle is too high for the old data, and tangential to the purposes of the modern data, we have been forced to compile our own model of the thermodynamic properties of saturated and wet mercury, striving only for accuracy sufficient to make reasonable predictions of the thermodynamic efficiency of a simple Rankine cycle.

The end result is a series of Charts and Tables appearing at the end of this Section and in subsequent Sections. They are used to discuss the flow of the fluid and to estimate the performance of engines. The reader not interested in the problems of constructing the underlying model may wish to skip to the end of this Section, circa Eq. (III-15).

In principle, all that is required to make the tables is a tabulation of specific heat (of any kind) over a path that spans the working range of temperature, together with sufficient P-V-T data [see Appendix A].

Up to the boiling point of mercury at 1 atm, the constant-pressure specific heat is well-measured, the heat of vaporization at room temperature has been measured, the PVT data of the vapor has been tabulated. The dry vapor is so thin as to constitute a nearly ideal gas obeying the equation of state $PV = RT$. For this region, almost any procedure that relies on real data* will give the same results. The entropy S and heat content H can thus be calculated for wetness x from

$$dH = C_p dT\big|_{liq} + VdP\big|_{liq} + d(1 - x)L \qquad \text{(III-1)}$$

$$TdS = C_p dT\big|_{liq} + d(1 - x)L \qquad \text{(III-2)}$$

where L is the heat of vaporization.

* Rather than differentiation and extrapolation of data models.

For our working range, between about 500 K and 1500°K, we use a more circuitous route because neither the specific heats nor the latent heat of boiling have actually been measured over the range. We proceed as follows:

(a) Model the available density data for saturated liquid with a simple formula.

(b) Model the pressure data of the wet vapor with a simple activation energy law.

(c) Assume a simple law for the temperature dependence of the constant volume specific heat C_v of the liquid, confirmed by data and by the correctness of the low temperature C_p deduced from C_v.

(d) Use experimental data to establish a simple approximation for the constant-volume pressure change $\partial P/\partial T$ along the liquid saturation line.

(e) Use the law of corresponding states to obtain a plausible law for the temperature dependence of the latent heat of vaporization L.

(f) Use the Clausius-Clapeyron equation to deduce the change in volume upon vaporization from L (rather than vice versa) and compare the result with the experimental data of Kikoin and Senchenkov[4].

(g) Compute the low-temperature difference between the resulting PVT data and the ideal gas law along the vapor saturation line to establish a so-called virial coefficient to be used in computing the H and S of the dry gas.

With the types of data worked out above, the thermodynamic equations for S and H become

$$dH = C_v dT\Big|_{liq} + T\frac{\partial P}{\partial T}\Big|_{liq} dV + VdP + d(1 - x)L \qquad \text{(III-3)}$$

$$TdS = C_v dT\Big|_{liq} + T\frac{\partial P}{\partial T}\Big|_{liq} dV + d(1 - x)L \quad . \qquad \text{(III-4)}$$

In these (and other) thermodynamic equations, a partial derivative represents the effect of holding a specific variable (in this case, volume V) fixed, while the total differentials represent the actual (experimental) path of integration. Thus for a boiling liquid dV and dT are related by the experimental density along the boiling line but $\partial P/\partial T$ is not related to the boiling temperature vs. pressure curve (except at the critical point) because $\partial P/\partial T$ requires that the liquid volume be held fixed.

A first step in the program outlined above is to fit available saturated-liquid density data of Postill et al[2], the data from the German literature[3] and that of Kikoin & Senchenkov[4] to formulae of the form

$$\rho_{sat} = \rho_1 + \rho_2 (1 - T/T_c)^m \quad . \tag{III-5}$$

In his classic paper on the Principle of Corresponding states, Guggenheim[11] introduced a slightly more complex formula with m = 1/3:

$$\rho_{sat} = \rho_1 + \rho_2 (1 - T/T_c)^{1/3} + \rho_3 (1 - T/T_c) \quad . \tag{III-5a}$$

There exists a critical review of density data in a doctoral dissertation by Schmutzler (see footnote 12 of El Hanany and Warren[3]) which has apparently passed privately among cognescenti but is apparently unavailable in the open letterpress literature. From occasional data points and curves published by the various authors involved with the German data, one can reconstruct this density curve along the liquid saturation line, x = 1, given in Fig. 4. To within the plotting accuracy of the data used in arriving at Fig. 4, this curve can be represented by a formula like Eq. (III-5) above 500°C with

$$\begin{aligned} \rho_1 &= 5.439 \\ \rho_2 &= 8.319 \\ m &= 0.315 \quad . \end{aligned} \tag{III-5b}$$

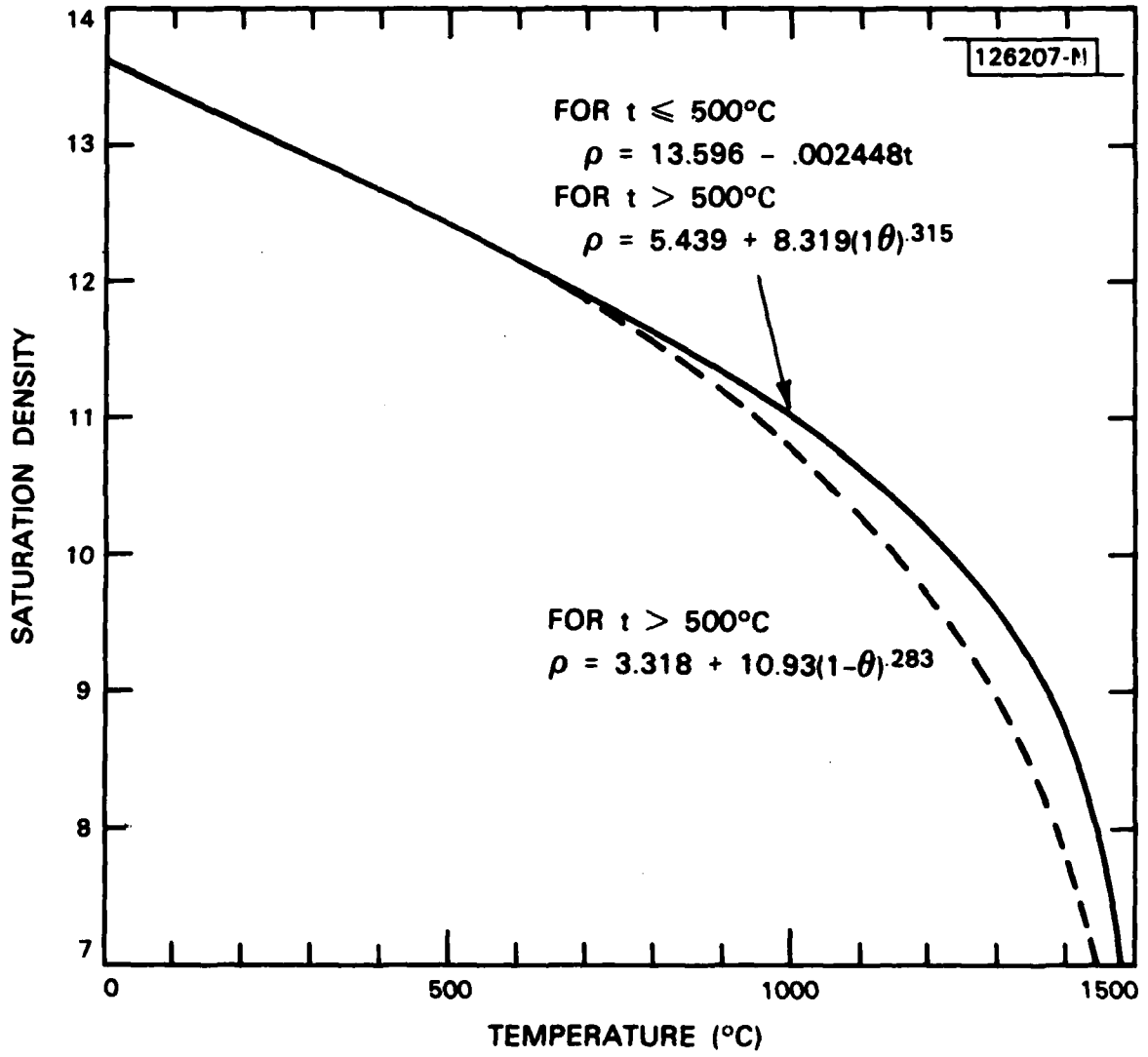

Fig. 4. Density of mercury reconstructed from various papers using Hensel-Frank-Smutzler model.

because this value of m is close to 1/3, the German data can be fitted to a Guggenheim relation, Eq. (III-ta) with *

$$\rho_1 = 3.3571$$
$$\rho_2 = 8.2702 \qquad \text{(III-5c)}$$
$$\rho_3 = -0.1737$$

Over the entire range between 500°C and the critical point, the difference between these two formulations is an order of magnitude less than the accuracy of the fit (and of the experimental data). Below 500°C, a simple linear extrapolation from 0°C past the known density at the 1 atm boiling point suffices for specific heat calculations.

While the presumptive recovery of the German model just described is consistent with the English data[2] (taken in the range up to 1050°C), it is only barely consistent to within experimental accuracies with the only collection of detailed P-V-T data, that of Kikoin and Senchenkov[4]. A saturation density curve from the latter data is plotted also in Fig. 4. It conforms (above 500°C) to Eq. (III-5) with the coefficients

$$\rho_1 = 3.14$$
$$\rho_2 = 10.93 \qquad \text{(III-5d)}$$
$$m = 0.283$$

Generally, to be able to compare our results with the published data of KiKoin and Senchenkov we have used the latter coefficients.

For present purposes there are four observations to be made about the two density curves in Fig. 4 and the formulas that fit them.

First. A wide range in the coefficients used in Eqs. (III-5) and (III-5a) result in curves that are actually quite close together. This suggests substantial flexibility in the selection of coefficients. For example, the

---

* The second set of data is derived from the first by setting the density and first two temperature derivatives in Eqs. (III-5) and (III-5a) equal at 1273°K. The number of significant figures in these formulas is not warranted by the data from which they were derived.

data (III-5d) can be also represented by the data:

$$\begin{aligned} \rho_1 &= 5.00 \\ \rho_2 &= 9.215 \\ m &= 0.371 \end{aligned} \qquad \text{(III-5e)}$$

with no observable difference over the range of temperature 700°K to 1600°K. The Hensel-Frank-Schmutzler curves appears to have been adjusted so as to yield Postill et al's value for the critical density, viz, 5.3 gr/cm^3. Our coefficients for Eq. (III-5) were obtained by matching formula and data at three points: 600°C, 1000°C, and 1400°C (873 K, 1273 K, and 1673 K, respectively).

Second. The divergence of the curves is comparable to the experimental uncertainties in the experiments on which they are based. This divergence is generally less than 1% up to 1000°C (1270°K), and generally less than 5% to within 100° of critical temperature.

Third. The density laws assumed in Eq. (III-5) and (III-5a) appear to be of the sort demanded by Nature over the entire range from room temperature to near T_c. The fit is easily improved by one or two orders of magnitude with simple corrections*. The price of not having sure density data is a corresponding uncertainty in the specific heat of the liquid and in the dependent computations of H and S. The following is a comparison of the calculations:

	English & German Data		English & Russian Data	
Temp (Deg K)	H (cal/mol)	S (cal/mol deg)	H (cal/mol)	S (cal/mol deg)
600	2120	5.09	2100	5.06
800	3404	6.94	3390	6.91
1000	4690	8.37	4740	8.40
1200	6035	9.56	6190	9.69
1400	7478	10.62	7795	10.88

*In computations, we have broken the whole range into two pieces, one below 500°C (773°K), and the remainder of the range, using a linear fit in the former and the power law fit in the latter.

Fourth. The range in which the density data is badly uncertain lies outside the present practical range of interest. Our interests in temperatures beyond 1300°K (1000°C) are severely constrained by the high working pressures that must be sustained, roughly 350 atm at 1300°K (rising to 550 atm at 1400°K). Indeed, our practical interest probably ends at 200 atm, where the difference between the density curves is of the order of 2%.

The second step is to fit the vapor boiling pressure data to an activation energy equation of the form

$$P = P_o \exp(-T^*/T) \qquad \text{(III-6)}$$

The International Critical Tables (ICT)[6] give $T^* = 7060°K$ for pressures above 1 atm. This value has been widely copied in the handbooks (especially when allowances are made for the inevitable misprints). The modern data between 1 atm boiling point and critical point suggest $T^* = 7172°K$.

Between 400°K and 800°K the Liquid Metals Handbook[12] gives

$$P = P_o \exp(-T^*/T - m\ln T) \qquad \text{(III-6a)}$$

as being accurate to within 2% of experimental data with $T^*=7617$ and $m=0.8$. Between the normal boiling point and the critical point, a similar equation which has the correct end points has $T^*=7454$ and $m=0.273$. For power extraction calculations, we have used either Eq. (III-6a) with the former data, or Eq. (III-6) with $T^*=7172$.

The third step is to calculate the specific heat of the liquid. Of all the paths for the measurement of specific heat, that taken at constant volume leads to the least variation over a wide range of conditions. This is so because only the internal energy of the substance is involved, whereas all other specific heats include work done against internal forces as the material changes dimensions. For an ideal monatomic gas, the molar C_v is simply 3R/2. For a simple solid, this doubles to 3R. A liquid C_v is

intermediate, tending to 3R at lower temperatures and 3R/2 at higher temperatures. For monatomic gases like argon, there appears to be no major anomoly in C_v near the critical point*. Postill et al[2] find that "between 100°C and 500°C along the saturated liquid curves C_v falls slowly and monotonically from 23.5 to 21.2 joules mole^{-1} C^{-1}, showing no sign of the minimum visible in C_p at about 300°C". This finding is consistent with the following assumed law for $T<T_c$:

$$C_v = 6.0 - 1.374T \times 10^{-3} \quad \text{cal/°K} \quad . \tag{III-7}$$

Postill et al[2] have also tabulated from their experimental data $\partial P/\partial T$ along the liquid saturation line up to about 1000°C. By taking tabular difference in the data of Kikoin and Senchenkov[4], one may extend the data in an overlapping range from 800°C up to the critical point. The results are shown in Fig. 5. We have used a simple broken line fit to this data

$$\begin{aligned} \frac{\partial P}{\partial T} &= 42.22 - 38.72\ T/T_c \qquad T > 573°K \\ &= 57.33 - 44.0\ T/900 \qquad T < 573°K \quad . \end{aligned} \tag{III-8}$$

Thermodynamically, it is possible (see Appendix A) to show that the specific heat along any path x is given by

$$C_x = C_v + T \frac{\partial P}{\partial T} \frac{dV}{dT}\Big|_x \quad . \tag{III-9}$$

At low pressure, up to a few atmospheres, there should be no observable difference between C_p measured at constant pressure and C_s measured along the saturation line. Using C_v from Eq. (III-7), ρ from Eq. (III-5) to set dV/dT, and $\partial P/\partial T$ from Eq. (III-8), one obtains in Eq. (III-9) values of C_s which are within 1% of the published data between 0° and 500°C.

*Some researchers have found a logarithmic pole in C_v observations taken within a few degrees of T_c.

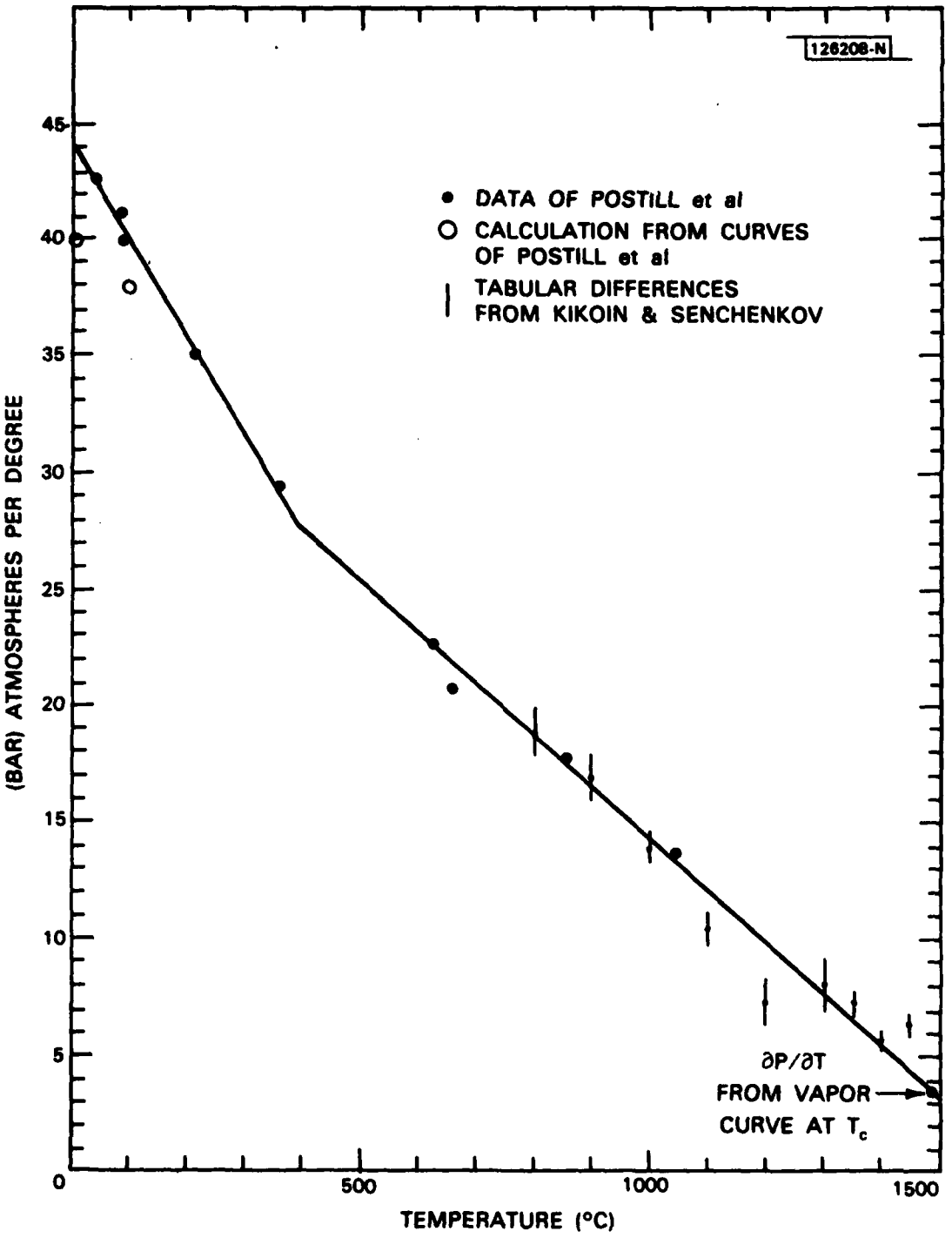

Fig. 5 Experimental ∂P/∂T near liquid saturation line.

Ordinarily, the heat of boiling L is measured at room temperature and, perhaps, at the normal (1 atm) boiling point. Latent heat of vaporization at other temperatures is usally deduced by measuring (or assuming from an equation of state) the boiling pressure-temperature law and the volume increase ΔV on vaporization. These are then related by the Clausius-Clapeyron equation

$$L = \Delta V / T \frac{dP}{dT} \quad . \tag{III-10}$$

However the measurement of L is made, whether directly from heat supplied or indirectly through Eq. (III-9), a plot of L vs. T for many substances, including argon, nitrogen, ammonia, and water seems to follow closely a universal law

$$L = L_o (1 - T^2/T_c^2)^m \tag{III-11}$$

with m being close to 0.4*. By analogy with argon as a monatomic gas, m for mercury has been taken to be 0.42. We choose L_o as 14.8 k cal/mol so that the equation will yield the accepted value of L at room temperature, 14.6 k cal/mol. Handbook quotations of L at the normal boiling point vary. The Liquid Metals Handbook[12] and other Atomic Energy Commission studies (e.g., Report ANL 5750[13]) give 13.98 k cal/mol. Our equation gives 13.97.

Eqs. (III-10) and (III-6) can then be used to deduce the volume change ΔV. This deduced change is compared with the high temperature experimental results of Kikoin and Senchenkov in Fig. 6. The close agreement, even to within a hundred degrees of critical temperature, can be taken as confirmation of the validity of the approximations used.

If all that is desired is a minimal formulation of the properties of a mixture of liquid and vapor below, and not too close to, the critical

*This manifestation of the Law of Corresponding States[11] appears to be our own discovery.

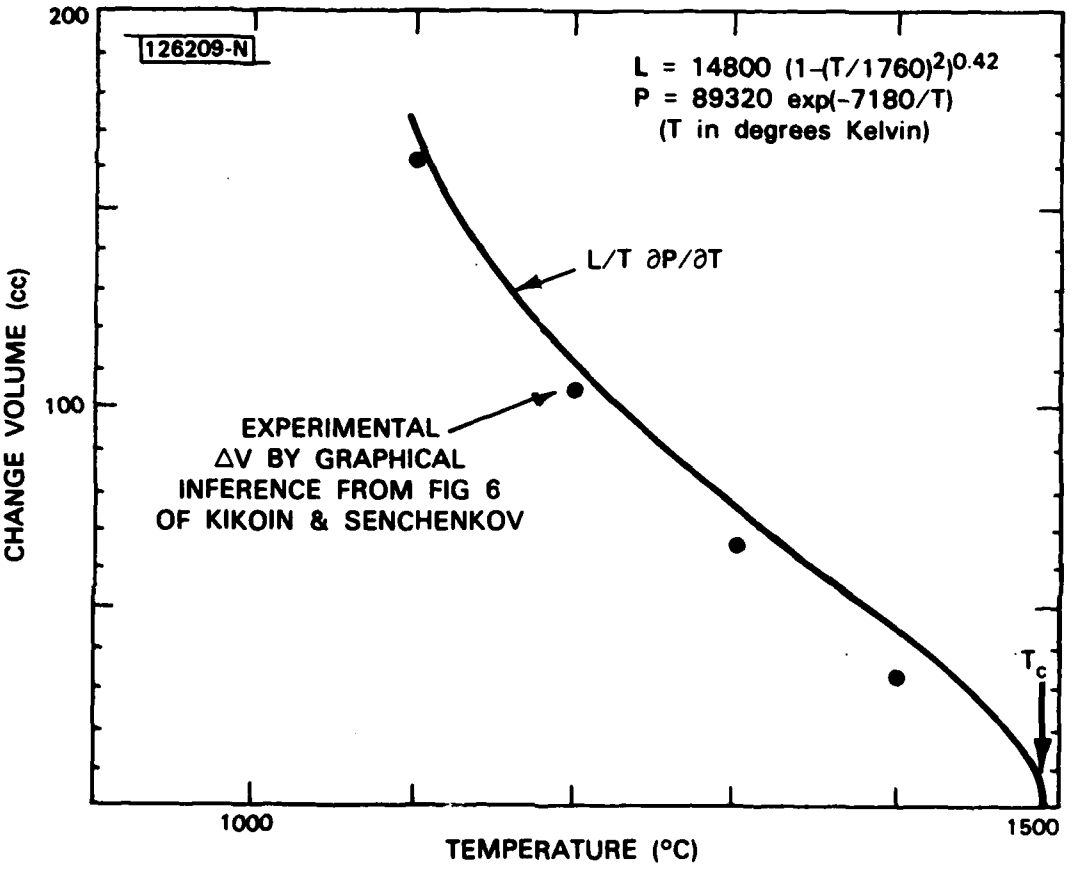

Fig. 6. Comparison of model with experimental data near critical point.

point, the preceding equations may be integrated, partly analytically and partly numerically to obtain H and S to an estimated 10% and $\pm$0.1 accuracy, respectively. In doing so, we have used the Russian density data rather than the German, which results in slightly more overall heat to be handled, and slightly less efficiency in isentropic expansion, both consequences being on the side of conservative estimation.

Results are given in the accompanying Table III-1.

It would be a severe limitation on our results, however, if we did not explore the superheat region also. First, there may be some advantage in power extraction in introducing deliberate superheat, just as with steam. Even more important are the non-equilibrium phenomena of the throttling of a high speed nozzle stream in a supersonic shock, and non-equilibrium expansion with supercooling. Downstream of a shock, the equilibrium state of a gas stream that was saturated is now superheated; the dynamic condition may also be in the superheat region. With supercooling, the droplet mist is not in equilibrium with the residual gas.

The Clausius-Clapeyron equation is a universal equation of state for the liquid-vapor dome. It must join a more conventional equation of state for the dry gas at the dry-vapor dome boundary. If the gas supercools, it will follow the conventional equation within the dome. The two equations of state have nothing physically in common except that they must give the same values at the vapor saturation line.

The equation of state for a non-ideal gas is usually written in the form of an ideal gas equation with correction terms. In principle, any pair of thermodynamic state variables can be taken as the independent variable in such an equation. For many purposes P and T are such a pair, but they fail to define the state of the fluid within the liquid-vapor coexistence dome. We shall use V and T, which do define the state of the fluid generally (except at the triple point where the solid can also join the equilibrium).

TABLE III-I

THERMODYNAMIC PROPERTIES OF MERCURY
(cal..mol..cc)

Data and Formulas Used

Tc = 1760 K Pc = 1500 atm; Lo = 14800 cal/m

Rho = $3.140+10.930(1-T/Tc)^{0.283}$ T>500C; $L/Lo=(1-T^2/Tc^2).42$

P = exp(12.103-7617/T-.8001n(T/630)) if T<500K

P = exp(11.397-7172/T-.0041n(T/630)) if T>580K

Cs = 6 - 0.001374T + (TdP/dTlv)(dV/dT)

T desk	P bar	Cs cal/°	Ho cal	Hvl	Hv	So cal/°	Svl	Sv	Vdif cc
300	0.0	6.38	172	14618	14790	0.60	48.73	49.33	810405796
400	0.0	6.44	813	14474	15287	2.44	36.18	38.63	2384229
500	0 1	6.46	1458	14286	15744	3.88	28.57	32.46	78865
600	0.6	6.43	2103	14052	16155	5.06	23.42	28.48	8586
700	3.2	6 37	2743	13767	16511	6.05	19.67	25.71	1780
800	11.4	6.58	3387	13429	16816	6.90	16.79	23.69	551
900	30.8	6.71	4055	13031	17086	7.69	14.48	22.17	222
1000	68.2	6.87	4741	12565	17306	8.40	12.56	20.97	107
1100	130.9	7.07	5450	12020	17470	9.07	10.93	19.99	59
1200	225.4	7.33	6189	11382	17570	9.69	9.48	19.18	35
1300	356.8	7.68	6966	10627	17592	10.29	8.17	18.47	22
1400	529.0	8.18	7795	9717	17512	10.88	6.94	17.82	15
1500	744.1	9.02	8701	8588	17289	11.47	5.73	17.19	10
1600	1003.0	10.80	9745	7093	16838	12.10	4.43	16.53	6
1700	1305.3	18.10	11163	4756	15920	12.90	2.80	15.70	3

There are two general forms for the modified P-V-T equation of state with V and T as independent variables

$$PV = RT + r_a(T,V) \qquad \text{(III-12a)}$$

$$P(V - V_o) = RT + r_b(T,V) \quad . \qquad \text{(III-12b)}$$

Evidently, the equations are equivalent. The latter represents an attempt to simplify the form of the residual, $\underline{r}$, by subtracting from the volume of the fluid a volume V_o hypothetically occupied by the fluid molecules as hard spheres.

Equation (III-12b) was proposed by VanderWaals*. Bertholots modification sets

$$r_b = -a/TV + \ldots \text{ neglect} \qquad \text{(III-13)}$$

which fits mercury somewhat better than VanderWaals omission of the T factor. Further flexibility can be introduced by using V^m, m arbitrary, in place of V.

The modern tendency is to use Eq. (III-12a) in the form of a "Virial Equation" with inverse powers of V:

$$r_a = B(T)/V + C(T)/V^2 + D(T)/V^3 + \ldots \quad . \qquad \text{(III-14)}$$

In any case, if the residual r(T,V) is known in the dry gas region, then there are standard textbook formulas available to obtain H,S, etc., in this region also. An obvious step is to compute r(T,V) from the Clausius Clapeyron formulation, in the hope that the results can be extended analytically into the dry gas region. This is a nevertheless delicate step, in that much depends on fitting the residual thus obtained to an expected form.

*with r_b equal to a/V^2.

Roberts[5] has attempted to produce a Virial expansion from the Russian data, but that data is not fully consistent in the dry gas region, and does not, in any event, extend down to the pressure range of interest (except for a single point at 900°C and 200 atm). We have used here the Berthelot equation

$$P = \frac{RT}{V - V_o} + \frac{a}{TV^2} \qquad \text{(III-15)}$$

with V_o = 10 cc/mol and $\underline{a}$ equal to 2.075×10^8 cal/cc.

The pressure so calculated along the gas saturation line of our model is within $\pm$3% of the pressure from Eqs. (III-6) over the entire range from 0°C to within 100° of the critical point. An even more sensitive test of the consistency of all of the assumptions is to compute from the model the C_v of the ideal gas by the methods of Appendix A, for comparison with 3R/2. The incompleteness of real data does not justify this step except as an indication of general trends. Nevertheless, the C_v so obtained is generally within $\pm$20%, and usually within $\pm$10% of the correct value, in spite of being derived as the differences of quantities an order of magnitude larger (see Appendix A).

The T-S diagram for a mixture of saturated liquid and vapor mercury is shown as Fig. 7 for temperatures between 500°K and 1750°K. A simplified Mollier chart (omitting pressure and volume data) showing enthalpy as a function of entropy, wetness, and temperature is shown in Fig. 8.

Within the evaporation dome, lines of constant T are also lines of constant P. Figure 7 shows the pressure trajectory according to the Berthelot Equation as the trajectory followed in the dry gas region and its non-equilibrium projection into the dome. Presumably if supersaturated vapor expands isentropically to encounter a pressure trajectory headed the wrong way, it will spontaneously condense. But we really do not know the shape of the non-equilibrium curves; we draw them on various charts to be able to consider non-equilibrium expansion of the gas qualitatively, not quantitatively.

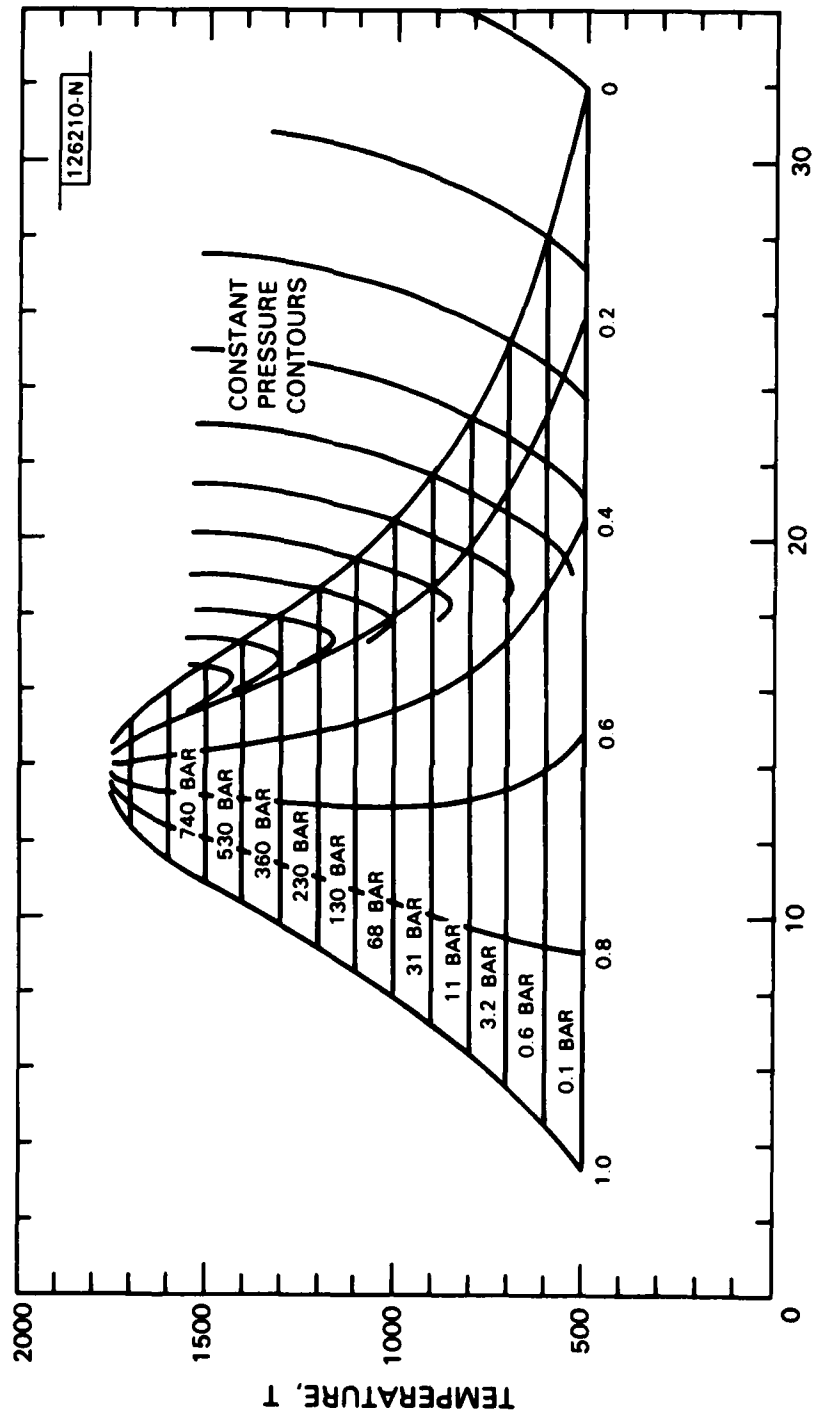

Fig. 7 T-S diagram for mercury.

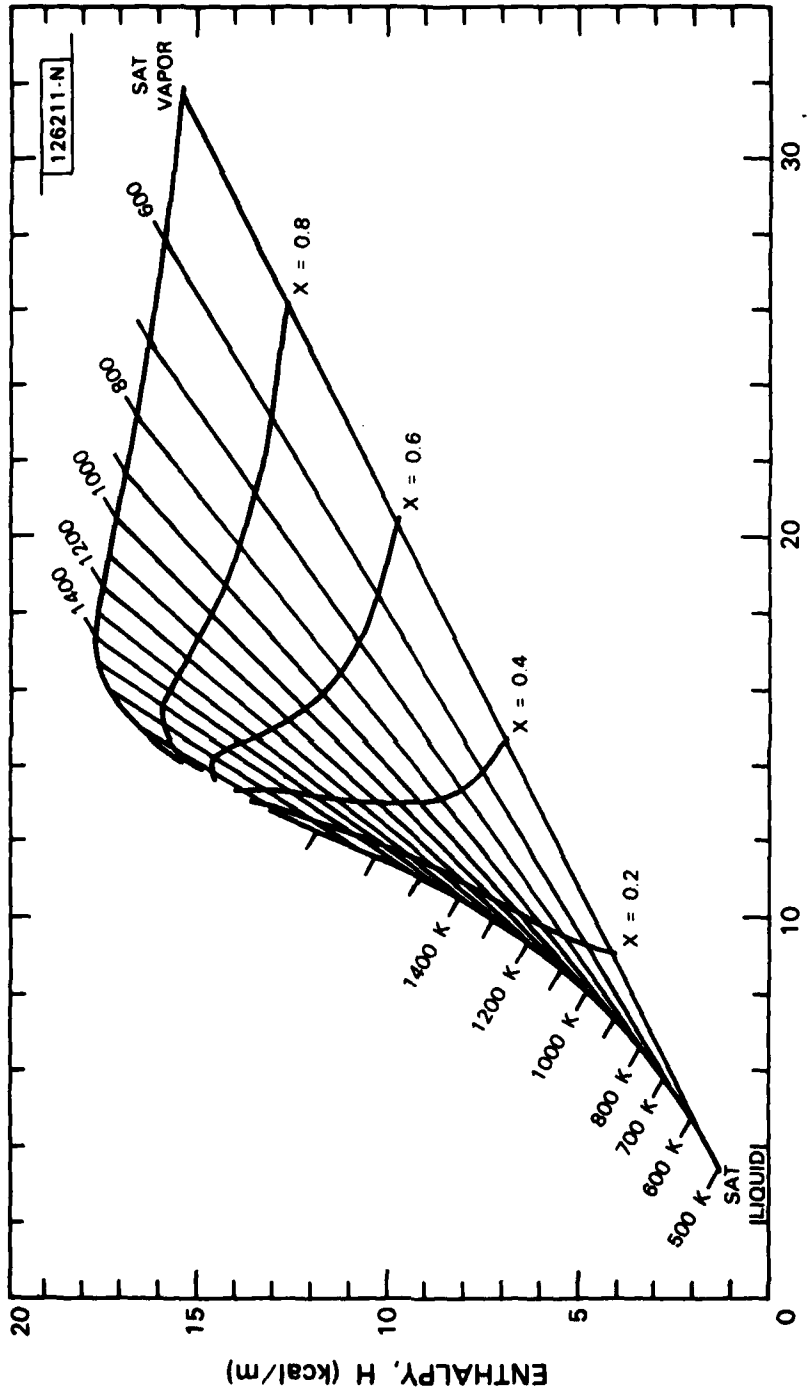

Fig. 8 Mollier chart for mercury.

The constant pressure trajectories on the H-S diagram (Fig. 8) show no anomalies. The two variables are connected everywhere by the thermodynamic identity

$$\left.\frac{\partial H}{\partial S}\right|_P = T. \qquad \text{(III-16)}$$

The isobars outside the dome are simply continuations of the straight lines inside the dome, smoothly curving away from linearity as the temperature changes. There is, however, a sharp break in the constant-temperature trajectories at the dome boundaries, because outside the dome, H tends to be a function of temperature only. These trajectories on the H-S diagram are used in discussing the differences between a Rankine cycle and a Carnot cycle in Section VI below.

One derived parameter that is needed to characterize fluid flow in an expansion nozzle is the local velocity of sound a for isentropic flow:

$$a^2 = \left.\frac{\partial P}{\partial \rho}\right|_S = \frac{1}{\rho}\left.\frac{\partial H}{\partial V}\right|_S . \qquad \text{(III-17)}$$

This calculation is made on the basis of condensation into a fine mist of droplets which are small enough to move with the gas. The resulting speed of sound is plotted against S entropy in Fig. 9 to facilitate investigation of nozzle flow. Note that under the fine mist assumption the gas becomes very dense as $x \to 1$ with the result that the speed of sound at $x \to 1$ is very low. If the droplets are too big or too few to vibrate with the gas but can still exchange heat with it, the velocity of sound will be that shown as $x \to 0$ for all values of x. Finally, if condensation and evaporation cannot reach equilibrium on the time scale of the expansion, then Fig. 9 is not applicable.

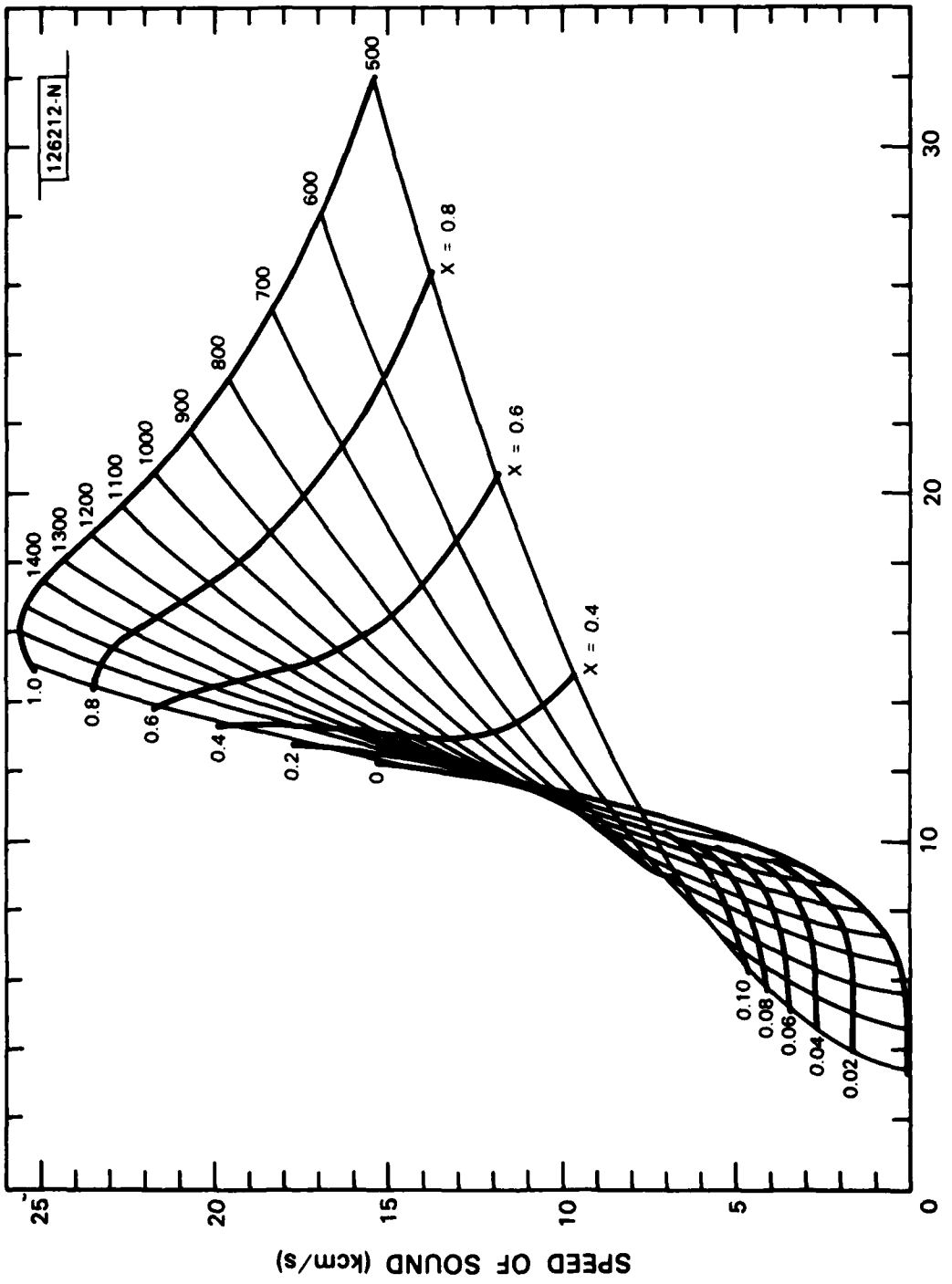

Fig. 9 Speed of sound in mercury.

PART 2

RADIATIVE TRANSFER BOILER

Chapter Summaries

Chapter IV
MERCURY BOILER
(First Part)

The wetting and corrosion problems normally associated with the use of mercury boilers are avoided by spraying droplets into the "boiler" tube and by relying on radiative heat transfer between the tube wall and the resulting droplet mist. Published experimental data for the electrical conductivity of mercury is used with both approximate and exact equations for the electromagnetic reflectivity to establish the insensitivity of such heat transfer to droplet size, over a temperature range of 600°K to 1400°K and for droplet radii down to a few tenths of a micrometer. Radiative transfer theory is then used to establish conditions under which the mist exhibits diffuse absorption in the range 75% to 100% for source temperatures between 1000°K and 1400°K. Heat transfer is at the rate of 50 to 150 kW/m^2 with the boiler walls roughly 150° hotter than the boiling liquid.

Chapter V
MERCURY BOILER
(Second Part)

A radiative heat transfer boiler has very low thermal mass. The working fluid cannot be relied on as a coolant, so that alternative means must be found for rerouting source heat not demanded by the eventual mechanical load. When the boiler is at the focus of a solar concentrator, then the optical absorption of the mist can be used to switch the absorption of sunlight. In general, other cooling is required, which may take the form of a secondary low-pressure boiler and heat-pipe condenser system.

IV. MERCURY BOILER (First Part)

The fundamental problem of boiling heat transfer is to prevent a layer of gas from forming between the hot shoe and the liquid being boiled. Ideally, the boiling layer should be so thin, and wet the hot shoe so thoroughly, that all vaporization takes place from the free surface. Under laboratory conditions, heat fluxes in boiling have been achieved which are close to the heat fluxes at the surface of the sun. Thin film boiling and condensation is used today on a less grandoise scale in heat pipes.

Liquid metals are well-adapted to the requirements of film boiling on account of their high thermal conductivity in the liquid state and on account of their ability to wet other metals. However, when mercury was first being considered, boiler design had not moved far from an enclosed pot of water on the stove; and the fundamental problem was to get mercury to wet the container at all. Eventually, this problem was solved by adding to the mercury small amounts of reactive metals, in particular magnesium, to attack and dissolve the oxide layers that were preventing wetting.

The resolution of the wetting problem revealed a new layer of difficulties. The mercury now appeared to attack the boiler tubes in use in the power plant even though it did not attack them in static tests in the laboratory at much higher temperatures. The problem was eventually traced to differential solubility. Even though only trace amounts of iron are soluble in the liquid, the amount varies with temperature so that metal was being constantly leached from the tubes in the hotter parts of the boiler and deposited in the colder parts. Researchers were able to show that a few degrees Fahrenheit temperature difference were sufficient to drive the process. Eventually an inhibitor was found in the form of the addition of parts per million of titanium.*

---

*A similar problem appears to have arisen in the development of the SNAP-8 boiler with the leaching of Cr from stainless steel resulting in the eventual use of a Tantalium boiler [27].

Even if you may not know the details of a erosion process that occurs in a flowing liquid, one way to reduce it is to reduce the amount of liquid in the system. When this was tried, mirabile dictu the heat transfer characteristics of the boiler improved! In its maturity, the mercury power plant was running with 1/3 the volume of liquid in its tubes that would have been needed in an equivalent water boiler[1]. It is an interesting footnote to this story that the G.E. scientists also solved the problem of fixing mercury so that a room temperature spill of liquid would not constantly release mercury vapor into the atmosphere. The inhibitor in this case is thallium.

We shall not utilize this history directly in the construction of a mercury vaporizer. At 1000°K, the radiation flux from a black body is 57 kW/m^2, a respectable figure compared with pot-on-the-stove boiling heat transfer. At 1000°C (1273°K) the flux rises to over 150 kW/m^2. While it requires a source about 150°K hotter to permit most of such a heat flux to be absorbed at these temperatures, there is nevertheless the prospect of direct radiative heat transfer between a hot wall and a mist of mercury droplets. In such a vaporizor contact heat transfer would be only a "back-up" mode for those droplets that hit the wall and stick to it.

To boil droplets by radiative heat transfer is a process simple in concept, complex to the point of defying exact analysis in detail. However, by using approximations based on radiative transfer theory it is possible to make some quantitative assertions.

First, obviously, the droplets themselves must have enough physical surface to absorb the heat. If V is the total volume of liquid and a is the droplet radius, then the nominal area A_o obtained by adding πa^2 for all spherical droplets is

$$A_o = 3V/4a \quad . \tag{IV-1}$$

If V is measured in cm^3 and a in μm, then A_o is in m^2.

Not all of A_o can be effective in absorbing radiation, because a metal sphere is only partially absorbing. For a black body radiating in the range of 1000° to 1300°K, the radiation spectrum peaks in the general vicinity of 2 μm wavelength. In this wavelength region mercury behaves towards radiation more-or-less like a simple metal with a room temperature conductivity near 10^6 mho/m[9]. Studies of the radiation-scattering properties of metal spheres in the IR spectrum use a parameter η

$$\eta = 60\,\sigma_e\lambda \quad . \tag{IV-2}$$

Van de Hulst[10] then gives, for sufficiently large spheres or sufficiently large values of the parameter η, the fraction Q_{abs} of droplet projected area πa^2 that effectively absorbs as (asymptotically)

$$3\sqrt{2/\eta} < Q_{abs} < (8/3)\sqrt{2/\eta} \quad . \tag{IV-3}$$

In recent years, the electrical conductivity σ_e of mercury liquid at saturation has been well-established up to high temperatures.[2-4] Thus we can establish the complex index of refraction as a function of wavelength and boiling (or condensing) temperature and can calculate the exact scattering coefficients to unpolarized radiation by the "Mie" method[10]. For a given effective black body radiation temperture, these results can be averaged with respect to wavelength to give curves of normalized absorption cross-section vs particle radius for various combinations of radiation temperature and droplet temperature, such as those shown in Fig. 10.

These results demonstrate substantial insensitivity to droplet size down to the submicron range, even at the lowest temperatures (corresponding to 5 μm peak flux wavelength). Over a wide range of conditions, the breakpoint, at which is absorption drops below its asymptotic limit, is at 0.2 μm droplet radius.

This insensitivity to droplet size permits the use of micron size droplets in the thermal wavelength region. As the droplet evaporates, the

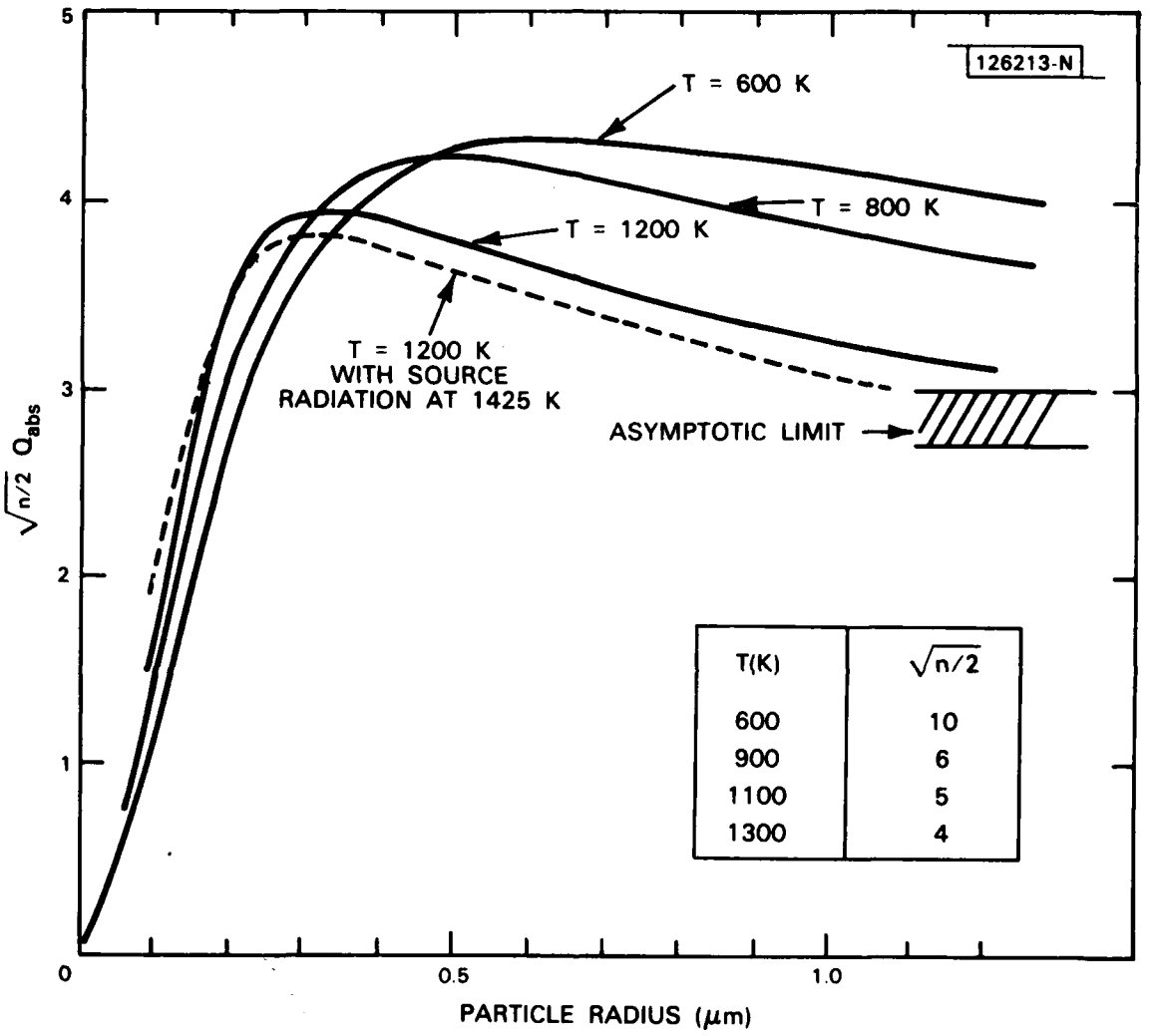

Fig. 10. Dependence of normalized absorption cross-section on droplet radius and temperature.

heat input per unit area of surface does not change, for wavelength reasons, until the volume is a negligible fraction of its initial value. By integrating a rate equation one may conclude that once a droplet comes up temperature, its radius decreases linearly with time until it reaches about 0.2 μ, then more slowly until the droplet radius drops to about 0.1 μ, at which point little further change occurs. The remnant particles may be swept out of the boiler with the compressed vapor to serve as nuclei for later condensation; or they may be evaporated by other processes, including contact with the container walls.

From Eqs. (IV-1), (IV-2), (IV-3), and the discussion of the previous paragraph, one may conclude that if 1 μ radius droplets are a useable size, roughly 2 to 4 cc of liquid mercury might be required per square meter of effective absorbing surface. The basic result is that the volume of liquid required is comparable to a liquid layer roughly as thick as the droplet diameter spread uniformly over the effective black body radiator area. By any normal standards, this is a very dry boiler indeed.

The second requirement is that the radiation actually get to the droplets. Consider boiler which consists of concentric cylinders, separated a modest fraction of either radius. If A_w is the area of one wall and A_{abs} is the effective absorption area of the droplets to heat (coming from one side), then the ratio A_{abs}/A_w is the Optical absorption thickness of the mist, τ_{abs}. If there were no further complications due to scattering, then $\exp(\tau_{abs})$ of the radiation from one wall will reach the other, so that radiation would be absorbed with an efficiency ζ

$$\zeta = 1 - e^{-\tau_{abs}} \qquad \text{(IV-4)}$$

Evidently, if A_{abs} is merely equal to A_w, and no scattering is present, the process can only be 63% efficient.

But droplets not only absorb light, they also scatter it. To describe what happens, it is necessary to introduce the concepts of a scattering

cross-section Q_{sca} and an average back-scattering cross-section Q_b (which is necessarily less than Q_{sca}). For very large droplet radii $Q_{sca} \rightarrow 2$ * and $Q_b \rightarrow 1/2$. VanderHulst remarks[10] that unless η is very large (10^8) the knee of the scattering curve occurs at larger droplet radii than the knee of the absorption curve. Thus, for very small droplets, absorption can dominate scattering and an optically thick mist ($\tau_{abs} >> 1$) will be highly absorbing.

However, if $2\pi a/\lambda$ is not small, scattering will be significant. Its effect is two-fold: it inhibits the penetration of radiation into the mist, but it increases, through multiple scattering, the absorption of the radiation that does penetrate. Suppose that the radiation from the boiler wall has an angular distribution like the equilibrium angular distribution deep within a cloud of the mist. (It doesn't, but the assumption is conservative, and the error made is not great.) Suppose that the radiation that reaches the far wall is small and/or similarly reflected. Then it is possible to use radiative transfer theory to find an equation for the diffuse reflectivity ρ

$$1/\rho + \rho = 2(1 + Q_{abs}/Q_b) \quad . \tag{IV-5}$$

The resulting diffuse absorption is plotted in Fig. 11, as a function of droplet diameter and temperature conditions.

Evidently for any distribution of droplet sizes, there is an optimum boiler fill of the order of magnitude A_w (for total absorption area) beyond which the rate of heating per unit mass in the boiler falls, even if the total heat transfer per unit area of hot shoe increases slightly.

The final consideration is to determine the steady state distribution of droplet size in the boiler. To bring the droplet to temperature ΔT requires an amount of heat roughly equal to 6.7 ΔT cal/mol for mercury.

---

* Q_{sca} for a large object is twice the physical cross-section because there is both a shadow cast and a diffraction pattern.

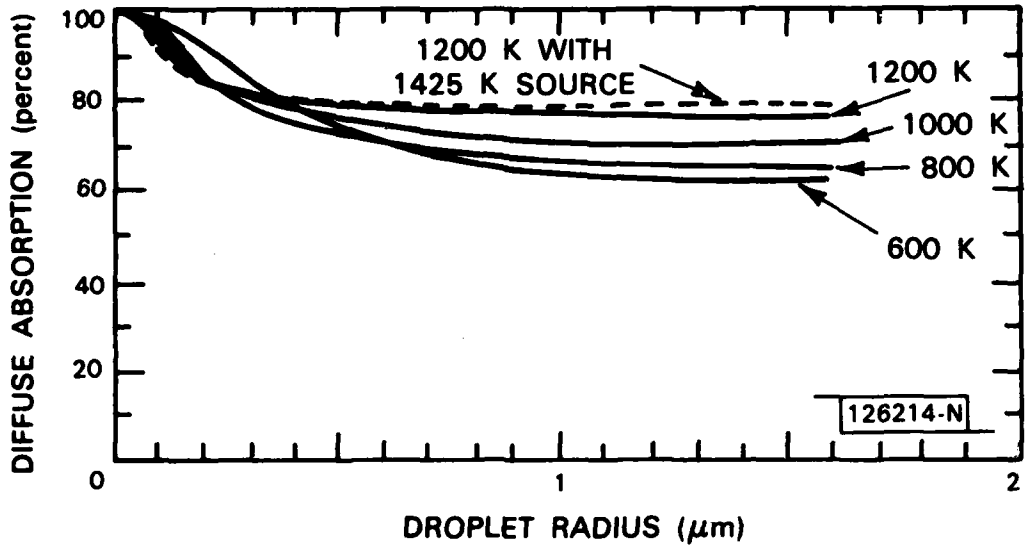

Fig. 11 Asymptotic diffuse absorptivity for droplet mist.

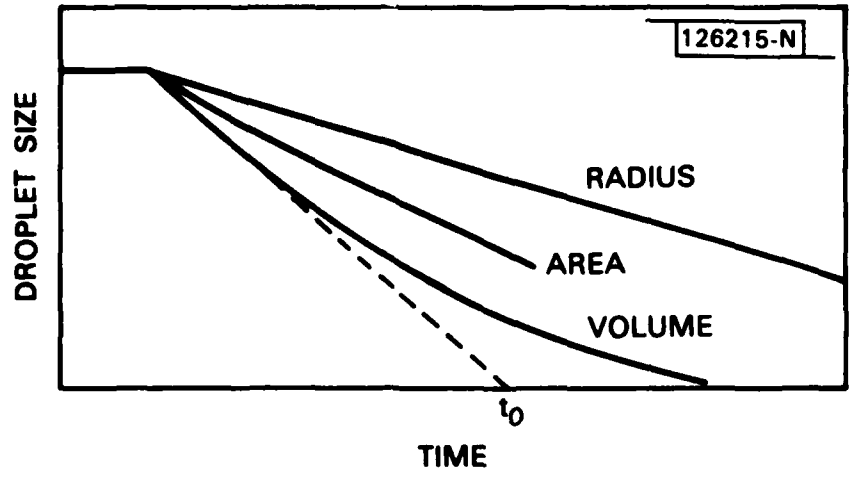

Fig. 12 Droplet size as a function of time.

The latent heat of vaporization is roughly 13 kcal/mol near 1000°. Suppose that ΔT is 500°K. Then the amount of heat required for vaporization is roughly 4 times that supplied to raise the temperature.

If, therefore, the droplet went on absorbing heat at the same rate, it would require 4 times as long to vaporize as to heat. It starts out this way, but as we have noted, it is the droplet radius that drops linearly, not its volume. Solving the dynamic equations reveals that the actual time to zero radius is 3 times again as long as the initial rate to zero volume.

The situation is shown in Fig. 12 where all the measures of droplet size are plotted versus time. At time t_o at which all of the droplets would have evaporated at the original rate, the area has dropped to 4/9 of its original value. At $2t_o$ all but 1-1/2% of the droplet is gone. The average area during the first interval is 72%. The average area during the second interval is 22%. Thus, if one constantly replaces the mist at the rate that it would have evaporated at the original rate, the actual droplet area is nearly the same as for a fixed charge at the beginning of heating; and droplets do not remain at any size much longer than 2 or 3 times the nominal evaporation time t_o.

The actual evaporation rate is quite fast. If a charge of .4 cm^3 is required per m^2, then there are 0.05 kg to be evaporated at 330 kJ (total) per kg by 50 to 150 kW. Evaporation takes on the order of tenths of a second after injection.

V. MERCURY BOILER (Second Part)

The high rate at which the required amount of mercury can be vaporized at temperature poses a series of design issues (on top of the requirement that the vaporization vessel and its connectors withstand 3000 psi working pressure at 1000°C) related to controlling the supply of heat relative to the supply of mercury.

Ordinarily, in the design of a boiler the working fluid is also a coolant for the boiler parts. Thus boilers are routinely controlled by adjusting the supply of fuel, not by shutting off the supply of working fluid. Ordinarily, also, there is enough liquid in the boiler at any one time to continue to cool it, through the release of steam through safety valves if necessary, through a slow shutdown, even if normal fluid flow should be blocked. Here, the boiler is nearly dry. Moreover, the sources of high temperature power, whether they be nuclear or solar, are not easy to shut down on a short time scale.

Thus, we must provide alternatives to the working fluid for cooling and regulating the temperature of the working parts of boiler and heat source. Several possibilities are:

(a) Provide an alternate path for the heat that will absorb the heat not utilized by the mercury.

(b) Put the mercury in series with heat flow to a cooler. Radiation not absorbed by the mercury simply passes on to the cooler.

(c) Make the presence of the "mercury" essential to the physics or chemistry of producing the heat.

A prime example of the third possibility is the uranium reactor in which heavy water (D_2O) is both the coolant and the moderator. As you lose coolant you also lose moderator and, in principle, the plant shuts down. It is always possible to postulate scenarios in which blankets of steam form between the

coolant and the fuel, so that cooling fails even though moderator is present; in practice cooling and moderator controls are kept separate because they must operate on phenomena with different inherent time lags.

While mercury is not a suitable moderator, Li^7 is. It is conceivable that a combination of light metals could take the place of mercury, and that the cycle might be one involving a chemical decomposition such as the formation and decomposition of LiH with energy extraction in an electrolytic fuel cell rather than in a heat engine [20].

Possibility (b) is easiest to impelement at the focal plane of a solar collector which is focussed in at least one dimension (Fig. 13). Without focussing, the sun is good for a little over 1 kW/m^2 on the ground, 1.3 kW/m^2 in space. With focussing in one dimension, the density can rise 100 kW/m^2, and with focussion in the second dimension, several hundred kW/m^2 are practical with simple optics. In principle, all that is necessary is to spray the mercury into one end of an optically transparent boiler tube made of, say Al_2O_3 (Lucalox or sapphire), and to withdraw Hg steam from the other end, the required technology being similar to that employed (except for end seals) in the so-called "high" pressure sodium vapor lamp. The absorptivity of mercury mist in the visible is about 20% at normal incidence, probably about 25% total absorption for spherical droplets. According to Eq. IV-5, this is enough to produce a mist with roughly 60% absorptivity inside the boiler tube. If the mist isn't there, the sunlight simply passes through the other wall of the tube and is lost.

In order not to cool the outer boiler wall in an uncontrolled fashion, it is contained in an optically transparent envelope from which air has been removed. (See Fig. 14). There are, in principle, a variety of sophisticated techniques for making this double-walled arrangement a "greenhouse" that passes sunlight but contains the heat if it is absorbed by the mercury. In fact, it is probably simplest not to try to be too sophisticated. It would suffice to supply sunlight at a substantially greater flux density than the mercury would lose by black body radiation.

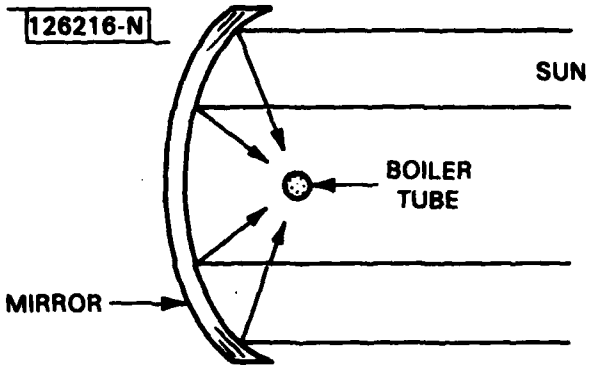

Fig. 13 Simple boiler and solar collector.

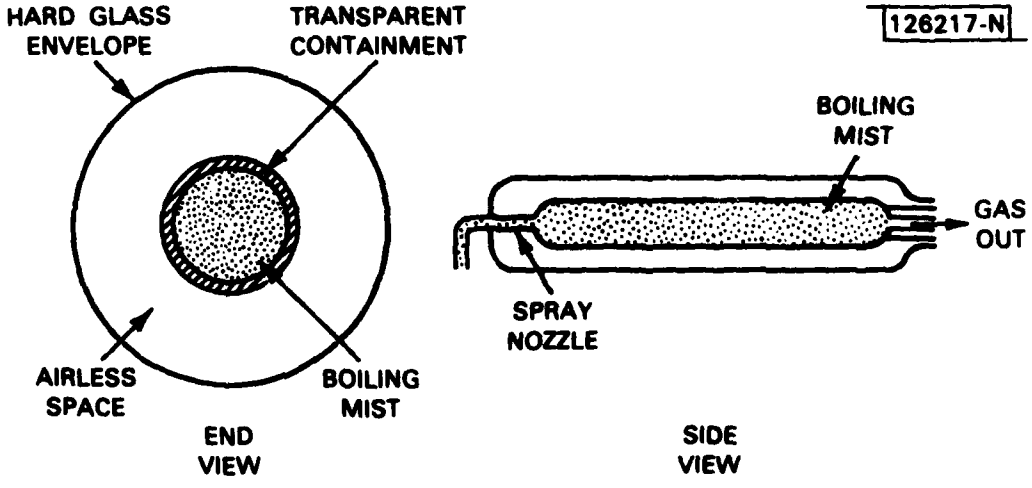

Fig. 14 Details of solar mist boiler.

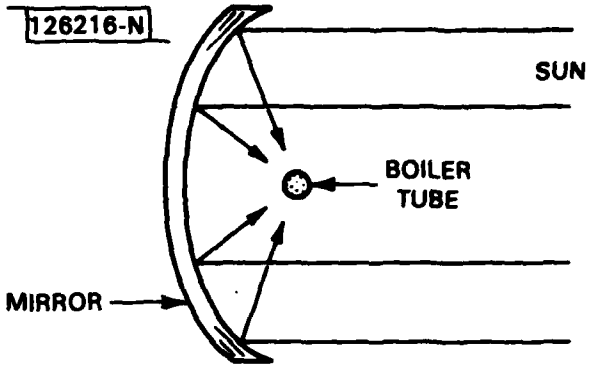

Fig. 13 Simple boiler and solar collector.

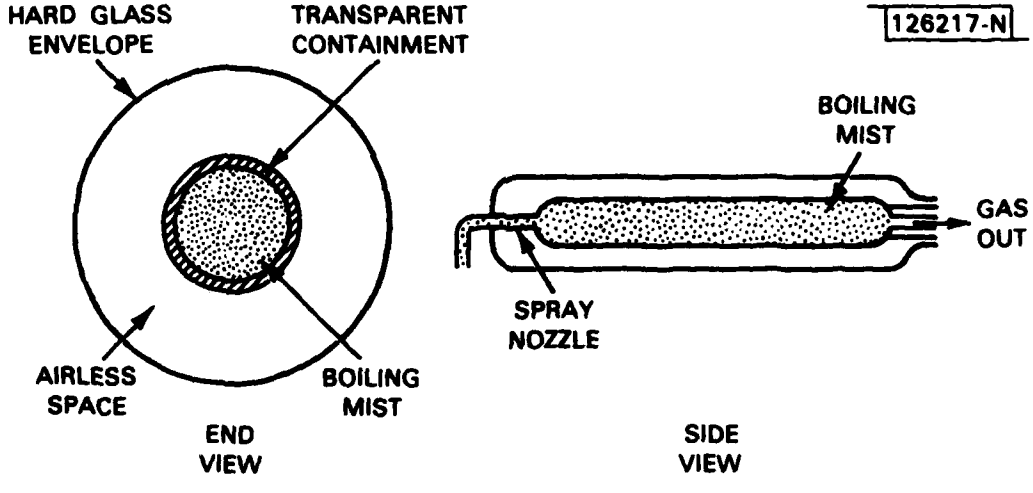

Fig. 14 Details of solar mist boiler.

The solar source is unique in that is lies in an entirely different wavelength range than the heat of the working fluid, so that the fluid itself constitutes a sufficient radiation switch. Even when the source is thermal, so that the radiation is in close to the same wavelength band, it is possible in principle to put the mercury mist between the source and a radiative "vent" to the external world as in Fig. 15. A difficulty is that one no longer has a greenhouse, so that the boiler wall is in the position of not transmitting heat at the temperature of the boiling mist, but of passing the entire heat load if the mist should not be present. Evidently, the only passive means of accomplishing this is to allow temperatures to rise. In order that this rise be not too great is may be desirable to implement a heat pipe between the outer wall of the boiler and the exterior radiator envelope that becomes active at a temperature roughly 100°C above the normal working temperature.

A chemical system such as iodide decomposition may be a better means of transporting the working material back to the boiler surface than the conventional heat pipe wicks. The usual entropy of decomposition of a compound is about 45 cal/deg per excess mole of gas produced. The decomposition of LiPb, for which the enthalpy of formation is about 14.6 kcal/mole, should thus vaporize at roughly 300° above normal boiling point of lithium (1315°C) NaPb (ΔH_f = 4.5 kcal/mo) at 100° above the normal boiling point of Na (883°C). Thus, it may very well be possible to use a secondary cooling system of LiPb for a Lithium boiler, and a secondary cooling system of NaPb for a mercury boiler. (The compound NaPb is stable at room temperature in air.) See Fig. 16.

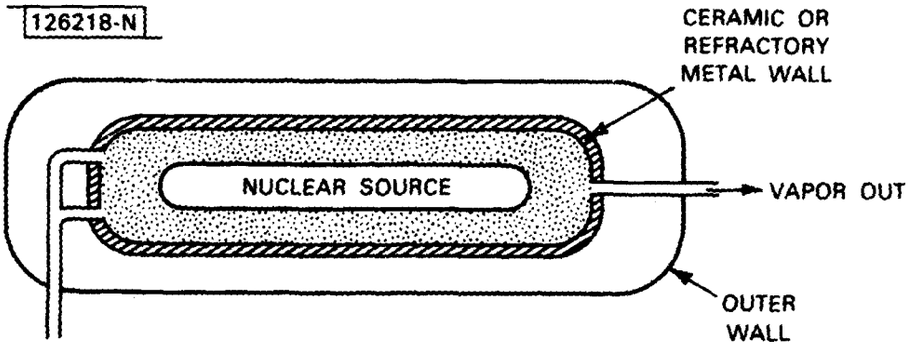

Fig. 15 Fire tube boiler.

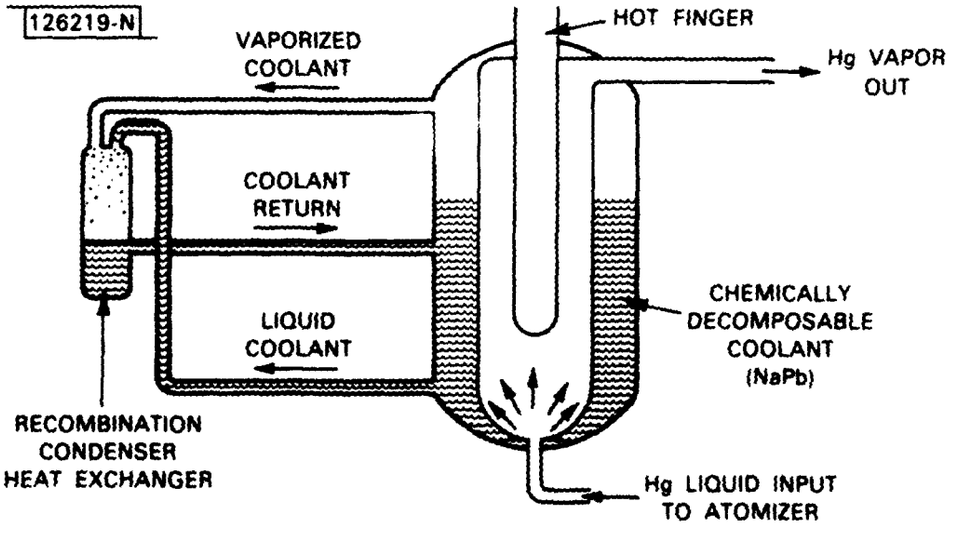

Fig. 16 Boiler with surrounding metal vapor coolant.

Part 3

THERMO-MECHANICAL ENERGY CONVERSION

Chapter Summaries

Chapter VI

ENERGY CONVERSION - STATIC EXTRACTION

The relationship between the enthalpy H of a working fluid and the work done in adiabatic processes is reviewed. The enthalpy-entropy (H-S) diagram for mercury is used to obtain the efficiency of ideal and modified Rankine cycles, permitting expanding vapor to become wet as in a piston expansion engine. The efficiency of a practical mercury Rankine cycle working between 1200°K and 600°K is found to be more than 90% of the ideal Carnot efficiency.

Chapter VII

KINETIC ENERGY EXTRACTION - DYNAMIC EQUILIBRIUM

An introductory analysis is made of the impulse turbien, in which expansion takes place in a stationary nozzle and in which the turbine reacts to the kinetic energy of the resulting flow. Ideal and non-ideal paths for the expansion are traced on the H-S diagram and on the P-V diagram. An equilibrium expansion from 1200° and 200 bar to 600° and 0.6 bar results in a 1 to 150 volume expansion.

Chapter VIII

KINETIC ENERGY EXTRACTION - SUPERSONIC FLOW

The speed on sound in Mercury vapor is calculated as a function of thermodynamic state variables. To avoid supersonic speed in the nozzle exits in a 1200°K to 600°K expansion, as many as a dozen successive stages of expansion might be needed. However, mercury is so dense that the speed of sound (150 to 250 m/s) is comparable with convenient peripheral speed for a turbine rotor. It is found that fully expanded flow at Mach 2.8 (M* 1.7) can be turned through 180° with only modest losses during startup. It is found that a single-pass extraction flow

at Mach 1.4 (M* 1.26) can be shocked down to a supersonic flow through the blades and be re-expanded at the blade exits with ony a few percent loss due to irreversibility. The equilibrium flow of mercury through the throat of a supersonic nozzle is considered both by analysis and by numerical integration of the thermodynamic properties of mercury vapor, with results presented as curves of flow vs nozzle area.

VI. ENERGY CONVERSION - STATIC EXTRACTION

In one sense, an energy conversion device such as a piston or turbine is simple, direct, and experimental. A hot, compressed vapor pushes on a piston which does work as the gas expands and cools. It is not a very efficient engine. A man named Newcomen discovered that if cold water is sprayed into the cylinder as the spent steam is being pushed out, the work available from each stroke increases enormously. This engine was efficient enough to pump out water from a coal mine while using only a small fraction of the new coal that could now be reached. It was not long before someone realized that a tremendous amount of heat was still being wasted by alternately heating and cooling the cylinder to room temperature, and so arranged to cool the exhaust steam in a separate condenser. The result added the name Watt to the languages of the world, and ushered in the industrial revolution.

But even if the parts are no longer cooled to room temperature, they still do alternately heat and cool as steam enters the cylinder and expands. The intrepid inventor would, if he could, make these parts out of a material with extremely low thermal conductivity and extremely low heat capacity so that this heating and cooling would not be a burden on the heat content of the steam. Glass almost is such a material. (See Table IX-I.) The writer has estimated a factor of 2 increase in the working efficiency of the gasoline engine if its cylinders and pistons could be made of glass*.

An alternative to non-heat-absorbing cylinder and piston walls is to make their area small relative to the volume of steam being handled. Since area increases as the square of dimension and volume as the cube, this means making everything as large as possible. Thus arises the infamous "economy of scale" of power plants.

In these contexts, the great advantage of the turbine is that under steady state conditions, the temperature at any given point on the turbine

*The difficulty in doing so is to find a way of supplying high-temperature lubrication. The tendency of glass to shatter can be controlled!

apparatus does not change with time. Thus, a small turbine can be efficient. Turbines have another advantage: they run at speeds of the same order of magnitude of the speed of sound in the gas and thus have a high power output per unit weight.

Even though turbines are much simpler than piston engines in terms of total parts count, they are relatively high technology because the high speeds and temperatures tend to stress components to their working limits with centrifugal force and vibration.

The objectives of this Section are two-fold:

(a) To obtain efficiency predictions for simple Rankine cycles using the data and curves developed in Section III, and

(b) To state the law of Conservation of Energy in a form that can be used for supersonic flow.

In this Section we assume generally instantaneous equilibrium. Later we shall take up possible practical consequences of non-equilibrium expansion.

If we were dealing with a closed (but variable volume) container which were moved from place to place while various things were done to - and with - it, then the proper measure of the energy inside would be the internal energy U, which is simply the sum of all possible potential and kinetic energy terms (mechanical, electrical, thermal, gravitational, etc.). U can be considered to be the net energy which must be added to the fluid inside the container to bring it from 0°K, at "rest" in zero field, to its present condition. If Q is the heat added and W the work done on the surroundings, the First Law (energy conservation) states

$$U - Q + W = \text{const} \quad . \tag{VI-1}$$

(The constant is arbitrary and depends on the assumed reference condition. In the scientific literature, a superscript "o" generally means 0°C as the reference state; a subscript "o" generally means 0°K as the reference state.)

If the fluid flows through a system of pipes, cylinders, etc., then some of the distribution of energy between U and W as defined above relates to the work required, for example, to remove the fluid from a pipe through which it flows. This work is counterbalanced by an exactly equal amount of work done by the next element of fluid that enters the pipe. In textbooks it is shown that this artifact of flow can be eliminated by adding a term PV to the internal energy to obtain the enthalpy H

$$H = U + PV \qquad \text{(VI-2)}$$

The first law of thermodynamics now reads

$$H - Q + W = \text{const} \qquad \text{(VI-3)}$$

in which W is now the net <u>external</u> work and no longer includes work merely exchanged between parts of the fluid as it flows through the system.

Unless one builds a suitable heat exchanger, it is difficult to exchange significant amounts of heat ΔQ between fluid and surroundings in a large scale system. Similarly, unless one deliberatly extracts work, ΔW is zero. Thus, the law for adiabatic flow becomes

$$H = \text{const} \quad . \qquad \text{(VI-4)}$$

This constancy of total H applies for flow through nozzles, throttling valves, through shock fronts, as well as through pipes of varying section. It does not depend on thermodynamic reversibility or whether the forces of friction convert the fluid to a state of higher entropy as it flows.

While the total $\mathcal{H}$ is preserved in any adiabatic process, it is convenient to divide $\mathcal{H}$ into a kinetic energy term and a static enthalpy term H that might be measured by an observer moving locally in the average flow direction of the fluid*. For our purposes we will consider only the thermo-mechanical contributions to the internal energy (neglecting, for example, the gravitational term which is the major contributor to the description of a hydro-electric plant). Thus we write

$$\mathcal{H} = \frac{1}{2} mv^2 + H = \text{const} \qquad \text{(VI-5)}$$

with H being the thermodynamic potential tabulated in Section III. Here m is the mass of one mole and $\underline{v}$ is the velocity of flow.

An important concept in the theory of fluid mechanics is the "tube of flow", which is an imaginary pipe (of variable cross-section) whose bounding surface is made up of "stream lines" parallel to the local directions of flow (or, if there is turbulence, the local direction of average flow). If Eq. (VI-5) is differentiated along a streamline, one obtains

$$mvdv + dH = 0. \qquad \text{(VI-6)}$$

If the flow process is adiabatic and is either (i) reversible or (ii) takes place in a region of constant cross-section** it is possible to show that dH can be replaced by VdP to obtain the differential form of Bernoulli's Equation

$$mvdv + VdP = 0 \quad . \qquad \text{(VI-7)}$$

---

*This separation may be useless if the flow is turbulent on a sufficiently large scale.

**Flow through a shock front is an example of the latter.

Fundamentally (except for case (ii) where it is a restatement of the law of conservation of momentum) this is a specialized result, not a substitute for a proper statement of the First Law, which states that for an adiabatic process ($\Delta Q=0$) the external work is given by the change in enthalpy.

$$\Delta W = \Delta H \quad . \tag{VI-8}$$

Next, we trace the simple Rankine cycle on the H-S diagram on the assumption that all flows take place sufficiently slowly that there is no practical distinction between H and H.

Let us start at the output of the boiler at point (3) in Fig. 17. The mercury has been fully evaporated, until all that remains is droplet nuclei. The state of the fluid is saturated vapor. The fluid is led to a large, low-thermal-mass cylinder in which it expands isentropically doing work ΔH_{34} on the piston.

As a practical matter, the fluid does not expand to a fixed enthalpy as the figure suggests but to a fixed volume. If the fluid leaves the boiler at about 900°C and 200 atm pressure the required expansion in volume is about 150-fold, an order of magnitude greater than that used in Diesel engines. The expansion path from 3 to 4 is shown on an H vs. V diagram in Fig. 18. A real engine carrying out such an expansion would probably utilize multiple expansion in a sequence of cylinders of increasing bore and stroke.

Because the expansion is presumed to take place slowly, liquid condenses around the droplet nuclei as the fluid does work; the state of the fluid at the end of the expansion is part liquid, part vapor. The fluid is next led to a condenser where the reduction to liquid is completed.

Ideally, condensation takes place at constant temperature; the amount of heat that must be extracted at constant temperature is then

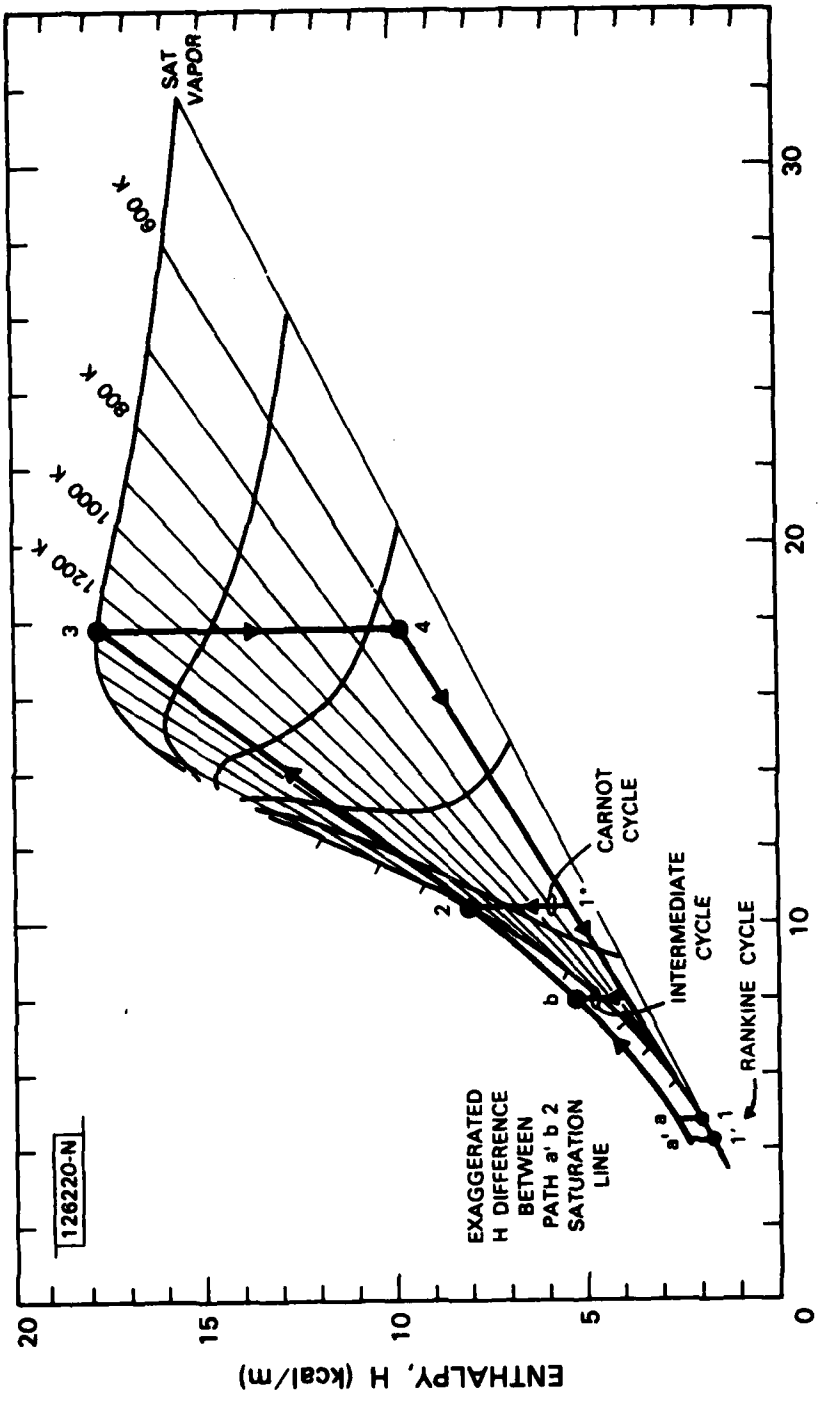

Fig. 17 Cycles on H-S diagram.

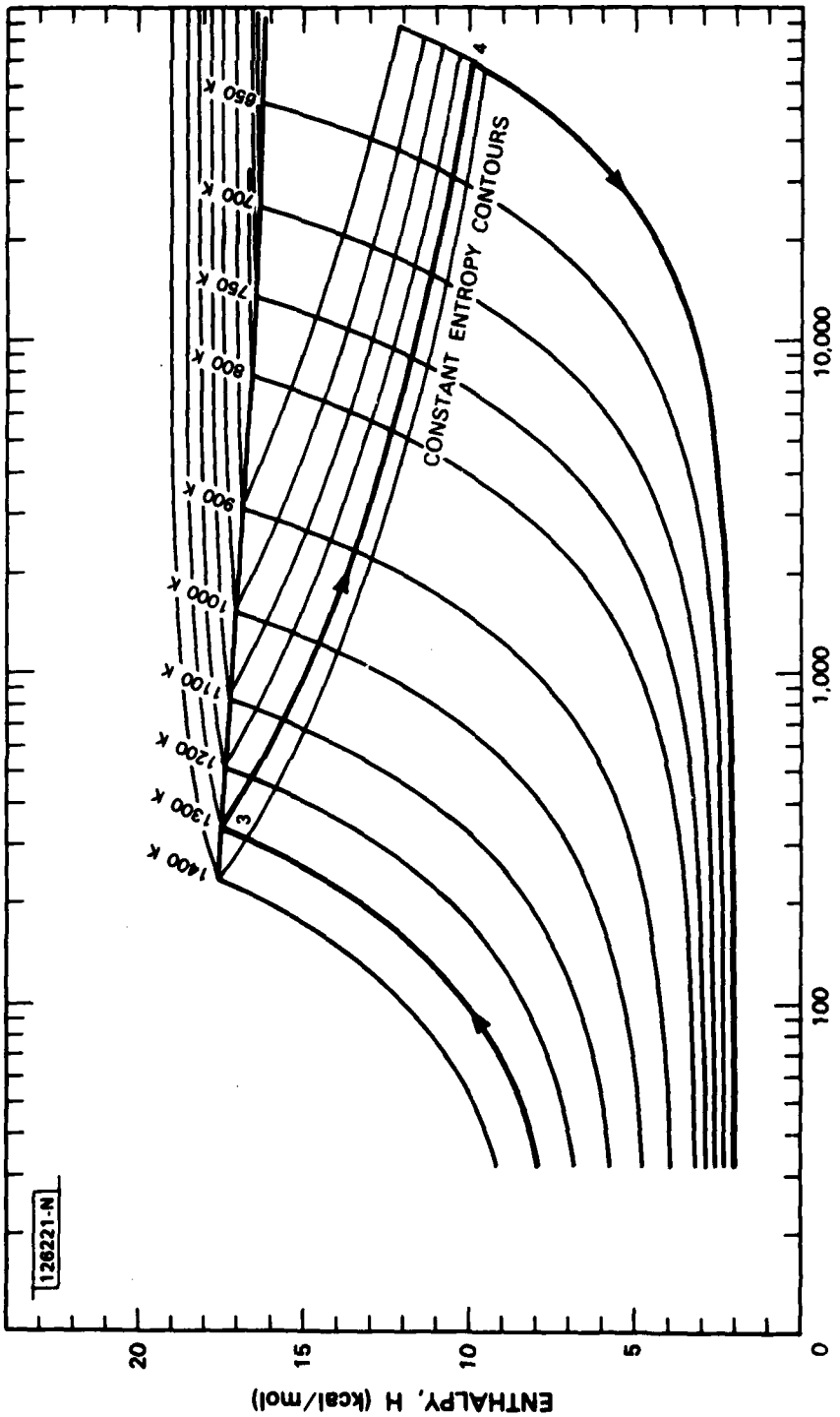

Fig. 18 Enthalpy-volume for Hg cycle.

$$\Delta Q_{41} = T\Delta S_{41} \quad . \tag{VI-9}$$

No net work is expected in the condenser. One can, of course, "prove" this from the Clausius-Clapeyron equation (see Section III) by demonstrating a change ΔH exactly equal and opposite to ΔQ in Eq. (VI-9). But this would be going the long way around. One can eliminate Q from explicit consideration in a constant temperature process by introducing the free energy G

$$G = H - TS \quad . \tag{VI-10}$$

For a <u>reversible</u> constant temperature process $\Delta(TS)$ is $T\Delta S$, which is ΔQ. Thus

$$\Delta W + \Delta G = 0 \quad . \tag{VI-11}$$

But two phases can be in equilibrium with one another only if there is no state of lower energy. It follows that both ΔW and ΔG are zero for condensation at equilibrium.*

As a practical matter, the temperature in the condenser will be somewhat lower than that at the piston outlet. As a result, the state at the inlet to the boiler feedpump moves from 1 to 1' at lower H and lower S (see Fig. 17). The result is that more heat must be discarded in the condenser (or supplied in the boiler) for a given useful output, ΔW_{34}, than would otherwise be the case.

In the feed pump, the condensed liquid is compressed adiabatically to somewhat above boiler pressure, to points a or a'. The higher pressure is necessary to overcome pressure loss in the atomizer nozzle.

---

*For constant temperature electrochemical reactions ΔG is not zero; the "work" which is available is then electrical.

Now, mercury is one of the most incompressible of fluids, dV/VdP amounting to only 5% per kilobar near the normal boiling point (630°K). There are two consequences of this fact. The first is that the power consumed by the feed pump is nominal - only a small fraction of RT_2 at the upper temperature as compared with a heat vaporization RT*, $T^* >> T_2$. More important is the fact that the trajectory of heating at constant pressure is nearly coincident with the liquid saturation line and is nearly parallel to it (see Appendix A, Eq. (A-8)).

As a result, the heat supplied by the highly irreversible heating of the cold injected liquid is nearly exactly the same as if the liquid had been heated reversibly along the saturation line. Because no work is being exchanged with the world outside the flow in the boiler, the heat supplied is simply ΔH.

There is slight work in going from 1 to an isotropically is ΔH_{1a}. (The change is exaggerated in Fig. 17.) Hence, the total energy supplied as work of compression and boiler heat is ΔU_{12}

$$\Delta U_{12} = \Delta H_{1a} + \Delta H_{a2} = \Delta H_{12} \quad . \tag{VI-12}$$

The final step in the boiler is the evaporation from 2 to 3, which requires heat of vaporization L_{23}.

In summary, the heat balance for the cycle is as follows:

Heat input:	$\Delta H_{a2} + L_{23}$
Work output:	$\Delta H_{34} - \Delta H_{1a}$
Heat discarded:	$\Delta H_{1a} + \Delta H_{a2} - \Delta H_{34}$
Efficiency:	$\dfrac{\Delta H_{34} - \Delta H_{1a}}{L_{23} + \Delta H_{12} - \Delta H_{1a}}$.

(VI-13)

Figure 19 shows efficiency vs. temperature for an 0.6 atm pressure condenser (600°K), calculated from the H-S diagram. At 1200°K boiler temperature, the Rankine efficiency (at 46%) is 92% of the Carnot efficiency.

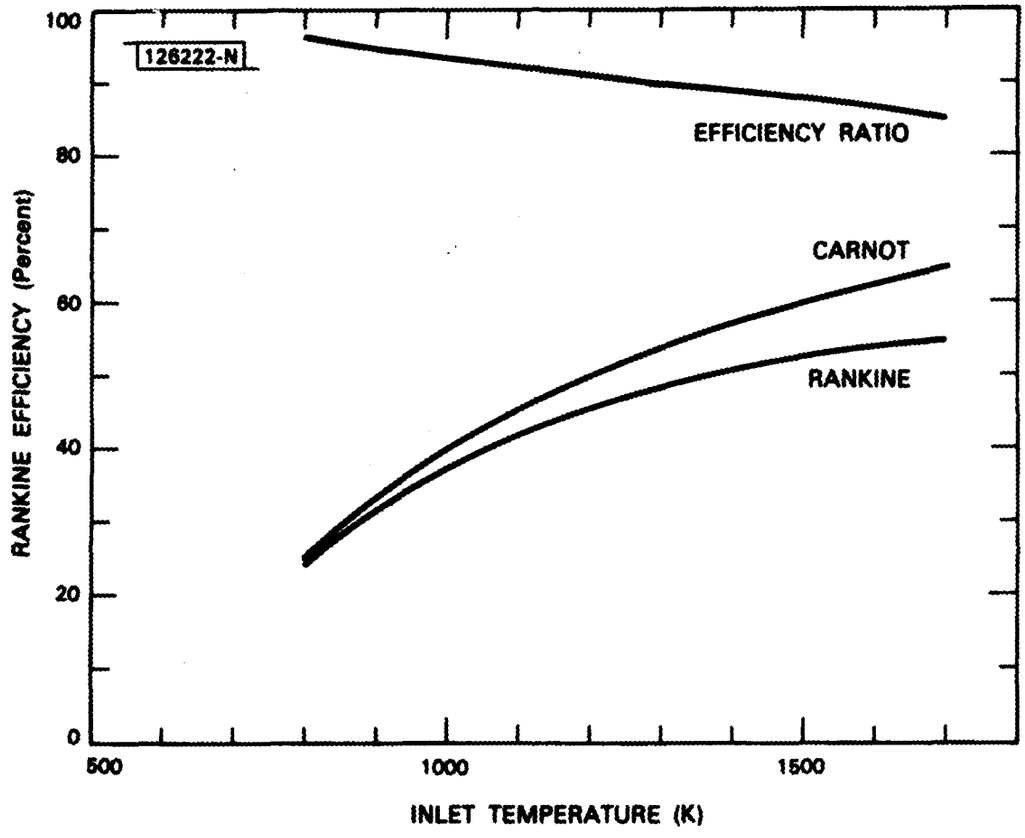

Fig. 19 Rankine efficiency mercury.

We may well inquire what happens if the fluid is not condensed all the way to liquid. If this is so, the point a is no longer at minimum H and S.

Instead, it moves from a point 1" on the condensation line to some point b along the trajectory a' ... a ... 2. In the limit, the point b coincides with point 2, and the isentropic compression 1*-2 is just what is required to complete a Carnot cycle, 1*-2-3-4-1*.

Such a Carnot cycle is indicated diagramatically in Fig. 20. The point O is the intersection of the projections of the boiling and condensation lines. For any isentropic compression 1"b", the net work out is $\Delta H_{34} - \Delta H_{1"b"}$. The heat supplied is $\Delta H_{03} - \Delta H_{0b"}$. It follows from similar triangles that the ratio of net output to net input, the Carnot efficiency, is independent of the position of the compression 1"b". Evidently, to the extent that the actual path of heating remains close to the projection O2, the cycle efficiency will be close to that of the ideal cycle even though the heating is irreversible.

As the point b (in Fig. 17) moves away from the Carnot cycle at point 2 towards the Rankine cycle at point a, the theoretical cycle efficiency drops slightly and the volumetric capacity of the feed pump drops dramatically. The effect of permitting roughly 5% of the vapor to remain uncondensed is shown by the intermediate curve in Fig. 21. This drop in required feed pump capacity tends to increase the practical efficiency, in that feedpumps are not perfectly efficient. The result is that the maximum actual efficiency may be reached between the Carnot and Rankine cycles, but rather closer to the latter than to the former.

The major result of this investigation of energy extraction in the static Rankine cycle is the recognition that the fluid need not be fully condensed, and that this incomplete condensation may be a theoretical advantage, requiring mainly an increase in the capacity of the feedpump. Alternately, a fixed-rate feedpump sized to handle some vapor along with the liquid can be used over a range of throughputs; the slack will be taken up by changes in the relative amount of vapor, and the cycle will adjust accordingly.

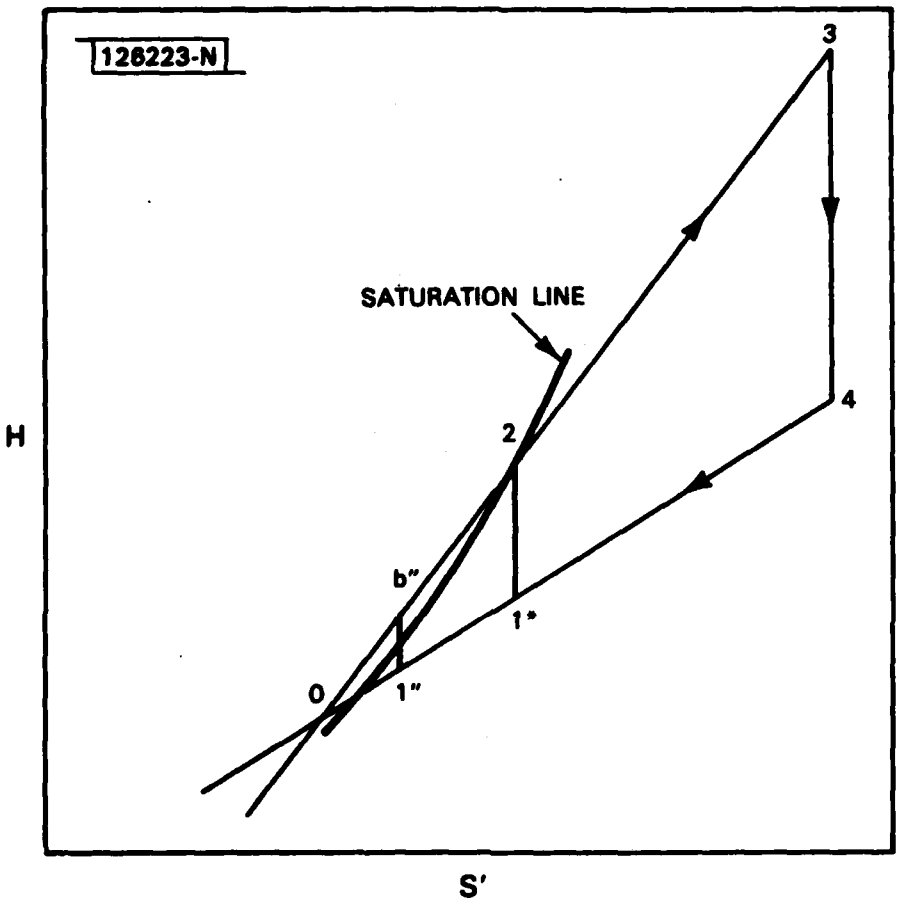

Fig. 20 Simplified cycle diagram.

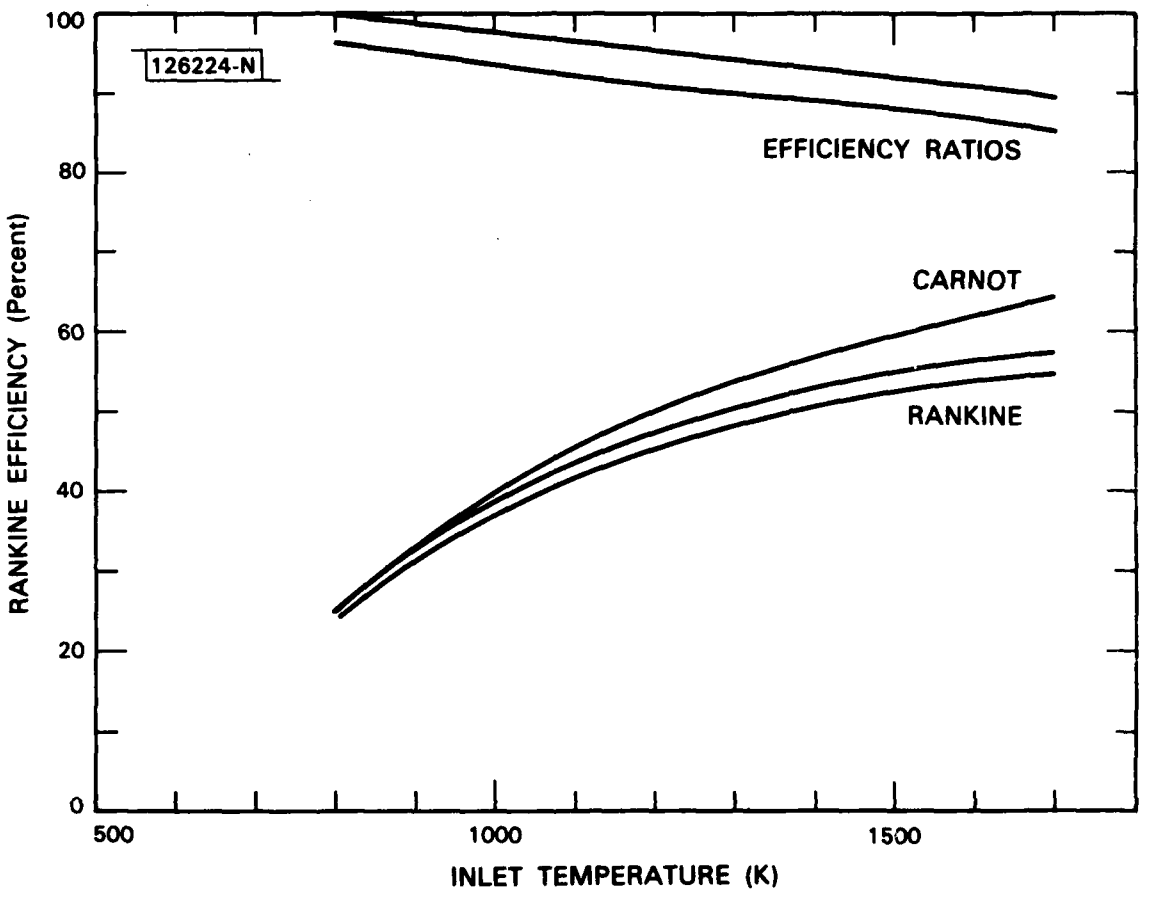

Fig. 21 Efficiency for several cycles.

VII. KINETIC ENERGY EXTRACTION I - DYNAMIC EQUILIBRIUM

Conceptually, the opposite extreme to the fluid doing work by slow expansion against a piston is the complete conversion of the available energy to kinetic energy of motion. The resulting fast-moving fluid stream the exerts force on a moving turbine blade by change of direction of momentum. In fact, energy can be extracted by both processes in the same machine. Nevertheless, turbines are basically high flow rate devices, so that one must understand what happens when a gas is moving fast enough so that internal compressibility can alter the flow (supersonic flow).

The advantage of the turbine is the high power density implied by the flow rate. For small power plants this energy density is perhaps too high, a fact which leads us to consider seriously supersonic flow within the turbine. With mercury, such flow is not limited to crossflow; the density of mercury is high enough to bring the speed of sound in the fluid well within the range of practical turbine blade speeds, 300 m/sec to 500 m/sec, so that supersonic flow parallel to the direction of blade motion is also practical. In this section, and the next, we continue to assume instantaneous equilibrium and homogeniety of the flow, except as it passes through a shock front. We deal here with three topics: energy extraction in an idealized turbine, its description on the H-S diagram, and the volumetric expansion ratios that are implied by the use of a condensing fluid.

A. The Turbine

The basic elements of turbine power extraction are:

1. A nozzle in which expansion results in the conversion of thermal energy to kinetic energy of flow, and
2. Moving reaction blades which extract energy from the flow by changing its direction.

The nominal operation of these elements is shown in Fig. 22.

The ultimate objective of blade design is to have the flow leave the blades in a direction opposite to the blade motion, and with as little

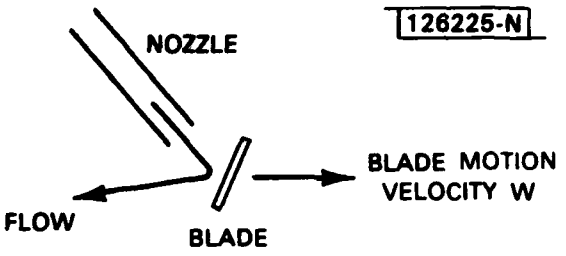

Fig. 22 Geometry of power extraction.

velocity as possible. In the process of changing direction, the fluid flow with velocity v_n at the nozzle has the blade velocity w vectorially subtracted from it twice: once as the flow approaches the blade, and once as the flow leaves the blade. Evidently, this double subtraction of the (fixed) blade velocity w will succeed in reducing the magnitude of v to low values in a single pass through the turbine only over a narrow spectrum of input velocities and output directions. Such a single-pass velocity reduction requires that w be comparable in magnitude with the original v_n, between 1/2 v_n (for nozzle flow parallel to the blade velocity) and v_n (for nozzle flow perpendicular to the blade velocity).

B. Dynamic Energy Extraction on the H-S Diagram

The apparent thermodynamics of energy extraction in the turbine depends on one's frame of reference, inasmuch as U and H depend on an observational definition of "at rest." If one takes a frame of reference on a nozzle fixed in position with respect to the boiler and condenser, H_n at the output of the

nozzle is the same at H_b at the output of the boiler. Work ΔW is extracted by the forces of changing momentum against the moving blades in the turbine, hopefully at constant entropy S. The H of the emerging fluid is $H_b - \Delta W$. The end result appears on the H-S diagram as a path identical with the path followed by the slowly expanding gas in a cylinder discussed in Section VI.

If one takes a reference point first on the nozzle, then on the turbine blades, and finally at the condenser, what one observes is a succession of stepwise constant-H processes:

H_b at the nozzle
An intermediate H on the turbine blades
$H_b - \Delta W$ at the condenser

In this case H changes in steps as reference changes, but otherwise the processes in the nozzle and in the turbine rotor appear to be constant-H processes.

These two uses of H indicate both the strength and the weakness of picking a thermodynamic variable that keeps track of only one parameter of a system. It does what is was supposed to do, and tells nothing else about the state of the system. In order to describe what is actually happening to the <u>fluid</u> (rather than the system energy) we must deal with H as defined in the previous Section,

$$H = H - 1/2\ mv^2 \quad . \qquad \text{(VII-1)}$$

If changes in potential energy in the gravitational or centrifugal force field were important, we would have to subtract such terms also.

In order to exhibit the details of what is happening to the fluid, as distinct from what is happening in the system, we must follow an element of fluid. For the fluid

$$\Delta H = \Delta U + \Delta PV = \Delta Q - \Delta W + \Delta PV \qquad \text{(VII-2)}$$

in which ΔQ, ΔW, and ΔPV are for the particular element of fluid. Even if the system heat exchange is zero and the system work done is zero, ΔQ and ΔW may not be zero individually. For example, some work ΔW can go into friction and be returned as heat ΔQ without affecting ΔH, but in the process S increases by ΔS

$$T_{eff}\,\Delta S = \Delta Q \qquad \text{(VII-3)}$$

in which T_{eff} is the effective temperature at which the frictional process occurs. Eventually, this increase in entropy will result in an additional amount of heat $T_{cond}\Delta S$ that has to be discarded at the condenser, heat which has to come from the available system work. The situation is shown on the H-S diagram in Fig. 23.

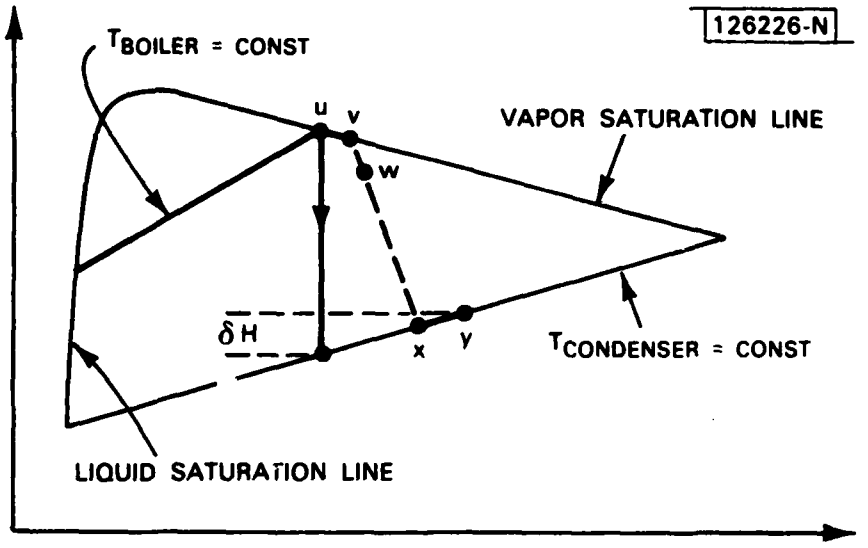

Fig. 23 Effect of entropy increases.

Ideally, fluid at the boiler output at u would do work reversibly and isentropically to point z on the condenser line, directly below u on the diagram. The figure shows four possible sources of entropy increase. Step uv represents fractional pressure drop between the boiler and the nozzle inlet. Step vw indicates the expansion between the nozzle inlet and its throat. Step wx is the expansion in the supersonic part of the nozzle; the increase in entropy is due to both friction and turbulence. Finally, as the fluid passes through the turbine, there will be additional friction and turbulence, resulting in a further increase in entropy to point y. The net result is a decrease δH in the available external work, and an exactly equal increase in the amount of heat that must be thrown away in the condenser.

The entropy increases shown in the figure are not intended to be to scale. The actual estimation of ΔS for paths uv and vw can be made from empirical friction coefficients to obtain ΔQ's, to be divided by the (well-determined) temperature in those regions. A similar calculation can be made for the path xy.

The increase in entropy along the major expansion path, w ... x, also depends on empirical data, but, for reasons that will emerge in Section X, it is not clear exactly what the state of the fluid will be at intermediate points along the path. Hence, it is not clear exactly what empirical data is applicable to the estimate.

If, indeed, the sum of all of the entropy increases is not modest in comparison with the entropy of condensation, then the cycle as a whole will be inefficient and not useful. Keeping these increases under control is a component design problem at a level of detail generally beyond the scope of our present discussion, although at key points we shall point to possible difficulties and make estimates to show that suitable control in design is feasible.

The path uvwxy is shown by dashed lines in the figure because we really do not know it. To the extent the end points are known, it is legitimate to assume any convenient intermediate path. Thus, if the path from u to y is reversible, or to the extent that the intermediate points are known, or to the extent that one may interpolate a path between points, one can write Eq. (VII-2) in differential form as*

$$dH = TdS + VdP \quad . \tag{VII-4}$$

The expression for $\partial H/\partial S$ at constant P comes from Eq. (VII-4) with dP set equal to zero. Differentiating Eq. (VII-1) along a line of flow yields

$$mvdv + dH = 0 \quad . \tag{VII-5}$$

Combining Eqs. (VII-4) and (VII-5) produces

$$mvdv + TdS + VdP = 0 \quad . \tag{VII-6}$$

Bernoulli's equation comes from Eq. (VII-6) by setting dS equal to zero. Inasmuch as V is m/ρ, ρ being the density of the fluid, an alternate form of Eq. (VII-6) is

$$\rho vdv + \frac{\rho}{m} TdS + dP = 0 \quad . \tag{VII-7}$$

Equations (VII-5), (VII-6) and (VII-7) as well as Eq. (VII-1) are the basis for our discussion of supersonic flow below. Generally, we will assume the effect of dS to be small, setting $dS \to 0$, with the effect of S to be added in

*The reduction uses dq=TdS, and dW=PdV. Eq. (VII-4) is an alternate thermodynamic definition of H.

later as a perturbation. In the case of supersonic shocks, the differential form of the equations cannot be used within the shock region; one estimates ΔS from the calculated initial and final states of the fluid.

C. Volumetric Implications Energy Extraction From A Fluid

As a gas emerges from a simple Rankine cycle boiler it is hot and highly compressed, but the molecules are nevertheless well-separated from the short range forces that held them together as a liquid. In the absence of condensation, such a vapor would very nearly obey the ideal gas law $PV = RT$. The maximum energy extractable per mole of such a gas (without additional input of heat) with a source at T_1 and heat rejection at T_2 is ΔH_{max}

$$\Delta H_{max} = \frac{\gamma}{\gamma-1} R(T_1 - T_2) \qquad \text{(VII-8)}$$

γ being the ratio of specific heats, which is 5/3 for monatomic mercury and 7/5 for polyatomic air.

In order to extract the energy ΔH using ideal gas expansion requires that the volume increase in the expansion ratio E

$$E = (T_1/T_2)^{1/(\gamma-1)} \quad . \qquad \text{(VII-9)}$$

For a 50% yield of available ΔH, T_1/T_2 would be 1/2. The expansion ratio for air would be 1 to 10; but for dry mercury the corresponding ratio is only 1 to 3.

The maximum energy extractable from an ideal gas (per mole) starting at temperature T_1 is found by setting $T_2 = 0$ in Eq. (VII-8). For dry H_2O and dry Hg starting at about 1200°K, this energy is roughly 8 kcal/mol and 6 kcal/mol, respectively. If the gas is able to condense as it expands, the condensation adds latent heat L to the available energy, in the amount of roughly 10 kcal/mol for water and 14 kcal/mol for Hg, so that the total is about 18 kcal/mol for each.

Since the condensing gas starts from the same initial conditions of pressure and volume as the (hypothetical) ideal dry gas, the final volume must be greater in order that the extra work be extracted as $\int PdV$.

The volume expansion for the condensing fluid must be calculated by the specialized methods discussed in Section III. For a fluid that begins its condensation on, or within, the gas saturation line, the isentropic expansion ratio between initial temperature T_1 and final temperature T_2 is

$$E \doteq \frac{T_2}{T_1} \exp\left[\frac{T^*}{T_2} - \frac{T^*}{T_1}\right] \qquad \text{(VII-10)}$$

where T* is the activation temperature for the pressure law, being about 7200K for mercury.

Figure 24 gives a logP vs. logV plot for condensing mercury, with several constant-S trajectories noted. The volume expansion for T_2/T_1 equal to 1/2 has risen from 1 to 3 for the dry gas to 1 to about 150 for the condensing vapor, while the available work per mole has risen from about 3 kcal to about 8 kcal on the H-S diagram.

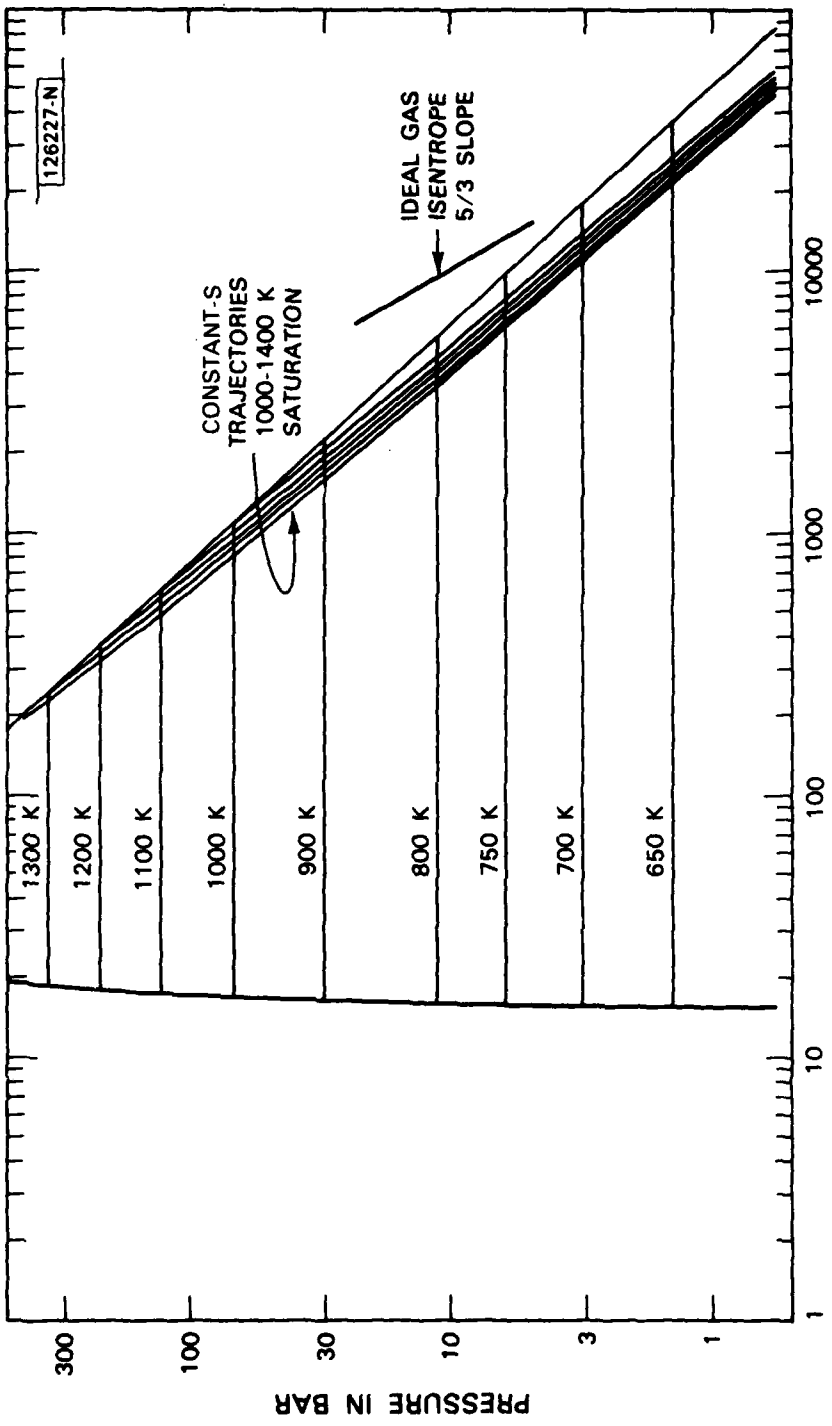

Fig. 24 Condensation paths on P-V diagram.

VIII. KINETIC ENERGY EXTRACTION II -- SUPERSONIC ENERGY FLOW

It is almost axiomatic that the conversion into kinetic energy of a majority of the heat content H of a compressible fluid requires supersonic flow. In this section, five topics are considered: the need for multiple-pass energy extraction if the flow is to be everywhere subsonic, the possibility of single-pass extraction with supersonic flow, the use of normal shocks and re-expansion to return the flow to the subsonic regime to turn it around as required for energy extraction, a demonstration of the plausibility of so turning a wholly supersonic flow at high Mach number, and a consideration of reversible expansion of wet vapor in a nozzle.

A. Speed of Sound and Multipass Subsonic Extraction of Energy

The local velocity of sound $\underline{a}$ is defined at constant entropy

$$a^2 = \left.\frac{\partial P}{\partial \rho}\right|_S \qquad \text{(VIII-1)}$$

Both $\underline{a}$ and H tend to be monotonic functions of temperature. Hence, as H drops because of a speed-up of flow, the temperature drops and $\underline{a}$ drops also. Thus a^2 can be considered to be a monotonic decreasing function of v^2, the square of the speed of flow*. On this basis, one can identify a number of corresponding speeds, as in the following Table VIII-1.

In order of decreasing magnitude, the relative sizes of the critical table entries are

$$v_{max} > a_o > a^* \quad . \qquad \text{(VIII-2)}$$

For an ideal gas, a_o and a^* are given by formulas:

---

* These velocities generally appear as squares in energy calculations. Obviously, $\underline{a}$ is also a monotonic decreasing function of v for v and a both greater than zero.

TABLE VIII-I

FLOW REGIMES

Flow Speed v	Sound Speed a	Explanation
0	a_o	speed of sound in stationary fluid
$v < a^*$	$a > a^*$	subsonic flow
v^*	a^*	speed of flow and speed of sound are equal, $v^* = a^*$
$v > v^*$	$a < a^*$	supersonic flow
v_{max}	0	all of energy H converted to kinetic energy at v_{max}

$$ma_o^2 = \gamma RT_1 \qquad \text{(VIII-3)}$$

$$ma^{*2} = (2\gamma/\gamma+1)\ RT_1 \qquad \text{(VIII-4)}$$

in which γ is the ratio of specific heats and T_1 is the rest temperature of the gas. For a non-ideal-gas fluid, a^2 can be calculated by finding $\partial\rho/\partial T$ and $\partial P/\partial T$ (both at constant S) and by then taking the ratio. Figure 9, reproduced here as Fig. 25, was constructed in that fashion. Another means of obtaining a^2 for a non-ideal-gas fluid is to find $V\partial H/\partial V|_S$, which is thermodynamically proportional to ma^2.*

Mach number M at any speed v is defined as v/a. Inasmuch as a→0 for $v \to v_{max}$, the Mach number at v_{max} is infinite. The specific Mach number M* is defined as v/a*. It remains finite as $v \to v_{max}$. Kinetic energy can always be written in terms of M*, since division by a* is mere normalization. For an ideal gas the kinetic energy is

$$KE = \frac{1}{2}\, mv^2 = \frac{\gamma}{\gamma + 1}\, M^{*2}\, RT_1 \qquad \text{(VIII-5)}$$

If this expression is combined with Eq. (VII-8) of the previous Section, with the condenser temperature T_2 set to zero, there results an expression for the maximum fraction $\underline{f}$ of thermal energy that can be extracted as kinetic energy in subsonic flow ($M \leq 1$):

$$f = \frac{\gamma - 1}{\gamma + 1} \qquad \text{(VIII-6)}$$

If one wishes to avoid the complications of supersonic flow with boiler-to-condenser temperature ratio T_1T_2 greater than $(\gamma+1)/2$, it is necessary to use several successive expansions and passages through turbine blades, extracting as most f in the first stage, f(1-f) in the second stage, and so on.

---

*As a check, we have obtained a^2 by the second method numerically and compared it with the result of the first method in the parameter range used in Fig. 31. The results were consistent to 3 significant figures.

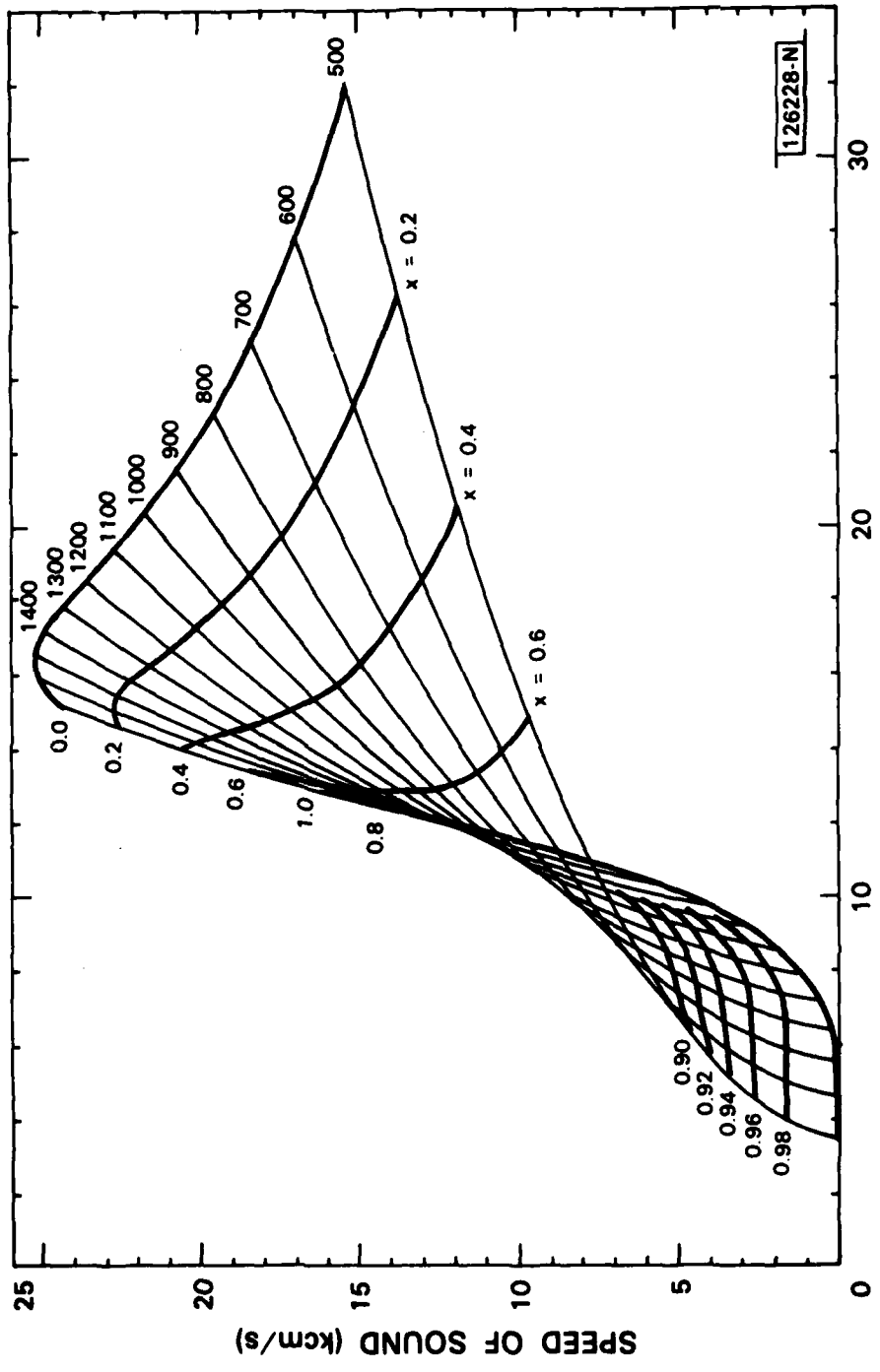

Fig. 25 Speed of sound mercury.

For a condensing vapor, f is much lower than for the corresponding ideal dry gas. Consider the energy which could be developed by expanding saturated vapor from boiler T_1 to condenser T_2. Let f_{12} designate the fraction of that energy which is available as kinetic energy of subsonic flow. Then Fig. 26 gives f_{12} for several values of nozzle inlet (boiler) and outlet (condenser) temperatures. For inlet and condenser temperatures of 1200K and 600K, respectively, f is 1/6, implying at least six stages of turbine expansion; more likely, the practical number would approach a dozen.

A dozen stages of turbine expansion would not be unrealistic for central station power plants. Similar numbers of expansion stages are used now in central station steam turbines, for a variety of (other) practical reasons. The main engineering problem would be to remove and recycle the low-entropy energy of the roughly 5% droplet content at the inlet of each turbine stage, so that only dry vapor would pass through the blades (see also Sections IX and X).

For energy conversion on the 5 to 100 kW scale, such as might be suitable for use in orbit (or in an automotive power plant) the throat dimensions of a subsonic nozzle become so small that one is forced to consider single stage expansion with supersonic flow through the turbine. At 200 atm and 200 m/sec, the power density is 100 kW/cm^2. In the central power station, such densities are welcome (100 MW per sq. ft. of cross-section); but they imply a 5 kW power plant that looks and runs more like a water wheel than like the conventional turbine with nozzles and around its entire periphery.

B. Supersonic Flow

Supersonic flow differs from ordinary subsonic flow mainly in that it cannot slow down reversibly. Any slowing down necessarily takes place through a shock front, because there is no way for a disturbance to propagate upstream to tell the onrushing fluid to slow down before it gets to the pile-up. Flow normal to a shock front always makes a transition back to subsonic flow; so, too, does the component of supersonic flow (at some other angle) normal to such a front.

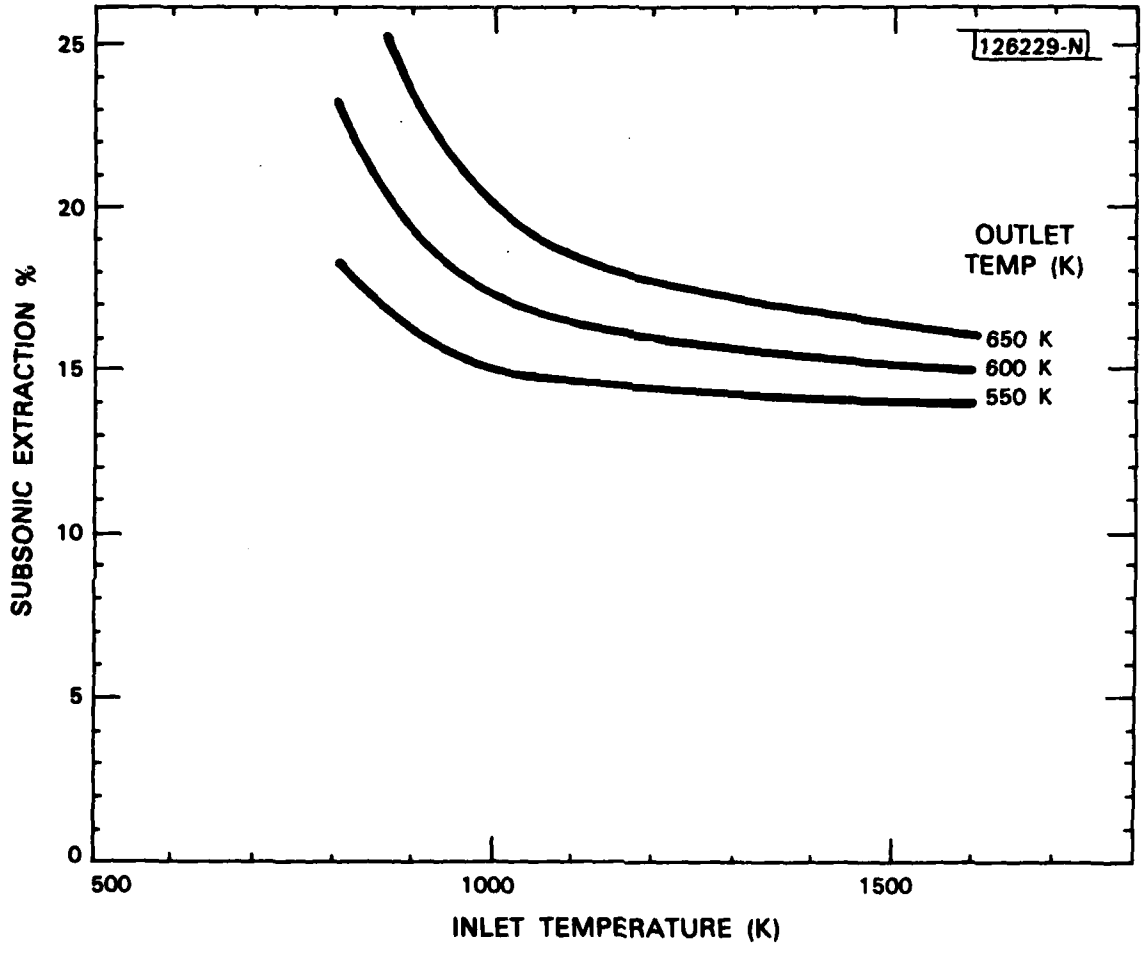

Fig. 26 Subsonic energy fraction.

The main difficulty with supersonic flow is in getting it to go around corners without losing in large entropy increases its capability for doing useful work. There are two ways of so doing. The first is to bring the flow back to subsonic flow through a normal shock. The subsonic flow can then be turned around the corner and re-expanded. (This process uses the turbine blades as secondary nozzles.) The second is to make the turn gradually, so that the flow considered as buckshot moving in a straight line does not meet a wall at greater than some modest angle α.

The first procedure implies high temperature in the subsonic flow region, and a larger volume expansion at the exit nozzle than at the shock compression, on account of the entropy increase. The second procedure is only nominally low temperature because the flow next to the confining walls must stagnate (see Section X). However, the gas-dynamic pressures are much lower than behind the shock. In fact, precautions associated with both methods must be practiced for each, because of the presence of high density droplets within the vapor if it is wet.

In the final part of this section we shall consider reversible expansion in a nozzle in which there is an opportunity for the gas to reach an equilibrium with the droplets of liquid it carries with it as a wet vapor. In the next section we shall consider gas and droplets as separate, interacting flows. But the time required for such interactions turns out to be long compared with the transit time through a shock front. As a result, we can assume in this section "frozen disequilibrium" in which droplets and gas constitute separate non-interacting flows beyond the main expansion nozzle. We shall consider only the dry part of the vapor; it can be considered to be accurately modelled as an ideal monatomic gas.

In assessing the practicality of using supersonic flow in mercury (as distinct from much lighter fluids), it is important to recognize the benign orders of magnitude involved. In Sections IV and VI we found on the H-S diagram an available enthalpy of output work of 7 to 8 kcal/mol for boiler

temperatures ranging from 1000° to 1500°K, and condenser temperatures in the range 550° to 600°K. If such amounts of energy are turned into kinetic energy of mercury, the resulting fluid velocity ranges from 530 to 560 m/sec, which is comparable with the state-of-the art in the peripheral speeds of commercial steam turbines.

In Section VII we noted that the ideal turbine speed for single-pass energy extraction is v/2, one half the nozzle exit velocity, when the nozzle flow is nearly parallel to the direction of turbine motion. If the nozzle flow makes an angle θ with the turbine motion, the factor 2 in the denominator is replaced by $1 + \cos\theta$, not much of a change for realistic θ. As a result, the ideal turbine speed for single-pass removal of all of the kinetic energy is well within the state-of-the-art in turbine construction, a situation unique to mercury as a practical working fluid.

It is important to recognize that the ideal turbine speed is a change-of-momentum result based on assumptions of reversible flow and no external pressure differential between the inlet and outlet sides of the turbine. The result is not affected by the compressibility of the gas. Equation (VII-6) valid for general fluid flow, is

$$mvdv + TdS + VdP = 0 \quad . \qquad \text{(VIII-7)}$$

(Recall that in this case $\underline{v}$ is streamline velocity, not vector velocity.) If we consider states at wheel inlet and exit (in the frame of reference of the wheel) for which dP is zero and for which dS is zero, the net change dv in streamline velocity must also be zero. The momentum mv can thus only change direction (in that reference frame) between inlet and outlet, regardless of what happens in between. Finite dS modifies the result slightly, as would a finite dP sustained by friction and tight clearances. Thus the optimum speed in a detailed design might differ slightly from the ideal $v/(1+\cos\theta)$, but not by very much. Here, we shall continue to use v/2 as typical of single-pass kinetic energy conversion.

At 600°K condenser temperature, the speed of sound in dry mercury is about 200 m/sec. Thus the Mach number of the fully expanded flow is roughly 2.8 (the corresponding M* is 1.71). The ideal turbine running at one-half the nozzle exit speed sees an approaching flow at Mach 1.4 (with M* at 1.26). The practical problem of turbine design is to actually turn the flow through roughly 180° - θ, so as to force the exit momentum (in the frame of the nozzle) and kinetic energy toward zero without incurring unacceptable pressure rises or entropy increases (both of which reduce the work output).

C. Flow Through Normal Shock

To actually turn the flow, the first possibility to be investigated is that the supersonic flow is choked by passing through a thin shock front perpendicular to the direction of flow. The flow emerging from the shock layer is subsonic. Such a flow can then be turned without further complications from compressibility effects. It is then re-expanded to supersonic flow at entrance pressure as it leaves the turbine.

Let us then consider a supersonic flow in a straight channel that encounters a transition layer perpendicular to the flow, in which, over an infinitesimal distance*, the velocity drops to a subsonic value, accompanied by increases in pressure, density, and temperature. For any given mass flow rate such a transition is always possible (part E below); the subsonic flow has the higher entropy and is therefore stable.

The enthalpy H is the same as both sides of the shock (no exchange of work or heat with the conforming channel). For an ideal gas, the critical velocity a* is therefore the same on both sides of the shock (to the extent that $a^*(H,S)$ varies only slightly with S in a non-ideal fluid, a* will be preserved across the shock for such a fluid also). For an ideal gas, elementary textbook formulas relate the supersonic M* and the subsonic $\hat{M}^*$ on the far side of the shock[14,15]

* The actual width is governed by diffusion phenomena beyond the scope of this discussion.

AD-A129 016 A HIGH PRESSURE MERCURY TURBINE CYCLE FOR USE IN SPACECRAFT AND TERRESTRI..(U) MASSACHUSETTS INST OF TECH LEXINGTON LINCOLN LAB R M LERNER 22 MAR 83 TR-577

UNCLASSIFIED ESD-TR-82-176 F19628-80-C-0002 F/G 13/2. NL

2/3

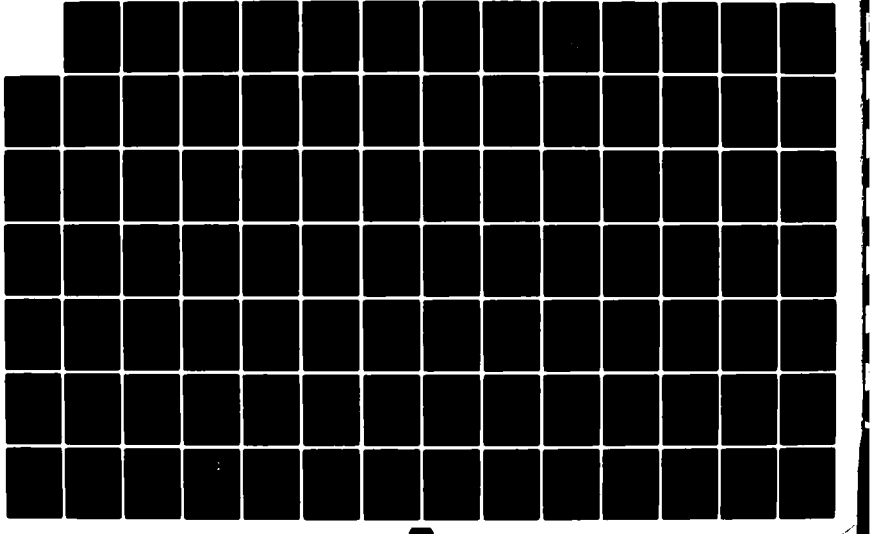

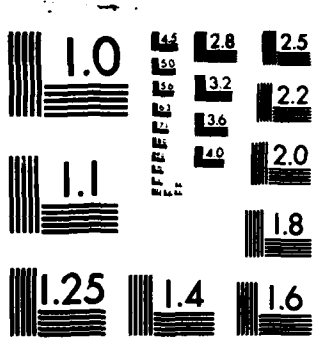

$$M^* \hat{M}^* = 1 \quad . \tag{VIII-8}$$

Continuity of mass flow through the shock then gives for the velocity and density ratios $v/\hat{v}$ and $\hat{\rho}/\rho$

$$v/\hat{v} = \hat{\rho}/\rho = E = M^{*2} \quad . \tag{VIII-9}$$

in which a carat over a symbol indicates the subsonic side of the shock. Because there is no time for the droplet component of the wet vapor to interact with the compressible gas component in, and just downstream of, the shock we make the "frozen disequilibrium" assumption and treat the dry gas as if it were ideal with no droplets present. This assumption justifies the use of formulas (VIII-8) and (VIII-9) for a shock in mercury vapor.

Textbooks[14] also give an ideal-gas formula for the pressure rise

$$\hat{P}/P = \frac{(\gamma + 1)E - (\gamma - 1)}{(\gamma + 1) - (\gamma - 1)E} \tag{VIII-10}$$

and discuss the problems of defining γ in such a way that formulas such as Eq. (VIII-10) remain valid for non-ideal gases[15].

Finally, from the ideal gas equation $PV = RT$, and remembering that E is M^{*2}, one can obtain $\hat{T}/T$:

$$\hat{T}/T = (\hat{P}/P)\,(\rho/\hat{\rho}) = \frac{(\gamma + 1) - (\gamma - 1)/M^{*2}}{(\gamma + 1) - (\gamma - 1)M^{*2}} \quad . \tag{VIII-11}$$

One interpretation of formulas (VIII-10) and (VIII-11) is to say that the pressure (and temperature) rise becomes infinite as the density (or velocity) ratio E approaches $(\gamma+1)/(\gamma-1)$. The truth is quite the other way around. E can approach this limiting value only as $M \to \infty$.

What we need to do next is to compare the shock pressure and volume ratios for a given $\hat{T}/T$ with those that might have accompanies a reversible deceleration which consumed the same kinetic energy and consequently produced the same temperature rise. For such a deceleration, the ratios P/P and ρ/ρ are given by isentropic formulas

$$\hat{P}/P = (\hat{T}/T)^{\gamma/(\gamma-1)}$$

$$\hat{\rho}/\rho = (\hat{T}/T)^{1/(\gamma-1)} \qquad \text{(VIII-12)}$$

The pressure and density ratios given by the isentropic formulas are generally larger than those for the shock. (For a monatomic gas the shock density ratio is limited to 4, and the shock pressure ratio to 4 times the temperature ratio.) The relatively expanded state of the gas behind the shock is accompanied by an increase in entropy ΔS with respect to reversible compression:

$$\Delta S = \left[\frac{\gamma}{\gamma - 1} \ell n \frac{\hat{T}}{\bar{T}} - \ell n \frac{\hat{P}}{\bar{P}}\right] R \qquad \text{(VIII-13)}$$

Now suppose that the subsonic flow behind the shock is turned through the required $180°-\theta$ angle. Further, suppose that the subsonic gas be re-expanded in a reversible nozzle to condenser temperature T before being exhausted from the channel. An amount of energy $T\Delta S$ that had been recoverable as useful work from the original flow must be discarded instead as heat to the condenser, $T\Delta S$ also being the work done in compressing the exhaust at temperature T back to outlet pressure P.

The accompanying Table VIII-II gives $T\Delta S$ as a percentage fraction of the original flow kinetic energy at Mach number M, as well as listing the

TABLE VIII-II
PARAMETERS OF NORMAL SHOCK

Gamma = 1.67

M	M*	Esh	Psh	Tsh	S-So	%TS/KE
1.0	1.00	1.00	1.00	1.00	0.00.....	
1.2	1.14	1.30	1.55	1.19	0.01	1.37
1.4	1.26	1.58	2.20	1.39	0.08	3.89
1.6	1.36	1.84	2.95	1.60	0.19	6.38
1.8	1.44	2.08	3.80	1.83	0.35	8.45
2.0	1.51	2.29	4.75	2.08	0.54	10.04
2.2	1.57	2.47	5.80	2.35	0.75	11.18
2.4	1.62	2.63	6.95	2.64	0.97	11.95
2.6	1.66	2.77	8.20	2.96	1.21	12.42
2.8	1.70	2.89	9.55	3.30	1.45	12.67
3.0	1.73	3.00	11.00	3.67	1.69	12.75
3.2	1.76	3.09	12.55	4.06	1.93	12.71
3.4	1.78	3.18	14.20	4.47	2.17	12.57
3.6	1.80	3.25	15.95	4.91	2.40	12.37
3.8	1.82	3.31	17.80	5.37	2.63	12.12
4.0	1.84	3.37	19.75	5.86	2.86	11.83
4.2	1.85	3.42	21.80	6.38	3.08	11.53

Gamma = 1.40

M	M*	Esh	Psh	Tsh	S-So	%TS/KE
1.0	1.00	1.00	1.00	1.00	0.00.....	
1.2	1.16	1.34	1.51	1.13	0.01	1.61
1.4	1.30	1.69	2.12	1.25	0.08	4.79
1.6	1.43	2.03	2.82	1.39	0.22	8.15
1.8	1.54	2.36	3.61	1.53	0.41	11.15
2.0	1.63	2.67	4.50	1.69	0.65	13.60
2.2	1.72	2.95	5.48	1.86	0.92	15.51
2.4	1.79	3.21	6.55	2.04	1.22	16.92
2.6	1.86	3.45	7.72	2.24	1.54	17.91
2.8	1.91	3.66	8.98	2.45	1.87	18.57
3.0	1.96	3.86	10.33	2.68	2.21	18.95
3.2	2.01	4.03	11.78	2.92	2.55	19.12
3.4	2.05	4.19	13.32	3.18	2.90	19.13
3.6	2.08	4.33	14.95	3.45	3.24	19.02
3.8	2.11	4.46	16.68	3.74	3.58	18.80
4.0	2.14	4.57	18.50	4.05	3.92	18.52
4.2	2.16	4.67	20.41	4.37	4.25	18.18

corresponding values of E, $\hat{P}/P$, and $\hat{T}/T$. For a Mach 2.8 initial flow, the Table gives $\hat{T}/T$ at 3.3. Where such a flow impinges on a blocked turbine rotor, stagnation temperatures ranging up to 2000°K can be expected. For a relative inlet velocity of M 1.4 at the moving blades, $\hat{T}/T$ is 1.39 so that if T is 600°K, $\hat{T}$ is roughly 835°K.

A remarkable feature of the Table is the low fraction - a maximum of 13% - of the kinetic energy that becomes fundamentally not recoverable on account of the irreversibility of the shock. This fraction is shown in graphical form as a function of M for two gases - monatomic (mercury) and diatomic (air) in Fig. 27. Evidently, the monatomic gas is superior in having a lower fraction of irreversibility in normal shock.

Figure 28 traces on the H-S diagram vapor leaving the boiler at 1200°K through expansion, presumed demisting, subsequent shock to superheat, and subsequent energy extraction with a condenser temperature at 600°K. The first equilibrium expansion from A to B gives a ΔH of roughly 7.2 kcal/mol as kinetic energy of flow, 40% of which is in the form of droplets. We assume that the droplets are put to one side (their energy, which is 40% of the total, to be extracted by other means).* The dry vapor is still moving with a kinetic energy of ΔH_{AB} per mole of vapor, at point C. If it were to be decelerated reversibly, with the conversion of nearly all of the kinetic energy back to heat, the compression would take place at constant entropy to point D. Instead, the compression goes irreversibly to point E at the same temperature (about 1800°K), with an increase in entropy ΔS of about 1.3 cal/mol deg K.

The diagram shows the continuation of the condenser pressure and constant temperature trajectories from 500°K boiling into the superheat

* This is the assumption of "frozen disequilibrium" referred to earlier.

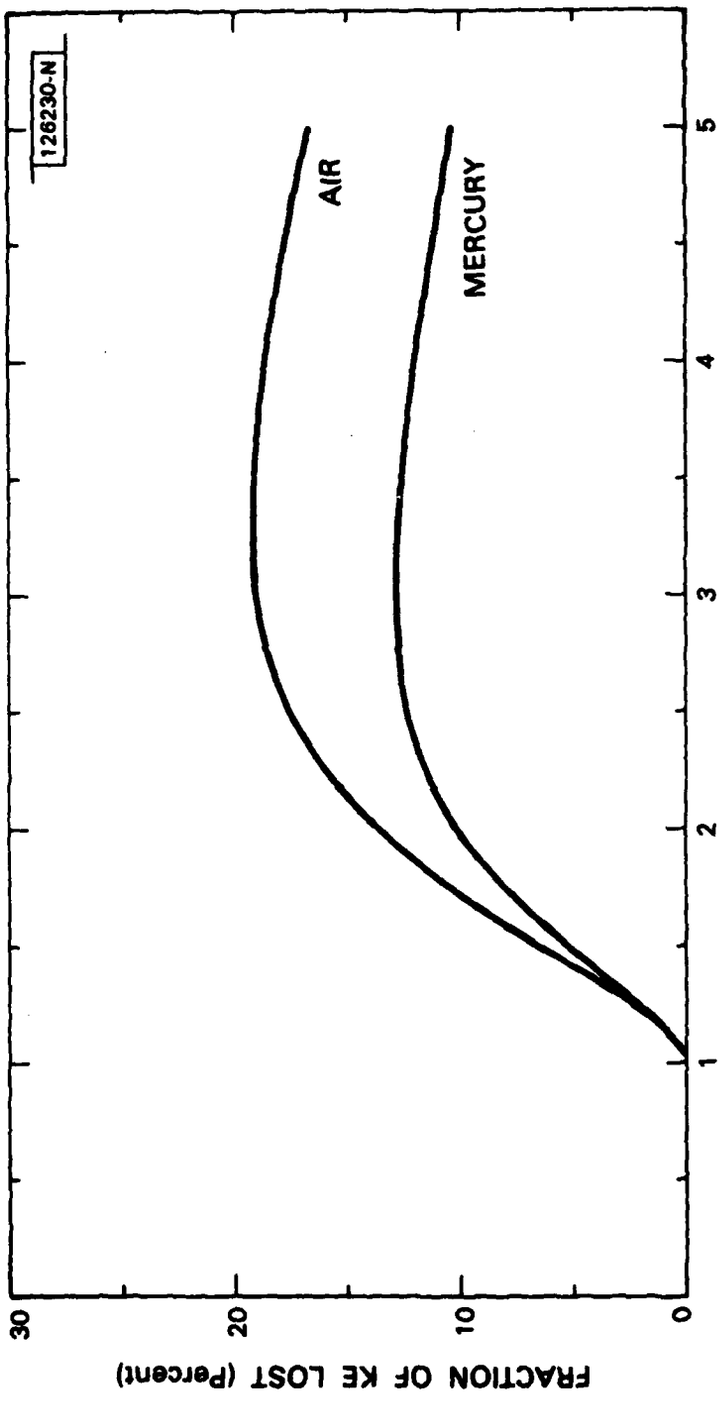

Fig. 27 Irreversible loss in K.E. for Hg and air in normal shock.

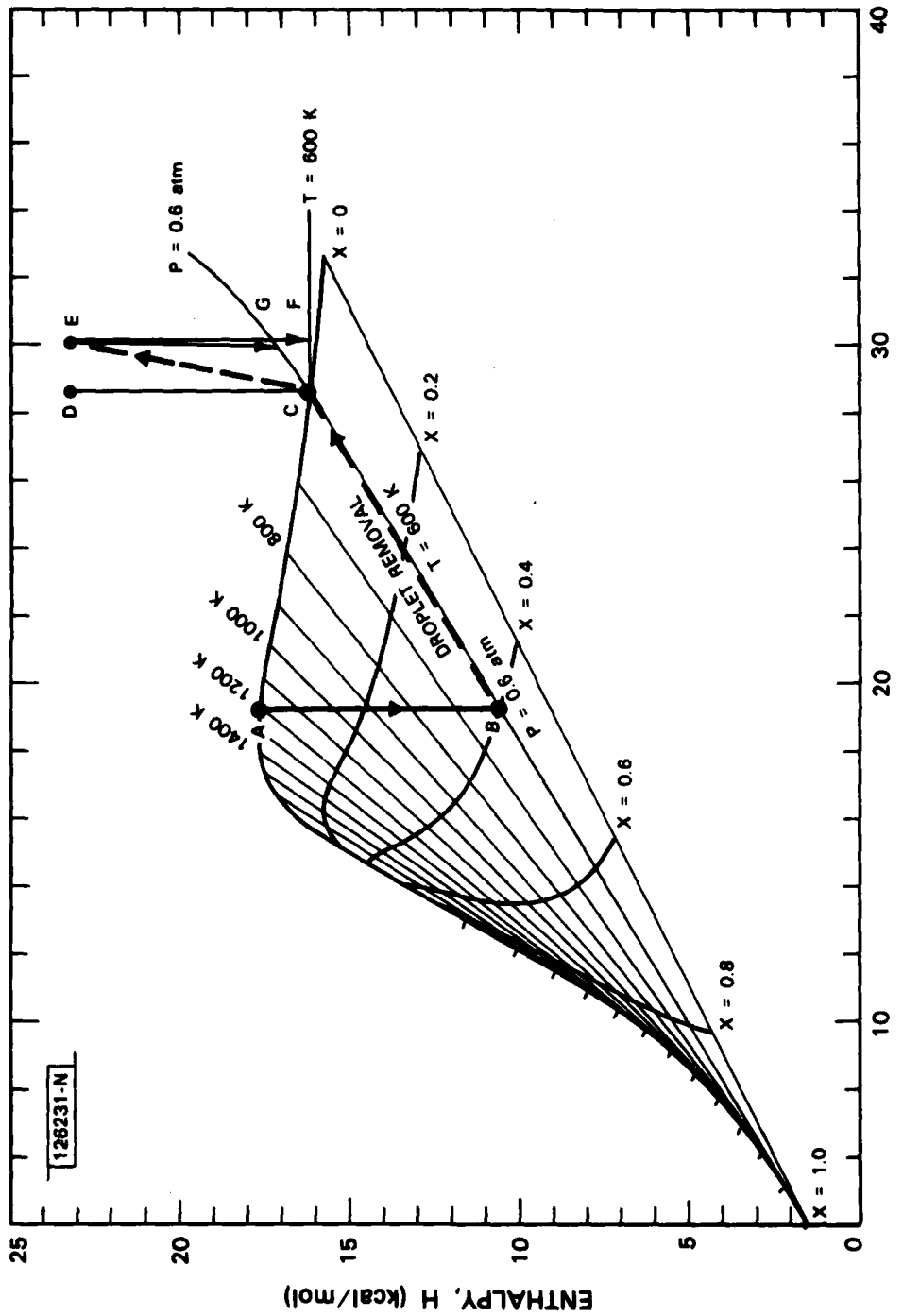

Fig. 28 Effect of shock on fluid state in H-S diagram.

region on an ideal gas basis (amply justified at these temperatures and pressures). All of the reheat enthalpy is extractable as work by isentropic expansion to 600°K along EF. But now the gas at point F is at a lower pressure than the condenser. Work $T\Delta s$ at T equal to 600°K must be done on the gas to get it back to condenser pressure. This work must come from the output enthalpy ΔH_{EF}. A simple means of accomplishing the desired result is to stop the output work expansion at point G, where the pressure is the same as that in the condenser, even if the temperature is a little higher. The work lost is ΔH_{GF} which is slightly greater than $T\Delta S$ because the average temperature along the trajectory P=const is somewhat greater than T:

$$dH = TdS \quad , \qquad dP = 0 \quad . \tag{VIII-14}$$

Figure 28 is drawn approximately to scale. The entropy change is significant. According to Table VIII-II the loss in the available kinetic energy of the gas is roughly 12%.

For flow within the half-speed turbine wheel, the situaton is qualitatively quantitatively different. The kinetic energy flow into the wheel is at only half speed but at the same flow temperature. Thus the enthalpy increase in the shock is at most one-quarter of ΔH_{AB}. On the scale of Fig. 29, the increase in entropy is almost below plotting accuracy. For all practical purposes, points D and E have coalesced, as have points C, F, and G. The overall loss due to entropy increase is less than 4% of the gas flow energy within the turbine, or less than 1% of the kinetic energy of the gas leaving the stationary nozzle.

D. Gradual Turning of Hypersonic Flow

For a single-pass turbine wheel operating at speed, normal shock to subsonic flow is a practical possibility, in terms of entropy penalty and in terms of temperature reached in the shock. If the turbine speed is slow, as it inevitably must be at start-up, the temperatures and pressures

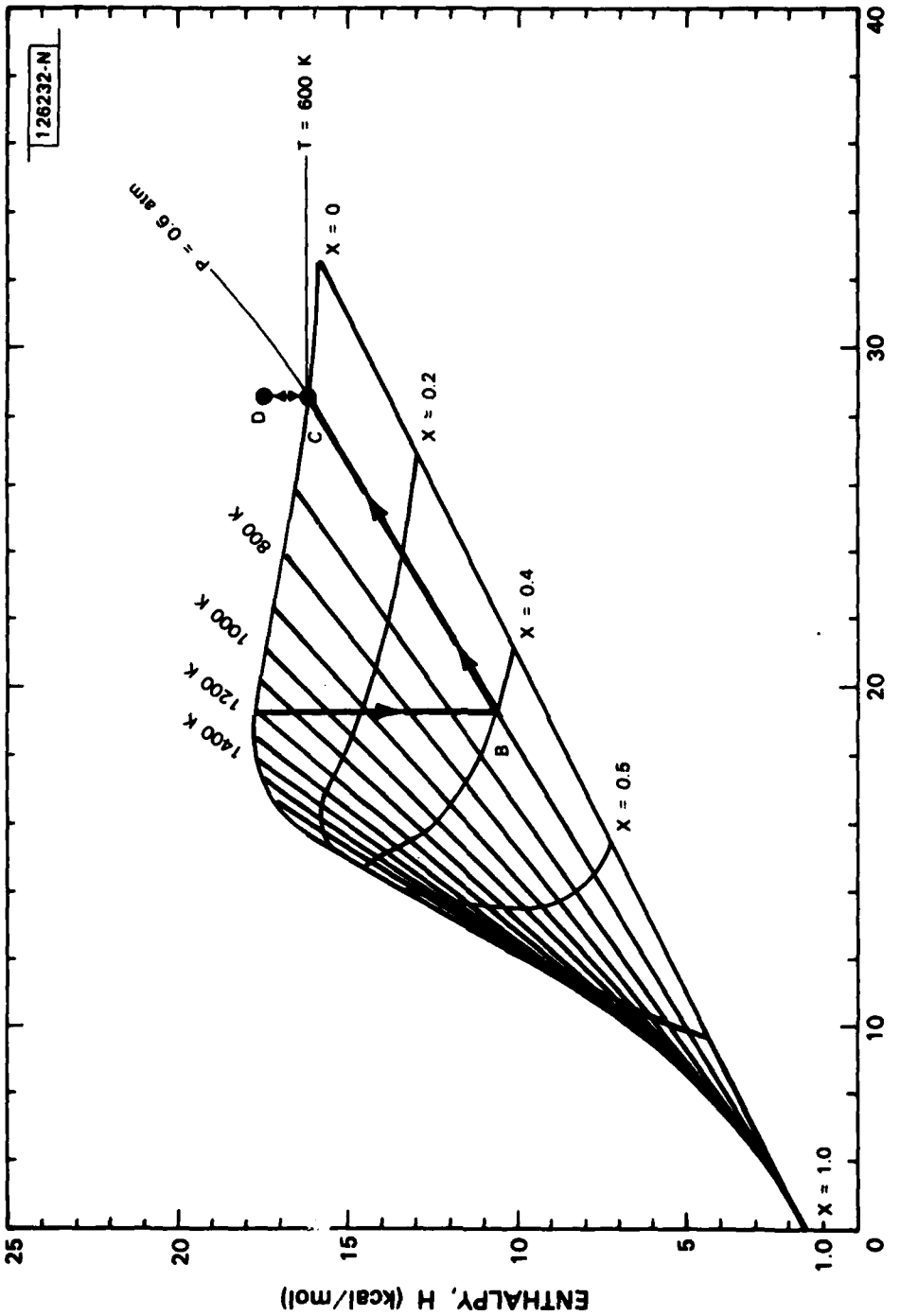

Fig. 29 Effect of shock on state for half-speed wheel.

behind a normal shock may be uncomfortably high. For such a flow, a viable alternative is to turn the flow through a sequence of small angles, α, so that the shock is nearly parallel to the flow. Flow parallel to the shock is nominally unaffected by it. Thus flow on both sides of such a shock can be supersonic (even though the component normal to the shock goes subsonic), and a mild, almost reversible shock is possible even at high Mach number.

A possible illustration of such a flow is shown in Fig. 30, in which a uniform two dimensional flow with M>>1 changes direction by angle α in a confining channel. The geometry has been chosen so that the flow simply changes direction at a single shock front connecting the two corners at which the channel turns. Such a single-shock geometry is possible at only one Mach number for a given choice of the transition length L (or vice versa); moreover, it does not work if the turn angle α is too large or if the Mach number M is too small.

In such a geometry, the shock angle $\hat{\mu}$ is very nearly equal to the Mach angle μ

$$\mu = \arcsin (1/M) \tag{VIII-15}$$

except when flow conditions are close to the onset of failure of the flow pattern. Geometric considerations provide the channel width ratio $\hat{w}/w$ and the velocity ratio $\hat{v}/v$ passing through the shock

$$\hat{w}/w = \frac{\sin \hat{\mu}}{\sin (\hat{\mu} + \alpha)} \tag{VIII-16}$$

$$\hat{v}/v = \frac{\cos (\hat{\mu} + \alpha)}{\cos \hat{\mu}} \tag{VIII-17}$$

Conservation of mass then provides the compression ratio E

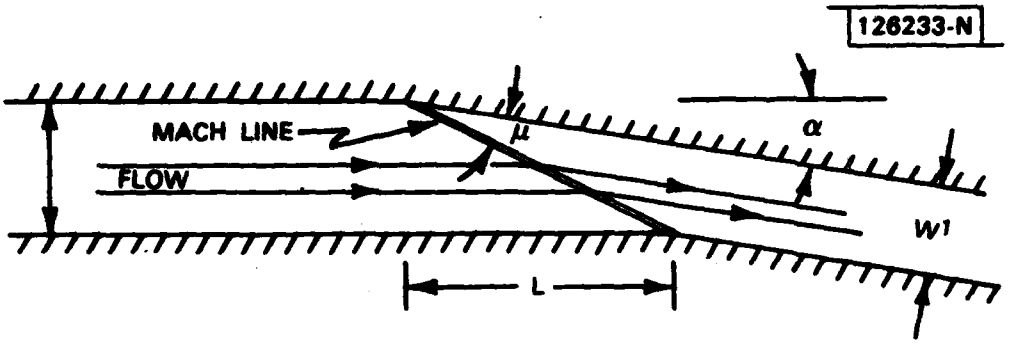

Fig. 30 Hypersonic flow through small angle turn.

$$E = \frac{\tan(\hat{\mu} + \alpha)}{\tan \hat{\mu}} \quad . \qquad \text{(VIII-18)}$$

All of the relationships cited earlier for the normal shock continue to hold for the inclined shock, provided one considers only the normal component of velocity M_n at the shock and a stagnation enthalpy H_n obtained by letting the normal comment of velocity (but not the tangential component) go to zero. One then finds[14,15]

$$M_n^* \hat{M}_n^* = a_n^{*2} \qquad \text{(VIII-19)}$$

with a_n^* computed from H_n instead of H. Equations (VIII-18) and (VIII-19) are, in effect, two different equations for the same ratio E; with the help of Eq. (VIII-17) to express a_n^* in terms of a^*, an implicit equation for $\hat{\mu}$ can be set up and solved numerically. Having found $\hat{\mu}$, it is possible to compute all of the other parameter ratios and to determine the entropy increase due to the shock[14].

Evidently, from Eq. (VIII-17), geometry requires that the velocity decrease in the turn, with the result that some of the kinetic energy of flow is converted back to thermal energy. To the extent that this conversion is reversible, the kinetic energy can be recovered by re-expansion. The fraction of the original kinetic energy reversibly exchanged for heat is shown in Fig. 31 as a function of turn angle α for several incident free-stream Mach numbers. A 25% conversion, which, in our examples above, would raise the stream temperature from 600°K to about 900°K, is possible in a Mach 2.8 flow at a turn angle of 15°.

The calculated entropy gain per turn is very small. What is shown in the Figure is the total fractional loss of available kinetic energy in N turns, each of size α followed by re-expansion, so that the total turn angle is 180°. Evidently, for the Mach 2.8 flow with a turn step of 15°, the cumulative loss in a 180° turn is 10%, producing an outlet temperature of about 700°C, a situation comparable to that for normal shock and re-expansion, but without the 2000°K intermediate temperature associated with the latter.

Of course, one would not actually try to implement a dozen stages of step turn and re-expansion. Our calculation is simple a plausibility argument that the supersonic turn is possible; and an estimate of the magnitude of effects to be expected when the unimpeded flow would strike the walls of the guiding channel at an angle α.

Up to the point in Fig. 31 at which each of the loss curves breaks off from the bottom curve, the shock angle $\hat{\mu}$ is within a degree or two of the Mach angle μ. Not many degrees beyond the point at which each of the individual loss curves is broken off there is no solution to the simple turn geometry. In particular, a flow that appears to turn easily and efficiently as a supersonic flow at Mach 2.8 and turn angle of 15° will not turn supersonically in the same geometry at Mach 1.4. Thus, it is plausible that the same turbine blade design might simply turn the supersonic flow without high

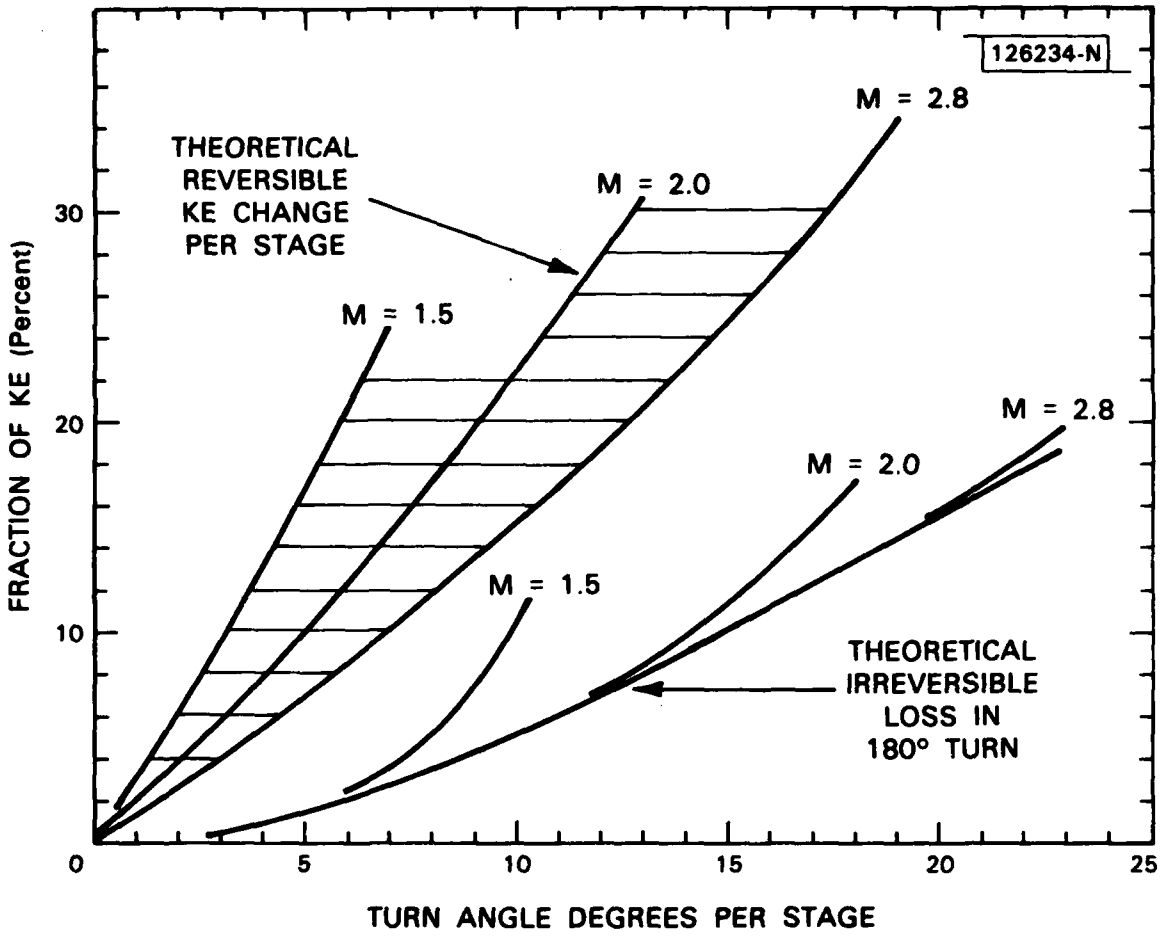

Fig. 31. Reversible and irreversible energy exchanges in supersonic step turns.

temperature shock* in start-up, but nevertheless support a normal shock so as to turn the flow subsonically when the turbine has come up to speed.

E. Flow in Expansion Nozzles

While densification of a supersonic flow can only occur irreversibly, expansion of a supersonic flow can occur reversibly in nozzles. Inasmuch as we need to consider the reversible expansion of a wet vapor, we cannot limit the discussion to ideal gas expansion. The procedure in this case is to formally integrate the flow equation using a^2 as a parameter, subject to a (determinable) functional relationship between a^2, H, and S. The result is an expression for density as a function of velocity. For almost all cross-sections conservation of mass flow then determines two stable flows, one subsonic and one supersonic. At the narrowest, cross-section, the flow is always at Mach 1, provided there is enough pressure drop across the nozzle as a whole to induce supersonic flow.

The equation of motion along a streamline (for $dS \to 0$) is

$$\rho v dv + dP = 0 \qquad \text{(VIII-20)}$$

which is derived from the general formula

$$\frac{1}{2} mv^2 + H = \quad = \text{constant} . \qquad \text{(VIII-21)}$$

If Eq. (VIII-20) be divided by ρ and dP written as

$$dP = d\rho \left.\frac{dP}{d}\right|_{dS=0}$$

$$\triangleq d\rho \left.\frac{\partial P}{\partial \rho}\right|_{S}$$

*There will be, of course, an unavoidable stagnation effect at the leading tips of the turbine blades during start-up.

one can recognize $\partial P/\partial \rho$ as the velocity of sound and write

$$v dv/a^2 + d\rho/\rho = 0 \ . \qquad \text{(VIII-22)}$$

We have already observed that (for any given S) a^2 is a monotonic decreasing function of v^2, which can be written explicityly through Eq. (VIII-21) if a^2 is known as a function of H and S. Thus Eq. (VIII-22) can be formally integrated to yield the density as an explicit function of velocity:

$$\rho = \rho_o \exp(- \int dv^2/2a^2) \ . \qquad \text{(VIII-23)}$$

The pressure change can be found formally from Eq. (VIII-20) in much the same way, by replacing ρ in that equation by the rhs of Eq. (VIII-23). The formal result is

$$\Delta P = \frac{1}{2} \int dv^2 \ \rho_o \exp \left(- \int dv^2/2a^2 \right) \ . \qquad \text{(VIII-24)}$$

The advantage of those forms for ρ and ΔP is not that they help with calculations in any particular case; it is that they help us make assertions about the nature of the flow independently of the details of a particular set of P-V-T data. For an ideal gas, a^2 is directly proportional to H

$$a^2 = (\gamma - 1) \ H/m \qquad \text{(VIII-25)}$$

so that, with the help of Eq. (VIII-21), the integrations (VIII-23) and (VIII-24) could be executed analytically. The first of these integrations yields a logarithm, thus getting rid of the exponential and returning the calculation to the familiar power laws of ideal gas calculations.

In general, for a real fluid, one can try to fit the data to various analytical relationships, such as

$$a = \alpha (H + h)^k \qquad \text{(VIII-26)}$$

with α, k and h all functions of S. To the extent that Eq. (VIII-26) is a valid approximation, the integral in Eq. (VIII-23) can be executed to give

$$\rho = \text{const} \times \exp[(H + h - mv^2/2)^{1-2k} \Big/ \alpha^2 m(1-2k)] \quad . \qquad \text{(VIII-27)}$$

By expanding the binomial in the argument of the exponential in powers of $mv^2/(H+h)$, it is possible to show by algebraic manipulation that

$$\rho = \rho_o \exp\left[- \frac{v^2}{2a_o^2} \left(1 + k \frac{mv^2}{2(H + h)} + \ldots \right) \right] \qquad \text{(VIII-28)}$$

with all powers of the normalized kinetic energy in the parenthesis having positive coefficients. Thus, for almost all k, ρ decreases at least exponentially as the square of v (or as the square of M*). The one case for which Eq. (VIII-27) fails is the ideal gas, for which $k = 1/2$*; but in that case, the answer is known: ρ depends in power law fashion on M*, rather than exponentially as in Eq. (VIII-28).

Figure 32 is a plot of a vs H for fixed S over the region of the H-S plane that would be used for equilibrium expansion of mercury in a simple Rankine cycle. A good first approximation to the a vs H relationship shown there is

---

* In the case $k = 1/2$, the passage from Eq. (VIII-27) to Eq. (VIII-28) involves the evaluation of 0/0 terms.

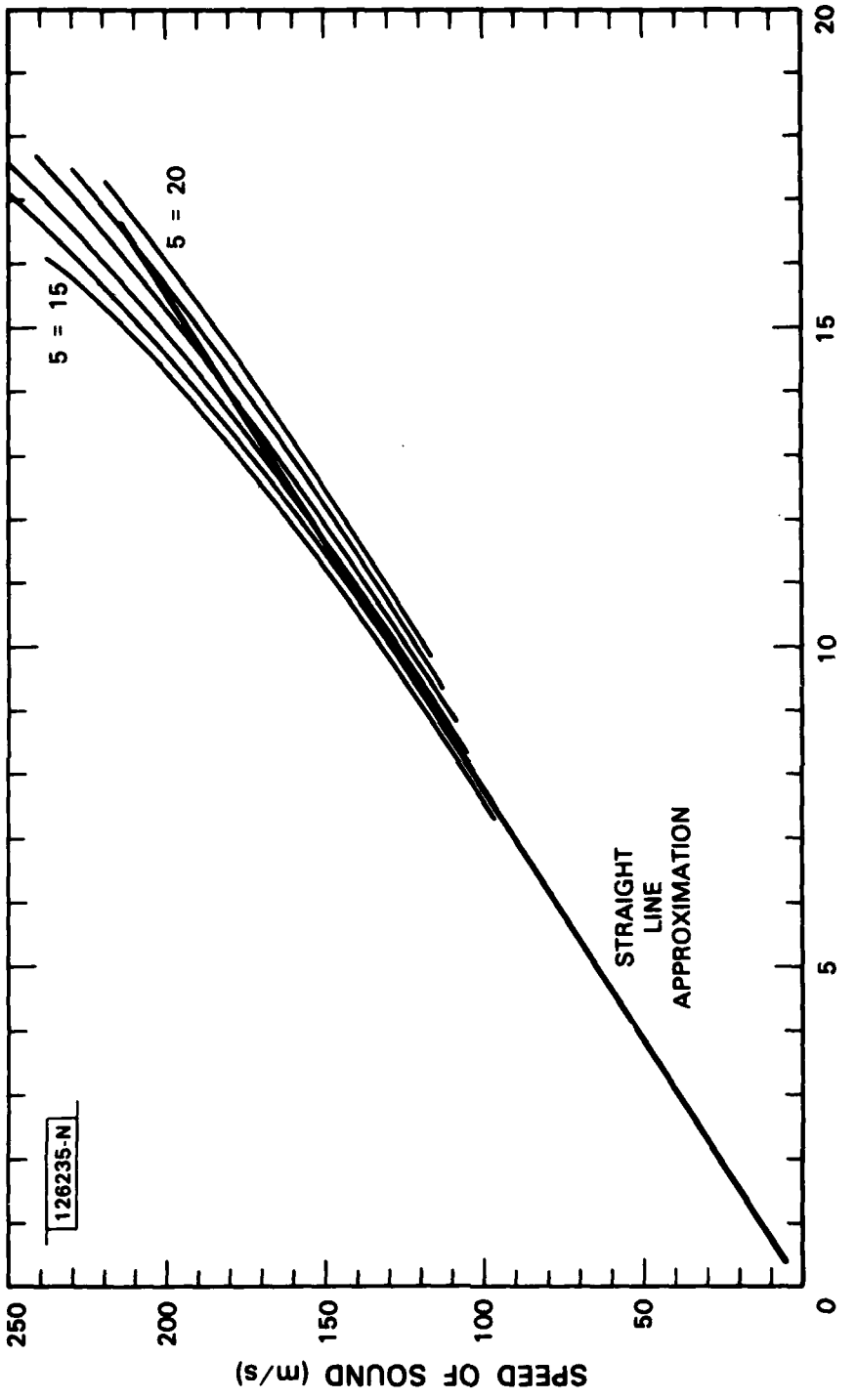

Fig. 32 Speed of sound vs enthalpy.

$$h(S) = 0$$
$$k(S) = 1 \qquad \text{(VIII-29)}$$
$$\alpha(S) = 3.1 \text{ mol-m/kJ-sec} \quad .$$

(In Eq. (VIII-29) calories have been converted to Joules to avoid mixed units.) A better approximation has positive h and k equal to about 1.5.

A plot of actual equilibrium density (in the form of its reciprocal, specific volume) is given for wet mercury vapor in Fig. 33, computed from the data developed in Section III, with density derived from wetness fraction and velocity from enthalpy differences, for isentropic expansion from the given inlet temperatures T_1. The Figure shows 100° steps in T_1 from 1000°K to 1400°K). Note the nearly quadratic shape of the curves on the semilog scale (for modest velocity), exectly as one might expect from the formal arguments just given. The Figure also indicates several constant-expanded-gas-temperature trajectories in 50° steps from 550°K to 650°K.

Now let us consider flow in a nozzle, which is a channel whose cross-section A varies gradually with distance so that the flow in any cross-section is uniform at u_o (grams) per second. Conservation of mass requires the same flow u_o through every cross-section, so that

$$A\rho v = u_o = \text{constant} \quad . \qquad \text{(VIII-30)}$$

If we substitute for ρ its formal determination from Eq. (VIII-23) we obtain

$$v \exp\left(- \int dv^2/2a^2 \right) = u_o/A\rho_o \quad . \qquad \text{(VIII-31)}$$

Except for A, the quantities on the rhs of this equation are fixed; A itself can be presumed determined by geometry. The function on the lhs rises from 0

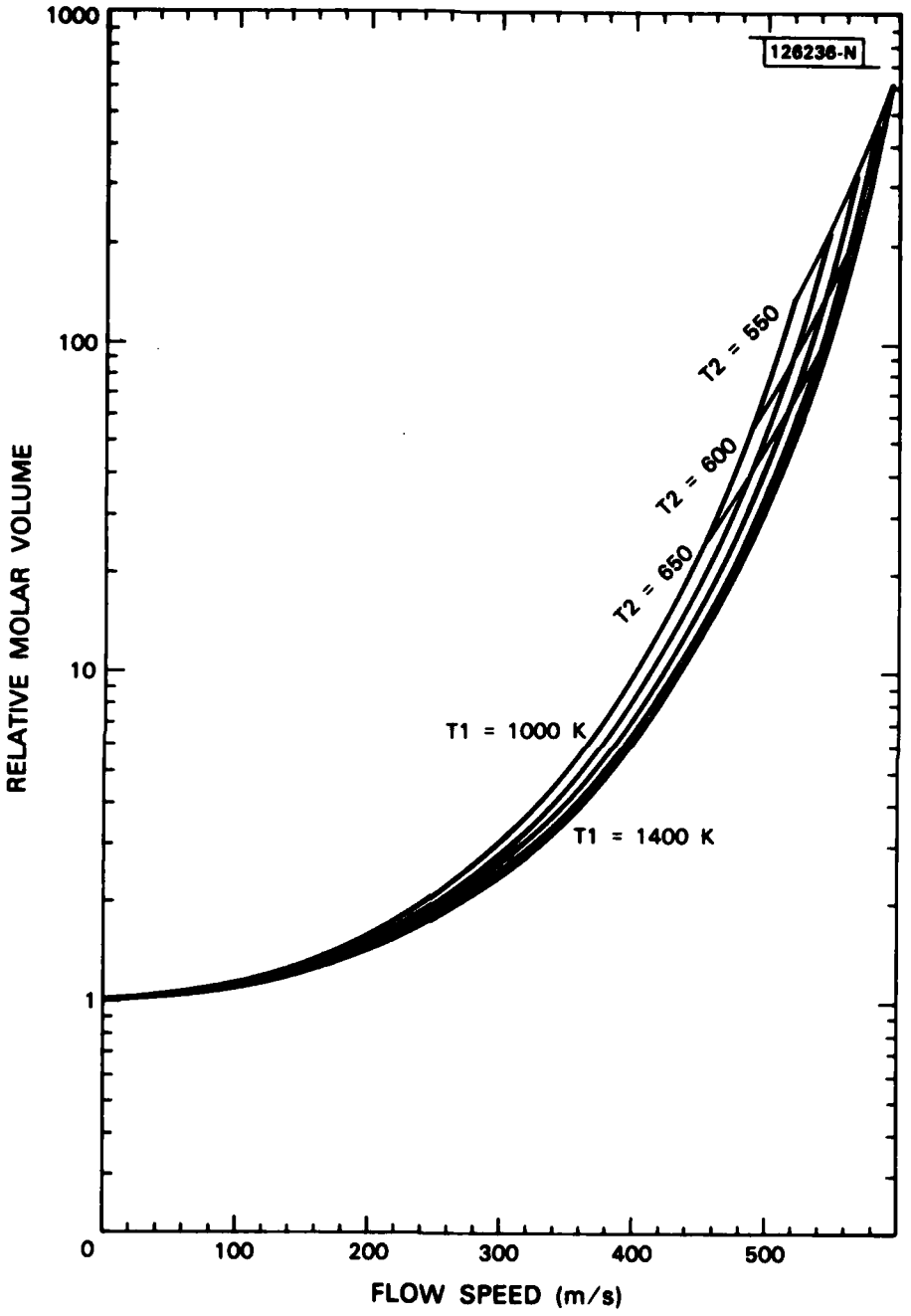

Fig. 33 Molar volume vs nozzle speed.

when v is zero to a simple maximum and then drops back towards zero as $v \to v_{max}$. This behavior is shown in Fig. 34. Differentiating the lhs of Eq. (VIII-31) to obtain the value of the maximum results in the general condition

$$v = a \quad . \tag{VIII-32}$$

That is to say, the maximum occurs when v=a*, the onset of sonic flow, Mach 1.

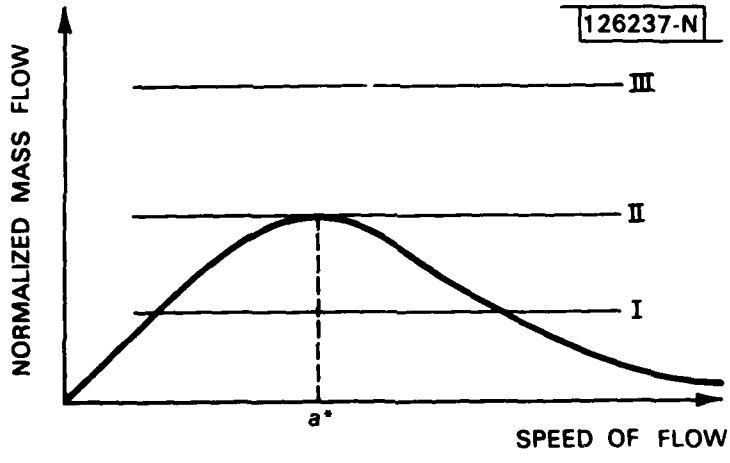

Fig. 34 Normalized flow conditions.

We may regard the quality on the rhs of Eq. (VIII-31) as a kind of normalized density of mass flow. If this flow is assumed to be too large, as a result of hoping for too big a u_o for a given A and ρ_o, the rhs plots as position III in Fig. 34. There is no solution for $\underline{v}$ if $u_o/A\rho_o$ is in position III.

As one lowers ones expectations by raising A or dropping u_o, the first possibility of solution occurs with sonic flow at II. If one lowers his flow density expectations further to region I, <u>two</u> flows are always possible, one subsonic and one supersonic.

Figure 35 shows the relative area required to sustain a given mass flow through the nozzle for wet mercury at equilibrium (again calculated from data in Section III) for various static inlet temperatures from 1000°K to 1400°K in 100° increments, together with estimates for the critical flow velocity a* in each case. The Figure also shows contours of constant-expanded-gas temperature from 550°K to 750°K in 50° increments.

It follows from the foregoing general argument that in a nozzle of varying cross-section, the flow will always be determined at the minimum cross-section. Either the flow at that point will be subsonic, or there will be enough pressure drop across the nozzle to require the flow at the minimum cross-section to reach Mach 1. The mass flow per unit area at this cross-section <u>cannot increase further</u> so that its maximum value is u_{max}

$$u_{max} = \rho^* a^* A_{min} \quad . \tag{VIII-33}$$

Thus the flow (under enough pressure) is divided into two distinct parts by the constriction A_{min} ... subsonic flow up to the constriction, Mach 1 velocity at the constriction, and supersonic flow beyond the constriction. Evidently, Mach 1 flow at the throat is independent of downstream conditions (which in any event could not propagate upstream to affect flow in the throat).

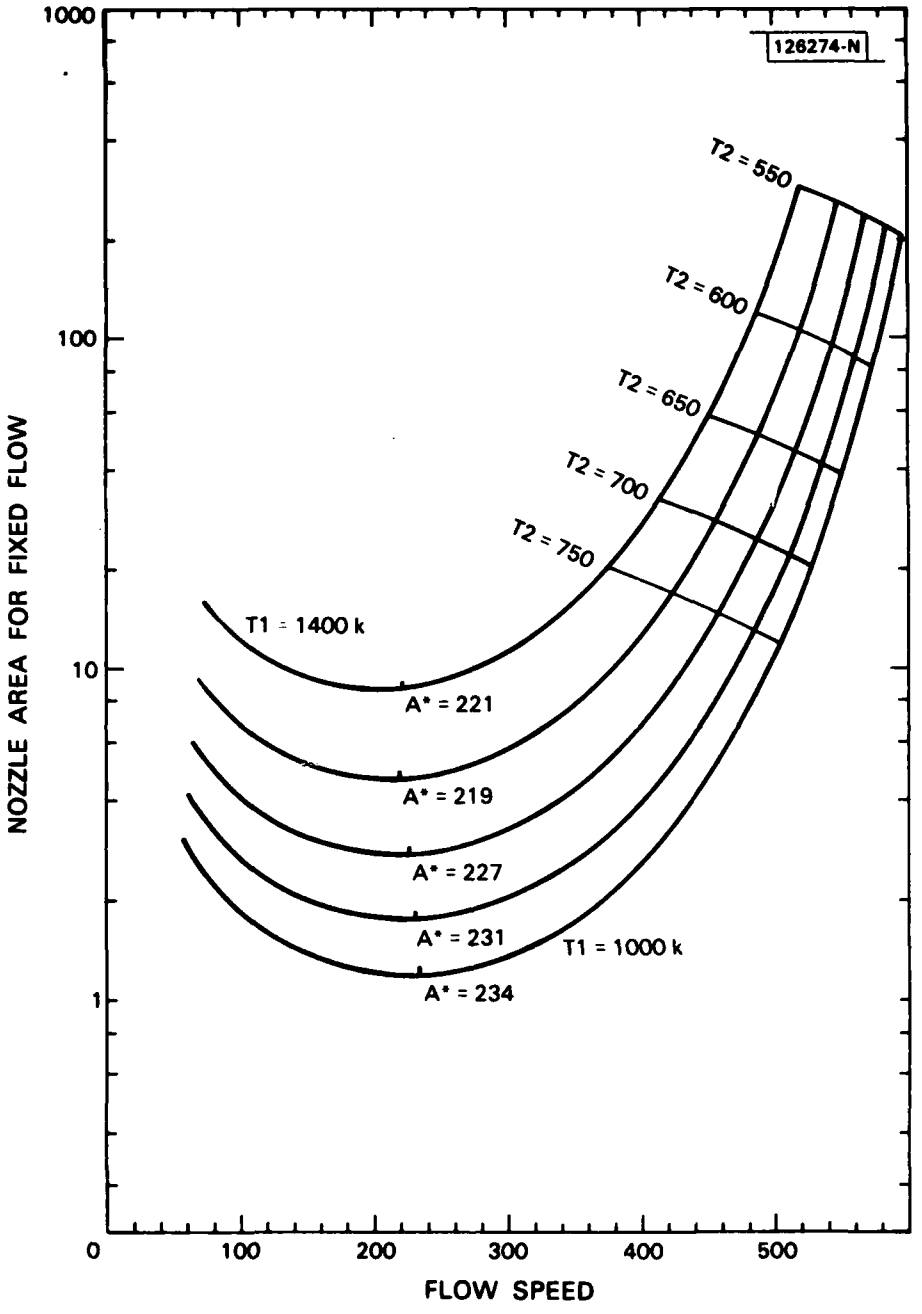

Fig. 35 Nozzle area vs nozzle speed.

The regulation of nozzle flow by conditions at the nozzle throat has wide ranging implications with respect to the stability of the overall system of turbine, feed pumps, boiler, etc. in which the nozzle is embedded. The critical speed a* is determined primarily by the nozzle inlet temperature T1, not by inlet pressure conditions. Moreover, a* is nearly the same* for a given T1 (within 5%) whether one considers equilibrium flow as in Fig. 35, or the "frozen disequilibrium" flow of an ideal gas starting from the same temperature. On the other hand ρ^* is determined primarily by the density of the inlet fluid shown, since by Eq. (VIII-26) and Fig. 33, as well as an ideal gas calculation, ρ drops by roughly a factor of 5/3 between inlet and throat.

On the other side of the boiler from this throttling device of fixed capacity is a feed pump which also tends to be a device that naturally controls the flow rate through the system. In between these two is a boiler of fixed available power and limited thermal mass of working fluid. If the two regulators, feed pump and nozzle throat, call for different flow rates, what will happen?

The situation in which the feed pump starves the boiler appears to be self-regulating under all conditions, provided there is adequate alternate cooling for the heat source (see Section V). In this case, the temperature rises somewhat, but ρ_1 at the inlet drops to a much greater extent than a* rises, thus reducing the flow through the throat.

On the other hand, if the feed pump stokes the boiler faster than the nozzle wishes to withdraw vapor, the stability is by no means certain. Much depends on the extend to which the unevaporated droplets can be swept out of the boiler along with the rest of the fluid flow, and the extent to which the presence of these droplets stabilizes (or destabilizes) flow.

---

* In the practical range $1000°K \leq T1 \leq 1400°K$.

The situation in which the boiler "drowns" is easy to imagine -- an excess injection of droplets by the feed pump, followed by a drop in temperature, resulting (not only in a modest drop in a*) in a precipitous loss in ρ^* as a consequence of the sensitivity of the boiler curve to temperature changes, resulting in a further decrease of nozzle throughput, further accelerating the drowning action.

There is a similar, but to the satellite engineer, more familiar, set of problems associated with operating a fairly "dry" condenser. Here, the problems are the same as those that appear as instabilities in the operation of heat pipes. Presumably, at the very least, they can be tackled with the same bags of tricks that have worked to stabilize heat pipe operation.

We do not propose to analyse and solve the system stability problems that can arise when a collection of components, each by itself well-behaved, are connected together in a closed loop. What we have done here is to call attention to the Mach 1 throat of a supersonic nozzle as one possible origin of such system difficulties. The flow depends entirely on the upstream conditions, not on the ones downstream. Any adjustment of source power conditions to meet the actual load downstream of the nozzle will have to be accomplished by some other means than depending on self-regulation of the flow.

We close this section by drawing a parallel between the pressure regulation at the discharge of a supersonic nozzle and the discharge from turbine blades sustaining supersonic flow.

Inasmuch as supersonic flow has no way of signalling nozzle exit conditions upstream, some adjustment of flow must occur in the vicinity of the nozzle outlet to match conditions into which the nozzle discharges. In Fig. 36, the discharge is assumed to be into a plenum at some fixed pressure. Evidently, if the plenum pressure is exactly the same as the dynamic pressure (measured by an observer travelling with the fluid) at the nozzle exit, the nozzle flow will simply continue out into the plenum, with no (conservative) forces acting to change its shape, until its momentum is dissipated in turbulence (Fig. 36a).

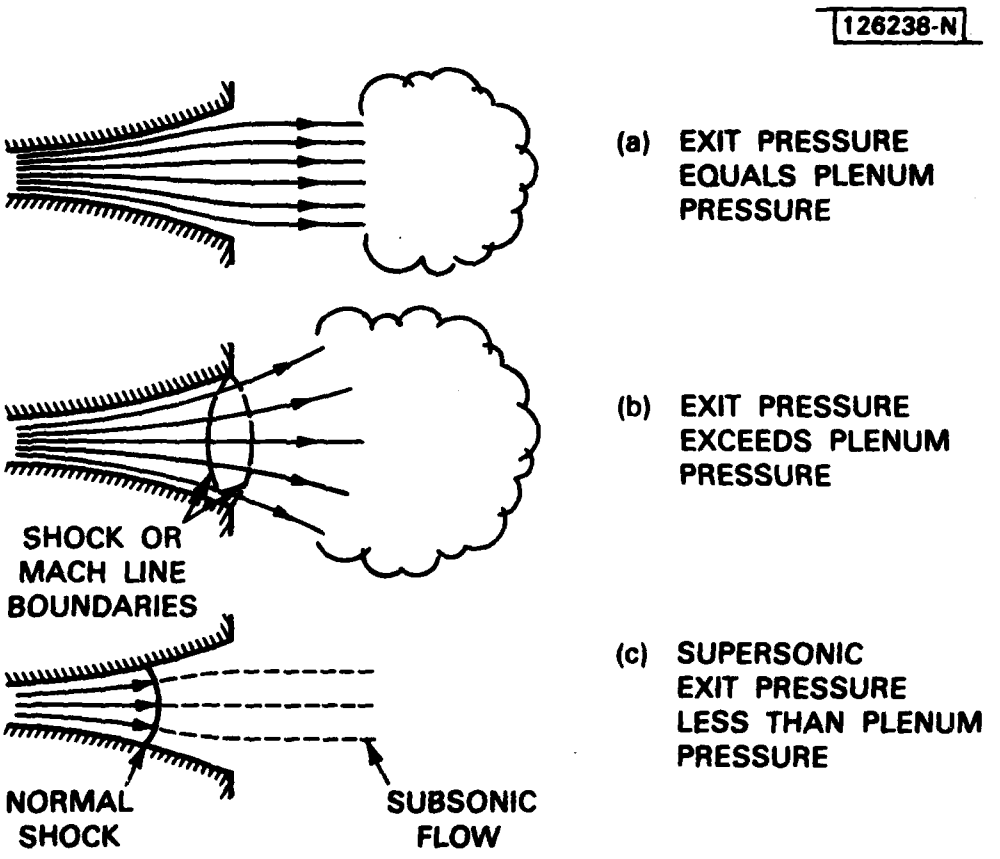

Fig. 36 Exit from nozzle into plenum.

If the dynamic pressure at the nozzle outlet is greater than that of the plenum, then the flow speeds up and expands with increase in entropy at the nozzle outlet (Prandtl-Meyer expansion), turning a corner as it does so (Fig. 36b). Here, there is a region near the nozzle outlet, bounded by Mach lines, in which the flow actually turns. Although the flow speeds up, the average momentum along the original flow direction remains unchanged. Although the all kinetic energy in the original flow might have been extracted in a simple change-of-direction machine, this is no longer feasible because the flow itself is expanding over an enlarged fan of directions.

The final case (Fig. 36c) is the one in which the supersonic flow arrives at the nozzle outlet only to find the plenum pressure too high for a supersonic exit. As a result a normal shock front forms, which works its way back upstream by cummulative pile-up until it reaches an equilibrium position. The flow at the outlet of the nozzle, and upstream as far as the shock, is subsonic. The kinetic energy of flow has been reabsorbed into thermal energy with an increase in entropy ΔS.

In discussing the turbine as a device which changed the direction, but not the magnitude, of the input momentum we argued that in

$$\rho v dv + TdS + VdP = 0$$

a small net dP between inlet and outlet of a turbine blade implied small dv because dS could also be assumed small. But here is a case in which dv can be substantial even if VdP is quite modest, because ΔS through the shock is significant.

Let us now consider three analogous cases in the flow through the turbine. Suppose, first, an exact match of outlet pressure to plenum pressure. There can be ideal change-of-direction energy extraction in which an input molar momentum mv becomes zero at the output, and a molar kinetic energy mvw is extracted.

Next, suppose that the plenum pressure is raised so as to produce a severe normal shock somewhere within the blade passageways, so that the exit velocity is slow with respect to the blades, nearly $\underline{w}$ with respect to stationary reference. The kinetic energy yield to the wheel is then $m(v-w)w$. In this case, the best choice of w is $v/2$. The result is that the assumed severe shock causes the power output of the wheel to drop by a factor of two from balanced conditions. Positive plenum pressures (with respect to turbine blade exhaust) should be avoided (except possibly when the blade flow Mach number is low enough to imply nearly-reversible compression in the shock).

Finally, if the plenum pressure is lower than that of the exhaust, the resulting irreversible acceleration of gas in the blade throat results in no changes in the net output momentum. Consequently, there is no change in the net force (or power output) on the turbine. There is, nevertheless, a waste of kinetic energy that might have otherwise been extracted at the lower condenser temperature implied by the reduced plenum pressure.

Thus, total useful expansion will be governed by nozzle geometry if the plenum pressure is equal to, or lower than, that determined by nozzle geometry.

PART 4

REAL FLOW IN NOZZLES AND BLADES

Chapter Summaries

Chapter IX
NON-EQILIBRIUM FLOW PHENOMENA

Droplets can exchange energy with the surrounding vapor only by friction or by thermal conduction, both of which are processes that introduce significant time lags. Droplets in wet mercury steam travel several thousand diameters beyond a velocity discontinuity or change of direction in the vapor flow. Droplets of sufficient size will not follow flow streamlines through the turbine blades, but will strike them, with impact conditions not unlike buckshot striking armor plate. Analysis of impact forces and potential causes of temperature rise at contact (including so-called "cavitation") indicates advantages of micron to submicron droplet size and glancing angles of incidence on impact. Unless the total droplet area is large enough, there is not suffient time for the mercury vapor to condense as it expands through the nozzle, returning the heat of condensation by thermal conduction to the vapor to permit it to do work. Even with the deliberate introduction of enough droplet nuclei to condense the vapor into droplets of only a micrometer radius, $100^{o}K$ temperature differential between the droplets and the expanding vapor may be needed to drive the heat transfer. A substantial reduction of the heat transfer design constraint can be effected by deliberately introducing wet steam into the expansion nozzle. A variety of configurations for the entire cycle are considered in order to be able to satisfy separately droplet size requirements for proper operation of the boiler and of the expansion nozzles.

Chapter X

NOZZLE DESIGN AND NOZZLE LOSS

The three constraints on nozzle design are the power at the nozzle throat, the permitted friction, and the temperature disequilibrium permitted between droplet mist and expanding vapor; each may be improved at the expense of the others. Graphical analysis is made of several nozzle designs having a constant temperature difference between mist and vapor. For 30 kW to 40 kW power flow through the throat, a nozzle operating on vapor 50% wet has 1/3 the length and 1/3 the friction losses of one who inlet vapor is dry. A nozzle for the 100 to 300 kW power range has a 5 mm throat, a length of about a meter, and total losses of about 10%. A nozzle for 2 kW would have a 0.5 mm throat, a 5 cm length, and losses over 35%.

IX. NON-EQUILIBRIUM FLOW PHENOMENA

Thus far, we have assumed that the droplet mist forms rapidly when thermodynamic conditions are favorable; and we have put aside the effects of the droplets on the flow on the far side of a shock. In fact, the formation of the droplet mist cannot be presumed. Although it is possible to give an adequate description of what happens if it happens, the actual formation of the mist is a question that must be resolved by epxerimental control of condensation nuclei.

If droplets are formed, they will persist with initial (supersonic) fluid stream velocity on the far side of a shock. The tendency is for these droplets to travel several thousand diameters beyond the shock front before giving up most of their differential velocity to friction with the (slower moving) post-shock gas flow. However, heat transfer limits the size to which droplets can grow in making the transit through a nozzle; similarly heat transfer limits the amount by which they can shrink in the disequilibrium beyond a shock. Thus, a thousand droplet diameters is likely to be a short distance in absolute terms, on the order of mm to cm; the transfer of most of the droplet excess momentum back to the flow as a whole, therefore, tends to take place on a practical scale.

In this section we explore these phenomena in greater detail. In particular, for droplets already formed, we shall describe the frictional dissipation of velocity difference behind the shock, the forces exerted by droplets impinging on channel walls, and the existence of temperature disequilibrium between the droplets and the enveloping gas on account of finite rates of heat transfer (and surface tension). We shall also consider the mechanisms that can drive and inhibit the formation of droplets and the need for very large numbers of droplet nucleation centers to reach condensation equilibrium in a nozzle of reasonable physical length, and strategies for coping with situations in which the number of nuclei turns out to be too small to support nucleation in a single nozzle. These considerations lead to a proposed system configuration for use on board a satellite.

A. Frictional Readjustment of Droplet/Gas Energy Imbalance Beyond Shock

Passage of a fluid through a normal shock is a constant H process, regardless of what happends to the individual components of a non-homogeneous fluid system. Let us suppose that for every 1-x moles of vapor arriving at the shock, there are x moles of droplets. Immediately beyond the shock the two flows, which had arrived at the same speed, are moving at different speeds, so that the concentration of droplets appears to be less than x. This situation persists so long as the speed differential persists. But eventually the forces of friction restore equality in velocity between the two flows, and return the droplet fraction to x (provided they have not meanwhile suffered evaporation). Two questions arise: what are the consequences of this return to common speed on the state of the flow? What is the order of magnitude of the forces involved and the time or flow distance over which they must act to restore such common-velocity flow?

The calculation of what happens to the state of the fluid is straightforward mechanics. Let the common flow velocity upstream of the shock be v. Just downstream, it is $\hat{v}$ for the vapor and v for the droplets

$$\hat{v} = v/M^{*2} \qquad \text{(IX-1)}$$

Thus the total molar kinetic energy just downstream of the shock is

$$KE = \frac{1}{2} mv^2 \left[x + (1-x)/M^{*2}\right] \qquad \text{(IX-2)}$$

Conservation of momentum gives the eventual downstream velocity (at fixed cross-section) as v'

$$v' = v \left[x + (1-x)/M^{*2}\right. \qquad \text{(IX-3)}$$

If one divides both sides of Eq. (IX-3) by a*, one obtains the eventual downstream M*:

$$M^{*'} = xM^* + (1-x)/M^* \quad . \tag{IX-4}$$

It is quite possible for this new M* to be greater than unity; i.e., the re-sorption of the momentum of the droplets can bring the flow back to supersonic flow, but, evidently, at a lower Mach number than the original. If this happens, there may have to be a (series of) secondary normal shock(s) to bring the flow to a subsonic quasi-equilibrium in which it can turn a corner*.

In the illustration of M 1.4 flow at the entrance to the turbine blades (given in Section VIII) M* was 1.26 and the value of x for original expansion from 1200°K to 600°K was roughly 0.4. From these numbers one calculates an eventual downstream M*' of 0.98, so that the flow (barely) remains subsonic even after the equilibration of the differential momentum of the two components.

If one calculates the downstream KE' from the velocity given in Eq. (IX-3) and adds the kinetic energy that was reconverted to vapor heat in passing through the shock, one can obtain by subtraction the fraction ξ_2 of the initial KE that is returned to heat during equilibration:

$$\xi_2 = x\,(1-x)\,(1 - 1/M^{*4}) \tag{IX-5}$$

while the fraction ξ_1 initially returned to vapor heat was

$$\xi_1 = (1 - x)\,(1 - 1/M^{*4}) \quad . \tag{IX-6}$$

---

*The corner must not be too sharp even in subsonic flow, lest turbulence losses be high (see Section X).

Evidently, for modest x, the frictional heat of equilibration is equally modest compared to the energy returned (nearly reversibly) to heat in the shock. The dependence of the total returned heat ξ on x is weak for modest x

$$\xi = (1 - x^2)\ (1 - 1/M^{*4}) \quad . \qquad \text{(IX-7)}$$

In Section VIII it was found that most of the energy fraction ξ_1 is returned to heat reversibly. Without conducting a detailed analysis it is not possible to state exactly how much of ξ_2KE is irrecoverable on account of entropy increase. The upper bound is the assumption that none of it is recoverable. In the example we have been carrying along with x = 0.4 and M* = 1.26, this upper bound is 15% of the KE before the shock. Inasmuch as the KE of the turbine flow in this example is 1/4 of the KE being extracted, an upper bound to the effect of ξ_2 on the overall energy extraction is a 4% loss (out of 100%) in extraction efficiency.

B. Forces Exerted by Droplet Impact

For every radius of flow curvature, there is a droplet size small enough that the droplet follows the flow rather than penetrating the boundary layer next to the turbine blade surface. This fact is used in some kinds of aerosol separators to collect mist droplets down to the micron size while passing smaller ones[16]. Extrapolation of the design equations for such apparatus to the velocites, vapor viscosity, and droplet density of mercury would lead one to expect that droplets under a micron diameter might not, in fact, strike the turbine blades at a 1 cm radius of flow curvature and 100 m/s flow velocity. Further analysis of the potential benefits of this particular consequence of droplet size control is beyond the scope of the present study. We shall conservatively assume that all mist droplets travel in straight lines with such impact forces at surfaces as would result from such straight line paths. The particles (or their fragments) are then assumed to be captured by the flow and sent headlong in new straight lines towards the walls, as in the Newtonian model[15] of fluid flow.

If a stream of fluid strikes a stationary surface with a velocity of approach v_a, then the steady-state pressure exerted is $c_\theta \rho v_a^2/2$, where c_θ is between 1 and 2, being greatest when the flow leaves with the speed of approach, being least when the flow simply slides parallel to the surface after striking it. If droplets moving at a nozzle exit speed of 560 m/s strike stationary blades at normally incidence, the steady-state pressure can be as high as 40,000 atm or 600,000 psi. Even with the turbine up to speed, the pressure of a normal impact at full velocity is 10,000 atm or 150,000 psi. By keeping angles of approach under 30° from grazing incidence, actual pressures can be controlled to be an order of magnitude less than those calculated for normal incidence impact.

The extreme impact pressures (600,000 psi at startup and 150,000 psi at running speeds) are beyond the high temperature hardness of most tough metals, but they are not necessarily beyond the hardness range of some ceramics (e.g., Si_2N_2) or some intermetallic components that might be used to "case harden" the surface of a blade material chosen for its mechanical and thermal toughness.

Of course, blade orientations and stream flow directions can generally be chosen to produce much lower v_a than the extreme values assumed above. An impact angle of a little under a third of a radian leads to pressures only a tenth of those above. Thus, it is legitimate to consider the handbook strengths of such materials under direct impact as providing the margin of safety in the expectation that actual flow geometries will result in working impacts an order of magnitude (or more) more benign.

During transient impact, the pressure can rise higher than the steady state values calculated above, the order of magnitude being $\rho v_a c$ rather than ρv_a^2, c being the speed of sound of compressional waves in the mercury liquid. The speed with which a mercury droplet might strike turbine blades is small compared with the (compressional) speed of sound in either mercury liquid or the blade material. Consequently, the dynamic situation is

completely analogous to lead buckshot striking armor plate. The ideal armor is tough and hard, and is thick compared to the size of the buckshot.

During the first few nanoseconds of impact, before a sound wave can propagate across the impinging droplet, the interface of contact must move at the speed of approach. The governing parameters which determine the ratio in which the two materials yield are the acoustic impedances ρc for liquid and blade. Most high strength materials have ρc comparable to that of Hg. But ρc for Mo alloys is 3 times that of Hg (and tungsten 5 times that of Hg). Thus, initially, there is a pressure wave in the blade material for which the initial displacement velocity, v_d, ranges from 1/2 down to 1/6 (for tungsten) of the approach velocity v_a.

Let us suppose that there is a maximum strain, δ_m, that the blade material can withstand without suffering irreversible changes. Then there is a critical displacement velocity, v_{crit}, given by

$$v_{crit} = \delta_m c \qquad \text{(IX-8)}$$

above which the blade will suffer damage. For a hard or tough material, the dilational velocity c is about 5000 m/s, and the dynamic δ_m is roughly 1%. Thus v_{crit} is roughly 50 m/s. Such a material could therefore be expected to stand up to repeated impact at 100 m/s from Hg at roughly equal ρc, and up to 200 m/s if the ρc ratios are favorable as in the case of Mo or W alloys. The transient acoustic pressure which corresponds to v_{crit} is approximately $\delta_m \rho c^2$. It is of the same order of magnitude, in the present case, as the steady state pressure.

The comments of the preceding paragraphs apply whatever the size of the impacting droplets, so long as they are small compared to the thickness of the surface they hit and so long as the impact time is small compared with

the time required to nucleate a variety of static yield mechanisms.* However, effects which tend to produce high temperatures at the impact interface do depend strongly on droplet size; they are generally referred to as "cavitation" phenomena although they are only superficially related to true cavitation erosion (which is the result of the repeated expansion and collapse of gas bubbles in a liquid).

The average temperature rise of an impacting droplet is bounded by its kinetic energy divided by its specific heat. For Hg vapor expanding from the vapor-gas saturation boundary at 1200°K to 600°K, this reconversion of kinetic energy to heat can lead to an average temperature rise of at most about 1100°K.** For droplets from an expansion over the same temperature range, starting with 50% wetness, and impacting on moving turbine blades at normal incidence, the actual possible average temperature rise is limited to about 150°K.

Now, various elasto-acoustic effects can result in the concentration of kinetic energy from within a volume V_o into a much smaller volume V_T on a time scale t given by the difference in linear dimension of the volumes divided by the speed of sound. The mechanism for converting this concentrated kinetic energy into heat can be simple (reversible) adiabatic compression, because the ratio of specific heats of a liquid such as mercury is nearly as large as that of a gas, ranging upwards from about 1.2 at room temperature.

However, because of thermal conductivity, heat so generated will diffuse away from the region in which it is generated, increasing the dimensions of the reduced volume V_T by an amount τ during time t:

---

* These include diffusion at grain boundaries, slip, grain size change, crack propagation, etc. These effects result in apparent yield parameters (for ordinary tensile strength, for instance) which are much higher in strain and much lower in stress than those which correspond to δ_m in Eq. IX-8.

** The assumption is that there is no time to form and blow off steam; otherwise, the average impact temperature cannot exceed boiler temperature.

$$\tau = \sqrt{2\alpha t} \qquad \text{(IX-9)}$$

where α is the thermal diffusivity of the medium. α is roughly 0.07 cm^2/s for Hg at 600° to 1000°K; roughly 0.4 $cm^2 s$ for Mo in the same temperature range.

Evidently, if in any given medium τ exceeds the difference in dimension $\Delta\ell_o$ between the volumes V_o and V_T, the concentration of heat does not take place (even if the concentration of kinetic energy does so); in such a case, the temperature rise within the material cannot exceed the average bound obtained by dividing average kinetic energy by average heat capacity. From Eq. (IX-9), it follows that the temperature rise will be benign whenever the dimensional difference $\Delta\ell_o$ is sufficiently small, as in Eq. (IX-10):

$$\Delta\ell_o < 2\alpha/v \; . \qquad \text{(IX-10)}$$

In the worst case, the mechanism releasing kinetic energy from V_o is instantaneous, so that the velocity $\underline{v}$ appearing in the r.h.s. of Eq. (IX-10) is the speed of sound in liquid Hg. This situation would result in $\Delta\ell_o$ of hundredths of a micrometer for benign temperature rise guaranteed. Ordinarily, however, the energy concentration must be at the interface with the turbine blade in order to cause damage to it, for which case V_o itself can be created only on the time scale of the speed of approach, v_a. Under such circumstances, the proper $\underline{v}$ to use in Eq. (IX-10) may be an order of magnitude smaller than the speed of sound. $\Delta\ell_o$ for guaranteed benign temperature rise is then on the scale of tenths of a micrometer.

Moreover, it is large temperature rise in the blade material that will cause damage. The transient heat capacity of most materials that might be used for turbine blades is much greater than that of Hg. The transient heat capacity of any surface during a time $\underline{t}$ is roughly β_t (energy stored per unit area and unit interface temperature rise):

$$\beta_t = 2\rho C_p \sigma t \qquad \text{(IX-11)}$$

C_p being the ordinary specific heat, ρ the density, and σ the thermal conductivity of the material. The following Table IX-I lists the $\rho C_p \sigma$ product for a number of materials.

TABLE IX-I

TRANSIENT HEAT CAPACITY PRODUCT
(JOULES PER DEG-SEC-CM^2)

Material	$\rho C_p \sigma$
Glass (Silica)	0.003
Mercury	0.05
Silicon Nitride	0.05
Alumina	0.3
Berrylia	0.6
Aluminum	1.0
Beryllium	1.2
Molybdenum	0.75
Tungsten	0.75

Evidently, the heat which might be stored in the blade material at an interface can be an order of magnitude higher than what might be stored in Hq liquid during the same time. The effect is as if $\Delta\ell_o$ in the mercury had been correspondingly increased. Thus, at an interface between Hg and a suitably chosen blade material we expect benign impact temperature rise if the dimensions of the heat generating volume are roughly a micron or less; this will be the case if the droplet itself is of the order of a micron in size. As for thermal events occuring within the mercury, they are isolated from the interface by the opacity of the mercury to radiation and its low thermal diffusivity. We conclude that so-called "cavitation" phenomena of

mercury droplet impact can be controlled by the proper choice of turbine blade material for service as armor plate (high v_{CRIT}) and high transient interface heat capacity, provided the droplets are small enough, in the micron size range.

C. Droplet Temperature Disequilibrium

The reader may suppose himself familiar with the condensation and evaporation of water droplets from mists in air; but such familiarity would be a poor guide for considering the corresponding phenomena when vapor on a window plane, for instance, is limited by the rate at which the condensable molecules of water can diffuse through the air to the window; thus, the vapor pressure near the window is substantially lower than that in the room as a whole, even though the room air is at nearly constant temperature. If the non-condensable air is removed, the situation is entirely different. Water molecules can now reach the window at the speed of sound if need be. What now limits the rat e of condensation is t he rate at which the heat of condensation can be removed. The room is now at nearly uniform pressure, but local temperature variations exist; in particular, the temperature near the "window" is lower than elsewhere. The situation with mercury condensation and evaporation in the vicinity of micron-size droplets is essentially a constant pressure (rather than constant temperature) process, in which the rates of condensation and evaporatin are determined by the flow of heat rather than by the flow of mass.

If there is any disparity in the sizes of droplets there will be no true equilibrium even in an apparent "steady state," if the droplets are small enough. The driving force in this case is surface tension, which

squeezes a droplet; as a result of the squeeze, molecules seek to escape by evaporation, raising the vapor pressure for a given temperature. If all the liquid is in a mist of equal-radius particles ("monodisperse"), then the resulting pressure increase is from P_o to P, given by Kelvin's equation

$$\begin{aligned} \ell n(P/P_o) &= 2M\Gamma/RT\rho_\ell r \\ &= r_c/r \end{aligned} \qquad \text{(IX-12)}$$

in which Γ is the surface tension, r the droplet radius, and r_c is obtained by combining all the other factors on the rhs of the equation. For water at room temperature, r_c is roughly 10 Å (10^{-3} μm); for mercury at 600°K, r_c is roughly 25 Å.

In terms of temperature change for a given pressure, the boiling temperature drops from T_o to T

$$T/T_o = 1 - (r_c/r)\ (T_o/T^*) \qquad \text{(IX-13)}$$

with T* being the activation temperature from the usual pressure law (T* = 7172°K for mercury). We shall put off any discussion of what might happen as $r \to 0$. We note that for micron radius droplets, $T-T_o$ is a fraction of a degree.

If there are a variety of sizes of droplet, then each size will be at its own temperature, some higher and some lower than the average vapor temperature. As a result, there will be a net flow of heat to the cooler, smaller droplets from the warmer, larger droplets. This flow of heat is accompanied by a flow of mass in the opposite direction; the smaller droplets lose mass while the larger ones receive it. The pathway for the flow of heat can be conductive or radiative. In Section IV we found that, even for the radiative path at 1300°K temperatures across hundred degree differentials, the time scale for

significant changes in the size of micron droplets was tenths of a second. Thus, although large droplets do tend to grow at the expense of smaller ones, and although a monodisperse mist is unstable with respect to one with a range of droplet sizes (polydisperse), the time scale of such changes is extremely long compared with the passage times of the flow through nozzles and turbine blades. For practical purposes, we can neglect the surface tension effect on a fully developed droplet mist.

Now, while the shock front slows the vapor flow normal to it to the subsonic range, it does not so affect the very much denser droplets, which emerge with velocity and temperature virtually unchanged. The droplets on the supersonic side were at rest with respect to the vapor stream. Now they are moving ahead through it with substantial, perhaps supersonic velocity. It is very difficult to say in detail what happens. Perhaps the frictional forces to which they are now subjected simply tear them to shreds. Certainly the stagnation pressures are enormous when compared to surface tension. At the very least, the droplet would have to configure itself to equalize the surface pressure; because metallic thermal conductivity is orders of magnitude higher than that of a vapor, the distorted droplet must be essentially isothermal throughout its volume. Since the equilibrium temperature at the front of the droplet corresponds to the stagnation pressure there, the droplet can, in principle, get very hot by simply gobbling up mass as it moves.

It was for reasons such as these that we declined above to estimate the degree of reversibility involved in the re-establishment of velocity equality between droplets and vapor streams. Nevertheless, we shall briefly consider the droplets to be solid spheres in order to estimate the distance required for velocity equilibration.

The drag force on a slow-moving sphere in a medium whose viscosity is η is given by F_η

$$F_\eta = 6\pi r\eta\Delta v \qquad \text{(IX-14)}$$

while the force on a sphere moving through a Newtonian fluid of non-interacting particles is F_m

$$F_m = \pi r^2 \rho_v (\Delta v)^2/2 \qquad \text{(IX-15)}$$

with ρ_v being the vapor density. The ratio of these two forces is

$$F_m/F_\eta = 12\ r\ \Delta v/2\nu \qquad \text{(IX-16)}$$

in which ν is η/ρ_v, the "kinematic viscosity." The non-numeric terms on the rhs of Eq. (IX-16) constitute a dimensionless number known as the "Reynolds number," Re. It is an emperical fact that over decades of variation in individual parameters, the frictional forces on an object appear to depend only on its geometry and Re. The transition from subsonic to supersonic flow regimes leads to no fundamental change in this assertion, except for modest adjustments related to convenience in defining ν when different parts of the fluid are at different temperatures.

Ordinarily Re is taken to be

$$\text{Re} = \frac{\Delta v\ \ell}{\nu} \qquad \text{(IX-17)}$$

in which ℓ is a dimension of the object measured in the direction of flow and Δv is the velocity difference between the object and the free stream. For a sphere or cylinder across the stream ℓ is taken to be the radius rather than the diameter. However, in the case of pipes and other channels, ℓ is taken to be the average diameter.

The dynamical forces exerted on an object are usually sated in terms of a drag coefficient C_D, or friction coefficient C_F, for forces acting in a direction along the flow, with the force referred to a convenient area, A.

$$F/A = C_D \rho (\Delta v)^2/2 \qquad \text{(IX-18)}$$

C_D being tabulated as an emperical function of Re.

For 1 μm radius spheres in mercury vapor at 650°K and 1 atm pressure and $\Delta v \sim 2 \times 10^4$ cm/sec, Re is in the decade between 10 and 100. Higher pressures and temperatures produce somewhat greater Re, still generally less than 3000. For this range of Reynolds number, the flow pattern around the object is still largely laminar and the friction forces predominantly viscous. For Reynolds numbers between 10 and 1000 the drag is given roughly by

$$C_D \doteq 10 / \sqrt{Re} \quad . \qquad \text{(IX-19)}$$

From the deceleration force given by Eq. (IX-18), the drag coefficient of Eq. (IX-19), and the mass m' of the sphere

$$m' = \frac{4}{3} \pi \rho_\ell r^3 \qquad \text{(IX-20)}$$

one can obtain the deceleration of the sphere. By integrating the velocity-time history one concludes that the equilibrium distance (referred to the flow) is roughly δx

$$\delta x = \frac{2\sqrt{2}}{15} \sqrt{Re} \frac{\rho_\ell}{\rho_v} r \quad . \qquad \text{(IX-21)}$$

For the data given above, Re is 20 and ρ_ℓ/ρ_v is about 5000. Thus, for this case δx is about 3000 droplet radii. If the droplets shred to small size, the stopping distance will be much less in both absolute and relative terms.

D. Spontaneous Mist Formation

Suppose that we cool pure dry mercury vapor, free of aerosols, along an isobar (constant pressure) to point A on the vapor saturation line as shown on the TS diagram in Fig. 37. Let us now continue to cool. Why should the

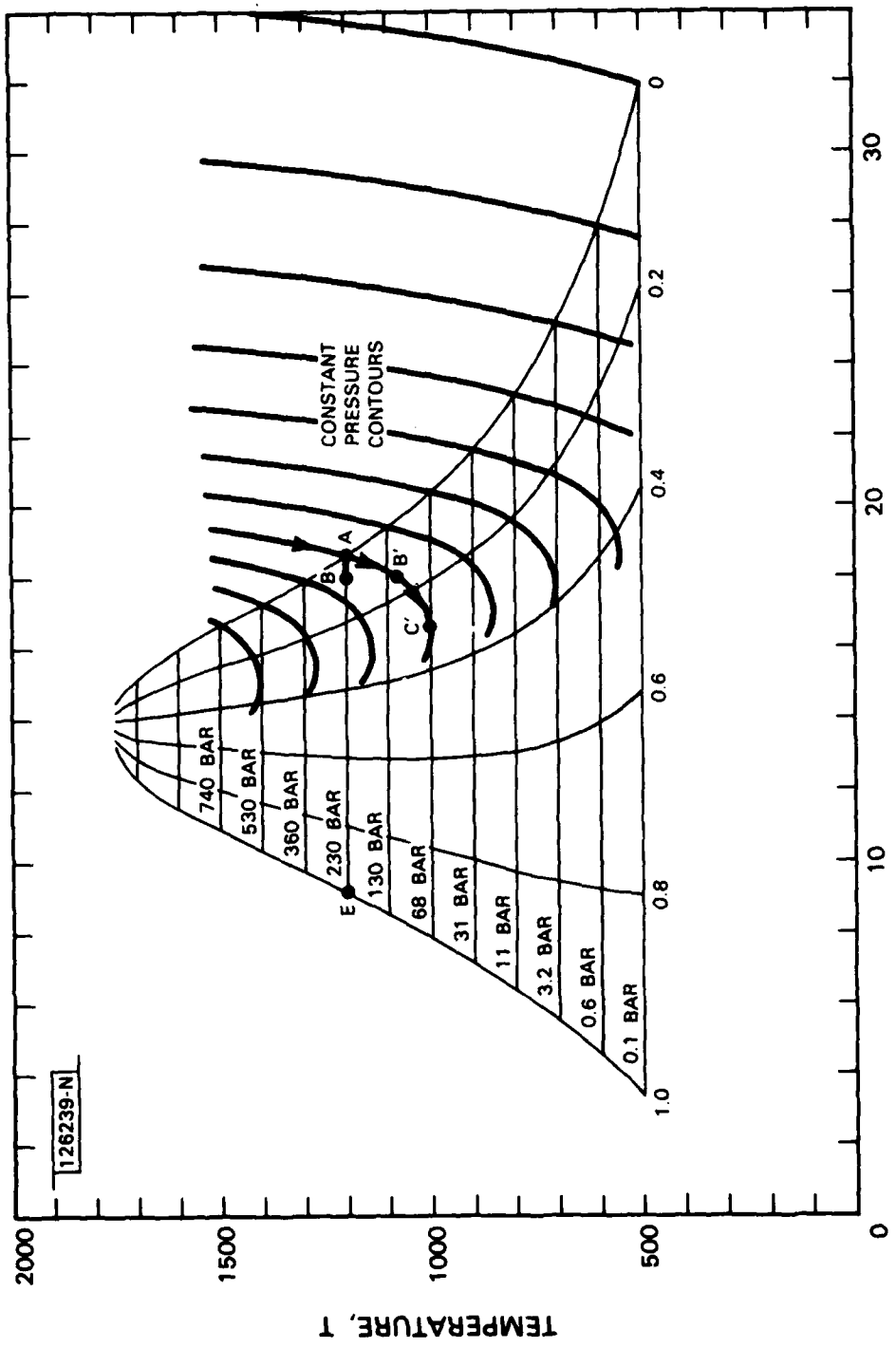

Fig. 37 Alternate dynamic condensation paths.

substance leave the homogenous isobar and become two-phase? True enough, the partially condensed vapor at B on the boiling line has a lower free energy than the homogenous gas at B', but what drives the change? The answer is, nothing drives the change. The gas simply supercools along the homogenous isobar.

Indeed, the forces of nature oppose the change. If a few atoms should randomly agglomerate, two effects tend to fragment the resulting nascent droplet:

1. The squeeze of surface tension (see above).
2. The temperature rise in the microenvironment following the release of specific heat of condensation.

There are two corresponding possibilities for spontaneous nucleation. One is that, with the pressure determined, the temperature could fall so low that the equilibrium pressure over the smallest possible droplet is below the environmental pressure, so that nucleation begins. Putting into Eq. (IX-13) a reasonable guess as to what might be the "smallest possible droplet" (capable of a statistically significant surface tension) yields apparently reasonable numbers for spont neous nucleation of water vapor (atmospheric water vapor is known to spontaneously nucleate at about -40°C). Similar "guestimates" for mercury based on a surface two monolayers thick, suggest spontaneous nucleation at half nominal condensation temperature. However, Eq. (IX-13) is not a means of <u>predicting</u> spontaneous nucleation; it is simply a means of classifying a minimum droplet radius or effective surface thickness <u>if</u> spontaneous nucleation occurs.

The second possibility is that the dry gas isobars in Fig. 37 are followed to the point C' at which the slope of the isobaric trajectory changes sign. This change in sign marks the transition from a stable positive specific heat to an unstable negative specific heat for the local environment of a nascent droplet. In this new region of instability, the release of heat by the droplet can cool the microenvironment, thus driving and stabilizing droplet formation.

Other means for getting the fluid past the local barrier to spontaneous condensation can be postulated, depending on one's perception of the nature of the local barrier. Both of the possibilities suggested above are useful mainly as frameworks for experimental results. Taking Kelvin's formula to atomic dimensions is an abuse of the statistics from which it was derived. Similarly, Fig. 37 extrapolates the Berthelot equation (see Section III) into a region in which we have no experimental evidence of its correctness in representing the isobars.

The only way to settle what really happens with mercury vapor is to boil it, cool it, and see what happens. The alternative is to provide droplet nuclei of sufficient size, and in sufficient numbers, that the questions about how condensation gets started simply do not arise. The droplet boiler is a natural source of such nuclei of the order of 0.01 to 0.1 μm in diameter, being the unevaporated cores of the injected boiler droplets. While this source of mist nucleation does not elminate the need for empirical evidence, it does provide the basis for engineering calculations with respect to growth rates and numbers of nuclei required to sustain such growth rates. In the next subsection we suggest the use of steam mode deliberately "wet" to provide controlled condensation.

E. Heat-Transport-Limited Mist Dynamics

Let us consider a steady flow with droplet nuclei moving along with the flow. At any point in time, t, the typical droplet has radius z. Let us further suppose that the nuclei are the remnants of injecting into the boiler droplets of radius r.

Thus, the number of droplets per mole, N, is found to be

$$N = \frac{M}{\rho_\ell} / \frac{4\pi r^3}{3} \quad . \tag{IX-22}$$

Although a growing droplet can exchange heat with the channel walls and other droplets by radiation, a change in the overall ratio of liquid to vapor requires that heat of condensation be exchanged between droplets and vapor.

This heat exchange cannot occur by radiation because mercury vapor is transparent at thermal radiation wavelengths*.

The mechanism for the heat exchange is conduction through the vapor (as dry gas). Such thermal conductivity rises with temperature; but for first order calculations we shall take the thermal conductivity, σ, to be 10^{-4} W/cm. Even at the Reynold's numbers of differential velocity just beyond a shock, the effective boundary layer thickness for thermal conduction is roughly one spherical radius; for low rates of relative droplet and vapor motion, classical heat flow theory gives the effective distance as exactly one spherical radius.

The rate at which heat can leave a spherical droplet having radius ζ is then dQ/dt W per mole:

$$dQ/dt = 4\pi\zeta\sigma\Delta TN \quad . \tag{IX-23}$$

On the other hand, if L is the molar latent heat of condensation (in Joules), we also have

$$dQ/dt = 4\pi\zeta^2 L \frac{d\zeta}{dt} \frac{\rho_\ell}{m} N \quad . \tag{IX-24}$$

Combining these two equations by eliminating dQ/dt (and N) gives a differential equation for the growth rate of the droplets as a function of the temperature differential ΔT between droplets and vapor:

$$\zeta d\zeta/dt = m\sigma\Delta T/L\rho_\ell \quad . \tag{IX-25}$$

This equation can be integrated directly to give the time required for the droplet to grow from some small size to wetness x. It can also be used to develop an equation for the profile of a nozzle that maintains a constant temperature difference between droplets and vapor. The details are carried as liquid density, heat of vaporization, etc.) are approximately constant over the working temperature range, one result of these calculations is a ratio

*Indeed, if the vapor were not transparent, the droplet boiler could not work as described in Sections IV and V. In this respect, steam (H_2O) and Hg are different, H_2O vapor having significant IR absorption.

relationship between speed of flow and distance along the nozzle (for small initial velocity and droplet size)

$$V/V_f = (Z/Z_f)^{3/7} \qquad \text{(IX-26)}$$

in which the velocity reaches V_f in distance Z_f. If the final wetness is X_f, then integration also yields

$$Z_f = (\tfrac{4}{7} V_f) \{L \rho_\ell x^{2/3} r^2/2m\sigma\Delta T\} \qquad \text{(IX-27)}$$

with the quantity in braces being the time t_x required under static conditions for the droplet to reach size $x^{1/3}r$. If we take L as typically 5×10^4J and m/ρ_ℓ as 15 to 20 in the hot region, and measure r in μm as r_μ, we obtain approximately

$$Z_f \doteq (\tfrac{4}{7} V_f) \{0.15 x^{2/3} r_\mu^2/\Delta T\} \quad . \qquad \text{(IX-28)}$$

For 1 μm droplets entering the boiler, a ΔT of 25°K implies about 1 meter of nozzle length and about 3 ms in time for expansion from 1200°K to 600°K, without reference to the nozzle diameter. Nozzle friction losses, however, do depend on the ratio of nozzle length-to-diameter. Nozzle friction will be low for a megawatt power plant having several centimeters of throat diameter (see Sect XC); friction will be difficult to control for simple expansion through a fraction of a millimeter throat diameter for a kilowatt power plant. Nozzle friction is the only problem of scale encountered in this study, in which "bigger" appears to be "better."

To get a better feel for the practical aspects of the situation, let us consider a flow of 1 mole per second with equilibrium expansion between 1200°K and 600°K. We have already calculated output and waste heat for such a flow at roughly 30 kJ and 35 kJ, respectively. Thus the flow represents an input of 65 kW to the turbine and an output of 30 kW from the turbine. In the process of converting heat to kinetic energy, the nozzle must condense roughly 20 kW of droplets. The nozzle throat area is about 2.5 mm^2 and the nozzle outlet is about 95 mm^2 (see Fig. 35 for ratios).

With micron size droplets the 20 kW heat exchange of nozzle condensation must flow through a boundary layer whose thermal conductivity is only 10^{-4} W/cm. Thus, in spite of micron thickness, the resistance of this layer is measured in degrees per watt. Thus the area over which 20,000 W heat exchange would occur would also be of the order of 20,000 cm^2.

Now, if a mole of mercury is broken up into liquid droplets with average radii of r_μ microns, the available area for heat transfer is Ar.

$$Ar \doteq \frac{50 \times 10^4}{r_\mu} \ cm^2 \quad , \qquad \text{(IX-29)}$$

apparently compatible with the above area requirement. But the flow is moving at several hundred meters per second through the nozzle; and we require that equilibrium be established in, say, a tenth of a meter. Thus the actual heat transfer rates required are tens of MW rather than tens of kW!

Evidently, there are four ways to meet the resulting inadequacy of the heat transfer situation within the nozzle:

1. Decrease the boundary layer thickness, or
2. Increase the area, or
3. Increase the thermal conductivity of the gas,
4. Increase the time available for droplet formation, or
5. Eliminate droplet size changes by using wet vapor at the nozzle inlet.

Brute force accommodation to slow nucleation rates by reintroducing multi-stage expansion is shown in Fig. 38. Here, each stage of (supersonic) expansion takes place in a time short compared with that required for the full formation of the droplet mist. The condensation appropriate to the pressure then occurs at leisure (and at constant H) in a plenum. The resulting droplet mist is extracted, concentrated, and returned to the boiler and the dried gas goes on to a second stage of non-equilibrium expansion in which the process is repeated. An so on, as many times as are necessary to reach condenser pressure and temperature. Note that in this scheme the droplets have no significant kinetic energy; consequently they do not have to be handled at high velocity.

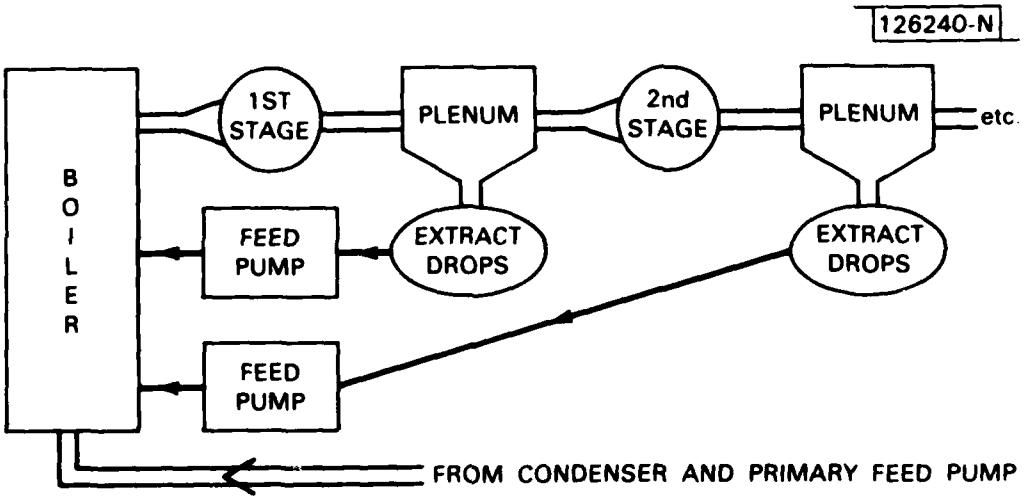

Fig. 38 Multi-stage expansion with intermediate equilibration plenums.

The operation of a system of this sort is shown on the H-S diagram in Fig. 39. The actual dry-gas isobars shown, being unjustified extrapolations of the Berthelot equation, are suspect; but the principles illustrated are none-the-less valid. In the Figure, there are three stages of expansion and subsequent condensation along the path ABCDEFGHJ in place of a single equilibrium expansion along the path AA'. After each expansion, there is an irreversible condensation BC, EF, and HJ. Following each of the two intermediate plenums, there is droplet removal along paths CD and EG. (The entrophy increases here are not real. They are the result of renormalization to show all processes on the same diagram.)

As shown on the diagram, the efficiency for the expansion AA' is 45%; that for the multiple expansion plant is 33% (which, if it could be believed, would still be respectable for a satellite power plant compared with 7% for a thermoelectric converter). On its face, the multiple-expansion plant is too complex for use in a satellite; but the qualitative fact is that the entropy gain in the first expansion is low compared with the entropy gain in subsequent expansions, while the wetness after the first expansion ($x = 0.1$) implies a substantial fraction of the eventual ($x \approx 0.4$) droplet radius*. Thus, instead of demisting the output of the first plenum, the wet gas may be expanded directly with nearly the full heat exchange area available [see Eq. (IX-26)], and with roughly three times the nozzle throat area as for the first expansion (see Fig. 35).

Another possibility is to increase the thermal conductivity of the gas by the introduction of a secondary gas such as He or H_2. In the pure state, these gases have thermal conductivity 20 to 30 times that of mercury vapor. However, in mixtures the effect of the light gas is reduced. Moreover, it is difficult to inject significant amounts of such gases either into the boiler or the nozzle without expending undue compressor power. Nevertheless, if such gases are used as buffer gases in the condenser, some will find its way into the boiler output, and perhaps thereby double the mixed vapor conductivity with respect to pure mercury.

---

*Recall that droplet radius varies as the cube root of x.

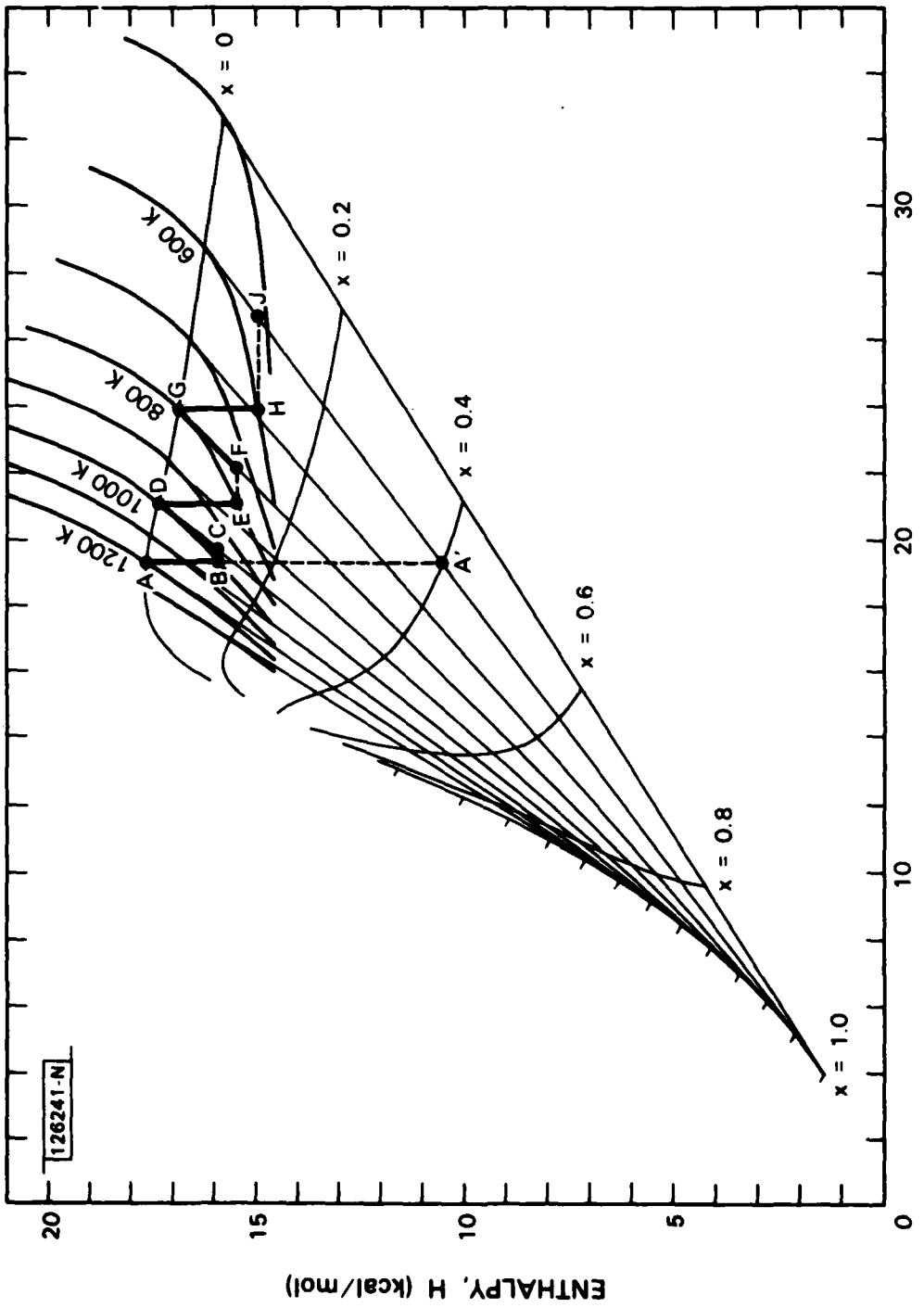

Fig. 39 Multi-stage expansion on H-S diagram.

While the incidental benefit from buffer gas circulation and from single-stage dry expansion may each amount to a factor of two in condensation heat exchange rate, the first two entries in the list - droplet area and boundary layer thickness - tend to act together to change order of magnitude, especially in the high pressure regime in which the droplet radius is large compared to a gas mean free path length. As the droplet radius goes down towards 0.1 μm, however, three limitations appear. First such droplets are difficult to produce from a liquid stream; second, they are below the evaporation size limit for the boiler; third, the effective thermal conductivity of the vapor may drop as the particle size goes below an atomic mean-free-path.

To utilize small droplets effectively requires a system with parallel paths, as shown in Fig. 40. This is a system which has wet, rather than dry, vapor emerging from the boiler. Consequently, there is an excess of droplet area in the system at all times. There is a separate nozzle loop A into which liquid is injected, designed for the sole purpose of maintaining a sufficient density of aerosol in the boiler output.

The result is wet vapor at an expansion nozzle inlet. Now, initially dry vapor requires a major change in wetness through condensation as it expands from A to A' in Fig. 38. But wet vapor expanding from P to Q between the same temperature limits entails little, if any change in droplet size x. Thus, the introduction of wetness helps in two ways; it provides extra area to accelerate condensation if it is needed; and helps eliminate the requirement for condensation in the first place! These phenomena are discussed again in Sections X and XI.

If the design is for a central station power plant, submicron droplets may be overkill, in which case the loop A, pump B, and their controls maintain the maximum droplet size that permits the expansion nozzle to function properly. In the central station power plant, the mercury condenser will also be a water boiler. Because mercury is a liquid metal, film condensation is not inhibited by the liquid layer formed; the area design of the condenser will be almost entirely determined by the heat transfer characteristics of the steam side.

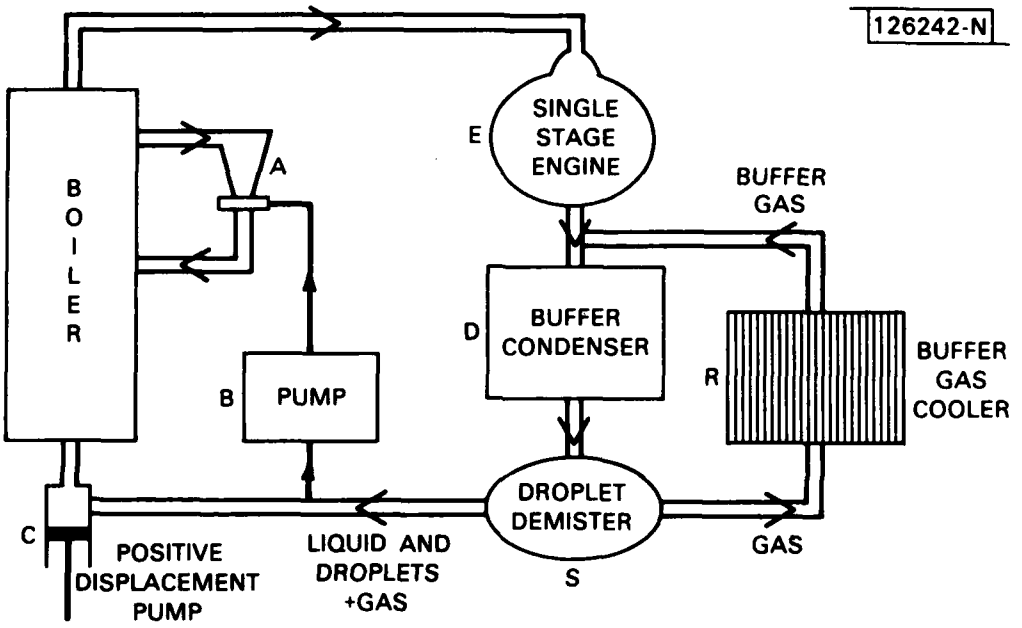

Fig. 40 Single-stage turbine engine with buffer gas condenser and microdroplet regeneration.

Liquid condensed can simply flow by gravity to a collection pump; there is no need for a buffer gas in the condenser.

In a satellite the possible weight of mercury accumulating in a condenser without the assistance of gravity flow presents a problem. A radiation design by Buden[19], using heat pipes and potassium as the condensate, was sized at about 8.5 kg/m^2. Assuming the wicks to be carrying 100 μm equivalent film thickness of liquid mercury in place of potassium would add about 1 kg/m^2 to the design weight, with corresponding greater weights for larger amounts of liquid in transport. Moreover, one must exercise care that the returning mercury liquid is able to wet whatever wicking system is provided. The satellite alternative is not to allow the mercury droplets to wet the condenser walls by carrying them as aerosols in an H_2 or He buffer gas at the low pressure of the condenser. The fractional micron droplets plus uncondensed vapor are mixed with buffer gas at the inlet to a buffer condenser. Most of the mercury vapor is condensed onto droplets with cooling by heat exchange with the buffer gas. The majority of droplets are separated from the gases in a dust-eliminator type of separator[17], and are coalesced into liquid (or at least into a semi-liquid mass of droplets). Some of this liquid is used via pump B to generate submicron nuclei in loop A, for example, by means of a supersonic jet whistle[16]. The rest is pressurized to boiler pressure in a positive displacement pump that can handle both liquid and gas. The vapor output (with concentrated aerosols) is bypassed from the displacement pump output directly into the boiler. The liquid at C is injected via an atomizer which need not produce droplets of any set size. The buffer gas from S, with some unseparated small aerosols, is circulated and further cooled in a separate radiative cooler.

Thus the mercury never reaches the boiler or condenser walls, except incidently and temporarily. Boiling takes place from, and condensation to, droplets. Droplet sizes are maintained in a separate control loop, not by the main boiler injection spray. Concentration of droplets into liquid after condensation takes place in a volume designed for the purpose, either as a

centrifuge or as Calder-Fox separator[18], not on the extensive surface of a heat radiator.

The particular means of executing the functions illustrated in Fig. 40 are by no means limited to using the cores of boiled or re-injected droplets. One can, for example, introduce into the system a mercury-wettable colloidal aerosol (having particle diameter $\leq 0.1\ \mu$) so that the cores of all droplets are non-ephemeral. In this case, we would seek to obtain a densified aerosol mixture rather than a liquid from the condenser output. Only residual fluid that might happen to agglomerate would be injected into the boiler as liquid; the bulk would be returned as compressed buffer gas plus aerosol. In such a case, one might be able to rely on passage through shock fronts, and wall contact in the turbine, to shred multicore agglomerates. The loop A in the Figure might then become a vestigial function, or be combined with the residual liquid reinjection system. Finally, in order to control the wetness of the fluid at the boiler inlet, a feed W of controlled size droplets may be implemented.

With all of those variants possible, it is Fig. 40 that we seriously propose for a system configuration for use on satellites.

X. NOZZLE DESIGN AND NOZZLE LOSSES

In this Section (and Appendix B) we obtain profiles and performance for nozzles designed on the assumptions that there is a constant temperature difference between the droplets of condensate and the bulk of the vapor as the fluid expands, and that this temperature difference is small enough not to have a major influence on the relationship between droplet temperature and fluid velocity at any given cross section. It follows from this analysis that the friction loss in the nozzle depends mainly on the ratio of nozzle length to throat diameter. On the one hand, the throat diameter is determined by the nominal power level of the nozzle output; on the other hand, the length of the nozzle is inversely proportional to the assumed temperature differential, and is substantially shorter when the inlet fluid is wet than when it is dry.

By trading off losses due to friction against losses due to entropy increase across the finite temperature differential, it is estimated that nozzle expansion of wet Hg vapor is possible at the 100kW to 300kW output level with losses, and geometry, comparable to that of supersonic nozzles operating on non-condensing air. The loss estimates are 8% to 10%; and the average flare semicone angle is about 10°. For power levels under 30kW or over 500kW, there are difficulties. In the low power case, friction becomes too high and/or the temperature differences within the nozzle become too large to justify the assumptions made. In the high power case, the nozzle becomes too short and acquires too wide a flare to justify the assumptions. No attempt is made in this Section to investigate criteria for nozzle design other than constant temperature difference. The low power case is discussed further in Section XII.

A. Nozzle Design, For Constant Temperature Difference.

Designs for supersonic nozzles typically have friction losses which are 5% to 10% of the nominal output kinetic energy (KE). But such designs are for the expansion of air without change of state. For condensing flow there will be a tradeoff between losses due to the failure to maintain equilibrium between vapor and condensate on the one hand, and losses due to friction as the nozzle is

lengthened to allow time for equilibrium to be reached as the flow passes through it. There is an additional loss, which we shall not consider here, if the walls of the nozzle are maintained at other than the "adiabatic wall temperature" established by the flow itself.

Expansion data for nozzle flow at equilibrium are given graphically in Figs. 33 and 35. The thermodynamic model of Section III can be applied to the case of heat-transfer-limited condensation, as discussed in Section IX, by the numerical method outlined in Appendix B, to obtain flow and nozzle profiles for near-equilibrium conditions. Profiles for one such design of nozzle is shown in Fig. 41 (on an exaggerated radial scale), in which it is assumed that condensation is taking place on the remnants of 1μm droplet mist injected into the boiler with a constant temperature difference ΔT of 25°K between the droplets and most of the vapor. The constant-temperature-difference nozzle is not the only, or even the best design possible. It is used here as a means of establishing the nature and order of magnitude of design problems.

The nozzle shown in Fig. 41 is long (over 100 cm for 1200°K and 600°K respective inlet and outlet temperatures) for two reasons:

(a) There is initially very little droplet area to support the exchange of heat between droplets and vapor.

(b) There is a substantial change in droplet size as the vapor condenses. Accordingly, there must be time in which to return heat of condensation to the uncondensed gas.

Figures 39 and 40 introduced the concept of producing boiler output with controlled wetness and controlled droplet size. If one starts with vapor with roughly 50% to 60% wetness, there is very little change in net droplet size during expansion, although the droplets themselves still must be cooled at the gas component cools. However, the droplet area for heat exchange is now as great at the beginning of the expansion as it is at the end of it. Taken together, these factors result in a factor of 4 or more decrease in the length of the nozzle for given inlet, outlet, and disequilibrium temperature conditions.

Figure 42 shows a series of nozzle profiles for initial wetness in the range from dry up to 60% wet, with droplet size after complete condensation

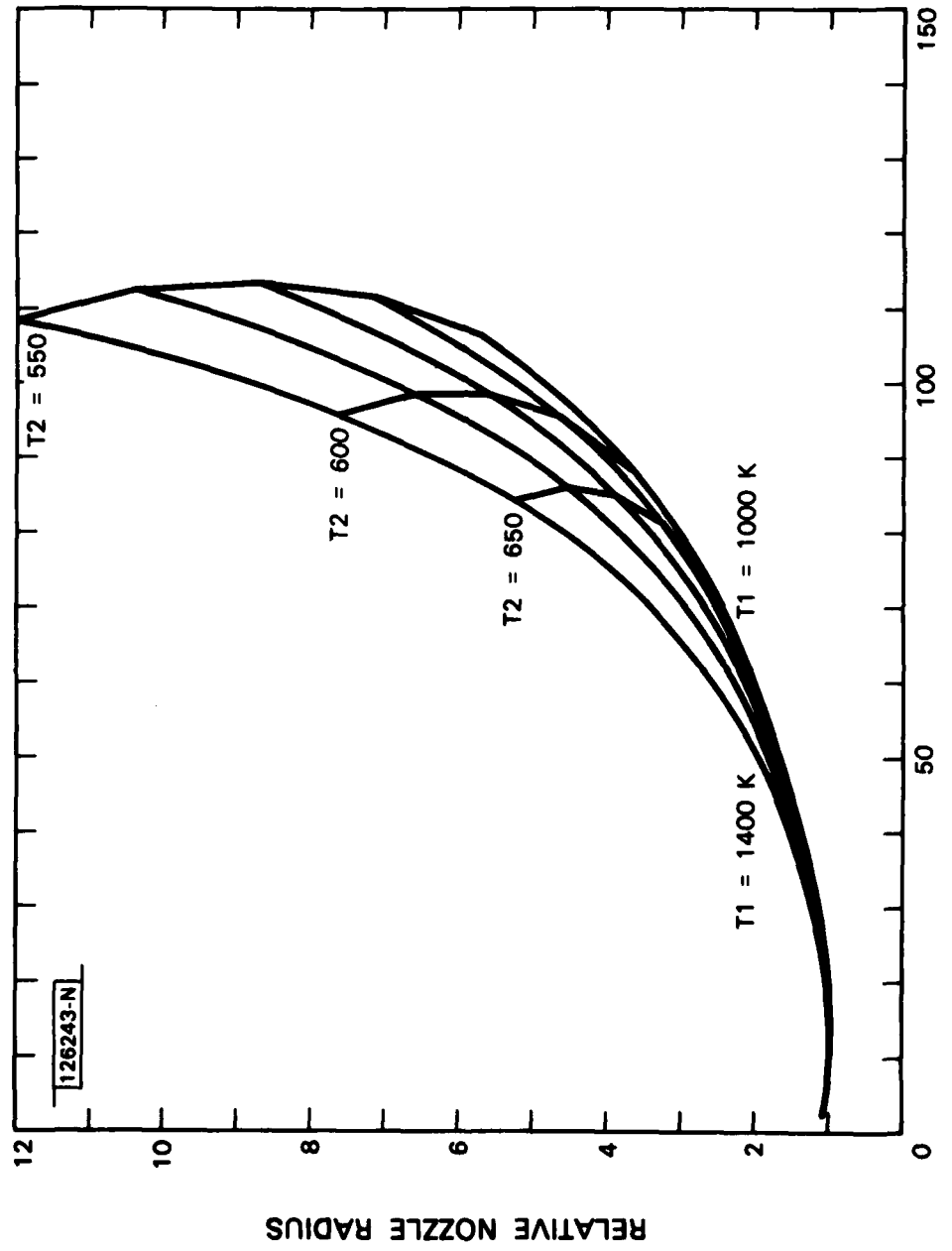

Fig. 41 Nozzle radius vs nozzle length.

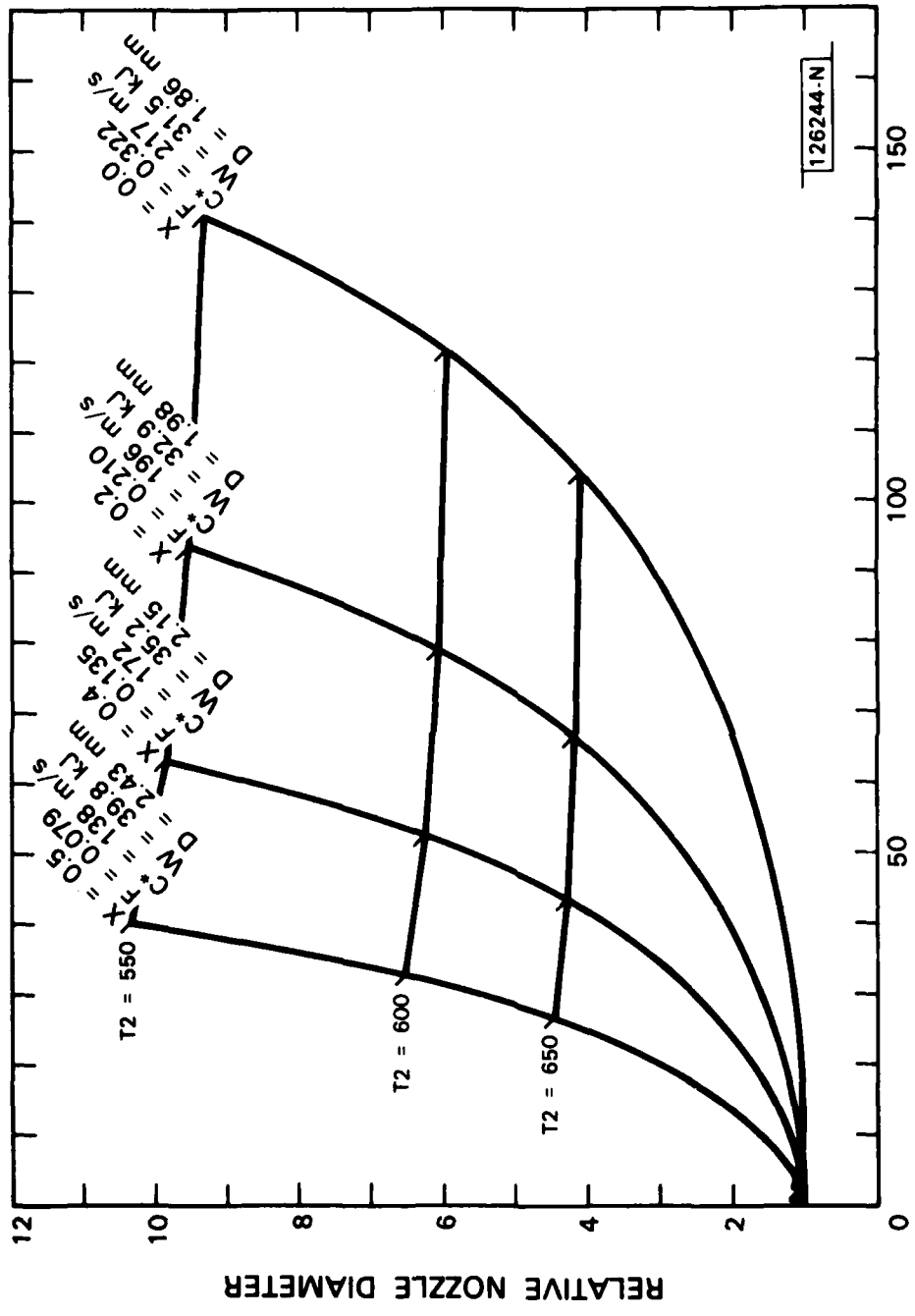

Fig. 42 Nozzle diameter vs nozzle length for wet vapor.

being 1μm, and the temperature differential between droplets and vapor being 25°K. The length of an actual nozzle of a design illustrated in either Figure scales with actual temperature differential, ΔT, and actual fully condensed droplet size, r_μ in μm, as in Eq. (X-1)

$$L_{NOZ} = L_{Figure}\, r_\mu^2\, (25/\Delta T) \qquad (X\text{-}1)$$

Table X-I gives some of the details of flow through a nozzle designed in accordance with Fig. 42.

TABLE X-I

NOZZLE FLOW PARAMETERS

Initial Wetness X	Throat Velocity (m/s)	Length 1200° to 600° (cm)	Friction 1 cm Throat % of KE	Typical Throat (mm)	Typical Power Flow (kW)
0.0	215	121	32	1.9	31
0.2	210	74	21	2.0	33
0.4	170	53	14	2.2	35
0.6	140	33	8	2.4	40

The second column of Table X-I shows the throat velocity dropping as the initial wetness increases. There is a proportional drop in the velocity at the nozzle outlet; both decreases are due to the presence of droplet mass as "dead weight" in the expanding gas stream.

The final two columns in Table X-I give typical throat diameters and corresponding nominal KE power level in the nozzle output. Inasmuch as the throat velocity is fixed by inlet temperature only, the power handled by the nozzle will scale as the square of the throat diameter. Thus, for the conditions concontemplated in the Table, the power output of a nozzle with a 1cm throat diameter is slightly over 1/2 MW, while to reach down to a nominal level of 2 kW requires a throat diameter of 0.5mm. for the conditions to which Table X-I applies (25° temperature differential and eventual 1μm condenser droplet size).

The fourth column of the Table gives frictional losses, calculated by methods outlined below, for a 1cm nozzle diameter (1/2 MW power level). They are high. They can be made lower by decreasing nozzle length (higher temperature differentials or smaller droplets) or by increasing throat diameter (higher power level). While an increase in throat diameter is surely desirable on a central station power plant scale, in a satellite the problem will be to control losses as the throat diameter is scaled below a millimeter. While a decrease in droplet diameter is theoretically possible without violating the assumptions of Section IV, as a practical matter the 1μm radius assumed may already be at the low end of what is technically reasonable. Consequently, we must examine the losses that may be ascribed to disequilibrium of temperature and those that may be ascribed to friction to see where the best mix of the two may lie.

B. Disequilibrium Entropy Loss.

The thermodynamics of non-equilibrium systems is a complex subject which we shall not attempt to enter here. The formulas of Section IX and Appendix B are worked out on the assumption that ΔT is very small, so that it is unnecessary to correct cross section and velocity computations for the difference between an adiabatic expansion $\Delta Q=0$ and the assumed isentropic expansion $\Delta S=0$. Generally speaking, so long as the entropy loss due to finite ΔT between liquid and vapor is small, the required adjustments to the calculation of cross-section and length do not change the scaling law of Equation (X-1)---or the friction calculations below---significantly.

The increase in entropy due to finite ΔT can be estimated by considering the heat dQ exchanged between droplets and vapor while the system is in the temperature range T, T+dT for droplets and T-ΔT, T-ΔT+dT for vapor. The entropy of the flux leaving the droplets is dQ/T. The entropy arriving at the vapor is higher, dQ/(T-ΔT). Consequently, the entropy increase dS is the difference:

$$dS = dQ\ (1/(T-\Delta T) - 1/T) \qquad (X-2)$$

Let us assume that dQ/dT is constant over the range between T_1 and T_2; and that the total heat exchanged from the droplets is Q_{12}. Then by integrating Eq. (X-2) between T_2 and T_1 as limits, and by expanding the resulting logarithms in power series, we obtain for the total entropy increase approximately S_{12}

$$S_{12} = (Q/(T_1-T_2)\ (\Delta T/T_2 - \Delta T/T_1) \qquad (X-3)$$

On the one hand, T_2S_{12} is the waste heat that must be discarded at the condenser on account of the entropy increase. On the other hand, Q is somewhat less than the work W nominally available. (The remainder of W comes from the H of the vapor without condensation).

The ratio Q/W varies from about 0.8 for an expansion starting with dry vapor down to about 0.5 for an expansion starting roughly 50% wet. Thus, for 1200° and 600° inlet and outlet conditions we obtain for the inefficiency due to entropy increase roughly

$$= (Q/W)\ (0.5\Delta/600) \qquad (X-4)$$

Evidently, for disequilibrium loss of about 6-7% with inlet vapor 50% wet, one can tolerate ΔT up to about 150°K. One cannot safely design according to these formulas with ΔT very much larger; at some sufficiently large ΔT (about 200° to 250°K if the constant pressure contours of Figs. 7 and 37 are correct) there will be spontaneous nucleation of the vapor, followed by the formation of a very large number of very small droplets whose total area we cannot analyze a priori. (There is also additional potential loss associated with the establishment of the ΔT in the first place. It can be partly avoided by injecting the seed droplets into the nozzle vapor at the lower temperature).

C. Nozzle Friction Loss.

In Section IX, in particular in Eqs. (IX-18) through (IX-21), we introduced the concept of coefficient of drag for the dynamic forces on a body

moving with respect to a fluid. The corresponding concept for wall friction is the friction coefficient C_f which relates loss per unit area of wall to the free-stream "dynamic pressure" $\rho v^2/2$. Suppose that the wall friction coefficient applicable to a flat surface or to a short length of tube is given. Then if the tube diameter is D, the fractional decrease in KE per unit length is given by*

$$dKE/KE = 4C_f\, dz/D \tag{X-5}$$

The coefficient C_f depends on the Reynold's number Re. In a conical nozzle the flow is at no point "fully developed", so that it is not clear whether the "typical length" used in specifying Re should be the nozzle diameter or length along the nozzle. Happily C_f is a very weak function of Re if Re is above 10^4. We take

$$\begin{aligned} 4C_f &= 0.02 \text{ for subsonic flow} \\ &= 0.01 \text{ for supersonic flow} \\ &= \text{neglect for first few nozzle entrance diameters of length.} \end{aligned} \tag{X-6}$$

Using the methods of Appendix B, the loss in Eq. (X-5) can be integrated along the length of the nozzle to provide an estimate of the overall friction loss as a fraction of the nominal KE at the nozzle outlet. The fractional friction loss for nozzles such as those shown in Figs. 41 and 42 is then given by ζ_f

$$\zeta_f = f_n \frac{L_{NOZ}}{d_{throat}} \tag{X-7}$$

where f_n is a friction factor for the particular nozzle design (determined from

---

* This equation applies equally to a circular or rectangular cross section at high Reynold, number. The friction increases by only 15% if the cross section has a 3:1 aspect ratio, as might be desirable to confirm to the geometry of blade inlets as a turbine wheel.

the integrat. ⁿ⁾ and d_{throat} is the nozzle throat diameter. For the nozzles in the Figures, f_n is approximately 0.25%. It is a weak function of actual inlet and outlet conditions; more accurate assessments of f_n can be obtained by dividing the tabulated loss in the fourth column of Table X-I by the nozzle length given in the third column.

A nozzle with a 1 cm throat in Fig. 41 is thus out-of-scale with respect to friction at the design 25° temperature differential and dry vapor at the inlet. The friction loss over the 120 cm length is 33%; the disequilibrium loss is only 1.5%. With the selection of ΔT at 100° to 125°, the nozzle has a 25 to 30 cm length, and total losses due to both causes of about 14%. By using 50% wet fluid at the inlet, the nominal nozzle length drops to about 11 cm and the nominal overall loss to about 6%. But in this case there are other design complications: the resulting nozzle is too short relative to both its throat and outlet diameters for the methods which we have been using to be applicable. Evidently, the analysis and design of a nozzle suitable for use on a central station power plant scale cannot be undertaken by the approximations used here.

Table X-II gives the dimensions and losses for a number of possible power levels for nozzled designed according to the above methods with nominal 1200° and 600° inlet and outlet temperatures as 50% wet fluid at the nozzle inlet.

TABLE X-II

NOZZLE DESIGN AND PERFORMANCE

Nominal Power Level kW	Nozzle Throat mm.	Nozzle Length mm.	Nozzle Outlet Diam. mm.	ΔT °K	ΔS Loss %	Cf Loss %	Total Loss %
2	0.55	55	3.5	200	10	25	35
10	1.2	70	7.8	150	6	13	19
30	2.1	70	14	150	6	8	14
100	3.8	85	24	125	5	5	10
300	6.6	125	42	100	4	4	8

From this Table, we note that the 100kW and 300kW nozzles have losses typical of supersonic nozzles operating with air, and comparable flare between throat and outlet, about 1/3 overall or about 10° semi-cone angle.

At the lower power levels there is an appreciable efficiency problem. One possible means of getting around this problem is considered in Section XII, in which the flow is taken through a rotating joint on the rotor axis and expanded against Coriolis force as a virtual piston for part of the energy extraction.

PART 5

APPLICATIONS ENGINEERING

Chapter Summaries

Chapter XI
OVERALL PERFORMANCE

A variety of losses in a practical mercury cycle are identified: pipe and turbine blade friction; windage and bearing friction; losses due to non-equilibrium heat transfer in boiler, nozzles, and condenser; feedpump and atomizer losses; and other miscellaneous losses. Sums of conservative estimates of such losses run from 30% at the 100 kW level up to 40% at the 10 kW output level. In a careful integrated design, overall losses may be lower, ranging from 10% at the central station scale up to 20% at the 30 kW satellite power plant scale. Overall efficiency from a hot shoe at 1100°C to a condenser at 300°C for a 30 kW satellite power supply is estimated to be 35% of the thermal input; using a bottoming cycle, central power plant efficiency is estimated to be 55% of thermal input.

Chapter XII
FEASIBILITY OF LIGHT WEIGHT POWER SUPPLY

Total weight and pounds-per-Watt for a variety of source and power conversion technologies are compared. Detailed estimates of weight and performance are made for boiler, waste heat radiator, turbine, and alternator. A possible application to RTG heat sources at the 10W/lb, 1 to 3 kW output level is suggested, using a reaction turbine. It is speculated that a LASL proposal for a 1MW reactor in space can be scaled down in weight and power level with 100 kW of ouput at 1oo W/lb. A developmental program to obtain 30 kW output for satellite use from a 10-meter diameter focussed solar collector is suggested, also sized for 100 W/lb (without storage for shadow).

Chapter XIII
DISCUSSION OF RESULTS

The devices and techniques orientation of this report is contrasted with the system engineering approach needed to assemble and integrate an actual system exploiting the technology. The techniques which have been introduced avoid the major system problems of the old low-pressure mercury system and the SNAP-8 program, at a cost of introducing new technology. It is urged that laboratory level testing of all system components excercise those components well beyond their intended stress levels to avoid limited-lifetime surprises at the pilot plant or full system level of application.

XI. OVERALL PERFORMANCE

At several stages of the discussion in preceding sections, it has been necessary to evaluate potential performance of a system component, either by making assumptions or by choosing operating ranges from curves and diagrams. In each case, the attempt was made to assume (likely) worst-case conditions, and to provide upper bounds on losses, rather than to delve too far into the design of individual system components. At the same time, we have completely neglected effects that are of secondary engineering importance. Good examples of the latter are (i) design temperature differentials between boiler hot shoe and output fluid, and (ii) losses from piping and turbine casings. In the former case, the engineering problem is the pressure, which has already reached 3500 psi at 1200°K, not the hot shoe temperature, which can be several hundred degrees higher in current nuclear power source designs. In the second case, the energy density in the moving fluid is so high that it is extremely difficult to remove significant amounts of it unless (as we have seen) one deliberately engineers for heat exchange.

In this Section we make estimates of bounds on friction and other incidental losses to arrive at bounds on the overall inefficiency of the cycle that is postulated in Fig. 40. The resulting bound on the loss is generally no more than 30% of the theoretical efficiency, with the actual loss probably no more than 10 to 20% of theoretical efficiency.

A. System Losses

In drawing up a system overview of potential performance of the mercury cycle as a practical heat engine, we shall provide upper bound to losses deemed significant and to neglect losses deemed insignificant. Moreover, we shall examine in detail only one set of inlet and outlet conditions, namely a turbine inlet temperature of 1200°K and outlet temperature of 600°K, for which the Carnot efficiency is 50% and the simple Rankine cycle efficiency (see Fig. 19) is 46%.

Figure 43 identifies a variety of losses that might be associated with a single-pass mercury heat engine of the type outlined in Fig. 40 at the end of Section IX. The Figure lists 14 loss mechanisms beyond those already included in the statement that the efficiency of the Rankine Cycle is 92% of the ideal Carnot Cycle for the temperature range assumed and for the properties of mercury calculated in Section III. Evidently, if these additional losses are not to get far out of control, each individual loss must be held to an average of one or two percent. Some of these additional losses have already been discussed in earlier Sections. The others will be dealt with here.

Some of the entries on the list in Fig. 43 fall into the category of losses that can be "neglected." Since we consider the temperature of the fluid entering the condenser (not the actual cold shoe temperature), item (k) is not germaine to the calculation. If friction losses in the nozzle and turbine blades can be held small, the corresponding losses in piping and condenser can be held very low indeed. We shall lump all such "negligible" losses together, including items (b), (c), (k), and (l) and assign to them an arbitrary "miscellaneous" 10% of the theoretical mechanical output.

We have already observed, in Section VII, that losses like the feedpump loss are subject to a design tradeoff. If all the feedpump does is to compress liquid, the energy of compression is a few Joules per mole, wholly negligible, even with low feedpump efficiency, compared with 65 kJ per mole at the boiler output. However, if 5% vapor content is allowed passing through the feedpump, the feedpump must supply 1 kJ per mole at, say 80% efficiency. (While some of the energy so supplied is recirculated cycle energy, the conservative assumption is that <u>all</u> of the resulting 1.25 kJ represents a system <u>loss</u>). On the other hand, it was noted in Section VII that recompression at 5% vapor should improve the theoretical cycle efficiency from 92% of Carnot to about 96% of Carnot, for a slight net gain over the assumed 1.25 kJ required to run the

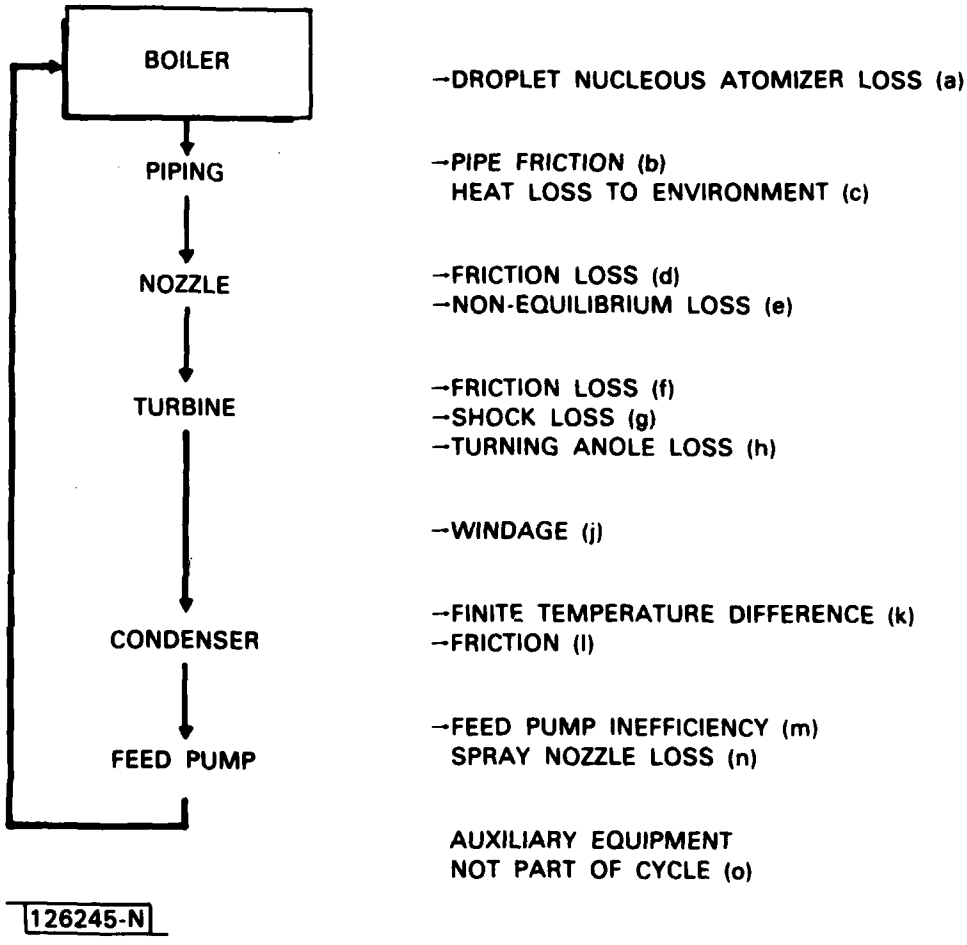

Fig. 43 Sources of loss.

compressor. Thus, in either case, we can add the feedpump compression power to the "miscellaneous" list.*

The items labelled as atomizer losses, namely items (a) and (n) in Fig. 43 cannot be dealt with so summarily. To form a droplet, it is necessary to supply surface energy in the form of surface "tension", Γ. If a mole of mercury is formed into 1 μm radius droplets at condenser temperature, the surface tension amounts to 20 J/mol. The surface energy varies inversely with droplet radius, rising to 200 J/mol for 0.1 μm droplet dimensions. Most nozzles and other devices for forming droplets of colloidal dimensions do so with an efficiency of one or two percent. However, for ultrasonic atomizers, the efficiency can be as high as 10%. Let us suppose, as an upper bound, that all of the fluid is atomized on each circulation into 1 μm droplets at 1% efficiency or into 0.1 μm droplets at 10% efficiency. Thus, either (a) or (n) of Fig. 43 (but not both) could carry an energy overload of 2 kJ/mol, which is roughly 3% of the molar energy at the boiler output.**

There are two kinds of losses in the nozzle and turbine blades besides the increase in entropy in the shockfront. The latter loss was found in Section VII to be at most 1/8 of the 25% of nozzle kinetic energy seen by blades, a net maximum of 3%. In addition there is friction in the boundary layer that separates a flow from its bounding channel, and induced turbulence in the flow itself as it turns a corner. It is shown in textbooks that the adiabatic wall temperature next to a supersonic flow is neither the initial temperature T_1 of the flow at low speeds, nor the temperature T of the high

---

* If the vapor at the nozzle inlet is deliberately made wet, as discussed below, in order to make possible nozzle designs with reasonable physical length, then this recompression has much greater leverage on the efficiency of the cycle and may be a sine qua non to thermodynamically efficient operation.

** It is not unusual for trace additives to cause a factor-of-two reduction in the surface tension of liquid metals. For example, 0.05 mole percent. Cs causes such a reduction in Hg. The author has obtained preliminary experimental evidence that small amounts of In or Ga also alter the surface tension of Hg.

speed free stream; rather it rises above T by a fraction, P_r, of the difference $T_1 - T$. Here, P_r is the Prandtl number

$$P_r = \frac{C_P \sigma}{\mu} \qquad \text{(XI-1)}$$

which is about 0.65 for mercury vapor over a wide variety of conditions. Since we have assumed the heat losses through nozzle and piping walls to be negligible, the formula for wall temperature T_W

$$T_W = P_r T_1 + (1 - P_r)T \qquad \text{(XI-2)}$$

is valuable mainly for estimating the temperature environment in which the wall materials must function, especially as operating conditions change.

The dynamic loss as the flow turns a corner results from the fact that the distance to be travelled along the inner radius of the bent channel differs from the distance travelled along the outer radius. For a one-dimensional flow, one can calculate that if pile-up of mass is to be avoided, a rotary motion is imparted to the flow as it turns the corner which (at subsonic speeds) consumes roughly $w^2/12R^2$ of the KE of the flow, w being the width of the channel, and R its average radius of curvature (see Fig. 44). Evidently, if $w/R < 1/3$ the kinetic energy loss will be less than 1% of the KE in the curved channel. Since this loss is principally in the turbine blade channels, where the KE is only 1/4 of that at the nozzle outlet, we can assign this loss, with $w/R < 1/3$, to the "miscellaneous" category of individually negligible losses.

A possible blade configuration is shown in Fig. 45. Here, flow entering the blades at A encounters a normal shock near the throat at S and slows down further in the "stagnation" chamber B while turning through a substantial fraction of 180°. Having turned, the flow returns to sonic speed at throat E and exits supersonically at C. Evidently, the losses in chamber at B are a part of "miscellaneous." The loss in the inlet shock has already been bounded.

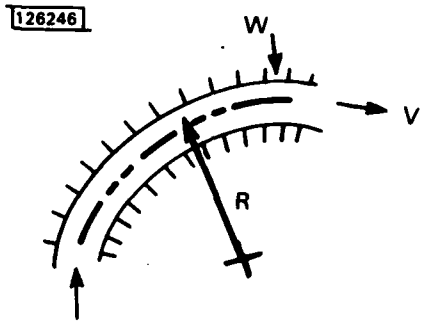

Fig. 44 One-dimensional flow turning corner.

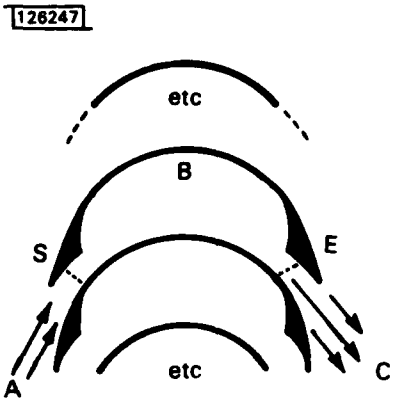

Fig. 45 Blade configuration.

The losses in the outlet nozzle, and the additional losses at the inlet nozzle are still bounded by expressions like Eq. (X-7). Inasmuch as the throat-to-length ratio can be held in reasonable bounds on the turbine blades (because no further condensation takes place), and because the apparent kinetic energy of blade flow is only 1/4 that of the main expansion nozzle, such friction losses are in the 1% rather than the 10% class.

The one remaining loss that we must discuss is the friction and windage loss. Experience with energy-storage flywheels strongly suggests that the windage loss will be very much larger than the bearing loss in a high speed machine using either magnetic or fluid-dynamic bearings. The flow leaving the wheel, of course, presents no windage problems; but it is not possible to make the flow leave the wheel on all parts of its high speed surfaces.

All wheels operating at peripheral speeds comparable to the speed of sound are potentially efficient centrifugal pumps. If the pumping action is not anticipated, the results of uncontrolled circulation can increase the windage losses substantially. But with intelligent design, and a reasonably close-fitting casing, the fluid within the casing will circulate circumferentially at one-half the angular velocity of the wheel, and the (radial) pumping will be confined to two thin boundary layers, one adjacent to the wheel and the other adjacent to the casing.

Under such circumstances, it is possible to define a coefficient C_M that relates the frictional torque to speed and area in much the same way that C_F relates friction force to speed and area. For (both sides of) a thin disc having radius r and spinning with angular velocity ω, standard formulas for the torque, T, are[22]

$$T = C_M \frac{1}{2}\rho\omega^2 r^5 \qquad \text{(XI-3)}$$

$$T = C_M \frac{1}{2}\rho v^2 r^3 \qquad \text{(XI-4)}$$

where the second formula is obtained from the first by substituting the peripheral velocity v for ωr.

Reynolds number in such cases is computed from v and r. It is gener. in the range 10^7, for which C_M is nearly constant at 0.005, and for which the boundary layer is roughly 0.001 r thick. Similar formulas hold for the outside surface of spinning cylinders, with cylinder length taking the place of one power of r.

Evidently, from Eq. (XI-3), for a given angular velocity only the largest-radius parts of the rotating assembly need produce significant windage loss. The actual power loss, P, is found by multiplying T by ω:

$$P = C_M \frac{1}{2} \rho v^3 r^2 \quad . \qquad \text{(IX-5)}$$

From Table III-1, we take ρ at 600°K and 0.6 atm pressure to be 0.0024. Using r equal to 4.5 cm and v equal to 280 m/sec, one finds a windage loss of 267 W. The use of wet vapor at inlet and outlet would raise ρ somewhat; but this increase is more than offset by the reduction in v as a result of extracting less energy per mole passing through the nozzles on account of wetness. Millner[18] made measurements on the windage loss of a slightly larger wheel than the one assumed here, mounted on magnetic bearings in air. He states that his drag loss at low pressure would have been 19 W at 50,000 rpm. Scaling his result to atmospheric pressure according to his measured pressure vs. loss curves suggests a windage loss of 200 W, comparable to the losses calculated from Eq. (IX-5) for the present case.

Note here a question of scale. If we postulate that a 0.5 cm blade height is reasonable for a 9 cm diameter wheel, while the nozzle exit area for 1 mol/sec, 30 kW mechanical, flow is only about 1 cm^2. It follows that this wheel is an order of magnitude under-utilized in power throughout capacity for a given friction. The proper mechanical output for such a wheel is 350 kW, for which the windage loss is <0.1%. In this connection, the force acting

around the periphery of the wheel is 1250 newtons to produce 350 kW at 280 m/sec, a distributed force of almost 300 lbs. Undoubtedly, the wheel for such a power level would be made larger than that postulated here, even at the cost of an increase in windage losses to around 1%, so as to permit shaft and bearing designs adequate to cope with the possible dynamic unbalance in forces of this magnitude. On the other hand, at the smallest scale, with at total output of only a few kW, the use of wet vapor at the nozzle inlet permits a reduction in peripheral speed to about 200 m/s; the windage loss for a 9 cm disc drops correspondingly to about 95 W (to which must be added an allowance for bearing friction).

Finally, we must consider item (o) in Fig. 43, losses due to equipment outside the nominal cycle. The point of view taken here is consistently that of satellite design where weight is at a premium and the use of high cost, high technology control systems and rectifiers is not precluded. Thus, we assume that the generator is mounted on the same axle at the turbine wheel and that, being always under some load, it functions as part of the bearing system for that axle. According to Eq. (XI-3), if the generator diameter is less than 2/3 of the wheel diameter, the resulting windage torque will be an order of magnitude under that of the wheel, per unit area; thus generator windage and bearing losses are included in the turbine windage and bearing losses.

Another implicit satellite component is a momentum wheel to offset the angular momentum of the turbo-generator combination. Together, these components function as part of the stabilization system of the satellite. We have just noted, from Millner's evidence[18], that the friction loss of this momentum wheel, which can spin on a magnetic bearing in a vacuum, is small compared to that of the turbine. Both the generator and the momentum wheel are considered further in Section XII. Here, we assign the generator electrical losses to the load, and consider the friction of generator and momentum wheel to be either part of the "miscellaneous" category or to be part of the satellite housekeeping overhead for orientation stability, not chargeable to the power source.

B. Loss Summaries

We now tabulated the various losses. They are of two types, those which are nearly constant fractions of mechanical output, and those which vary with mechanical output in some other manner. The principle occupants of this latter category are the friction losses and the temperature disequilibrium losses which are adjusted along with friction.

Table XI-I give frictional losses for 2, 10, 30 and 100 kW nominal nozzle output power, assuming 1200°K to 600°K expansion and 50% nozzle inlet wetness with 1 μm condensate droplet size. We have used 150 W friction and windage loss for a 9 cm wheel, 300 W loss for a possible 14 cm wheel for 100 kW. Nozzle dimensions and losses are taken from Table X-II.

TABLE XI-I

OUTPUT LEVEL DEPENDENT LOSSES

Nominal Output kW	Wheel Friction Windage kW	Wheel Friction Windage %	Nozzle Throat mm	Nozzle ΔS Loss %	Nozzle Friction %	Total Loss %
2	0.15	7.5	0.55	10	25	42
10	0.15	1.5	1.2	6	13	20
30	0.15	0.5	2.1	6	8	15
100	0.30	0.3	6.6	5	5	10

An overall summary of the losses tabulated in Fig. 43, as estimated above, is given in Table XI-II. Estimates of the power-level-dependent losses from Table XI-I are included. Evidently, for the 2 kW level of turbine input the sum of fractional losses is too large to be meaningful. Indeed, for this case other losses, such as those due to geometric underutilization of the available turbine blade entrance area, might have been included if the nominal total

TABLE XI-II

LOSS SUMMARY

	Loss Type	Estimated Loss Fraction for Power Level of 2KW	10KW	30KW	100KW
a.	Nucleus formation	Included in item (n)			
b.	Piping	"	"	"	"
c.	Heat to environment	"	"	"	"
d.	Nozzle friction	25%	13%	8%	5%
e.	Non-equilibrium loss	10%	6%	6%	5%
f.	Turbine blade friction	"	1%	"	"
g.	Turbine shock loss	"	3%	"	"
h.	Turning angle dynamic loss	Included in item (n)			
i.	Friction and windage loss	8%	2%	1%	0.3%
j.	Condenser temperature differentials	Included in item (n)			
k.	Condenser system friction	Included in items (m) & (n)			
l.	Feedpump inefficiency				
m.	Spray nozzle loss	"	6%	"	"
n.	Miscellaneous	"	10%	"	"
	Totals	63%	41%	35%	30%

losses were not already so high as to indicate the need for a feasibility investigation beyond the scope of the present study. On the other hand, the sum of all the inefficiencies for a nominal mechanical turbine input of 30 kW is less than 35%, leaving at least 65% of the theoretical Rankine output intact. Thus, for this latter case, the overall efficiency appears to be at least 30% of the boiler output.

While this lower bound is not quite up to central station power plant efficiency, it is respectable indeed compared with any current technology satellite power supply. For an actual careful integrated design, it is not unreasonable to suppose that all of the system losses can be limited to about 10% on a central power station scale (1 to 100 mW), rising to 20% for a 30 kW satellite or automotive scale power system. Thus we can anticipate the possibility of a prime mover thermal efficiency at 35% to 40% of boiler output, for the conditions assumed, for a single-pass turbine system. However, it is obvious from Table XI-II that one cannot be this optimistic about the 2 kW power level for a satellite. Further thoughts with respect to the 2 kW to 5 kW level in a satellite are to be found in Section XII.

In a satellite, from which waste heat can be discarded only by radiation, there is a weight penalty for low condenser temperature that can easily drive the overall power system design to accepting lower efficiency in return for higher Watts-per-pound of system. This tradeoff is more thoroughly discussed in Section XII.

In a terrestrial power plant, the economics are different. A condenser temperature at 500°K is close to the critical temperature of water-steam. The heat discarded from the mercury cycle can thus be used in a supplementary steam cycle, by means of which another 15% to 20% of the original boiler output can be extracted mechanically. Thus, in a terrestrial power plant one might expect 55% overall efficiency using the high pressure mercury cycle as the base cycle and by using a conventional medium pressure steam plant as a "bottoming" plant. This possibility should be contrasted with the old G.E. system in which low pressure mercury was used as a "topping" plant for (what today would be called) a medium pressure base steam plant, for which the overall efficiency was about 37%.

XII. FEASIBILITY OF LIGHT WEIGHT POWER SUPPLY

The requirement of weight is not unique to satellite power supplies. It applies to every vehicle that must generate power while it moves. By automotive (0.3 kW/lb) and aircraft (1-3 kW/lb) power plant standards, satellite power supplies seem very heavy, but the bookkeeping is different. The bookkeeping for a spacecraft must include everything, fuel (if used), energy conversion, power conditioning, and disposal of waste heat.

An estimate of 10 W/lb is standard for space-borne solar cell power supply for raw bus bar power without battery. A vehicle so supplied would expect to remain silent, and to cope with thermal cycling, during eclipse. (Such silence may be inconsequential for some application or for some orbits). Inasmuch as the silicon solar cell technology for spacecraft is a mature art, anything better would have to be based on other technologies.

In addition to technology, there is a practical weight limit on satellite power supplies, bounded by the size and weight of a satellite that can be conveniently launched into a given orbit. Although proposals have been made to build supersatellites by docking maneuvers from multiple launches, most applications planning is done on the basis of single-launch constraints. Using the Space Shuttle as a staging platform, the planned IUS (Inertial Upper Stage) can place about 5000 lbs with 24 hr orbit. Whatever amount of power that is to be used in a satellite so launched must come from a power source whose weight is small compared with 5000 lbs. Although one can imagine demands for high power in both low orbit and interplanetary satellite, we shall consider here only weight modest compared to 5000 lbs.

Possible power is given as a function of allocated weight and specific source power for several source technologies, existing and postulated, quantized to 5 dB increments, in Fig. 46. The quantization places the RTG of the LES-8/9 class and battery-assisted solar cells in the same box, although the latter may also be 5 dB higher in specific power than the former.*

---

*The LES-8/9 radioisotope source weight 46 lb and the overall weight was 87 lb for 2.4 kW of output, of which 150W was available electrically.

126248-N

TOTAL WEIGHT (lb)	SPECIFIC POWER (Technology Used)			
	3W/lb CURRENT RTG SOLAR CELL AND BATTERY	10W/lb SOLAR CELL RAW BUS HG CYCLE TG	30W/lb (Proposed) REACTOR TG	100W/lb (Proposed REACTOR
30	0.1 kW	0.3 kW		
100	0.3 kW	1.0 kW HG-TG		
300	1.0 kW	3.0 kW		30 kW SOLAR
1000			30 kW	100 kW
3000			100 kW	300 kW

Fig. 46 Output power as a function of permitted weight, specific power and technology.

The three bordered areas in the figure represented technology that will be considered further below. The box at the bottom of the 30 W/lb column represents a proposal by Buden of Los Alamos [19] for a 100 kW_e source that utilizes a 1.2 MW reactor, sodium heat pipes, a (proposal) 9% efficient thermopile and potassium vapor heat transfer to a 1 MW radiator. The Buden proposal weighs nearly 4000 lbs, which is far too much for a 5000 lb satellite. The bordered pair boxes at the bottom of the last column of the figure represent proposals, considered below, to reduce the weight of the Buden system by using the more efficient mercury conversion cycle. The box just above this, at the 30 kW power level, is a proposal, introduced here, to use a solar concentrate to power an Hg boiler. The final bordered area, in the middle of the figure, represents the goal with which this study began, to mate the radioisotope thermal source of the LES-8/9 technology to a high efficiency heat engine to achieve several kW (rather than several hundred W) of satellite prime power.

Below, we make weight estimates for the various major components of the energy conversion system, and use these estimate to discuss each of the three cases just described.

A. Weight Estimates

Ultimately, weight is determined by the capabilities of various materials and the degree of engineering conservation appropriate to the application. Overdesign which affects only the probability of subsystem failure after launch is subject to reduction of margins; overdesign which affects the safety of personnel or a population may be determined by political rules as well as by engineering review.

The toughest engineering design problems with the Hg heat engine occur in the "boiler" where the combination of high pressure and high temperature, together with the high corrosion potential of liquid metal, combine to severely constrain the choice of materials that can be used. The physics experiments of the 1960's established that molybdenum, alumina, and to a lesser extent

beryllia (which tended to spall at temperatures over 1500°K), are compatible with Hg under static conditions in a pressure bomb to nearly 2000°K, at pressures an order of magnitude higher than those used here, for repeated experimental runs of several days each.

Both high density alumina and high temperature Mo alloy (known to the metallurgical trade as "TZM") have caveats associated with their use in walled tubes--as in boilers--or as parts of turbine blades. TZM has its greatest strength only in the direction in which it has been mechanically "worked". Since tubes require their greatest strength, under pressure, in the circumferential direction, this fact poses a challenge to skill in fabrication. TZM must also have surfaces exposed to air above 400°C suitably protected from oxidation (before launch) and may need to have surfaces exposed to liquid mercury suitably passivated for operation above 500° or 600°C. Alumina is a ceramic, albeit available in extremely low porosity, high strength from (e.g., "Lucalox" tradename of General Electric Co.), but nevertheless subject to creep above 1000°C at the stresses anticipated at boiler pressure, unless manufactured with grain size and additives to control such plastic flow.

To conduct a search for better materials for high steady stress (as distinct from droplet impact) at high temperature is beyond the scope of the present study.

The total weight of a boiler or other high pressure component is determined by its density relative to its working stress. Between 1000°C and 1200°C this ratio is (by coincidence) approximately the same for both TZM alloy and fully densified alumina; for this regime we shall take the "handbook value" of the ratio to be 1 gr/cc/8000 psi, and shall use this ratio for design calculations.

For radiator temperatures near 600°K, there is a wide choice of high strength, high density materials compatible with Hg, including a number of steels. We shall assume that this list also includes oxide dispersion-hardened Al or Al-Be mixtures, or other suitable material with a density under 3 gr/cm^3, which can successfully contain hydrogen in this temperature regime.

With these assumptions in mind, we can give approximate weights for the major components of the power conversion system: the boiler, the radiator, the turbine, and the generator.

A(1). Boiler Weight

The boiler is that component of the system in which the problems of high mechanical stress in a corrosive atmosphere are the greatest. Above 600°C, for example, commercial Mo always may need some form of protection in the form of inhibitors, passivation, or ceramic interlayer.

For radiative heat transfer within the boiler, we assume a "hot shoe" which is not necessarily the prime heat source, but is connected to it by means of a sodium heat pipe (with Mo wall). We assume a standard boiler wall temperature equal to that of the energing Hg vapor at 1200°K and a hot shoe at 1400°K to 1450°K. A nominal layout of such a boiler tube, its hot shoe, and its end section are shown in Fig. 47. Although the fin tube hot shoe is at a higher working temperature than the boiler wall, conservative design calls for both to be able to withstand boiling pressure at the hot shoe temperature. Thus, we design for 8000 psi and 1400°K rather than the working pressure of 3500 psi and working boiler wall temperature 1200°K, even though we expect boiler control and safety systems to hold the pressure under 4000 psi.

If TZM is the tube wall material, the average wall stress is assumed to be 40,000 psi at 1400°L with 8000 psi gas pressure. Thus the wall thickness would be 1/5 the radius, or 1/10 of the tube bore. If alumina is the tube wall material (for which the end cap scheme of Fig. 47 is not applicable), the stress lower, but the overall weight the same as for TZM tubes.

Assuming TZM, the tubes have a 1 mm wall for a 1 cm tube diamter. Smaller tubes would result in thinner walls (and therefore a lighter boiler) down to some practical lower bound on wall thickness; larger tubes, heavier walls and a heavier boiler.

A boiler wall so designed with 1 cm diameter and 1 mm wall thickness would weigh 10 kg/m^2 of wall area. We assume an equivalent weight for hot

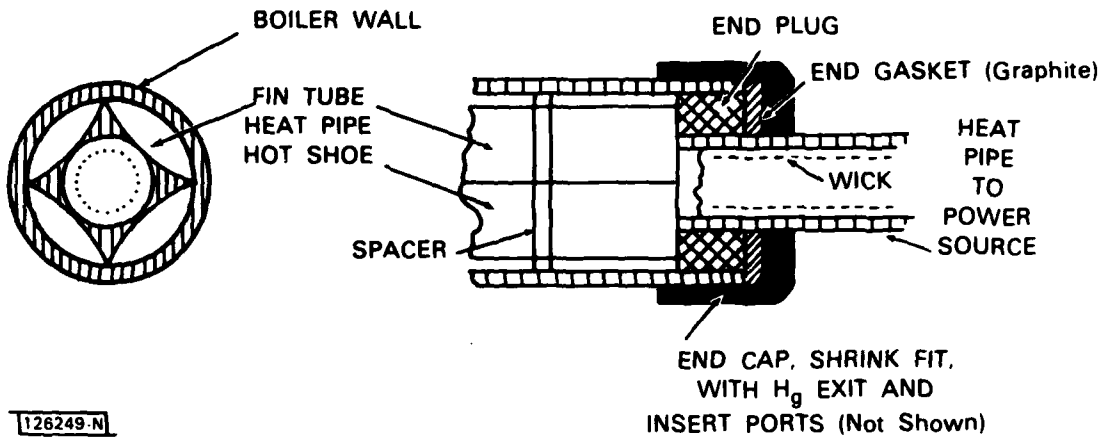

Fig. 47 Longitudinal and radial cross-sections of boiler tube.

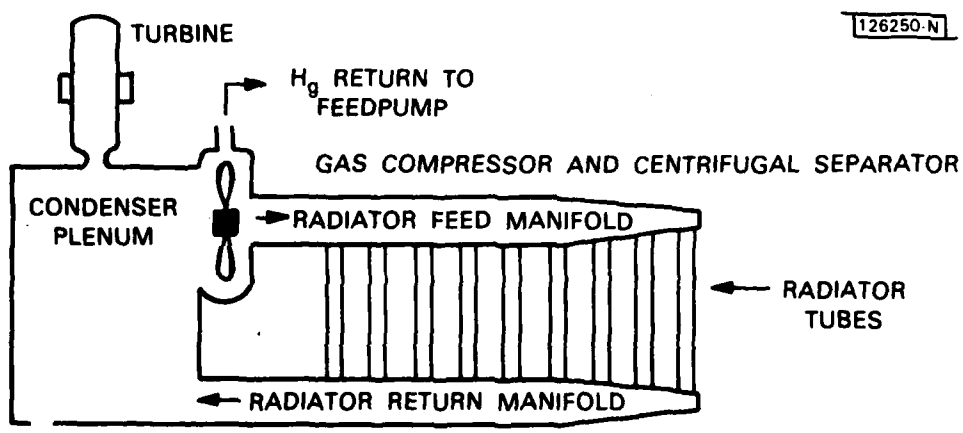

Fig. 48 Schematic layout of buffer gas condenser and radiator.

shoe and end caps, resulting in a total weight of 20 kg/m^2 of heat transfer surface. In Sec. IV, we found the effective absorption of the mercury cloud in such a boiler to be 0.8. Let us further assume that the hot shoe emisivity is 0.8. Then the resulting heat transfer by radiation ranges between 65 kW/m^2 for a 1400°K hot shoe to 85 kW/m^2 for a 1450°K hot shoe.

Combining these assumptions yields a specific weight W_{boiler} given by

$$W_{boiler} \sim (0.27 \pm 0.3)d_{cm} \quad kg/kW \qquad \text{XII-1}$$

for hot shoe temperature between 1400°K and 1450°K.

A boiler for 100 kW thermal output might thus be made up of a bundle of tubes 50 cm long and 12 cm in overall diameter, each tube being 1 cm across, the total package weighing about 60 lbs.

A(2). Heat Radiator

All rejection of waste heat from a satellite must take place by radiation proportional to the fourth power of temperature. Thus, heat rejection at low temperature implies a large, ultimately heavy, radiator. The notion, often repeated in populist literature, that a power plant in space can be as efficient as one pleases on account of the 4°K equilibrium temperature of outer space, overlooks the weight of the radiator.

Buden [19] proposes a light-weight radiator using liquid metal vapor (potassium) in a heat pipe. He exhausts 2 kW per kg of radiator system weight. This design is nevertheless heavy, for several reasons. First, it is necessary to use a relatively heavy metal, like Mo or stainless steel, to resist the corrosive effect of the liquid metal. Second, it is necessary to include metallic wicks to return the condensate to the central heat exchanger. Third, it is necessary to allow for the weight of the returning liquid metal absorbed on the wicks and flowing in the return channels. If necessary vapor were to be condensed directly in such a radiator, one would face the additional problem of making the mercury wet the metal on which it condenses. Finally, there is the practical problem that the vapor in such condenser tubes is generally below atmospheric pressure so that there are two separate leakage problems to

be solved, inward air leaks in atmosphere on the ground, and outward vapor leaks in vacuum in space.

The alternative to heat pipes, mentioned briefly in the figures at the end of Sec. IX, is to use a non-condensing buffer gas such as H_2 or He between the condenser and the radiator, as shown also in Fig. 48 (not to scale). In its simplest form, the turbine and coolant gas are mixed in plenum; the mercury droplets are separated centrifugally at the compressor.

There are now no wicks, no returning liquid in the radiator, and the radiator itself can be made out of almost any convenient material that can contain H_2 or He at 600°K. To achieve good heat transfer, the gas must move at a fair rate---about 100 msec---through the radiator tubes. This rate is sufficient to blow clean the tube walls of any condensate that might form as a result of stray vapor from the condenser plenum.* The system works best at radiator output heat fluxes under 10 kW/m^2 (i.e., under 1 W/cm^2), for which the price is less than 50° temperature drop between the condenser manifold and the radiator surface. Design equations, given in Appendix C, suggest that the friction loss can be kept at 1% of the heat radiated if the tubes are at least 3 cm in diameter and no longer than 1 m. (Longer tubes would require large tube diameter).

For such a radiator, a light, non-hydrogen-permeable alloy, such as oxide-strenthened aluminum, is appropriate, with wall thickness determined as much by stiffness considerations as by strength requirements. At a flux of 5 kW/m^2, with 1/2 mm walls and a 50% weight overhead for manifolds and other structure, such a radiator would have a specific weight of 0.5 kg/kW. This is comparable to the Buden radiator, except that the flux densities (5 kW/m^2 vs 16 kW/m^2) are substantially lower; and the temperature of operation is also significantly lower (550°K vs 775°K), resulting in higher cycle efficiency.

---

*See any textbook discussion of the Calder-Fox separator [16].

An overall optimization for minimum system weight will not be undertaken here; we shall, however, indicate some of the features of such a calculation. Suppose that the design is dominated by the weight of the radiator and that the actual mechanical output is a fixed fraction of the theoretical thermodynamic output. Then maximum power per unit weight is obtained from a thermodynamically inefficient configuraton, for which the (absolute) radiator temperature is 3/4 of the boiler temperature. However, the weight of other parts of the system generally is significant and also directly proportional to boiler output. This extra weight drives the optimum radiator (condenser) temperature downward.

We procede as follows. Consider the boiler working fluid to be at temperature T_1, at which it receives heat at a rate proportional to boiler area and, ultimately, boiler weight. Let the radiator be at temperature xT_1. Suppose that we size the boiler "area" to be equal to that which would provide all the boiler heat by radiative transfer at T_1. Suppose that the boiler weight is A units/m^2 of boiler "area", and that the radiator weight is B units/m^2 of effective radiator black body area. The flux emitted by the radiator is only x^4 per unit area of that received by the boiler; but only x of the boiler output is (ideally) discarded as waste heat. It follows that the total weight of boiler-plus-radiator is proportional to M_W

$$M_W = \frac{1}{1-x}\left(A + \frac{B}{x^3}\right) \qquad \text{XII-2}$$

Differentiation leads to the condition for minimum weight

$$x + \frac{x^4}{4}\frac{A}{B} = 3/4 \qquad \text{XII-3}$$

Even if the radiator walls are quite light compared to the boiler "walls", say A/B equal to 16, optimum x drops only a little, in this case to 0.5. The optimum so calculated is broad. For the above assumptions, the specific weight rises less than 50% for x in the range $1/3 \leq x \leq 3/4$.

Evidently, the weight of the boiler "walls" can be extended to include the prime source of heat and any other weight that is proportional to total heat flux, with similar results.

A(3). Turbine and Generator

It is not necessary to exhibit a mechanical layout of the turbine and its casing in order to bound the weight. In Sections VIII and IX, we assumed a turbine diameter of roughly 10 cm. It is reasonable to assume that the entire turbine package, with rotor, beamings, passageways, and casing, does not weigh more than a 12 cm diameter solid cylinder of steel, 10 cm long. Such a cylinder weighs 10 kg. For the lowest end of the power scale, with a mechanical output less than 2 kW, it is reasonable to cut this estimate by a factor of 2. At 100 kW output, and 200 m/s peripheral speed, the force on on the rotor circumference is only about 100 lbs, which can be adequately handled with the overall dimensions given.

Consider next a bundle of N equal conductors having total cross-section A moving with velocity v perpendicular to a magnetic field B, as in Fig. 49. Each conductor sees an electric field $\underline{E}$ numerically equal to vB, so that if the conductors are connected in series, the total voltage is E

$$E = NL_1 \underline{E} \quad , \qquad \text{XII-4}$$

L_1 being the length of each conductor in the field. The electric resistance is R

$$R = \frac{N^2 L_1 \rho_e}{A} \qquad \text{XII-5}$$

with ρ_e being the effective electrical resistivity of the conductors.

If the conductors are connected in series and if the resulting generator is connected to a load to generate power W at efficiency η, it is an exercise in elementary circuit theory to find that

$$W = \eta(1 - \eta)\underline{E}^2/R \qquad \text{XII-6}$$

The last three equations can be combined to give an expression for the physical volume of conductor, V_c, required to generate power W with efficiency η:

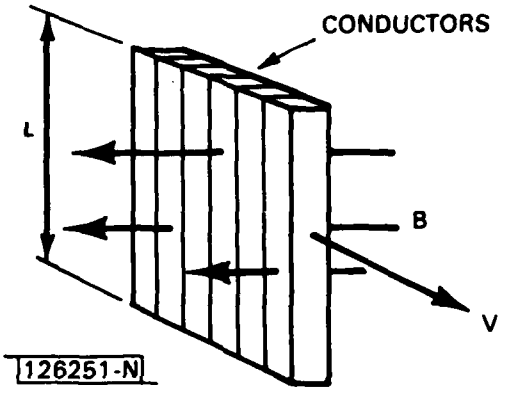

Fig. 49 Generator geometry.

$$V_c = A L_1$$
$$= W \rho_e / \underline{E}^2 \eta(1 - \eta) \qquad \text{XII-7}$$

For a given power level and efficiency, the only real engineering variable here is the electric field $\underline{E}$. Because the peripheral speed of the turbine is 200 to 300 m/sec, it will be difficult to build a generator in which the conductor velocity is under 100 m/sec. Using SmCo magnets, it should be possible to reach 0.6 to 0.7 Weber (6000 to 7000 ganes) in the conductor gap. Thus, one can consider $\underline{E}$ of the order of magnitude 100 volts/meter. If this assumption be used in Eq. XII-7 along with the room-temperature resistivity of copper (1.7×10^{-8} ohm-m) the result for a 99% assumed efficiency is a phenominal 0.2 cc per kw!

Now this result is in various ways naive. In an a.c. generator $\underline{E}$ is only the peak field; the average $\underline{E}^2$ is only half as great. In a real machine, the volume of unusable "air gap" or "slot-space" may be equal to that available conductors. If the winding must operate at elevated temperature, or be made of Al to save weight, the resistivity is twice as great as for room temperature Cu. There must be some allowance of volume for connecting conductors in series. There must be some consideration of the effect of local a.c. magnetic fields and eddy currents within the conductors themselves. Thus, one can easily account for a factor of 10 to bring the "conductor" volume to 2 cc per kW. Finally, for the assumptions made, there may be 3 or 4 cc of magnet for every cc of copper-plus-air-gap. Thus, we can account for 10 cc per kW. At an average density of 5 g/cc, this is 0.05 kg/kW.

Why, then, are conventional machines so much heavier? The best answer is that they are not, if one takes into account an order of magnitude lower $\underline{E}^2$ and the geometric constraints of 60 Hz design (for which $\underline{E}$ drops as the number of poles is increased to reduce the volume of iron). The generator postulated here operates at some multiple of 1 kHz, with whatever frequency and number of pole pairs are appropriate to satisfy other requirements of design.

The low (potential) specific volume of the generator makes it possible to include the generator as part of the turbine package, in that the volume of a 100 kW generator is about the same as what was assumed above for turbine housing and bearings. Indeed, the generator conductors are dynamically repulsive to magnetic fields, so that an integral generator can act as part of the bearing system for the turbine.

A4. Summary of Specific Weight

The four components just described, boiler, radiator, turbine, and generator, by no means constitute a complete description of the power source. There is, for example, the thermal source itself on the one hand, and the various pumps and plumbing that tie everything together (not to mention a control system) on the other hand. Nevertheless, the foregoing four together do constitute an irreducable minimum of structure for a heat engine for mechanical conversion from heat to electric power.

The weight of turbine and generator have been given in terms of electromechanical output. System efficiencies in Section X were also stated in terms of nominal mechanical output; but the boiler and radiator weights have been given in terms of thermal output. Let us assume that out of the total boiler outputs, 1/3 is connected to electrical output and 2/3 is radiated as waste heat. The specific weights of a conversion system are then as follows:

Boiler:	0.8 hg / kWe	
Turbine:	0.3 kg / kWe	(30 kW_e output)
Generator:	0.1 kg / kWe	
Condenser:	1.0 kg / kWe	
Total	2.2 kg / kWe	

Such a weight compares most favorably with the 50 kg/kW_e of the energy conversion system in the LES 8/9 RTG's, and the 8 kg/kW_e assumed by Buden [19] in his proposal for a 100 kW_e reactor system in orbit. On the other hand, this total does suggest an upper limit in the neighborhood of 200 w/lb for the Hg-turbine technology in orbit.

B. Use of Hg Cycle in Reducing the Weight of a Reactor in Orbit

Buden [19] has proposed an orbiting reactor with 1.2 MW thermal output and 100 kW_e electrical output using a thermopile as the means of converting heat to electricity at 9% efficiency. An artist's drawing of this reactor-TG is shown in Fig. 50. Buden gives estimates of the weight associated with various parts of this power plant, reproduced here as Table XI-1.

TABLE XII-I

PARAMETERS OF LASL SPACE REACTOR

Item	Dimensions	Weight	Power
Reactor	0.57m dia x 0.52m	440 kg	1200 kW_t
Shield		380 kg	
Thermoelectric Converters		285 kg	100 kW_e
Radiator	7m long; 62 m^2 area	510 kg	1000 k W_t

(The subscript "t" refers to thermal power, "e" refers to electrical power. Evidently, 100 kW is directly radiated as loss outside the actual radiator).

The primary weakness of the Buden power plant is its weight; it is too heavy to be used as a prime power source in a shuttle-launched high orbit mission, even though it is designed to be used in the shuttle. The simplest weight-reduction modification is to replace the TG with a boiler-turbine-generator system, and to reduce both the reactor output and size of the radiator to take advantage of the factor-of-three improvement in conversion efficiency. Here, the Hg system would be designed for the Buden hot shoe (1400°K as has been assumed in design examples) and 775°K radiator temperatures.

Several adjustments in Hg system layout would be necessary to accommodate to the higher condensor temperature, including the design of an Hg to Potassium heat exchanger and the acceptance of an overall laver efficiency than might be available at 600°K condensor temperature. Nevertheless, the higher exhaust temperature reduces some of the nozzle and turbine speed design problems while

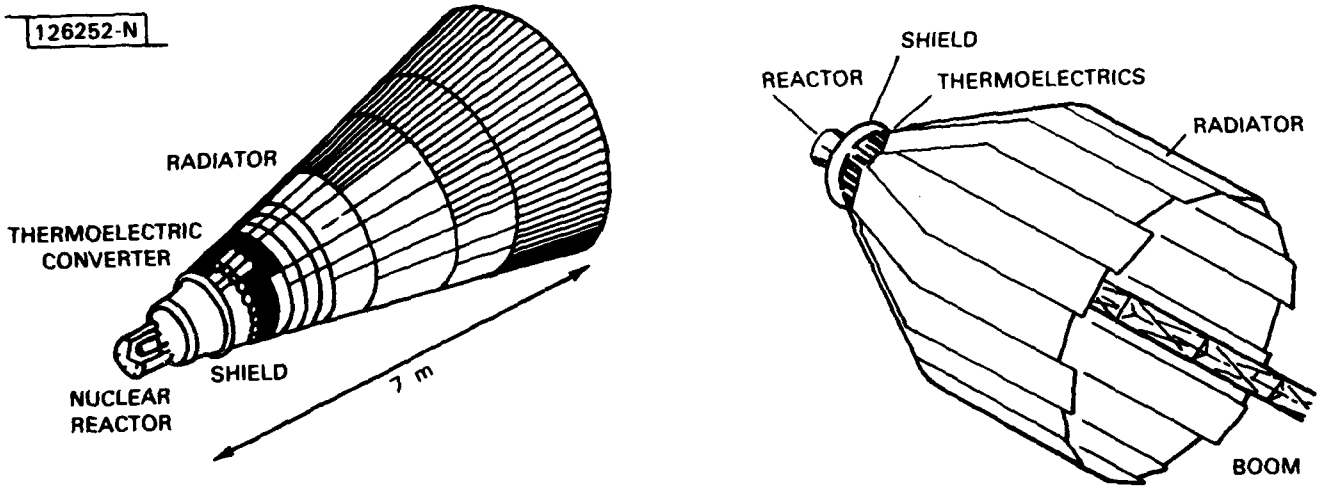

Fig. 50 Space nuclear reactor power supply.

TABLE XII-II

REVISED WEIGHT ESTIMATES

Boiler:	350 kW_t	x	0.22	= 77 kg
Turbine:				10 kg
Generator:	100 kW_e	x	0.05	5 kg
Radiator:	230 kW_e	x	0.5	115 kg
Structure:				75 kg
Total				282 kg

not significantly increasing those met in the design of the turbine blades. We therefore assume an overall 30% efficiency for the conversion to electrical output (35% thermodynamic x 85% system).

The weights of the revised system components are then as in Table XI-II. (We have reduced Buden's structure estimate by a factor of 2 on the grounds that much of it is used to support the very weight that is being so drastically cut.) If this total is added to the (unchanged) reactor (440 ks) and shield (380 kg) weight, the total is now 1100 kg or 2400 lbs. While this is still roughly half of the weight that can be put into synchronous orbit by a single IUS, the available power is so much higher than that normally available (by two orders of magnitude) that a system designer might well accept the resulting restrictions on the remainder of his payload.

Some further adjustments in weight may be appropriate within the framework just described. Some of the fuel can be off loaded as no longer needed at the lower power level. Some additional weight must be added for the heat exchanger which condenses mercury on one side of a wall while boiling potassium on the other side.*

Evidently, with the addition of the Hg turbine system, the major candidates for weight reduction became the reactor and the reactor shield. In both

*The two metal systems must be isolated. Hg and K form compounds with roughly 10 kcal/mol heat of formation.

AD-A129 016 A HIGH PRESSURE MERCURY TURBINE CYCLE FOR USE IN SPACECRAFT AND TERRESTRI..(U) MASSACHUSETTS INST OF TECH LEXINGTON LINCOLN LAB R M LERNER 22 MAR 83 TR-577 3/3

UNCLASSIFIED ESD-TR-82-176 F19628-80-C-0002 F/G 13/2 NL

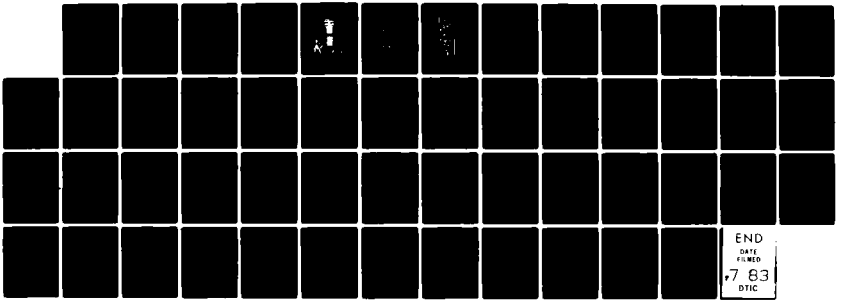

END
DATE FILMED
7 83
DTIC

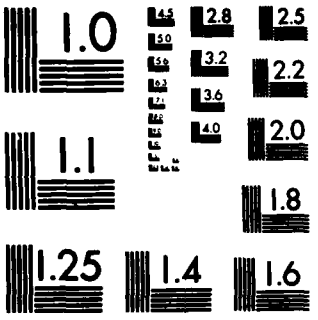

cases, a minimum thickness of material (neutron reflector and external shield) is included, so that weight does not drop in proportion to maginum design power. A discussion of such possible scaling is beyond the scope of this investigation.

On the other hand, it is appropriate to ask what happens if turbine and boiler are designed for 300 kW_e output, using the full 1000 kW_t input of the Buden design. The turbine and generator become somewhat larger than those assumed in Sections A3 and A4, on account of the strength of structure required and on account of the need to design for cooling and the presence of significant armature reaction. Estimated weights are as follows:

Reactor	440 kg	Boiler	220 kg
Shield	380	Turbine	20 kg
Structure	120	Generator	30 kg
Radiator	350		

Total: 1500 kg

The weight is now 3400 lbs, almost 90 W/lb. The extra 200 kW_e came at the marginal specific power of the Hg-system, about 200 W/lb.

100 kW_e and 300 kW_e are the power levels required to supply aircraft and ground-based communications transmitter systems, respectively. The power level is therefore attractive for use in a communication scenario in which a symmetric air/orbit or ground/orbit link could be appropriate. However the system designer must be assured that there will be weight left over in the booster for the rest of his payload.

C. 30 kW Solar Power Plant

The reactor and shield proposed by Buden [19] weighs roughly 0.7 kg/kW_t. We have already observed that we are not in a position to state that the favorable specific source weight would persist if the reactor were scaled to

lower maximum power. Moreover, the reactor presents a γ-radiation hazard to the satellite it serves.

A light-weight unfurlable solar collector constitutes a viable alternative to the reactor as a power source capable of tens to a hundred kW_t within current technology capability. The basic component is an umbrella-like structure manufactured by Lockheed [17] that has been produced in diameters up to 10m, and which weighs about 0.5 kg per m^2 of umbrella surface deployed. The surface itself is sufficiently accurate to collect the 1° optical width of the sun at a focus. To function as a collector of sunlight instead of being merely a reflector of radio waves, such an umbrella might require an appliqué of aluminized plastic film, with negligible additional weight penalty.

A 10 meter diameter umbrella of this sort could theoretically concentrate 100 kW_t of solar energy on a 10 cm diameter circle at 10 m focal length. We assume the boiler to be placed away from the focus, so that the beam area is $0.1m^2$. The boiler we assume to weigh no more than a solid block of alumina 5 on thick, with $0.1m^2$ area, having passageways inside for the mercury cloud. The back side of this block of alumina faces a mirror, so that it loses heat only from its front surface, even if no special greenhouse precautions are taken to conserve heat. Giving up this loss, the weight of reflector rises to 0.55 kg/kW_t; and the weight of the boiler is roughly 0.22 kg/kW_t (as in the hotshoe case!).

Thus, all of the estimates at the end of subsection A5 can be applied.* With the addition of 0.55 kg/kW_t for the collector, the total weight becomes 2.75 kg/kW_e, or 82.5 kg for a 30 kW_e plant. To this, we add an estimated 17.5 kg for pumps, pipes, atomizes, auxiliary motors, etc, to round out the estimate at 100 kg (or 220 lbs) for 30 kW, about 140 W per lb.

What is remarkable about this power plant is that the source requires no new technology. (Of course, the Hg converter is new.) In one giant leap the

*These estimates are, in fact, conservative. If the practical design reaches 85% overall efficiency, then the net efficiency for a 46% nominal Rankine cycle is close to 40%.

effectiveness of solar power supply has been increased by an order of magnitude!

D. 1.5 kW_e Radio-Isotope-Powered Supply

The radio-isotope power supply for the LES-8/9 satellites developed (and in 1980 was still developing) about 4.8 kW_t of thermal power for about 300 W of electrical output. The radio-isotope was Pu 238, an α-emitter with a half life of 86 years. Plutoninum oxide was used as the golf-ball size core of base-ball size units having carbon filament wrapping and iridium cases to provide mechanical containment (in case of a crash into a mountainside following an aborted liftoff); the canister was also designed for abort scenarios. The radioisotope is contained in two canisters for each satellite. Heat flow is radial, passing through the thermopile to the outer casing, which is also the radiator. Hot shoe temperature is 1030°C; radiator outside temperature 250°C to 300°C.

Fig. 51 shows a pair of RTG cansisters being put in position for a thermal vacuum test. Fig. 52 is a cutaway drawing of an individual canister, showing its overall construction. Fig. 53 shows a cutaway of the radio isotope heat source with a 1" diameter boiler tube inserted (by the artist) along the central axis of the heat source, resulting in minimum mechanical rearrangement internally. The weight of the radioisotope consisters for 4.8 kW is 42 kg (92 lb), of which approximately 11 kg (24 lb) is fuel. In this context, minimum boiler weight is not significant. A 1" tube designed according to (XII-1) would weigh 3 kg; but an extra few kg for other designs requirements would not be significant compared with 45 kg for minimal source plus boiler tube.

The hottest internal temperature for the LES-8/9 design hot can was about 1300°C. This now becomes the possible outside temperature, with insulation and a possible emergency cooling system replacing the thermocouples of the present design. The insulation of choice for such applications is stabilized zirconia felt. The problem of controlled external cooling is discussed in Section III in connection with Figs. 15 and 16. For the thermopile, the

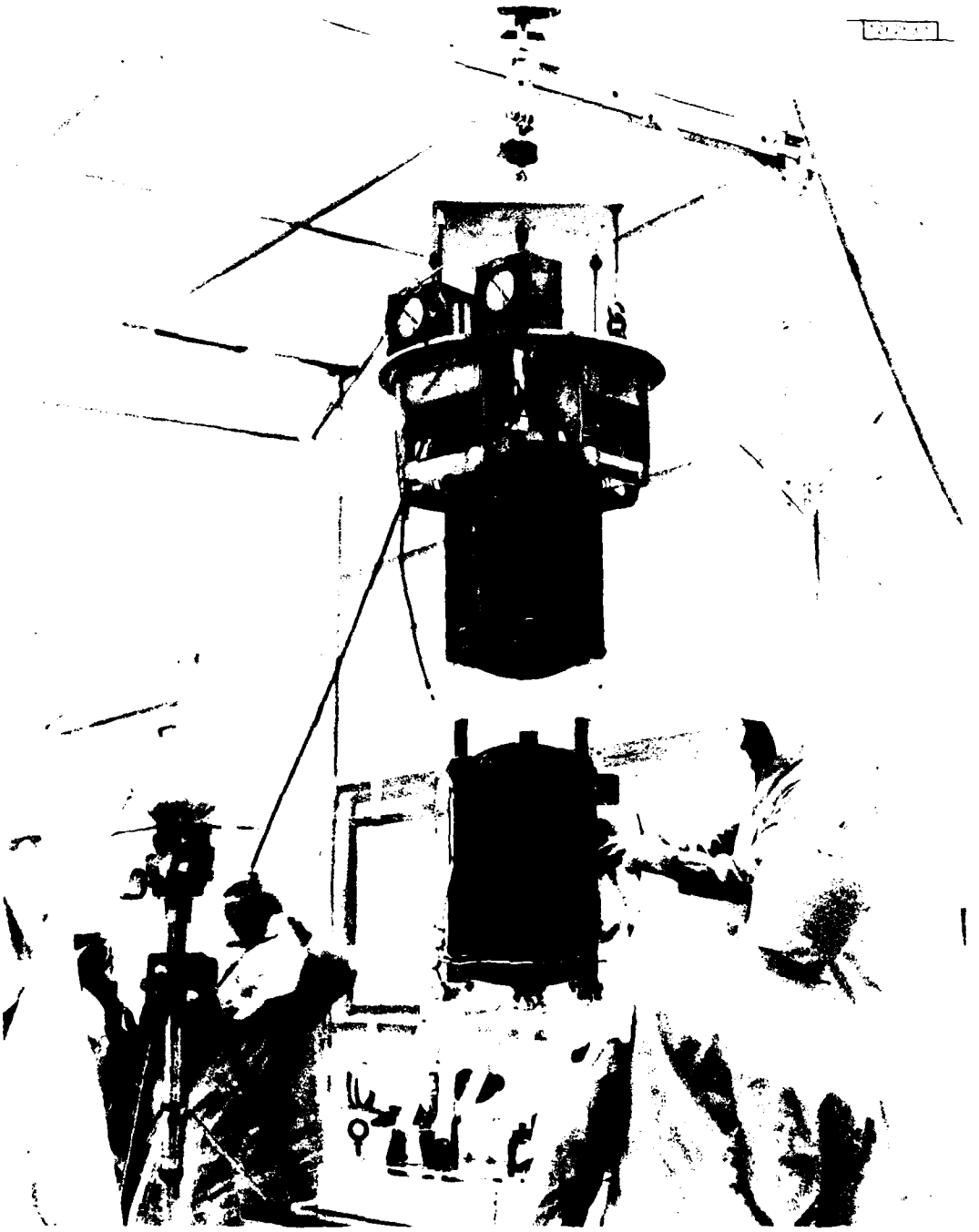

Fig. 51 RTG canisters being positioned for thermal vacuum test.

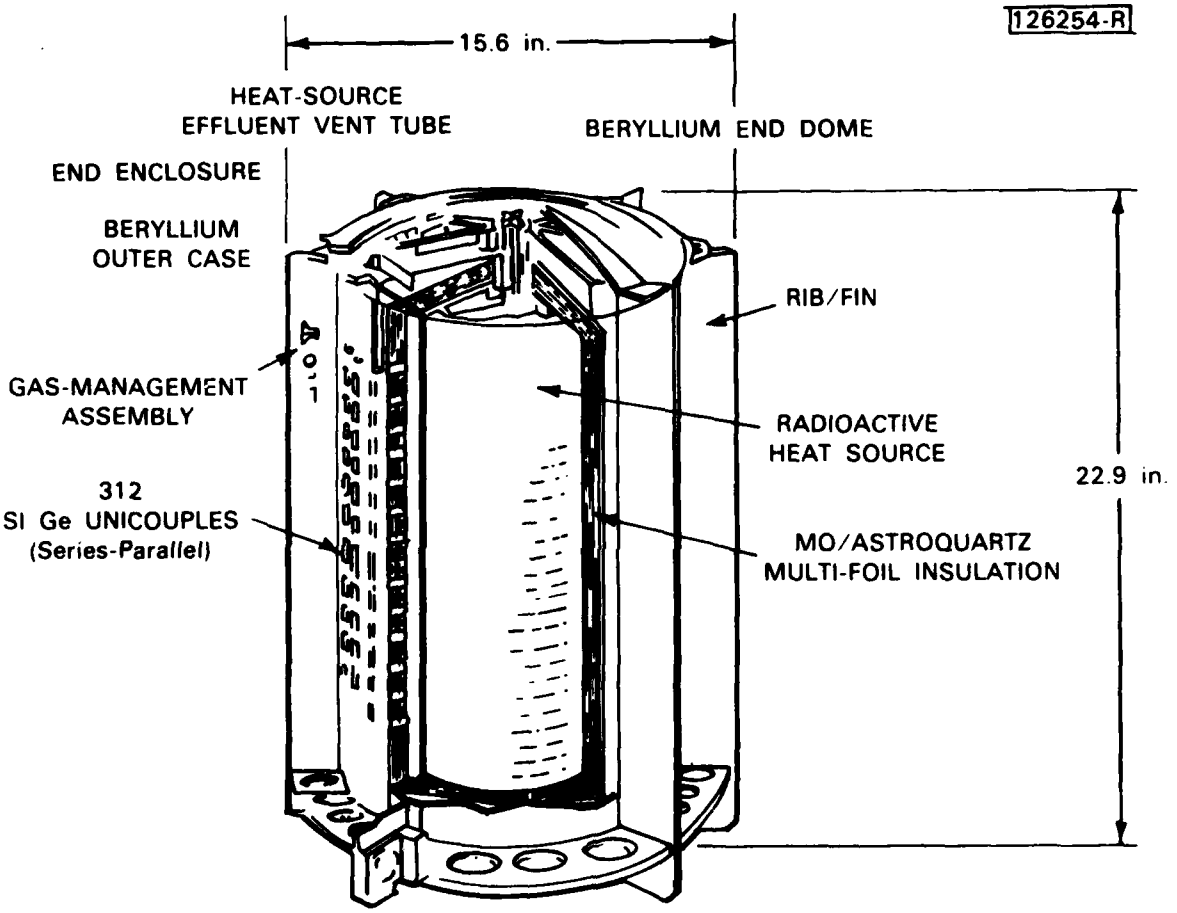

Fig. 52 Cutaway of LES-8/9 RTG canister.

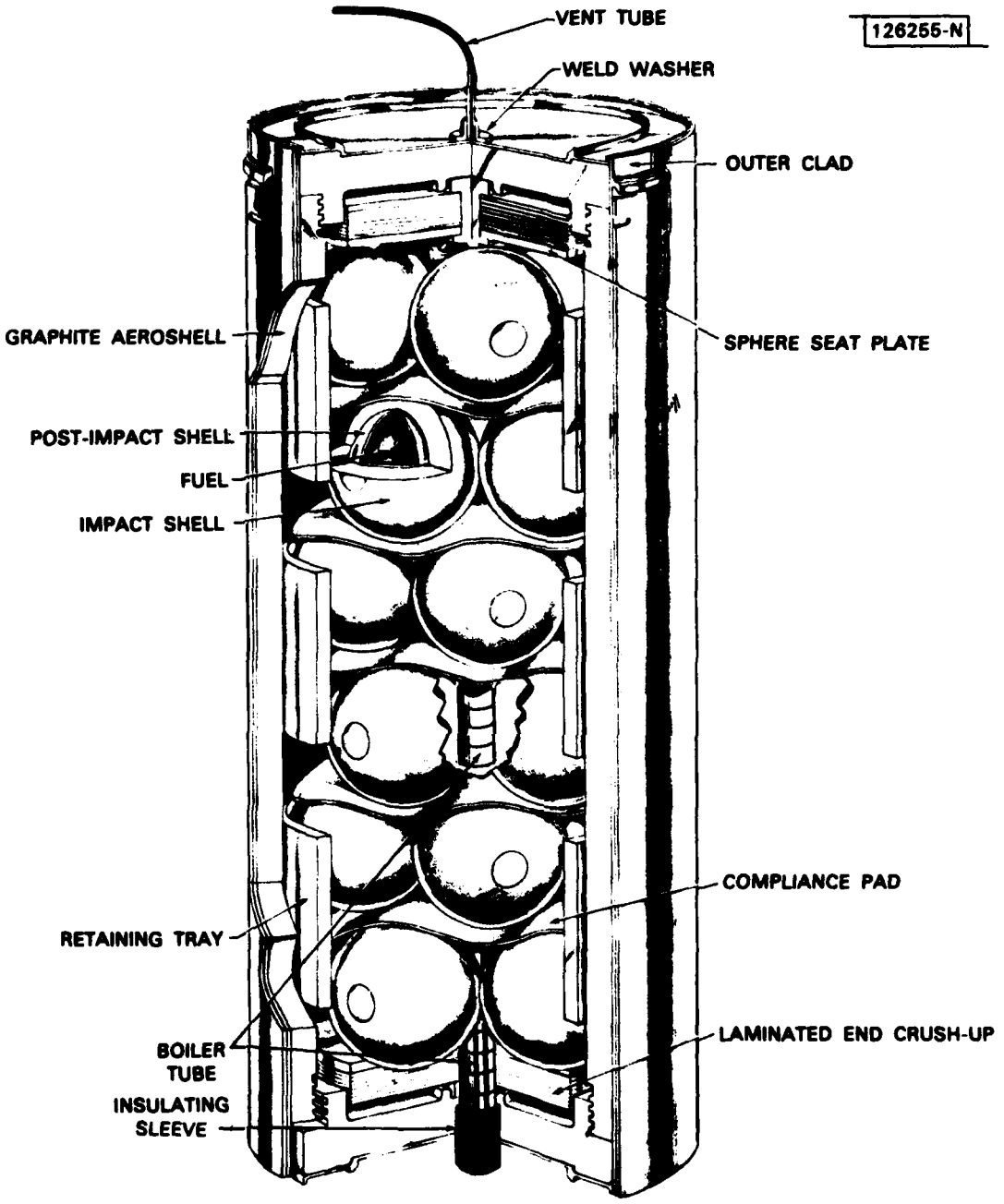

Fig. 53 Modified heat source with boiler tube.

difference in heat flow as the output is switched from full load to no load is insignificant. For a fully insulated canister, a loss of the boiler charge would leave the entire thermal output with no place to go.

An adaptation of the automatic cooling scheme of Fig. 16 to the present case is shown schematically in Fig. 54. Openings for the passage of vapor are provided through the insulation. These are shown in the Figure as direct paths, but in practice the hot can would not directly "see" the outer can. A wick is provided on the inner surface of the cool outer can to bring condensed liquid back to the hot inner can surface.

A backfill of low conductivity inert gas such as Xe is provided to provide a set pressure for the operation of the cooling system. Below this pressure there is minimal heat transfer by evaporation; above it, heat pipe action takes place. The switch is made over a 100°K change in hot can temperature.

Thus, in terms of the overall LES-8/9 RTG design, the semiconductor junctions are removed and replaced by insulation and a self-switching heat pipe cooling system. While the overall weight of this new arrangement can be expected to be somewhat less than the older one, we shall assume a total weight for the assembly (including boiler pipe) roughly equal to the 78 kg (172 lbs) required in toto for the 4.8 kW_t LES-8/9 subsystem. Recently, workers at G.E. have proposed hot can arrangements weighing 20% less than those built for LES-8/9 [22]. Presumably similar weight reduction is possible for the outer shell system, too. But such weight reductions are not significant on the scale of accuracy involved in our present estimates.

To avoid major individual temperature excursions of the cool can and the waste heat radiator as the thermal load shifts between them, the two can be constructed as a single assembly, as in Fig. 55. Here, the tubes for the gas cooling are supported by the fins of the cool can and are thus part of the fin structure. Only the 2.4 kW canister closest to the satellite is shown in the figure, with the radiator tubes terminating in distribution plenums for the condenser cooling gas. (See discussion of Fig. 48).

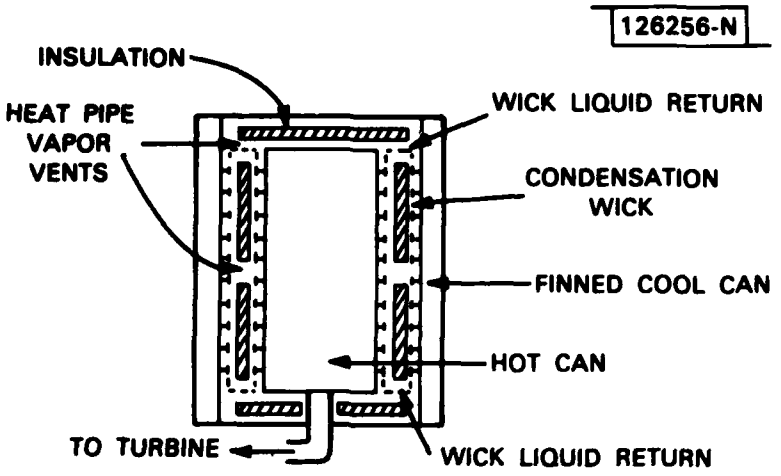

Fig. 54 Heat pipe automatic cooling system.

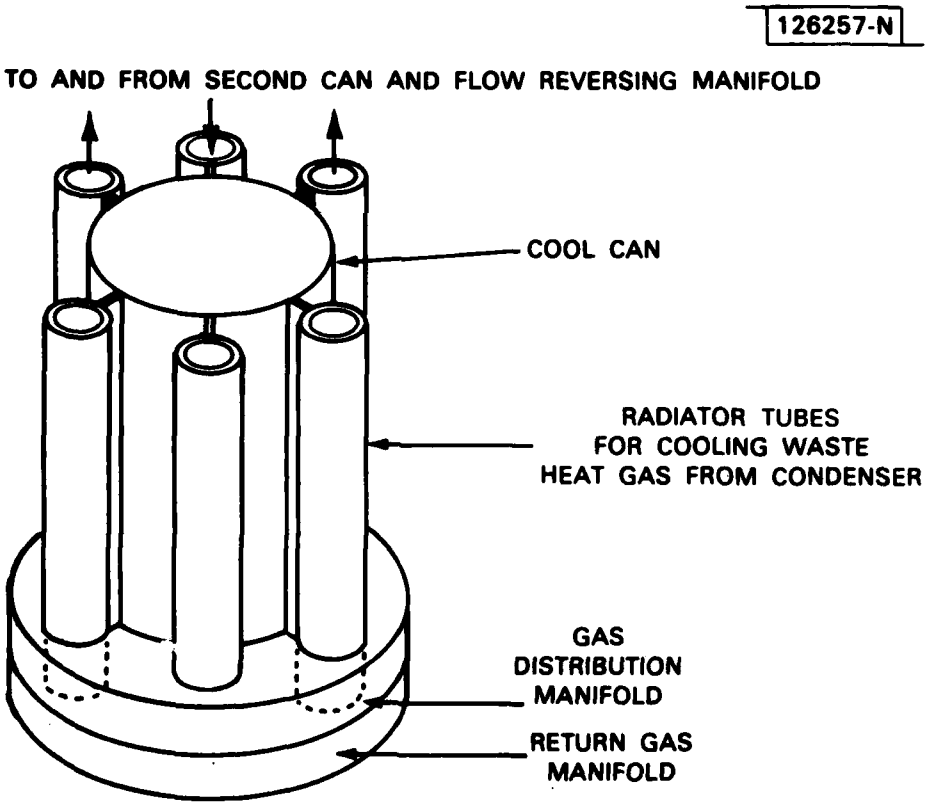

Fig. 55 Combination radiator and cool can.

We shall assume that the problems associated with the nozzle design and friction/windags losses of a 2 kW scale turbine can be solved, at least so as to obtain roughly 75% of theoretical cycle efficiency. Means for accomplishing this include reducing wheel diameter to cut windage losses and bringing the high pressure vapor into the wheel itself, along its axis of rotation, through a fluid dynamic bearing. Some of the expansion between wheel hub and periphery can then take place against Coriolis force as a virtual piston. The wheel then operates as a 4th of July pin wheel; fluid speeds in excess of peripheral wheel speed are unnecessary. See Fig. 56 and Appendix D.

Thus, the main causes of frictional loss (high speed in the supersonic part of the nozzle, entrance losses in the turbine blades, and friction associated with turning the flow) need not occur or are substantially reduced. Moreover, the droplets which form do not strike any surface at high speed.

Because the absolute amount of waste heat to be radiated is only a few kW, there is little problem in running the radiator at 550°K and the condenser at 600°K without a weight penalty that is significant in comparison to the 78 kg overhead of the source. As a result, the overall efficiency is still high: 0.75 x 0.46 is roughly 1/3, for a electrical output of 1.6 kW_e.

The added weight penalties for this conversion system are estimated in Table XII-III.

TABLE XII-III

1.5 kW_e OUTPUT WEIGHT ESTIMATES

Turbine, Generator	5 kg
Momentum Wheel	5 kg
Radiator, 3 kW_t	3 kg
Miscellaneous pumps, plumbing, and controls	9 kg
	22 kg

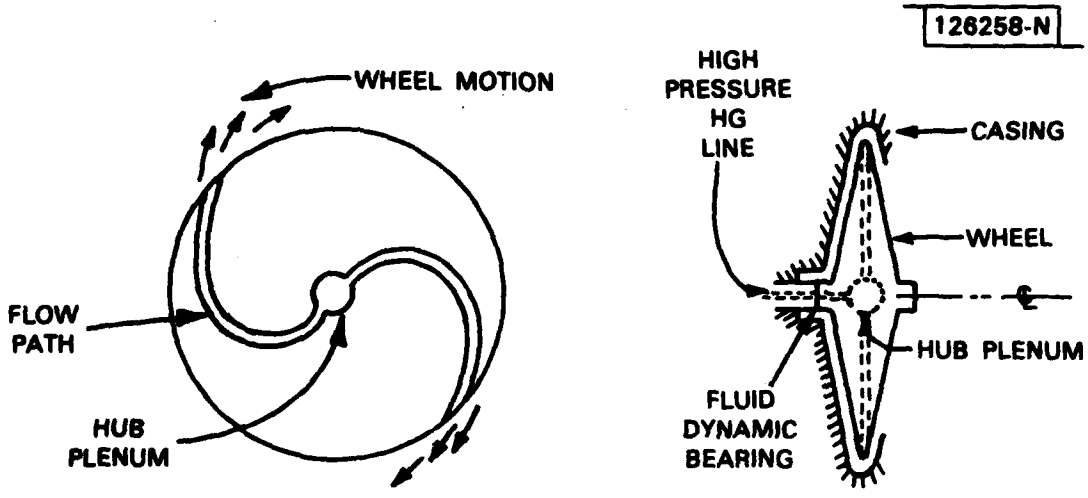

Fig. 56 Hub-fed pinwheel turbine.

In the Table, the weight of turbine and generator have been combined with the latter functioning as part of the bearing system for the former. An item "momentum wheel", and insignificant part of higher output power plants, has been added. This wheel is necessary to offset the angular momentum of the turbine generator combination. Taken together, the two function as parts of the overall satellite stabilization system. Radiator weight has been raised from 0.5 to 1 kg/kW to take account of structure (such as plenums) not significant as part of larger radiators.

XIII. DISCUSSION OF RESULTS

Even if we accept all of the experimental unknowns as having favorable outcomes, there remains the question, can the results be engineered into a workable satellite subsystem. As one peruses the reports on the low-pressure old G. E. and more recent SNAP-8 systems, one is impressed by the unfortunate system engineering consequences of a good idea that emerged from the laboratory too soon, that did not undergo adequate accelerated life testing of critical components. In both cases, by the time the difficulties were discovered and corrected it was too late to change the rest of the system in which these components were imbedded.

Figure 57 is intended to give a flavor of the system management problems that one faces in attempting to actually build a mercury-powered system into a satellite. The lower part of the Figure indicates by close proximity of the labelled boxes functions that affect one another. Note the inclusion of a number of practical considerations such as fluid reserves and contaminant control, which are not considered in the body of a report such as this one. (Although some sources of contamination and its effects can be anticipated, often both are discovered midway through a life cycle). The uppper part of the figure indicate economic interfaces with a non-technical support environment, any one of which can drive technology which looked practical at the component level into oblivion.

Figure 57 is presented primarily to remind the component developer why it is that the system engineer or financier often says to him, "you don't understand the problem." There is, of course, the danger that the reader will see that Fig. 57, though complicated, is nevertheless naive, and dispair of ever bringing a system to completion. The proper use of exercises like Fig. 57 at the component development level is to anticipate the system "domino-effect" of changing a component when something goes wrong with it, or when it turns out that two subsystems that worked well in isolation have a practical incompatibility.

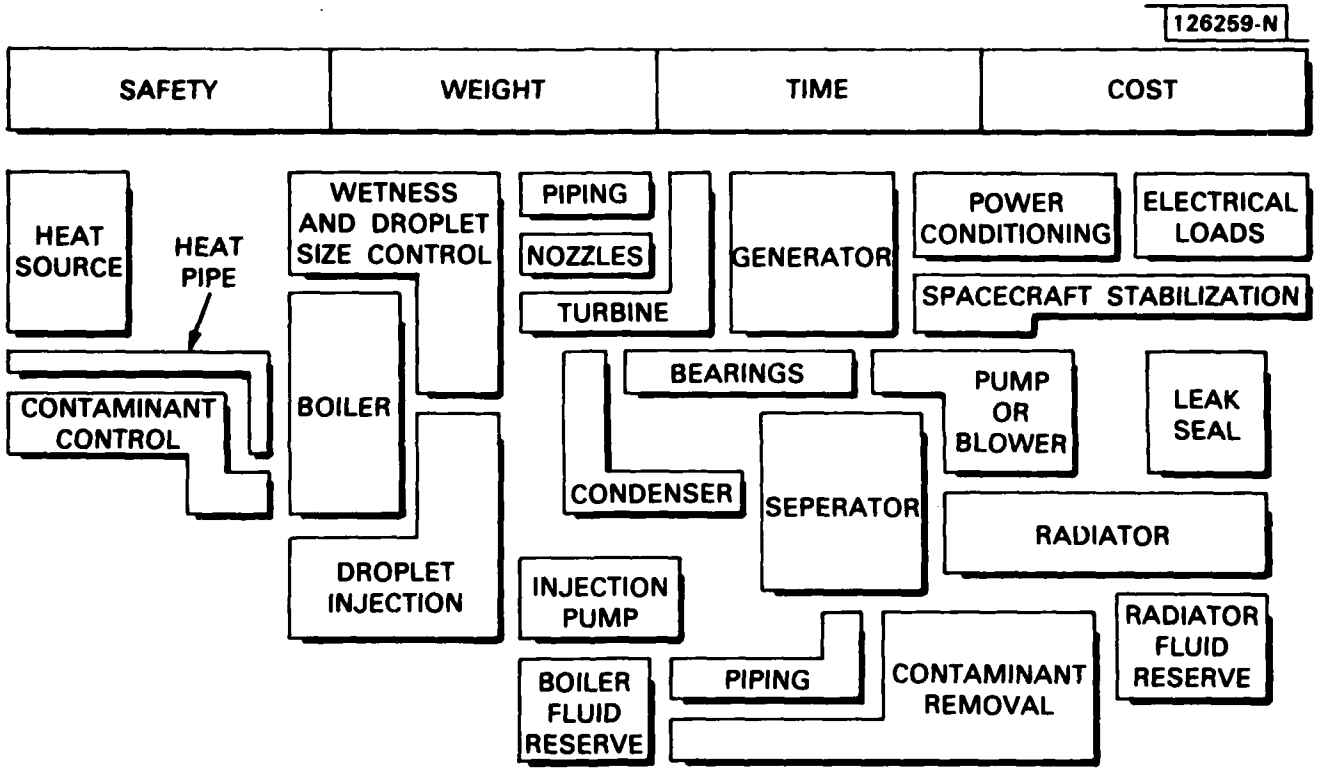

Fig. 57 System interrelationships.

The components of the high-pressure Hg system proposed here have been conceived in such a way as to do an "end run" on a number of troubles that plagued the low-pressure G. E. and SNAP-8 systems.

- The biggest single problem with the old systems was the dilemmna of wetting us. corrosion. The "end rum" is to use (non-wetting) radiative heat transfer in the boiler, and vapor-to-gas heat rransfer in the condenser.
- Another major difficulty with the old systems was the rotating seals and bearings. Notwithstanding the attempt to produce a mercury-wetted beaming as part of the SNAP-2 program, liquid metals are poor lubricants. The "end run" is the single-stage impulse turbine with integral-shaft alternator, which can be run with magnetic bearings, and no rotating seals. (It was the desire to avoid lubricated seals as much as "simplicity" that motivated the extensive investigations of the single-pass impulse turbine with supersonic flow).
- A further difficulty with the old systems was a lack of adequate accelerated life testing. Corrosion and contamination problems surfaced after a few thousand hours of operation of what was supposed to be the final installation. In retrospect, a variety of mechanisms with exponential dependence of rate on temperature (differential solubility, creep, embrittlement, formation of sludge with contaminants) were being exercised too close to threshold. The "end run" in this case is to assume that the boiler must be capable of continuous operation at a temperature some 200°C hotter, and at 2 1/2 times the pressure, of normal operation. Life testing under such conditions accelerates exponential failure mechanisms by factors of 10.

- Because of scale, the old G.E. system did not have unanticipated problems with system dynamics. (Structure, shutdown, accommodations to changing load). However, the original SNAP-8 design (a so-called two loop design) did not adequately anticipate the effect of having the thermal time constant of the boiler short compared to that of the reactor heat source. The "end run" has been to make the problem of control and an alternate path for excess heat stand out like a sore thumb. Both boiler and turbine in the high pressure system have very low thermal mass; and supersonic flow in the turbine effectively disconnects the flow rate at the discharge from flow in the boiler.

At the same time that we have identified or avoided certain known system problems, the new technology has created others.

- The control of sandblasting by small droplet size in an impulse turbine has not yet been demonstrated experimentally, so that the consequent system overhead cannot be fully anticipated.
- Because the fluid velocity in nozzles and blades is lower in a reaction turbine than in an impulse turbine, the former is more efficient and less vulnerable to droplet sandblast. Generally, however, the reaction turbine requires rotating pressure seals (example: the fluid dynamic beaming assumed in Fig. 56), which may be difficult to design for 5 to 10 years of unattended life.
- Light gas as a system contaminant is an everpresent hazard of any arrangement that contains radioactivity whether as reactor or radio-isotope. H_2 forms hydrides with Na and K in heat transfer loops. He diffuses though almost any material and can cause embrittlement of component parts. The proposal to use light gas as the heat transfer fluid in the radiator raises a significant compatibility problem, in terms of

inevitable leakage from one part of the system to another through spacecraft-enforced close proximity. The blocks labled "contaminant control" on the hotside, and "contaminant removal" on the coldside, are non-trivial parts of the system.

Given all these factors, it is worthwhile to take the next steps to solve the experimental problems of the high pressure mercury cycle, and if so, where should those steps begin?

To the first question, the author responds, yes, it is worthwhile. The high pressure mercury cycle is the only efficient cycle which is thermodynamically matched to the hot shoe and condenser temperatures of compact reactors, radio-isotope sources, or solar concentrators, whether in space, or (with a steam turbine as a bottoming cycle) on the ground. Although Fig. 57 is apparently complex, the individual component level resolution of the complexities, as discussed in earlier sections, appear to be mechanically and conceptually simple.

The second question is not as easy to answer. Some simple initial experiments at the component and information-acquisition level are outlined in the next section. But towards incorporation in what system should development be directed? Section XII considered superficially three possibilities: substitution of an Hg cycle for a thermoelectric in a reactor system; substitution of Hg cycle for a thermoelectric in a radio-isotope system; and use of an Hg boiler at the focus of a solar concentrator collector system. The first two have the attractive feature that they have the flavor of component substitutions in systems already conceived or in service. The disadvantage is the apparent absence of a funded mission for those "existing" systems. At the same time, even if no market has been developed, there are applications for developmental terrestrial power systems at almost every level of output. It is therefore suggested that an initial development of such a system be sized to be able to operate on the ground at the focus of a 30 ft dish antenna, retrofied with a shiny foil surface to produce a thermal level of about 30 to 50 kW_t. By using a modular concept for the heat flow, with a thermal

bypass around the boiler/turbine system, heat sources and radiators other than the ones selected for demonstration could be substituted (see Fig. 58). Moreover, the weight, space, and safety limitations associated with placing components at the antenna mount of a 30 ft dish, while not those of a satellite, are sufficiently close in both order of magnitude and kind to demonstrate the plausibility of using the technology on a satellite. Moreover, the economics of reproducing the power conversion hardware, while not those of central power plant hardware, are sufficiently close in scope as to demonstrate the plausibility of using the technology for terrestrial applications.

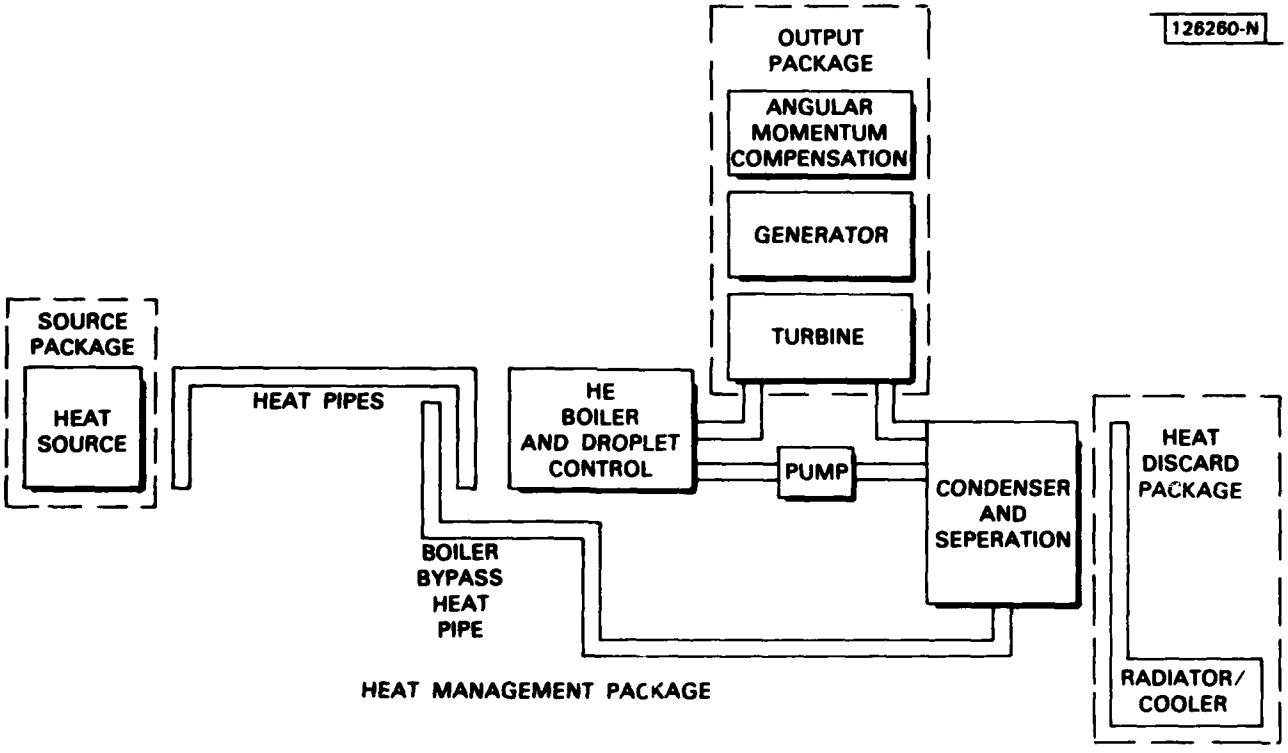

Fig. 58 Modular layout of heat management for substitution of input and output subsystems.

XIV. SUGGESTIONS FOR EXPERIMENTAL WORK

While the investigations of this report have sought to lean as heavily as possible on experimental results, it has been, nevertheless, a paper study. Although several novel suggestions have been offered---such as the radiative droplet boiler, the use of controlled wetness and droplet size in an expansion nozzle, and the use of dynamic expansion against Coriolis force as a virtual piston---in sufficient detail to make the construction of working models "merely" a matter of standard drawing board design and machine shop construction, such models have not been designed, built, and tested.

Suggestions for executing experimental work helpful to the construction of working models of system components and for assembling those models into demonstration systems fall into several categories. At one end of the scale are basic investigations to determine the accuracy of the models used and the breadth of materials actually available with which to execute designs. At the other end of the scale are the system optimizations and dynamic simulations necessary to determine which of several alternative energy extraction cycles would be suitable in a large terrestrial power plant, or in the design of a mercury boiler as an integral subsystem in a reactor rather than as an add-on through the intermediary of sodium heat pipes. In the middle lies the design, construction, and testing of actual atomizers, boilers, nozzles, bearings, heat exchangers, and turbogenerators.

At the basic level, one of the more important tasks is, in effect, updating the Liquid Metals Handbook with information about high temperature corrosion and passivation of modern materials. Such information may be proprietary or in not easily accessible reports. At the same time, there will be no substitute for an experiment with a selected subset of materials to determine not only resistance to attack by Hg, but also the effectiveness of known corrosion inhibitors at high temperature and stress level. (In this connection, it is to be expected that the attack on a material under stress will be concentrated at grain boundaries, which are a small fraction of the exposed surface. To the extent to which an inhibitor also interacts preferentially at such boundaries, trace

quantities may suffice to drastically alter corrosion stability).

At a fundamental physics level is a measurement of the pressure and heat of boiling of mercury over the temperature range. Here what is required is a more-or-less conventional boiler with some form of electric (i.e., measureable) heating, and a more-or-less conventional condenser, all mounted in a closed system with a buffer gas under adjustable pressure. Liquid is then simply boiled, condensed, and recirculated until enough has been refluxed to permit accurate assertions about the heat used to boil a given mass at a given temperature and pressure. It is not anticipated that the results of such measurements will make the difference between the success and failure of any given subsystem; but such measurements are required to be able to predict the best operating conditions to better than 10% accuracy, or to evaluate efficiency to within a few percent.

There are two intermediate investigations that are particularly interesting; both are part paper design, part experimental.

One such investigation explores the tradeoff between a fixed nozzle with droplet impact on the turbine blades against the radial flow configuration illustrated in Fig. 56. In their simplest form, both sets of experiments can be conducted at room temperature. In one case mercury is accelerated and broken up into droplets of controlled size and direction, and then allowed to impact test surfaces. Arrangements are then made to heat the surface (not the mercury) to working temperature, so that the experimenter can see what happens during the experiment without having to construct high pressure, high temperature windows. Similarly, many of the questions about the high pressure fluid dynamic bearing (which is really a low friction, high pressure rotating packing) can be addressed near room temperature using mercury or related liquid metal fluids, with room pressure gas as the backfill on the low pressure side of the bearing. Eventually, of course, if these experiments are successful, further data will be needed under operating conditions; but the more severe environment is not needed for the initial screening experiments.

Another investigation relates bearings to the generator part of the turbo-generator. We have remarked several times that a high energy-density electric generator functions a fortiori as a dynamic bearing for the turbine axle to which it is connected. (A possible definition of "high energy density" is a machine in which magnetic fields due to load current flow are a significant fraction, in magnitude, of the magnetic fields which produce the open circuit voltage. A high-density design might have reaction fields of 1000 gauss for 7000 gauss main fields.) Perhaps only the designers of cryogenic electrical machinery appreciate how fully the design of ordinary motors and generators is driven by the vagaries of easily demagnetized ferromagnetic materials. The advent of rare-earth-cobalt permanent magnets removes the need, and even the desireability, of using soft iron in alternating fields at room temperature. Some further ingenuity needs to be exercised in the design of permanent magnet generators that will take full advantage of the hysteresis-free field of such magnets and also the high angular rotation rates of the mercury turbine to produce field upwards of 100 volts/meter at the conductors. Generators of this kind could occupy not much more value than the turbine wheel itself and thus be part of the turbine assembly even when sized for full turbine output. (However, they are not 60 Hz machines).

The suggestions produced in the preceding paragraphs are intended to be typical of the kind of experimental work that needs to be done. This is not the place for an integrated proposal of an experimental plan leading, with milestones, through a series of prototypes to a spacecraft power plant or to a pilot scale system for a power station.

APPENDIX A

THERMODYNAMIC EXTRAPOLATION OF SPECIFIC HEAT DATA

Generally speaking, theoretical thermodynamics simply explores the mathematical consequences of the fact that we use more variables to describe the state of a substance than are mathematically necessary. Additional constraints come from the First and Second Laws, but the most convenient results come from the assumption that mathematical potentials such as entropy S and internal energy U are differentiable functions of several variables.

Thus, for reversible processes we can write the heat exchanged, dq either in terms of U or in terms of S as functions of T and V

$$dq = \frac{\partial U}{\partial T} dT + \left(\frac{\partial U}{\partial V} + P \right) dV \tag{A1}$$

$$dq = TdS = T \left(\frac{\partial S}{\partial T} dT + \frac{\partial S}{\partial V} dV \right) \quad . \tag{A2}$$

Eq. (A2) is simply a restatement of the meaning of partial derivatives and the definition of entropy. Eq. (A1) is not a definition. It is a statement of the First Law, that the heat supplied must go into either internal energy dU or into external work PdV. Evidently, we have too many symbols describing one set of facts and an additional (First Law) constraint. Inasmuch as dT and dV are arbitrary in relative size, their coefficients must be equal

$$T \frac{\partial S}{\partial T} = \frac{\partial U}{\partial T} \tag{A3}$$

$$T \frac{\partial S}{\partial V} = \frac{\partial U}{\partial V} + P \quad . \tag{A4}$$

Because all the parameters in these equations are assumed to be differentiables, S can be eliminated between them. To do so, one partially differentiates (A3) with respect to V and (A4) with respect to T to obtain two new equations. Utilizing all four equations and the mathematical identity

$$\frac{\partial^2 Z}{\partial x \partial y} = \frac{\partial^2 Z}{\partial y \partial x} \tag{A5}$$

(valid for all Z, x, and y for which the partial derivatives exist) one obtains

$$\frac{\partial U}{\partial V} + P = T \frac{\partial P}{\partial T} \quad . \tag{A6}$$

This is a typical thermodynamic result, in that it is as much a consequence of the fact that U and S are differentiable point functions (independent of the path by which the point (T,V) is reached) as it is a consequence of the principles of physics. Eq. (A6) may be substituted back into Eq. (A1) to eliminate the explicit dependence on $\partial U/\partial V$

$$dq = \frac{\partial U}{\partial T} dT + T \frac{\partial P}{\partial T} dV \quad . \tag{A7}$$

Eq. (A7) can be used to obtain the specific heat C_x along any path x through a point in terms of the constant volume specific heat C_v at that point. Constant volume implies $dV = 0$. It immediately follows that $\partial U/\partial T$ is C_v. Now, along an arbitrary path x, there will be a proportionally between dV and dT. It follows that the specific heat C_x can be calculated from C_v and the equation of state according to

$$C_x = \left.\frac{dq}{dT}\right|_x = C_v + T \left.\frac{\partial P}{\partial T}\right|_V \left.\frac{dV}{dT}\right|_x \quad . \tag{A8}$$

In particular, the specific heat at constant pressure, C_p, is

$$C_p = C_v + \left.\frac{\partial P}{\partial T}\right|_V \left.\frac{\partial V}{\partial T}\right|_P \qquad \text{(A9)}$$

which is the (less general) form of Eq. (A8) usually found in reference books.

Now $\underline{q}$ is not a point function. It depends on the path between two conditions of the fluid as well as the initial and final states. On the other hand, the entropy S defined by

$$dS = dq_{reversible}/T \qquad \text{(A10)}$$

is a point function, independent of the path (so long as the process is reversible). In mathematical language, dS is a "total differential" and 1/T is the "integrating factor" for the reversible exchange of heat. The integratability of dS in the multidimensional state manifold is the primary reason for dealing with S instead of $\underline{q}$.

In terms of S and C_v, Eq. (A7) becomes

$$dS = C_v \frac{dT}{T} + \frac{\partial P}{\partial T} dV \quad . \qquad \text{(A11)}$$

This form of the specific heat equation can be used in conjunction with Eq. (A8) to extend the knowledge of specific heat from any path x to any other path x' between the same temperature limits, which was the assertion made at the beginning of the Section on the thermodynamic properties of mercury.

Inasmuch as Eq. (A8) can be used to convert C_x to C_v at any given temperature on path x, and to convert $C_{v'}$ to $C_{x'}$ at that same temperature on path x', all that is necessary is to use Eq. (A11) to derive the relationship between C_v and $C_{v'}$ at any given temperature. For this purpose, consider on the (V,T) plane two trajectories at constant volumes V and V' through points x and x', as in Fig. A1, at temperature T. Futher, let y and y' be points on the respective constant volume trajectories at some other temperature T'. Then the entropy at y' can either be determined directly along the path x'y' by

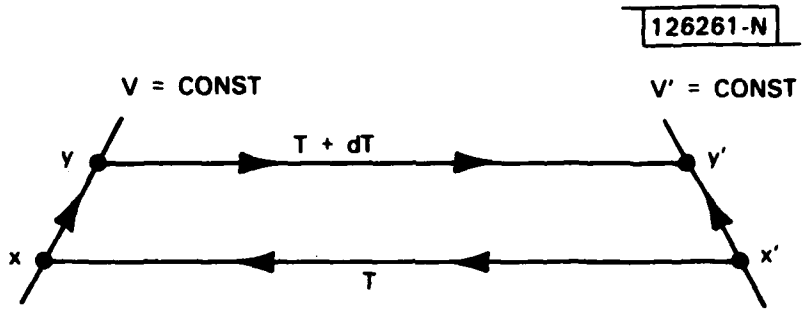

Fig. A1 Trajectories for determining specific heat C_v.

$$S_{y'} = S_{x'} + \int_{x'}^{y'} C_{v'} dT/T \tag{A12}$$

or it can be determined along the path x'xyy' by

$$S_{y'} = S_{x'} - \int_{v}^{v'} \frac{\partial P}{\partial T} dV + \int_{x}^{y} C_v \frac{dT}{T} + \int_{b}^{v'} \frac{\partial P}{\partial T} dV \quad . \tag{A13}$$

The entropies $S_{y'}$ in these equations must be the same, resulting in

$$\int_{T'}^{T'} C_{v'} \frac{dT}{T} = \int_{T}^{T'} C_v \frac{dT}{T} + \int_{V}^{V'} \left(\frac{\partial P'}{\partial T} - \frac{\partial P}{\partial T} \right) dV \quad . \tag{A14}$$

If we allow the difference between T and T' to shrink to differential size, the integrals with respect to temperature disappear and we are left with

$$C_{v'} = C_v + T \int_V^{V'} \frac{\partial^2 P}{\partial T^2} \, dV \quad . \tag{A15}$$

Evidently, this means of extending specific heat from volume V to V' at constant temperature requires that $\partial^2 P/\partial T^2$ remain defined and finite along the entire path. At possible points of failure of $\partial^2 P/\partial T^2$ to be well-behaved, such as the critical point and phase boundaries, further investigation of the nature of the discontinuity is required if Eq. (A15) is to be used properly. We shall consider only the case in which the path of integration crosses a saturation boundary.

When the path crosses a saturation boundary, the failure of Eq. (A15) is the failure of the difference under the volume integral approach zero as T-T' approaches zero. Instead, we have

$$C_{v'} = C_v + T \int\!\!\!\!\!\!-_V^{V'} \frac{\partial^2 P}{\partial T^2} \, dV + \left(\frac{\partial P'}{\partial T} - \frac{\partial P}{\partial T} \right) \frac{dV}{dT} \Bigg|_{\text{boundary}} \tag{A16}$$

where the bar through the integral indicates omission of the immediate vicinity of the boundary, while the second term introduces the discontinuity in C_v at the boundary. The differential form of the C_v equation usually found in reference books gives no hint of Eq. (A16):

$$\frac{\partial C_v}{\partial V} = T \frac{\partial^2 P}{\partial T^2} \quad . \tag{A17}$$

If we can assume that $\partial^2 P/\partial T^2$ is finite on either side of the boundary, then there are two cases, depending on whether dV/dT is positive or negative.

If dV/dT is positive, then the temperature T' can be reached from V without crossing the boundary, so that C_v and $\partial P'/\partial T$ are associated on the same side of the boundary. In this case the integral in Eq. (A16) vanishes as V'-V is made small enough and we are left with

$$C_v + \frac{\partial P'}{\partial T}\frac{\partial V}{\partial T}\bigg|_{\text{boundary}} = C_{v'} + \frac{\partial P}{\partial T}\frac{\partial V}{\partial T}\bigg|_{\text{boundary}} \quad . \tag{A18}$$

According to Eq. (A8) this is simply a statement that C_{boundary} is the same on both sides of the boundary. If $\partial V/\partial T$ is negative on the boundary, $\partial P'/\partial T$ is associated with C_v' instead of C_v; but because of the negative sign, the specific heat remains continuous across the boundary.

$$\Delta C_{\text{boundary}} = 0 \quad . \tag{A19}$$

Let us apply Eq. (A16) to a constant-temperature path from the liquid region near the boiling line, through the wet-vapor boiling region into the dry gas region. Let C_{vL} be the constant-volume specific heat of the liquid on the liquid side of the boiling liquid boundary; and let C_{vB} be the corresponding parameter on the boiling liquid side. From Eq. (A16) we have

$$C_{vB} = C_{vL} + T\left(\frac{\partial P}{\partial T}_{liq} - \frac{dP}{dT}\bigg|_{\text{boiling}}\right)\frac{dV}{dT}\bigg|_{\text{sat liq}} \quad . \tag{A20}$$

Now let C_{vv} be the constant volume specific heat of the dry vapor at the vapor saturation line. Then from Eq. (16) we have

$$C_{vv} = C_{vB} + T\int \frac{\partial^2 P}{\partial T^2}\bigg|_{\text{boiling}} dV + T\left(\frac{dP}{dT}\bigg|_{\text{boil}} - \frac{\partial P}{\partial T}_{gas}\right)\frac{dV}{dT}\bigg|_{\text{sat vapor}} . \tag{A21}$$

The integral in Eq. (A21) is trivial in that the integrand is constant (at fixed temperature) across the boiling region. Thus we obtain for C_{vv}

$$C_{vv} = C_{vL} + T \left(\frac{\partial P}{\partial T}\right)_{liq} \left.\frac{dV}{dT}\right|_{liq\ sat}$$

$$+ T \left(\frac{\partial^2 P}{\partial T^2}\right)_{boil} \Delta V + T \left(\frac{\partial P}{\partial T}\right)_{boil} \frac{d\Delta V}{dT} \qquad (A22)$$

$$- T \left(\frac{\partial P}{\partial T}\right)_{gas} \left.\frac{dV}{dT}\right|_{gas\ sat}$$

in which ΔV is the difference between the volume of saturated liquid and saturated vapor at temperature T. The first line of Eq. (A22) is the specific heat on the liquid saturation line, C_{sat}. The second line can be reduced with the help of the Clausius Clapeyron equation. The result is

$$C_{vv} = C_{sat} + T \frac{\partial}{\partial T} \frac{L}{T} - T \left(\frac{\partial P}{\partial T}\right)_{gas} \left.\frac{dV}{dT}\right|_{gas\ sat} . \qquad (A23)$$

Finally, let C_{vG} be the specific heat at some point well into the (nearly ideal) dry gas region, for which the gas obeys a nearly ideal equation of state

$$PV = RT + r(T,V) \qquad (A24)$$

r(T,V) being the "residual" which vanishes as T and V become large. Since the second partial temperature derivative of RT/V is zero, we find

$$C_{VG} = C_{vv} + T \int_V^G \frac{\partial^2 r(T,V)}{\partial T^2} \frac{dV}{V} . \qquad (A25)$$

<u>In principle</u>, one can work backwards from the known value of C_{vv} as $V,T \to \infty$, namely 3R/2 for a monotonic gas, through a known residual and known boiling heat of vaporization and pressure to the specific heat along the

liquid saturation line (and ultimately, if desired, to C_v of the liquid). The result could then be compared for consistency with the assumed and measured experimental properties of the liquid. Alternately, one can start with the properties of the liquid and carry the calculation in the other direction to see whether all of the assumptions are consistent with the 3R/2 constant-volume heat capacity of the rarified gas.

In actuality, the last two terms in Eq. (A23) are each an order of magnitude larger than their difference, so that the whole computation is highly sensitive to small errors in the models for L, P, and the departure of V from the ideal gas law. Since each of these models enters as a derivative, the main thrust of a calculation made according to the previous paragraph is to test the consistency of the derivatives of the various assumptions. If such consistency is obtained, the models themselves are consistent. But if the derivatives are not well consistent, it does not necessarily follow that the models are poor ones for calculating the total heat and entropy, which are obtained by integration, not differentiation.

The accompanying Table A-1 shows a model test calculation of this sort, using the Russian liquid density data, the simple activation energy pressure equation above 630°K and the Liquid Metals Handbook pressure equation below 630°K. The 4th column of the Table gives C_s along the liquid saturation line. The 5th column gives the error in reaching C_v at temperature and $V \to \infty$. The 6th column gives the largest individual term from Eqs. (A24) and (A25) which appears in the calculation of the ultimate C_v (3 cal/mol deg). Other columns give the pressure in bar, the ratio of pressures calculated along the gas saturation line by Eqs. (III-6) of the text and by inserting the given volume V into the Berthelot Equation of Section III of the text.

The final column gives the apparent residual left over from the Berthelot Equation along the gas saturation line, as a fraction of R. Presumably this remainder is a direct measure of the cummulative inconsistency of the assumed pressure, heat of evaporation, and equation of state relationships; the fifth column divided by C_s or $C_{v\infty}$ is an indirect measure, sensitive to the temperature derivatives of these same assumptions.

TABLE A-1
THERMODYNAMIC PROPERTIES OF MERCURY (P-V-T EQUATION)

Tc = 1760 K: Pc = 1500 atm: Lo = 14800 cal/m

Rho = $3.140+10.930(1-T/Tc)^{0.283}$ T>500C; $L/Lo=(1-T/Tc^2).42$

P = 84411 exp(7172/T) (=exp(17.247-7617/T-.81nT) if T<630K)

Vo = 10.000

log A = 8.317

Hcor = 0.000

K,V^{-K} 2.000

Cs = 6 - 0.001374T + (TdP/dTlv)(dV/dT)

Temp DegC	log10 Pbar	Pressure Ratio	Cs	dCv	Max Term	dR %
0	-6.58	1.003	6.38	0.84	54.77	-0.3
50	-4.76	1.002	6.43	0.37	46.49	-0.2
100	-3.44	1.001	6.46	0.08	40.46	-0.1
150	-2.43	1.001	6.48	-0.14	35.88	-0.1
200	-1.64	1.002	6.49	-0.33	32.30	-0.2
250	-1.01	1.003	6.50	-0.50	29.44	-0.3
300	-0.49	1.005	6.48	-0.65	27.10	-0.5
350	-0.06	1.006	6.46	-0.79	25.16	-0.6
400	0.32	1.019	6.42	-0.50	23.54	-1.9
450	0.64	1.024	6.42	-0.48	22.17	-2.3
500	0.92	1.027	6.54	-0.32	21.01	-2.6
550	1.17	1.028	6.60	-0.22	20.02	-2.7
600	1.38	1.028	6.67	-0.13	19.18	-2.6
650	1.58	1.026	6.74	-0.03	18.47	-2.3
700	1.75	1.022	6.82	0.06	17.88	-1.9
750	1.91	1.016	6.91	0.14	17.38	-1.4
800	2.05	1.009	7.01	0.20	16.99	-0.8
850	2.18	1.002	7.12	0.25	16.68	-0.1
900	2.30	0.994	7.24	0.28	16.48	0.5
950	2.40	0.986	7.39	0.30	16.37	1.1
1000	2.50	0.979	7.56	0.29	16.37	1.7
1050	2.60	0.973	7.76	0.26	16.49	2.1
1100	2.68	0.968	8.01	0.20	16.76	2.4
1150	2.76	0.966	8.32	0.13	17.23	2.4
1200	2.84	0.967	8.73	0.04	17.95	2.3
1250	2.91	0.972	9.29	-0.06	19.06	1.8
1300	2.97	0.982	10.12	-0.17	20.80	1.1
1350	3.03	0.999	11.53	-0.25	23.71	0.1
1400	3.09	1.026	14.48	-0.20	29.39	-1.4
1450	3.14	1.070	25.13	0.43	46.00	-3.3

APPENDIX B

DROP GROWTH IN CONSTANT TEMPERATURE DIFFERENCE NOZZLE

The objective here is to integrate the equations for droplet growth in an expansion nozzle on the assumption of conductivity-limited condensation over a constant temperature differential between droplet and the remainder of the vapor. If the droplet radius is ζ, then Eq. (IX-22) for droplet growth is

$$\zeta \frac{d\zeta}{dt} = \frac{m\sigma\Delta T}{L\rho_\ell} = \alpha \tag{B-1}$$

in which α is a weak function of temperature. The relationship between kinetic energy and wetness we take to be

$$d\left(\frac{1}{2} mV^2\right) = d(Lx) \quad . \tag{B-2}$$

Without any loss of generality, Eq. (B-1) may be rewritten in terms of x and fully-condensed droplet radius, r, using

$$\zeta = rx^{1/3} \tag{B-3}$$

so as to take the form

$$\frac{r^2}{3} x^{-1/3} \frac{dx}{dt} = \alpha \quad . \tag{B-4}$$

Finally, the substitution of dZ/v for dt yields

$$\frac{r^2}{3} x^{-1/3} v dx = \alpha dZ \quad . \tag{B-5}$$

Starting with a given x and V at Z equal to zero, one can integrate Eqs. (B-5) and (B-2) numerically. For any given dx, one determines from the

data in Section III on the H-S diagram the change in Lx. This is inserted into Eq. (B-2) to determine the change in v^2. The new x and v are inserted into Eq. (B-5) to give the increment in distance along the nozzle. From the flow velocity and temperature conditions, the area of the nozzle at the given Z is also determined as in Fig. 38. The process of numerical integration can thus be repeated for successive increments of condensation dx. It was in this manner that Figs. 41 and 42 of the text were obtained.

If α and L can be assumed not to vary significantly during the expansion, Eqs. (B-2) and (B-5) can be easily solved and integrated analytically. Integration of Eq. (B-2) yields

$$x - x_o = \frac{m}{2L} (v^2 - v_o^2) , \qquad \text{(B-6)}$$

v_o being the initial velocity at Z=0, and x_o the initial wetness. Evidently, Eq. (B-6) is oversupplied with constants. We shall write instead

$$x = x_o + \frac{m}{2L} v^2 , \qquad \text{(B-7)}$$

with the understanding that the new x_o includes the effect of v_o from Eq. (B-6). Putting x from Eq. (X-7) and dx from Eq. (B-2), at constant L, into Eq. (B-5) yields

$$\frac{\frac{r^2 m}{3L} v^2 dv}{(x_o + \frac{m}{2L} v^2)^{1/3}} = \frac{m}{L} \frac{\alpha \Delta T}{\rho_\ell} dZ . \qquad \text{(B-8)}$$

The expression on the l.h.s. of Eq. (B-8) is the differential of a Gauss hypergeometric function $2F_1$. If we adopt the convention that v is zero at Z equal to zero, then the integral of Eq. (B-8) is

$$x_o^{1/3}\,\alpha\Delta TZ = \frac{v^3}{9} r^2 \rho_\ell \; {}_2F_1\left(1/3,\ 3/2;\ 5/2;\ -\frac{mv^2}{2x_o L}\right) \quad . \tag{B-9}$$

For small values of the final argument, the ${}_2F_1$ function approaches unity. If, instead, the initial droplet size is very small, then textbook formulas (for example Abramowitz and Stegun, Handbook of Mathematical Functions, formula 15.3.7) can be used to obtain ${}_2F_1\ (1/3,\ 3/2;\ 5/2;\ -u)$ in terms of ${}_2F_1\ (1/3,\ -17/6;\ -1/6;\ 1/u)$ and ${}_2F_1\ (1/3,\ 0;\ 13/6;\ 1/u)$.

For the behavior when x_o is small compared to mv^2/L, it is easier to let $x_o \to 0$ in Eq. (B-8) and to find

$$\alpha\Delta TZ = \frac{v^{7/8}}{7} r^2 \rho_\ell \left(\frac{2L}{m}\right)^{1/3} \quad . \tag{B-10}$$

Applying Eq. (B-10) to both the general pair (Z,v) and the final pair (Z_f, v_f) yields Eq. (IX-23) of the text by division:

$$Z/Z_f = (v/v_f)^{7/3} \quad . \tag{IX-23}$$

Whereas Eq. (B-8) requires a hypergeometric function to integrate as a (v-Z) relationship, the replacement of dZ by vdt results in an elementary integral for the (v-t) relationship. Again adopting the convention that v is zero at t=0, the result is

$$\frac{M}{L}\,\alpha\Delta Tt = \frac{r^2}{2}\left(x_o + \frac{m}{2L} v^2\right)^{2/3} \rho_\ell \quad . \tag{B-11}$$

Suppose once more that x_o is negligible. Then this equation reduces to

$$v^{4/3} = \frac{4\alpha\Delta T}{r^2 \rho_\ell}\left(\frac{m}{2L}\right)^{1/3} t \quad . \tag{B-12}$$

Putting this equation into Eq. (B-10) produces

$$Z = \frac{4}{7} vt \quad , \tag{B-13}$$

which is also Eq. (IX-24). The actual value of t can be obtained directly by integrating Eq. (B-4):

$$t = \frac{r^2 \, (x^{2/3} - x_o^{2/3}) \, L \, \rho_\ell}{2 \, m \, \alpha \, \Delta \, T} \quad . \tag{B-14}$$

APPENDIX C

LIGHT GAS HEAT TRANSFER FOR CONDENSER AND RADIATOR

We consider here the performance of a condenser-radiator system for mercury which uses a light gas such as H_2 or He as the means of transporting heat from condenser region to the radiator surfaces. The radiator can then be constructed of any material that can contain these light gases at the radiator temperature, about 600°K. Inasmuch as the He molecule is actually smaller than the H_2 molecule, although the latter is lighter, the best gas both to contain and to use for heat transfer is H_2. Materials which have low permeability to H_2 include Al, Be, some (but not all) glasses, graphite, and high temperature plastics. We cannot consider the materials problems further here.

The parameters which are relevant to heat transport at 600°K and at 1 atm pressure are given in Table C-I, except that the properties for Hg vapor are those at the equilibrium pressure, 0.6 atm.

TABLE C-I

Properties of H_2, He, and Hg at 600°K

Property	H_2	He	Hg
Thermal Conductivity, σ (W/cm)	3×10^{-3}	2×10^{-3}	0.08×10^{-3}
Density, ρ (g/cm^2)	40×10^{-6}	90×10^{-6}	2300×10^{-6}
Viscosity, μ (μ poise)	125	250	500
Kinematic Viscosity, ν (cm^2/sec)	3	3	0.2
Volumetric Heat Capacity, $\bar{c}$ (Joule/cc)	600×10^{-6}	400×10^{-6}	250×10^{-6}

At these modest pressures, both the thermal conductivity and the viscosity depend on temperature only (not pressure) and scale as the 0.5 or 0.6 power of temperature; the P-V-T relations are those of an ideal gas.

Note first that the thermal conductivity of either H_2 of He is roughly 30 times that of Hg vapor. Thus, if the condenser plenum shown in Fig. 48 is large in volume compared with the product of nozzle length and nozzle exit area (as must be the case to keep the vapor speed in the plenum modest), the temperature difference between light gas and mercury droplets in the condenser is no more than 1/30 of the temperature difference between droplets and mercury vapor in the nozzle, at most a degree or two.

Evidently, if there is to be a heat transfer design problem with the light gas, it will be in the radiator tubes, not in the condenser plenum where Hg and light gas are comingled.

Heat transfer from fluids flowing in pipes has been the subject of extensive empirical investigation. Except in a thin boundary layer next to the wall, heat is moved by turbulent mixing rather than by thermal conductivity. The dimensionless-numeric characterization of flow conditions is the Reynolds number Re

$$Re = \rho v d/\mu \qquad \text{(C-1)}$$

with v the speed of flow and d the diameter of the pipe. It follows from Table C-I that if the flow speed is 100 m/sec, a pipe diameter of 3 cm is needed if Re for light gas flow is to be at least 10,000, as is required for the reliable formation of the boundary layer. Slower flow speeds would imply even larger pipe diameter to set up turbulent heat exchange conditions.

Empirical results for heat transfer are tabulated by giving a non-dimensional "Nusselt number," Nu, as a function of Reynolds number:

$$Nu = 30(Re \times 10^{-4})^{0.8} . \qquad \text{(C-2)}$$

(If Re exceeds roughly 3×10^5, the boundary layer itself becomes turbulent and a slightly different expression takes over; but in the radiator tubes such conditions are not reached.)

The actual heat transfer coefficient, h, per unit area of pipe wall is then given in terms of the thermal conductivity of the gas by

$$h = \sigma \, Nu / d \quad . \qquad (C\text{-}3)$$

Evidently, the Nusselt number can be interpreted as the ratio of the pipe diameter to the thickness of the boundary layer. The combination of Eqs. (C-1) through (C-3) results in a heat transfer coefficient that varies very little (as the -0.2 power) with pipe diameter; and roughly directly (as the 0.8 power) as speed of flow. Thus, for Re in the general vicinity of 10^4 and pipe diameter in the general vicinity of 3 cm, the boundary layer has an effective thickness of roughly 1 mm for any gas flow.

There are four major considerations in the design of a radiator. The first is the temperature at which radiation takes place. For 600°K, the maximum black body radiation is roughly 0.75 W/cm^2; at 550°K this drops to roughly 0.5 W/cm^2. The rest of the heat transfer system must be sized to supply heat at such flux levels. The second consideration is the temperature drop across the boundary layer, ΔT_b, due to the above heat flux. The third consideration is the temperature drop, T_g, in the fluid as it passes from radiator inlet to outlet as a consequence of the heat given up by the moving gas. The fourth consideration is the power required to maintain gas flowing through the pipes at the speeds necessary for modest temperature drops in heat transport and in heat flow through the boundary layer.

We begin by equating the heat flux W_d dissipated in radiation to the heat flux, q_h, which passes through a unit area of boundary layer when the temperature drop is T_b. From the preceeding equations:

$$W_d = q_h = 30\ \sigma\Delta T_b \left(\frac{vd}{\mu} \times 10^{-4} \right)^{0.8} / d \quad . \qquad (C\text{-}4)$$

Let us introduce the following notation, definition, and formula:

$$Re^* = Re \times 10^{-4} \quad . \qquad (C\text{-}5)$$

$$Pr = C_p\ \mu/m\sigma \quad . \qquad (C\text{-}6)$$

$$\rho = mP/RT \quad . \qquad (C\text{-}7)$$

Equation (C-5) is a definition of Re* so that it is unity when Re is 10^4. Equation (C-6) introduces the "Prandtl number," Pr, a dimensionless number which differes very little from fluid to fluid, being 0.66 for H_2 at 600°K and 0.72 for water at room temperature. Equation (C-7) is the ideal gas law, applicable to any gas at modest pressure.

Using Eq. (C-1) and Eqs. (C-5) to (C-7) one can algebraically manipulate Eq. (C-4) to take the following form

$$W_d = 30 \times 10^{-4}\ vP\ (C_p/R)\ (\Delta T_b/T)\ (Re^*)^{-0.2}\ (Pr)^{-1} \quad . \qquad (C\text{-}8)$$

In this equation W_d and vP are assumed to be given in consistent units. All of the parentheses are then dimensionless numbers. At any given system gas pressure, P, the equation asserts that the boundary layer temperature drop is inversely proportional to the speed of flow. Inasmuch as neither (C_p/R) nor (Pr) is a strong function of the choice of gas, the $v\Delta T_b$ product is not a strong function of the choice of gas. Modest preference goes to diatomic gases ($C_p/R = 3.5$) over monatomic gases ($C_p/R = 2.5$). (The equation can be applied to liquids only if one uses for P the ideal gas pressure that would be required to achieve the actual liquid density, rather than the system pressure. For liquids, the effective P is several thousand atmospheres, so that the equation does indeed state that liquids are better coolants than gases.)

To push the gas through the radiator tubes at velocity $\underline{v}$ requires kinetic energy and power to overcome friction. This power can only come from the turbine. Consequently, one must observe the constraint that $\underline{v}$ be low enough to keep the frictional loss at a small fraction of the turbine output.

Section X gives the frictional loss per unit wall area, q_f, as proportional to the cube of the flow speed

$$Q_f = C_f \rho v^3/2 \quad . \tag{C-9}$$

For $Re^* \geq 1$, the friction coefficient C_f varies slowly with Re^*. In the "Reynolds analogy" we put

$$C_f = 0.0075\ (Re^*)^{-0.2} \quad . \tag{C-10}$$

(There are more sophisticated formulations for C_f, some of which include the effects of tube wall roughness. Equation (C-10) suffices for present purposes.)

From Eq. (C-9) it is clear that the highest gas speeds for a given friction loss are attained with the least dense gas, all other things being equal. However, the variation of $\underline{v}$ with ρ is a weak one, so that increasing pressure in Eq. (C-8) (which also raises density) has a net beneficial effect, even though the maximum allowed $\underline{v}$ drops slightly as a consequence.

Let us suppose that the friction loss flux, q_f, is a small fraction, ζ_f, of W_d. Inasmuch as W_d is the waste heat from the turbine, ζ_f should be small compared with $\eta/(1-\eta)$, where η is the thermal efficiency of the turbine cycle, in order that the friction loss also be a small fraction of the turbine output.

If the coolant gas is H_2 at 600°K, we obtain for $\underline{v}$ from Eq. (C-9) and (C-10)

$$v = 8400(100\ \zeta_f\ W_d\ /\ P_{atm})^{1/3} \text{ cm/sec} \tag{C-12}$$

with W_d in W/cm^2 and P_{atm} in atmospheres. If the coolant gas is He, the corresponding result is

$$v = 6700(100\ \zeta_f\ W_d\ /\ P_{atm})^{1/3}\ cm/sec \quad . \qquad (C\text{-}13)$$

If these results are combined with Eq. (C-8), and an appropriate numerical adjustment is made for otherwise inconsistant units, we obtain the boundary layer temperature drops as

$$H_2:\ T_b = 45.4(T/600)^{2/3}\ (W_d/P_{atm})^{2/3}\ (100\ \zeta_f)^{-1/3}\ (Re^*)^{-0.13} \qquad (C\text{-}14)$$

$$He:\ T_b = 72.4(T/600)^{2/3}\ (W_d/P_{atm})^{2/3}\ (100\ \zeta_f)^{-1/3}\ (Re^*)^{-0.13} \quad . \qquad (C\text{-}15)$$

Evidently, for an interesting selection of parameters (T=600°K, P=0.6 atm, W_d=0.5, ζ_f=1%), the H_2 heat exchanger can be built with a boundary layer temperature drop under 50°K. Moreover, if the condenser temperature is raised in the interest of reducing the weight of the radiator, the turbine exhaust pressure rises more rapidly than TW_d, with the result being a slight net improvement in ΔT_b, even when ζ_f is lowered to compensate for the reduced efficiency of the thermal cycle. In such a case, the problems are mainly those of engineering materials which are both strong enough to contain the pressure at condenser temperature and low enough in the periodic table to be resistant to H_2 diffusion.

Finally, we need to calculate the additional temperature drop due to the requirements of heat transport by the gas itself. If the gas temperature drops by ΔT_g passing through a tube of length L, the total heat delivered is Q_t:

$$Q_t = \pi d^2 v \rho C_p \Delta T_g / m \quad . \qquad (C\text{-}16)$$

On the other hand, the total heat flux in the tube is found by multiplying q_h by the area of the tube wall:

$$Q_h = 30\,\sigma\pi Ld \times 10^{-4}\, v\rho\Delta T_b/\mu(Re^*)^{0.2} \quad . \qquad (C\text{-}17)$$

From Eqs. (C-16) and (C-17), one can find the ratio of ΔT_g to ΔT_b, using the Prandtl number for the quantities on the rhs of Eq. (C-6):

$$\Delta T_g/\Delta T_b = 3 \times 10^{-3}\,(L/d)\,(Pr)^{-1}\,(Re^*)^{-0.2} \quad . \qquad (C\text{-}18)$$

Evidently, so long as the length-to-diameter ratio of the tube is less than 30, the heat transport temperature drop will remain less than 10% of the drop through the boundary layer. Only if L/d is of the order of 100 or more will T_g become a major design consideration. In this connection, note that in order that Re be 10,000 for H_2 gas moving at 8500 cm/sec, the tube diameter must be at least 3.5 cm. Thus a tube with L/d for 30 is over a meter long; one with L/d for 100 would be 3.5 meters long.

APPENDIX D

FLOW IN CHANNELS ON A ROTATING DISC

Consider a coordinate system that rotates with a turbine wheel at angular frequency ω, and flow outward from the hub of the wheel in a confined channel as in Fig. D-1. At any radius r, the flow moves with speed u at an angle ψ to the radius, reaching a maximum velocity v_m at the outer radius r_m. For most efficient extraction of the kinetic energy of this flow as it leaves the wheel, v_m should be close to ωr_m and ψ should be close to 90°.

In the rotating coordinate system, the wheel appears to stand still, and the expanding gas flows through it, just as for a non-rotating expansion nozzle. However, the flow differs from that described in Sections VII, VIII, and IX in two essential ways. First, in addition to the kinetic energy of the local flow, $1/2\ mu^2$, there is a potential energy term, $-\frac{1}{2} m\omega^2 r^2$. Second, although the flow apparently does no work on the walls of the channel, there is a body force, the Coriolis force, against which the flow does work W.

The Coriolis force is given by F_c

$$F_c = 2m\omega \times \frac{dr}{dt} \tag{D-1}$$

and the work done against this force is obtained by integrating along the flow path s:

$$W = 2 \int_s \omega \times \frac{dr}{dt} \cdot ds \quad . \tag{D-2}$$

If H_i is the initial enthalpy of the fluid at the axis, it is divided between the work done and the remaining enthalpy H as the flow moves outward

$$H + W = H_i = \text{const} \quad . \tag{D-3}$$

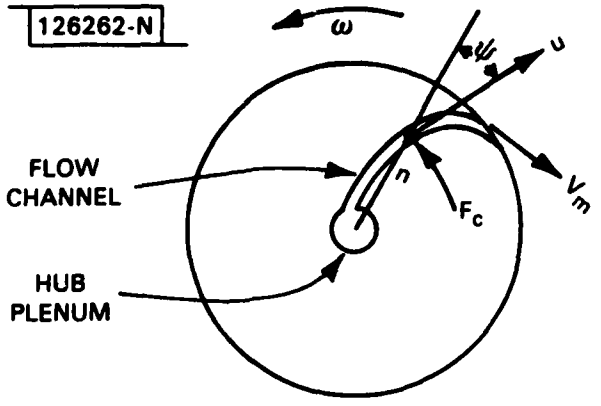

Fig. D1 Radial flow geometry.

The enthalpy H is made up of the enthalpy H of the fluid plus the kinetic and potential energy terms. Thus, for the rotating coordinate system, Eq. (VII-1) of the text is replaced by

$$H - H = \frac{1}{2} mu^2 - \frac{1}{2} m\omega^2 r^2 \quad . \tag{D-4}$$

Combining Eqs. (D-4) with (D-2) and (D-3) produces the conservation law

$$H_i = \text{const} = \frac{1}{2} m(u^2 - \omega^2 r^2) + 2 \int_s \omega \times \frac{dr}{dt} \cdot ds + H \quad . \tag{D-5}$$

Now we shall concern ourselves solely with the case in which the flow is perpendicular to the axis of rotation, for which the vector products in

Eq. (D-5) can be simplified. The conservation law then becomes

$$H_i = \text{const} = \frac{1}{2} m(u^2 - \omega^2 r^2) + 2\omega \int_s \sin \psi \frac{dr}{dt} ds + H \qquad \text{(D-6)}$$

where ψ is the angle between the radius and the direction of flow. The integral in this equation can be written as

$$\int_s \sin \psi \frac{dr}{dt} ds \quad , \quad \int_r u \sin \psi \, dr \quad , \quad \int_u u \frac{dr}{dt} \sin \psi \, du$$

in which path and limits are chosen appropriate to the particular variable of integration. By using the second form of the integral, we have

$$H_i = \text{const} = \frac{1}{2} m(u^2 - \omega^2 r^2) + 2m\omega \int_r u \sin \psi \, dr + H \quad . \qquad \text{(D-7)}$$

If, to be consistent with good kinetic energy extraction, we choose u to be equal to ωr_m at the periphery, and designate this velocity as v, then the net energy change from zero speed at the hub to v at the periphery is H_i-H:

$$H_i - H = 2m\omega \int_r u \sin \psi \, dr \; 2\Delta H \quad . \qquad \text{(D-8)}$$

We can reasonably assume that the wheel channel is so designed that the flow leaves nearly tangentially, $\sin \psi = 1$, with the result that in the frame of reference of the laboratory the exiting flow has no kinetic energy. It follows that H_i-H has been deposited in the wheel.

It is not unreasonable to assume a piecewise logarithmic spiral flow path, with ψ constant along each major segment of the path*. The largest extraction occurs when u is almost constant at nearly v,

$$\begin{aligned} \Delta H &= 2m\omega v r_{max} \sin \psi \\ &= 2mv^2 \sin \psi \end{aligned} \qquad \text{(D-9)}$$

*Allowing for short regions of transition between ψ's.

with a path chosen so that sin ψ is nearly unity. This is almost 4 times the ΔH that could be ascribed to the apparent kinetic energy of flow, $\frac{1}{2} mv^2$. Stated another way, in this case, nearly 3/4 of the energy transferred to the wheel came from the expansion against the Coriolis force as a virtual piston; only 1/4 came from the change in apparent momentum of the flow.

Other flow patterns produce other results, all the way from a high percentage of extraction by static expansion as above, to a high percentage of static pumping by reversing the sign of ψ. If sin $\psi \to 1$ and u is proportional to r, then the energy extracted is one-half that given in Eq. (D-9); if u is proportional to $\sqrt{r}$, then the ΔH is 2/3 that given in Eq. (D-9).

Evidently, in all these cases the energy extraction is comparable to what would be obtained from a stationary nozzle having an exit velocity of 2v. Thus, for the same degree of droplet vapor equilibration, the nozzle can be shorter by roughly a factor of 2; and the friction losses per unit area are reduced by up to a factor of 4.

Just as in the case of a non-rotating nozzle, flow in a rotating channel is determined by a minimum cross-section constriction. However, the flow at this point is not necessarily sonic in any coordinate system. The formal equation for expansion of the flow can be obtained in a manner analogous to that by which Eqs. (VIII-20) through (VIII-24) were obtained from Eq. (VIII-7), by differentiation of Eq. (D-7) followed by variable changes and integration.

Differentiation of Eq. (D-7) yields

$$dH_i = 0 = m(udu - \omega^2 r dr) + d \int 2m\omega u \sin \psi \, dr + TdS + VdP \quad . \qquad \text{(D-10)}$$

The assumption that dS is zero and the substitution of the speed of sound, a^2, for $dP/d\rho$, and ρ for m/V, yields

$$-\frac{d\rho}{\rho} = \{udu - \omega^2 r dr + d\int 2\, \omega u \sin \psi \, dr\} \; / \; a^2 \qquad \text{(D-11)}$$

for which the formal integral is

$$\rho = \rho_o \exp(-\int\{\}/a^2) \qquad \text{(D-12)}$$

with the braces representing their content in Eq. (D-11). The flow per unit are is ρu. It is maximum (and the corresponding minimum throat area fixed steady mass flow) occurs when

$$a^2 = u^2 + \omega^2 r^2 \frac{d\ell nr}{d\ell nu} \left(\frac{2u}{\omega r} \sin \psi - 1 \right) . \qquad \text{(D-13)}$$

If the throat is close to the axle, so that $r \to 0$, the terms added to u^2 on the rhs of Eq. (D-13) vanish, so that the throat conditions approach sonic flow, M*=1. But generally, the additional term on the rhs of Eq. (D-13) will be, by design, positive. The resulting throat speed will therefore be subsonic.

One easy nozzle design is one for which the flow reaches exit velocity in a throat close to the axis and then proceeds at nearly constant velocity u, with ψ close to 90°, to the periphery in a spiral. If u is fixed, then the net body force on the moving fluid is proportional to F

$$F = -\omega^2 r \, dr/ds + 2u \sin \psi \frac{dr}{dS} \omega \quad . \qquad \text{(D-14)}$$

The first term on the rhs of Eq. (D-14) is the component of centrifugal force, the second the component of Coriolis force, both along the direction of flow. Geometrically, dr/ds is cos ψ. Thus

$$F = \omega \cos \psi \, (2u \sin \psi - \omega r) \quad . \qquad \text{(D-15)}$$

If the flow is to be constant at v_{exit}, then Fv_{exit} represents the power expended, which must come from the internal H of the fluid. If ψ is held fixed, then this rate of energy extraction varies with radius:

$$Fv_{exit} = \omega \cos \psi \, (2 \sin \psi - r/r_{exit}) \, v_{exit} \quad . \qquad \text{(D-16)}$$

An alternative is to make the rate of energy extraction constant, which requires that

$$\cos \psi \, (2 \sin \psi - r/r_{exit}) = \text{const} \quad . \tag{D-17}$$

Since sin ψ is nearly unit for minimum exit velocity for a given energy output, this equation basically requires that cos ψ vary over a two to one range as r varies between zero and the periphery.

In a design of this kind, the temperature of the fluid tends to drop linearly with distance along the constant-speed length of the nozzle. The nozzle cross-section is then roughly exponential with distance. In this manner, a nozzle can be designed in which a throat diameter of 0.5 mm is increased to 6 mm in 75 mm beyond the throat section, with only about 50°K temperature differential between vapor and droplets necessary to maintain proper internal heat exchange at 50% wetness.

Because most of the work in this kind of nozzle is done against Coriolis force, the losses at the throat may be a substantial fraction of the kinetic energy without producing an overall loss of more than 10 or 15%, just as is the case with the kinetic flow in optimized turbine blades. Detailed design tradeoffs for Coriolis force nozzles are beyond the scope of the present work. Hence, we make no attempt to accurately estimate the loss in any particular case.

BIBLIOGRAPHY

1. "Power From Mercury Vapor" by W. LeR. Emmet, Trans. AIEE, Vol. 32, December 16, 1913, pp. 2133-2149.

   Other papers giving the history of this project are:

   "Mercury Vapor Unit Operates Successfully" by James Orr, Power, July 1, 1930, pp. 4-9.

   "The Mercury Vapor Process" by Smith & Thompson, Trans. ASME Vol. 64, October 1942, pp. 625-646.

   "Mercury for the Generation of Light, Heat, and Power" by Trans. ASME Vol. 64, October 1942, pp. 647-656.

   See Also Liquid Metals Handbook [12] Chapter 1, Section 3.5, and Chapter 4, Section 8.

2. "The Equation of State and Electrical Resistivity of Liquid Mercury at Elevated Temperatures and Pressures" by Postill, Ross, & Cusack, Phil Mag 18 (1968) pp. 519-530.

3. "Metal - Non-Metal Transition in Dense Mercury Vapor" by Hensel & Franck Reviews Mod Phys 40 No. 4, October 1968, pp. 697-704.

   "Absolute Thermoelectric Power of Dense Mercury Vapor" Schmutzler and Hensel, Phys Lett 35A No. 1, 3 May 1971, pp. 55-56.

   "Knight Shift in Expanded Liquid Mercury" by El-Hanany and Warren, Phys Rev Lett 34 No. 20, 19 May 1975, pp. 1276-1279. See especially footnote 12. The foregoing references are a sampling of those available.

4. "Electrical Conductivity and Equation of State of Mercury in the Temperature Range 0-2000°C and Pressure Range 200-5000 Atm." by Kikoin & Senchencov Physics of Metals and Mettallography (USSR) 24, No. 5, (1969) pp. 24-89. (Fiz Met Metall 24 No. 5, 843-858, 19670.

5. "Thermodynamic Properties and Viscosity of Supercritical Mercury" by A. S. Roberts, 2nd AIAA/ASME Thermophysics and Heat Transfer Conference, May 24-26, 1978, Conference Paper 78-868.

6. International Critical Tables, E. W. Washburn, Editor National Research Council/McGraw-Hill, New York, 1928. (Vol. III, pp. 104-106).

7. Thermophysical Properties of Matter, Vol. 4, "Specific Heats of Metallic Elements and Alloys", Touloukian & Buyco, Plenum Press, 1970.

8. Thermodynamic Tables and Charts, Raznjevic, Editor, McGraw-Hill, 1976.

9. "The Optical Properties of Liquid Metals" by N. R. Comins, Phil Mag 8, 25, 1972, p. 817.

10. Light Scattering by Small Particles by H. C. Van De Hulst, Wiley, NY (1957) Chapter 14, "Absorbing Spheres," esp. formulas for "region 3" on p. 290 and "region 5" on p. 291.

11. "The Principle of Corresponding States," By E. A. Guggenheim, Jour Chem Phys 13, No. 7, July 1945.

12. Liquid Metals Handbook, R. Lyons, editor, 2nd Edition U.S. Atomic Energy Commission/Bu Ships (1952) (Superintendent of Documents, Washington, DC).

13. Handbook of Chemistry and Physics, CRC Publishing Co., 53rd Edition (1972). (1973).

14. Supersonic Aerodynamics by E. R. C. Miles, Dover, NY (1961). See esp. Sections 1.10-1.12 and 7.1-7.12.

15. Hypersonic Flow, Vol. I (Invicid Flows), by Hayes and Probstein, 2nd ed., Academic Press, NY (1966) See esp. sections 1.4 and 1.5.

16. Processes for Air Pollution Control, G. NonHebel, 2nd Edition, CRC Press, Cleveland, 1972. See esp. Chapters 12 ("Removal of Dust From Gases") and 15 ("Mist Removal").

17. "The Wrap-Rib Parabolic Reflector Antenna" LMSC/A969503. Lockheed Missiles & Space Co., Sunnyvale, CA (10 April 1970).

18. "Flywheel Components for Satellite Applications", by A. R. Millner, MIT Lincoln Laboratory Technical Note 1978-4, 16 May 1978, pp. 77-79. DDC-AD-A060586

19. "100 kW$_e$ Nuclear Electric Power Source, by D. Buden, Los Alamos Scientific Lab., Paper # 79-2089, 14th International Electric Propulsion Conference, October/November 1979.

20. "Thermodynamics of the Lithium Hydride Regenerative Cell" by Johnson & Heinrich, Adv Chem Ser, 67, pp 105-120 (1964).

21. "Performance of the Multi-Hundred Watt Radioisotope Thermoelectric Generator Source for the LES-8/9 Satellites" C. E. Kelley and C. W. Whitmore, Technical Papers AIAA 7th Communications Satellites Systems Conference, April 24-27, 1978. An. Inst. Aer. & Ast., NY, 1978, pp 728-735 (AIAA 78-534).

22. "RTG Power Sources for the International Solar Polar Mission" AIAA Paper 80-9204 (15th IECEC), Am. Inst. Aer. & Ast. NY, 1980, [Conference held Aug. 18-22, 1980].

23. "Experiments on Drag of Revolving Disks, Cylinders, and Streamline Rods," by Theodore Theodorsen and Arthur Regier, NACA Report No. 793, Superintendent of Documents, Washington, DC 1945.

24. "Materials Technology Programs in Support of a Mercury Rankine Space Power System" by Phillip L. Stone, NASA TN D-7355, NASA-Lewis Research Center, Cleveland, September 1973.

25. "SNAP-8 Electrical Generating System Development Program (Anon) Aerojet General, Azusa, CA, July 15, 1971, (NASA CR-72860).

REPORT DOCUMENTATION PAGE		READ INSTRUCTIONS BEFORE COMPLETING FORM
1. REPORT NUMBER ESD-TR-82-176	2. GOVT ACCESSION NO. AD-A129016	3. RECIPIENT'S CATALOG NUMBER
4. TITLE (and Subtitle) A High Pressure Mercury Turbine Cycle for Use in Spacecraft and Terrestrial Power Plants		5. TYPE OF REPORT & PERIOD COVERED Technical Report 6. PERFORMING ORG. REPORT NUMBER Technical Report 577
7. AUTHOR(s) Robert M. Lerner		8. CONTRACT OR GRANT NUMBER(s) F19628-80-C-0002
9. PERFORMING ORGANIZATION NAME AND ADDRESS Lincoln Laboratory, M.I.T. P.O. Box 73 Lexington, MA 02173-0073		10. PROGRAM ELEMENT, PROJECT, TASK AREA & WORK UNIT NUMBERS Program Element Nos. 63431F/ 33601F Project Nos. 2029/6430
11. CONTROLLING OFFICE NAME AND ADDRESS Air Force Systems Command, USAF Andrews AFB Washington, DC 20331		12. REPORT DATE 22 March 1983 13. NUMBER OF PAGES 260
14. MONITORING AGENCY NAME & ADDRESS (if different from Controlling Office) Electronic Systems Division Hanscom AFB, MA 01731		15. SECURITY CLASS. (of this report) Unclassified 15a. DECLASSIFICATION DOWNGRADING SCHEDULE

16. DISTRIBUTION STATEMENT (of this Report)

Approved for public release; distribution unlimited.

17. DISTRIBUTION STATEMENT (of the abstract entered in Block 20, if different from Report)

18. SUPPLEMENTARY NOTES

None

19. KEY WORDS (Continue on reverse side if necessary and identify by block number)

Spacecraft power plant	Boiler with radiatve heat transfer
Mercury turbine	Radiative heat transfer
Rankine cycle	Thermodynamic peoperties of mercury
Solar energy	Wet steam turbine
Droplet boiler	Supersonic turbine

20. ABSTRACT (Continue on reverse side if necessary and identify by block number)

A high pressure thermomechanical cycle using mercury as a working fluid can be made practical at close to theoretical thermodynamic efficiency between a hot shoe temperature of about 1200°K (3000 psia "boiler" pressure) and 600°K condenser. Means are proposed for utilizing a simple "Rankine" cycle without superheat, in which liquid droplets are vaporized by radiative heat transfer after being sprayed into the boiler chamber as a mist; and in which vapor wetness is controlled (by the addition of further hot mist if need be) prior to expansion in a nozzle; and in which, after expansion, the kinetic energy of both droplet and vapor phases is utilized in a turbine. Potential non-equilibrium flow phenomena and potential turbine blade erosion by wet fluid are controlled by utilizing a condensate droplet radius of the order of 1 μm during expansion and power extraction.

20. ABSTRACT (Continued)

Rough calculations are made of boiler and radiator size and weight for use in orbit, at the 100/300 kW output power level for use as a replacement for a thermopile in a spaceborne reactor system, at the 30 kW output power level for use with a radioisotope thermal source or with a concentrating solar collector. Specific power for the 100/300 kW case ranges up to 100 W/lb. In all cases, the overall space plant thermodynamic efficiency is in the range 25% to 35%; in a terrestrial power plant a 40% practical efficiency is possible, ranging up to 55% if a conventional medium pressure steam plant is added as a bottoming cycle.

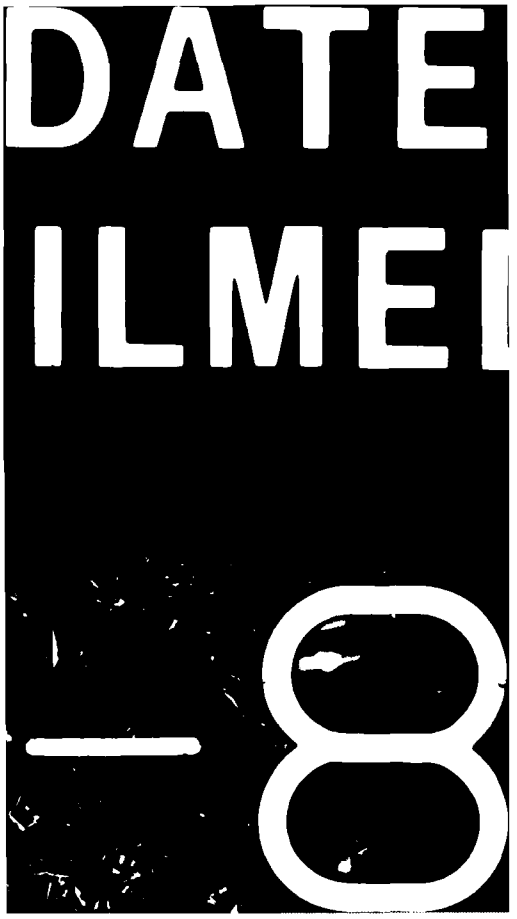
DATE
ILME
8